Role of WIP in metastasis and study of transcriptional regulation of N-Wasp

Amrita S Salvi

2016

ROLE OF WIP IN METASTASIS AND STUDY OF TRANSCRIPTIONAL REGULATION OF N-WASP

Amrita S Salvi

School of Biological Sciences

2016

ROLE OF WIP IN METASTASIS AND STUDY OF TRANSCRIPTIONAL REGULATION OF N-WASP

Amrita S Salvi

School of Biological Sciences

A thesis submitted to the Nanyang Technological University in partial fulfilment of the requirement for the degree of Doctor of Philosophy

ACKNOWLEDGEMENT

TABLE OF CONTENTS

CHAPTER 1: INTRODUCTION

VIII

LIST OF FIGURES

XII

LIST OF TABLES

LIST OF ABBREVIATIONS

2-OG	2-Oxoglutarate
3-AT	3-Amino-1, 2, 4-triazole
α-SMA	Alpha Smooth muscle actin
AD	Activation domain
APS	Ammonium persulfate
AR	Acidic region
ATP	Adenosine 5'-triphosphate
Arp2/3	Actin related protein complex
ARNT	Aryl hydrocarbon nuclear translocator
bHLH	Basic helix-loop-helix
BMP	Bone morphogenetic protein
BR	Basic region
BSA	Bovine serum albumin
c-TAD	C terminal activation domain
cDNA	Complementary DNA
Cdc42	Cell division cycle 42
C	Cofilin homology
ChIP	Chromatin immunoprecipitation
CR16	Corticosteroid and regional expression 16
ddH$_2$O	Double distilled water
DEG	Differentially expressed genes
DEPC	Diethypyrocarbonate
DMEM	Dulbecco's Modified Eagle Medium
DMSO	Dimethylsulfoxide
DNA	Deoxyribonucleic acid
dNTP	Deoxynucleotide Triphosphate

DTT	Dithiothreitol
EGF	Epidermal growth factor
ECM	Extracellular matrix
E.coli	*Escherichia coli*
EDTA	Ethylenediamine Tetraacetic acid
EMT	Epithelial Mesenchymal Transition
EPAS	Endothelial Per-Arnt-Sim
F-actin	Filamentous actin
FA	Focal adhesions
FBS	Foetal Bovine serum
FC	Focal complex
FAK	Focal adhesion kinase
FIH -1	Factor inhibiting HiF1
Fyn	Proto-oncogene tyrosine-protein kinase Fyn
G-actin	Globular actin
GAP	GTPase activating protein
GBD	GTPase Binding domain
GDI	Guanine Nucleotide Dissociation Inhibitors
GEFs	Guanine Nucleotide exchange factors
GFP	Green Fluorescent protein
Grb2	Growth Factor Receptor-Bound Protein 2
GTPase	Guanosine triphosphatase
HIF1α	Hypoxia-inducible factor A subunit
HIF1β	Hypoxia-inducible factor B subunit
HMGA2	High-mobility group AT-hook 2
HRE	Hypoxia Response element
HRP	Horse Radish peroxidase
Hrs	Hours

I-Smad	Inhibitory Smad
Id	Inhibitor of differentiation
IPAS	Inhibitory Per-Arnt-Sim
IRES	Internal ribosome entry site
IRSp53	Insulin receptor tyrosine kinase substrate
ISL1	Insulin gene enhancer protein ISL-1
JNK	c-Jun N-terminal kinase
LB	Luria-Bertani Medium
LiAc	Lithium acetate
LTBPs	Latent TGF-beta binding proteins
MAPK	Mitogen-activated protein kinase
MCS	Multiple cloning site
MEF	Mouse Embryonic Fibroblast
MET	Mesenchymal Epithelial Transition
Mins	Minutes
miRNA	MicroRNA
MLC	Myosin light chain
MMP	Matrix metalloprotease
Msx1	Muscle segment homeobox 1
N-WASP	Neural-WASP
N-TAD	N Terminal activation domain
N-cadherin	Neural cadherin
Nck	Non catalytic region of tyrosine kinase adaptor protein
NGS	Next Generation sequencing
NMR	Nuclear magnetic resonance
NK	Natural killer
ODDD	Oxygen dependent degradation domain
PAGE	Polyacrylamide gel electrophoresis

PBS	Phosphate Buffered Saline
PCR	Polymerase chain reaction
PEG	Polyethylene glycol
PEI	Poly-ethylenimine
PHD	Prolyl hydroxylase domain
PI3K	Phosphatidylinositol-3 (PI3) kinase
PIP$_2$	Phosphoinositide bis-phosphate
PMSF	Phenylmethylsulfonyl fluoride
POU3F2	POU domain, class 3, transcription factor 2
PRR	Proline rich region
pVHL	Von Hippel-Lindau protein
R-Smads	Regulatory Smads
Rac1	Ras-related C3 botulinum toxin substrate-1
Rcf	Relative centrifugal force
RFP	Red fluorescent protein
RNA	Ribonucleic acid
RNA-Seq	RNA sequencing
RNase	Ribonuclease
RPM	Revolutions per minute
RT PCR	Reverse Transcription PCR
SBE	Smad Binding element
SCAR	Suppressor of cAMP receptor
SCC	Squamous cell carcinoma
SDS	Sodium Dodecyl Sulphate
SFM	Serum free media
SH2	Src Homology 2
SH3	Src Homology 3
shRNA	Short hairpin RNA

SIP1	Smad-interacting proteins 1
Smurf1	Smad ubiquitination regulatory factor 1
TEMED	N,N,N',N'-tetramethylethylenediamine
TGF-beta	Transforming growth factor beta
Toca-1	Transducer of Cdc42-dependent actin assembly
TSS	Transcriptional start site
UTR	Untranslated region
VH	Verprolin homology
WAS	Wiskott Aldrich Syndrome
WASP	Wiskott Aldrich Syndrome protein
WAVE	WASP-family verprolin homologous proteins
WBD	WASP binding domain
WH1/EVH1/PH	WASP homology domain 1/ Ena-VASP homology domain 1 / Pleckstrin homology
WH2	WASP homology 2
WICH	WIP and CR16 Homologus protein
WIP	WASP-interacting protein
WIRE	WIP related

Abstract

Cancer cell migration and invasion involves actin cytoskeleton reorganization, which is regulated by the WASP family of proteins such as WASP (Wiskott Aldrich Syndrome Protein) and N-WASP (Neural-WASP). N-WASP and WASP interacting protein (WIP) play a crucial role in integrating signaling cascades leading to actin cytoskeleton remodeling. Compared to non-tumorigenic HaCaT cells, N-WASP expression was found to be low in the tumorigenic, non-metastatic epithelial cell line, HSC5 and high in the metastatic HaCaT derivative cell line, A5-RT3. Differential expression of N-WASP may play a role in determining the function of N-WASP during tumorigenesis. Characterization of N-WASP promoter was carried out by using GFP reporter assay, which led to the identification of a 393 bp regulatory region in N-WASP promoter critical for N-WASP promoter activity. Yeast one hybrid screen identified Msx1, an embryonic transcription factor as a binding element in N-WASP promoter.

N-WASP expression has been shown to be increased under hypoxia conditions. In the current study, it was found that N-WASP promoter activity was enhanced in the presence of Hypoxia Inducible factor (HiF1α) suggesting a possible regulatory mechanism exerted by HiF1α. Sequence analysis of the N-WASP promoter revealed presence of two hypoxia response elements (HRE) characterized by the consensus motif 5'ACGTG 3'. Site-directed mutagenesis and ChIP assay demonstrated one of the HRE to be the binding site of HiF1α under hypoxic condition.

RNA sequencing of HaCaT (non-tumorigenic keratinocyte) and A5-RT3 cell, which is a metastatic derivative of HaCaT led to the identification of 4488 genes which are upregulated and 1403 genes which are downregulated in A5-RT3 compared to HaCaT cells. WIP, N-WASP and

HiF1α were among the 4488 genes which were significantly upregulated in A5-RT3 cells in comparison to HaCaT cells. The role of WIP in migration, invasion and proliferation was studied in A549 human lung carcinoma cells. Overexpression of WIP was found to enhance the proliferative, migratory and invasive ability as well as confer anchorage-independent growth properties in A549 cells. Expression level of WIP was found to increase in presence of TGF-beta and its role in TGF-beta induced EMT was analyzed in A549 cells. Overexpression of WIP was found to enhance EMT progression whereas knockdown of WIP inhibited morphological changes associated with EMT. Knockdown of WIP led to significant reduction of RhoA in A549 cells which explains reduced migration, invasion and proliferation of WIP knockdown cells. Thus the data indicates an important function of WIP in metastatic progression.

CHAPTER 1: INTRODUCTION

1.1 Cytoskeleton

The cytoskeleton comprises of a three dimensional intracellular network formed by filamentous polymers which helps the cell to sense external environment and respond to stimuli. The cytoskeleton spatially organizes cellular content and maintains cell shape and size [1]. The three cytoskeletal filaments i.e. microtubules, intermediate filaments and actin filaments; along with their regulatory proteins form a dynamic network that can assemble, disassemble and maintain the integrity of intracellular components [2]. The large surface area occupied by cytoskeleton along with the high negative charge density on the cell surface helps in localization of many signalling molecules in response to specific transmembrane receptors [3].

1.2 Actin cytoskeleton

Actin is the most abundant eukaryotic intracellular protein and is encoded by a large, highly conserved gene family. Actin exists in both a globular G-actin monomeric form and a filamentous polymeric F-actin form. The actin cytoskeleton can alter the cell shape and size by rapidly assembling and disassembling itself through actin monomers leading to cell spreading and cell migration [4].

Cell migration is a vital step in various cellular processes such as immune cell chemotaxis, fibroblast migration as well as neuronal cell migration during normal physiological and pathological stages such as metastasis [5]. Cell locomotion is a complex event requiring

coordination of actin cytoskeleton, cell-cell and cell-ECM (extracellular matrix) adhesion etc [6].

Actin is an important component of protrusive structures such as filopodia, invadopodia and

lamellipodia, all of which are present at the migratory edge of motile cells (Figure 1.1) [7]. These

protrusive structures differ in their structure and function. However, all of them consist of an

actin core surrounded by adhesion and scaffolding proteins. These structures are important for

cell-ECM attachment as well as degradation of the ECM during migration [8]. Actin was found

to be present in the nucleus, indicating a role in chromatin remodelling, transcription and RNA

processing [9].
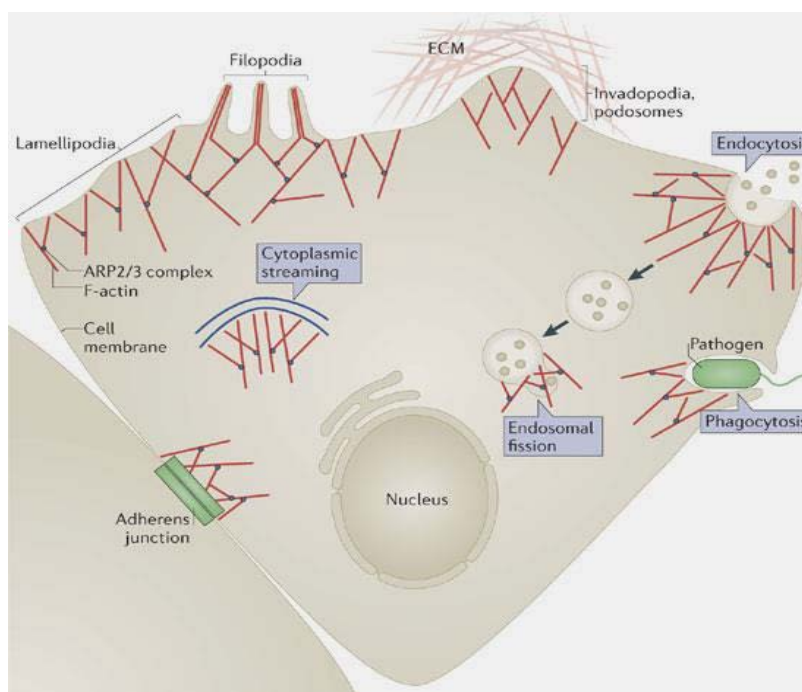
Figure.1.1: Schematic representation of actin cytoskeleton in a migrating cell
Actin-related protein 2/3 (Arp2/3) complex localizes to leading edge of migrating cells, adherens junction, phagosomes and endosomes. The leading edge of migrating cells consists of motile structures such as filopodia and lamellipodia. Invadopodium, actin rich structure possesses matrix degradation capacity which helps in tumor invasion and metastasis.
Reprinted by permission from Macmillan Publishers Ltd: [Nature reviews Molecular Cell Biology] [7], copyright (2013).

1.3 Actin cytoskeleton regulators

Migration of cell in response to extracellular stimuli is based primarily on the reorganization of actin cytoskeleton. Actin filament reorganization is mediated by actin binding proteins, which are classified based on their function as severing, monomer binding, nucleating, sequestering, capping and cross-linking proteins [10]. Actin is an ATPase and regulates the transition of actin from G-actin to F-actin form [11]. G-actin monomers are added to the barbed (+) and pointed (-) end of the actin nucleus to accelerate actin filament elongation [12]. Reorganization of actin cytoskeleton is also regulated by Rho GTPases (Guanosine Triphosphatase), which act as GTP-dependent molecular switches [13]. The formation of actin nucleus is the first step in formation of new actin filaments, regulated by actin nucleating proteins such as formins and the Arp 2/3 complex. Formins are actin polymerizing proteins which bind to the barbed end of actin filaments by bridging two actin subunits [14]. The Arp2/3 complex is a conserved 7-subunit complex consisting of Arp2, Arp3 and subunits ARPC1-5 (Actin-related protein complex 1-5) [15]. The Arp2/3 complex nucleation activity is enhanced via binding with nucleation promoting factors (NPFs). NPFs binds to the Arp2 and Arp3 subunits of the Arp2/3 complex bringing the two subunits together for formation of actin nucleus and F-actin [16]. NPFs help in the recruitment of actin monomers to the Arp2/3 complex and thus promote actin polymerization [17]. Member of NPFs consist of WASP family, WASP family verprolin homologous family proteins (WAVE 1-3) and WASP and SCAR (suppressor of a cyclic AMP receptor) homologue (WASH) [18].

1.4 WASP family of proteins

The WASP/Scar family of proteins play a crucial role in Arp2/3 complex activation which promotes actin polymerization [19]. The WASP family includes the WASP and Scar/WAVE subfamilies. The WASP subfamily consists of WASP and N-WASP, and the Scar/WAVE subfamily consists of Scar/WAVE1-3. WASP is only expressed in hematopoietic cells, whereas N-WASP is expressed ubiquitously although elevated levels of the protein are found in the brain [20].

Mutation in the *WAS* gene causes Wiskott Aldrich Syndrome (WAS), an X-linked disorder characterized by eczema, recurrent infections and severe thrombocytopenia. It is a primary immunodeficiency, which is fatal unless treated by bone marrow transplantation [19]. WAS patients show abnormalities in cytoskeletal structure of lymphocytes. The size of the lymphocytes and number of platelets is reduced in WAS patients. WAS T lymphocytes show a relatively smooth surface due to decrease of microvilli number [21]. Another significant feature is the diminished response of peripheral blood T lymphocytes to CD3 stimulation for cell proliferation [22]. Cellular and humoral immunity deficiency is common among WAS patients, although severity of symptoms varies among patients. The *WAS* gene was identified by positional cloning and it comprises of 12 exons spanning 9.5 kb [19]. Mutations have been identified all over the gene's sequence, but more than 50% of mutations in WASP were found in exons 1, 2 and 3, which code for the WH1 (WASP homology 1) domain [23].

1.5 Neural Wiskott-Aldrich syndrome Protein (N-WASP)

N-WASP is a 505 amino acid protein, which was first isolated from bovine brain as an isoform of WASP [20]. N-WASP knockout mice have embryonically lethal phenotype with defects in neural tube and cardiac tissue around embryonic day 11 [24-26]. Presence of N-WASP has been demonstrated in various actin-rich structures such as filopodia, dorsal ruffles, lamellipodia and invadopodia [27-32].

1.5.1 Domain structure of N-WASP

The WASP family of proteins show similar domain structure and multiple motifs, which interact with a number of proteins (Figure 1.2). N-WASP contains a WH1 domain (also known as Ena-VASP-homology-1 (EVH1)) or PH domain (Pleckstrin-homology Domain) at the amino terminus [20]. The WH1 domain interacts with verprolin family of proteins that include WIP [22], CR16 (corticosteroid and regional expression 16) [33] and WICH/WIRE (WIP and CR16 – homologous protein/WIP-related) [34, 35]. The WH1 domain is followed by a Basic region, which encodes the CRIB (Cdc42 and Rac interactive binding) motif. Following this Basic region is the GBD (GTPase-Binding Domain) region [36, 37] and the proline-rich region (PRR); the latter possesses binding sites for numerous SH3- domain-containing proteins such as cortactin, WISH, adaptor proteins such as Nck, Grb2 and Src-family protein-tyrosine kinase Fyn [38]. At the extreme carboxy terminus is the VCA domain. The VCA domain is a hallmark of all the members of WASP family of proteins. N-WASP VCA domain consists of two verprolin

homology domains (V) also termed at WASP homology 2 (WH2) followed by a short C domain

(central/connecting domain) and an A domain (acidic domain) (Figure 1.2) [10].
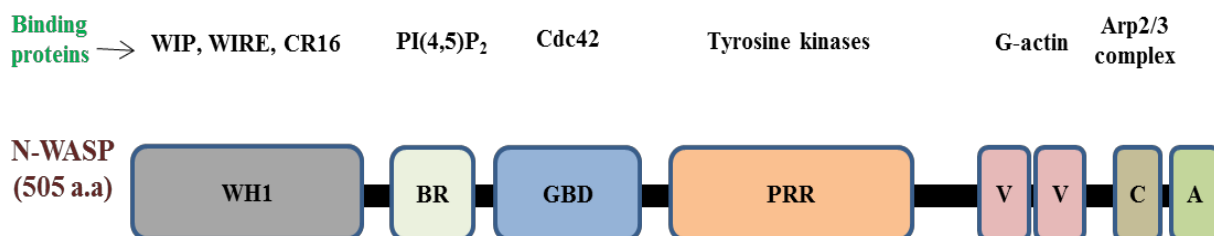
Figure.1.2: Domain structure of N-WASP

From the amino terminal to the carboxy terminal: WH1- WASP homology domain 1; BR-Basic region; GBD-GTPase binding domain; PRR-Poly-proline; V-Verprolin homology domain, C- Cofilin-homology or central domain; A- Acidic region..

In resting state, N-WASP adopts a closed conformation due to intramolecular interaction of the

carboxy terminus and the GBD (Figure 1.3) [39]. The affinity between the GBD and carboxy

terminus is reduced due to binding of activators such as PIP2 to the basic region or Cdc42 to the

GBD, respectively. This results in the opening of the closed conformation of N-WASP, which

exposes its VCA region that can bind and activate Arp2/3 complex and subsequently leads to

actin polymerization [10]. Dimerization of the VCA domain is also shown to regulate N-

WASP/WASP activity towards Arp2/3 complex [40]. Focal adhesion kinase (FAK) has been

shown to phosphorylate N-WASP at the conserved Tyr256 residue, which maintains N-WASP in

cytoplasm [41] and phosphorylation of N-WASP has been shown to enhance N-WASP

stimulated actin polymerization indicating that FAK may regulate N-WASP activity [42].
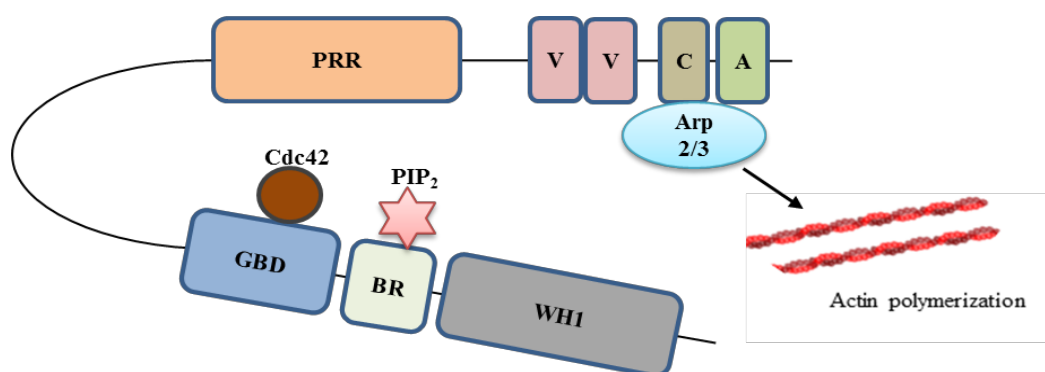
Figure.1.3: Model for N-WASP mediated actin polymerization

In its inactive state, N-WASP has an auto-inhibited conformation with sequences near its C-terminus binding to a region near its N-terminus. Its activation is dependent upon Cdc42 and PIP2 binding to disrupt this interaction, causing the N-WASP protein to 'open'. This exposes a domain near the N-WASP C-Terminus that binds to and activates the Arp2/3 complex. Activated Arp2/3 nucleates new F-actin.

1.5.2 Functions of N-WASP

N-WASP helps in coordinating signals from molecules such as small GTPases, SH3-domain containing proteins and phospholipids, and delivering those signals to the actin machinery leading to actin polymerization [20]. Studies in mouse embryonic fibroblasts (MEFs) have shown that N-WASP deficiency reduced cell adhesion to fibronectin and enhanced motility of cell, suggesting the importance of N-WASP in regulating cell adhesion and cell motility [43]. Conditional knockout of N-WASP in mice brain led to cranial deformities due to excess accumulation of cerebrospinal fluid and the mice did not survive past weaning stage [44]. N-WASP has also been shown to be essential for the fusion of skeletal muscles in developing mouse embryos [45]. N-WASP is present at sites of clathrin mediated endocytosis and plays a role in actin assembly for promoting vesicle fission and departure [46, 47]. Recent study has demonstrated that dynamin, a GTPase responsible for endocytosis, recruits WAVE complex followed by N-WASP during endocytosis of the interleukin-2 receptor [48]. N-WASP is also

important for regulating synapse formation in hippocampal neurons as well as for formation of dendritic spines [49]. Studies have also demonstrated the presence of N-WASP in nucleus [50, 51]. N-WASP forms a complex with the kinetochores and is important for chromosome alignment and progression of mitosis [52]. N-WASP also regulates transcription by interacting with the PSF-NonO complex which is associated with RNA polymerase II [51]. Expression of HSP90 is found to be regulated by nuclear N-WASP by modulation of Src kinase activity [50].

1.5.3 Role of N-WASP in cancer

Tumor cells turn highly invasive and metastatic by undergoing a cascade of events such as loss of cell-cell contact, degradation of ECM, increased cell migration, increased proliferation and increased survival [53]. These events are mediated by numerous biomolecules whose expression varies at each stage of cancer progression [54]. Recent studies have implicated the role of N-WASP in cancer progression and metastasis. Microarray studies have revealed that N-WASP is upregulated in liver metastases of human colorectal cancer compared with the primary tumor [55]. N-WASP expression is upregulated in hypoxia induced epithelial mesenchymal transition (EMT) and expression of N-WASP is essential for metastasis [56, 57]. A number of *in vitro* studies in cancerous cells have demonstrated the presence of activated N-WASP in invadopodia and lamellipodia [30, 31]. N-WASP has also been shown to promote cell motility, formation and activity of invadopodia and invasion in breast cancer cells [58]. A study in melanoma cancer cell has indicated the importance of N-WASP in motility and maintaining amoeboid cell morphology [59]. N-WASP expression is found to be increased in breast cancer and it has a crucial role in degradation of ECM by promoting the trafficking of matrix metalloproteases (MMPs) at

invadopodia structures [60]. On the contrary, another study shows N-WASP expression is downregulated in breast cancer cells and it was suggested that N-WASP is a putative tumor suppressor [61]. These studies suggest that N-WASP can act either as a tumor suppressor or as a promoter of metastasis depending on the stage and type of cancer. The importance of N-WASP in cancer cell invasion and migration can be attributed to its function in actin nucleation, motility and ECM degradation [60, 62, 63].

1.6 Verprolin family of proteins

The verprolin families of proteins are effector proteins involved in regulating actin cytoskeleton by directly interacting with actin or indirectly through actin regulatory proteins [64]. Verprolin (Vrp1p), a proline-rich protein, was first identified during a screen for vinculin-like gene in *Saccharomyces cerevisiae* [65]. Subsequent sequencing studies confirmed the presence of the genes encoding verprolins in most eukaryotic organisms [64]. The mammalian verprolin family consists of three proteins: [66] WIP (2) WIRE and (3) CR16 [64]. CR16 is a glucocorticoid regulated protein expressed in brain, testis, lung and colon [67]. CR16 knockout mice shows defect in spermatogenesis leading to sterility in males [68]. Human WICH/WIRE is responsible for actin cross-linking and causes induction of filopodia in N-WASP dependent as well as independent manner [69-71]. WIRE along with N-WASP helps to maintain the integrity of the zonula adherens (ZA) junction [72]. Yeast verprolin is essential for endocytosis, determining cell polarity and has been shown to bind to actin and myosin. WIP, a mammalian homologue of verprolin can rescue the non-receptor mediated endocytosis, growth and cytoskeletal defects in verprolin-deficient yeasts [73].
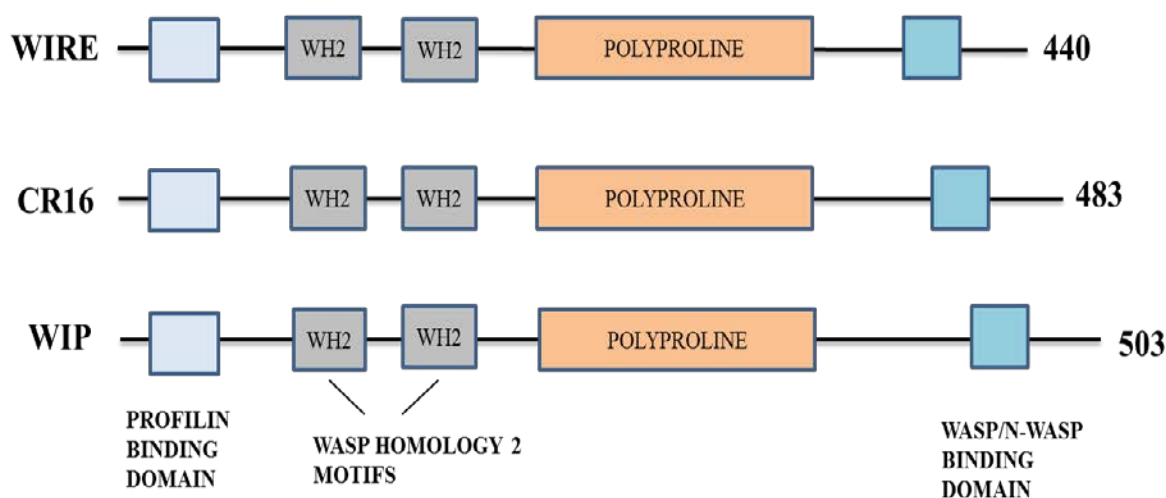
Figure.1.4: Schematic representation of the human verprolin family members: WIRE, CR16 and WIP.

The domain organization here shows the Profilin binding domain, Verprolin homologous domain (V), the Proline rich region and the WASP binding domain.

All three members of the mammalian verprolin family possess similar domain structures (Figure 1.4). The N terminus consists of a V domain (WASP homology domain 2), followed by a proline rich sequence and a WASP binding domain (WBD) at the C terminus [22, 64].

1.7 WASP Interacting protein (WIP)

WIP was identified as an WASP interactor through yeast two hybrid screening [22]. Subsequent studies revealed that WIP acts as a chaperone for WASP and recruites WASP at immunological synapses [74]. N-WASP mediated actin polymerization and filopodia formation is also regulated by WIP [69]. WIP protein is encoded by the *WIPF1* gene present on chromosome 2 and is encoded by 7 exons. Human WIP, a proline rich protein consists of 503 amino acids and

molecular mass of 55 kDa. Although WIP is ubiquitously expressed; higher expression is found in hematopoietic cells [22, 75].

To date, two WIP isoforms have been reported [76]. The first isoform Prlp2 is generated by alternative C-terminus splicing of last exon in *WIPF1* gene. The second isoform Mini-WIP is a truncated version of WIP with 402 amino acids and lacks the WASP binding region. Mini-WIP is suggested to regulate functions of WIP by competing with binding partners of WIP [76].

1.8 Domain structure of WIP

WIP has a multi-domain structure which facilitates its interaction with various proteins involved in actin regulation and polymerization. The N-terminal region of WIP known as V domain shares sequence homology to Vrp1p, an actin binding protein in yeast [77]. The V domain consists of 112 amino acids and contains two WH2 domains [78]. The binding of WIP to G-actin and stabilization of F-actin is mediated through the first WH2 domain containing the actin-binding KLKK sequence [69, 79]. Glycine rich stretch in the N-terminal region of WIP allows structural flexibility of V domain [80]. WIP consists of three ABM2 motifs (profilin binding actin-based mobility 2) (Figure 1.5) [22, 78].
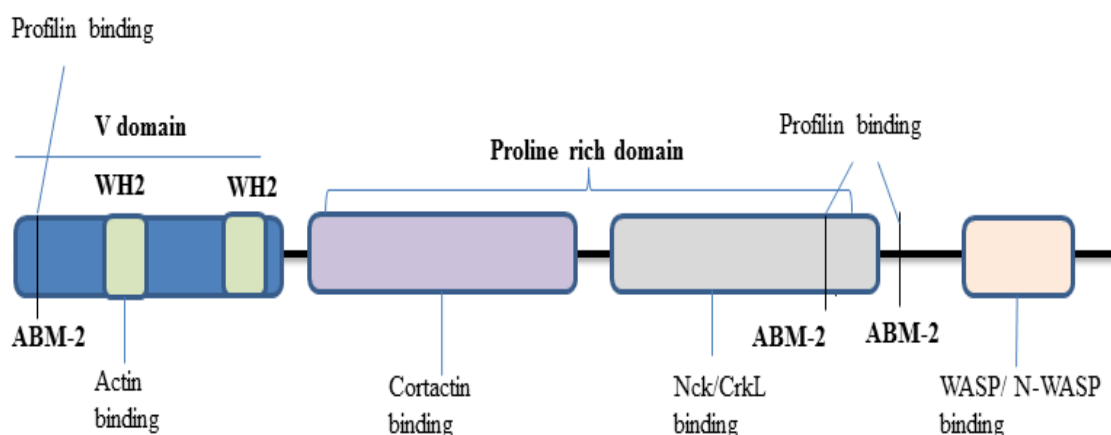
Figure.1.5: Schematic representation of domain structure of WIP showing interactions of WIP

From the amino terminal to the carboxy terminal: V domain (verprolin-homology domain) consists of two WASP-homology 2 (WH2) domains for actin binding and one or two actin-based motility-2 domains (ABM-2) for profilin binding. V domain is followed by proline rich motifs that bind to cortactin, Nck or CrkL. The WASP binding site resides at the C terminus.

Following the N-terminus WH2 region of WIP is the proline rich sequence which contains binding site for SH3 domain containing proteins such as Nck, and Crkl, which are adaptor proteins required for signal transduction events in lymphocytes [81, 82]. The proline region of WIP is also a binding site for cortactin, another SH3 domain containing protein which plays a role in actin cytoskeletal dynamics [83]. WIP binds to the WH1 domain of WASP and N-WASP through its C-terminal region [22]. This function is shared by other verprolin proteins, allowing binding of CR16 to N-WASP [84] and WICH/WIRE to N-WASP and WASP [35]. Nuclear magnetic resonance (NMR) studies have shown that amino acid residues 454-459, 461-468 and 476-485 of WIP come into direct contact with WASP/N-WASP during binding [85]. Binding of WIP to WASP and N-WASP helps to maintain the auto-inhibited closed conformation of

WASP/N-WASP. This prevents Cdc42 mediated N-WASP activation and thus stabilization of WASP/N-WASP in their inactive conformation [69]. WIP is essential for WASP stability, but not that of N-WASP, in human cells [69, 86, 87]. WIP interacts with profilin and actin through its proline rich region. Overexpression of WIP augments F-actin levels leading to ceribriform projections on the cell surface [22, 87].

1.9 Role of WIP

1.9.1 Role of WIP in immune cells

WIP expression is elevated in lymphoid cells and studies have demonstrated the importance of WIP for immune cell function. WIP and WASP mostly exist as a complex in T cells [88]. Several studies have demonstrated the importance of the WASP-WIP interaction in immune function [89]. Disruption of WASP-WIP binding by mutation leads to a rounded smooth cell surface in immune cells. This leads to diminished immune synapse and reduction of cytotoxicity in natural killer (NK) cells [90]. Mutation which introduces a stop codon in the WIP gene led to diminished WASP levels and caused an immunodeficiency similar to WAS [91]. The WH1 domain of WASP is the WIP-binding region and most of the mutations causing WAS are positioned in the WH1 domain [92]. WIP is important for formation and stabilization of podosomes in macrophages and phagocytotic activity of macrophages [93, 94]. Localization of WASP at the podosomes is regulated by WIP and WASP is rapidly degraded in the absence of WIP which adversely affects the podosome stability and its ability to degrade underlying matrix [93, 95]. Murine WIP knockout T cells showed defects in proliferation, polarization and

secretion of IL-2 in addition to disorganized actin cytoskeleton [74]. WIP plays a role in chemotaxis of monocytes [28]. It is vital for localizing WASP activity in actin based vaccinia virus motility and for localizing WASP to immune synapse after T-cell receptor engagement [96, 97]. Apart from WASP-dependent functions, WIP plays other roles independent of WASP. WIP can bind directly to actin and prevent disassembly of F-actin [79]. Overexpression of WIP in human Burkitt lymphoma B cells leads to increased content of cellular F-actin [22]. WIP is also important for formation of leading edge in migrating dendritic cells [78].

1.9.2 Role of WIP in non-immune cells

WIP plays a role in regulating neuronal maturation and synaptic activity during early neuronal development. Knockout of WIP in hippocampal neurons led to overgrowth of neuritic and dendritic branches as well as enlargement of somas. Thus, deficiency of WIP led to more mature synapses as compared to wild-type neurons [98]. Reports have indicated the importance of WIP in filopodia formation. Filopodia are thin finger-like protrusions of the plasma membrane which contain parallel bundles of F-actin [10]. Filopodia play a role in wound healing, cell migration and neurite outgrowth [99]. WIP is important for stabilizing actin filaments and inducing filopodia formation together with N-WASP [69].

1.10 Role of WIP in cancer progression

The role of WIP in immune cells and actin polymerization has been established [89]. However, its role in metastasis is not well-characterized. Microarray analysis of clinical colorectal cancer specimen showed that patients with reduced expression of *WIPF1* gene had better prognosis [100]. Studies in fibroblast have reported WIP as a negative regulator of fibroblast chemotactic migration similar to N-WASP [43] and overexpression of WIP in NIH3T3 fibroblast reduced cell adhesion, spreading and migration whereas knockdown of WIP had an opposite effect [101]. Interaction of WIP with N-WASP is critical for the formation of invadopodia, which are protrusive structures formed by metastasizing cancer cells to degrade ECM and form secondary tumors at distant sites [102]. Invadopodia consist of an actin core surrounded by MMPs, kinases and scaffolding proteins [103]. Actin regulating proteins such as N-WASP, cortactin, fascin and Arp2/3 complex are important for the functioning of invadopodia [104-106]. Binding of WIP to Nck helps in recruiting N-WASP-WIP complex to sites of invadopodia formation [31]. A recent study has demonstrated the role of WIP in regulating invasion in breast cancer cells. Knockdown of WIP in breast cancer cells led to a reduction in number of cells forming invadopodia as well as their degradative capacity [107]. Microarray studies have shown enhanced expression of WIP after EMT induction in prostate cancer cells [108]. Overexpression of WIP in breast cancer cells led to formation of peripheral membrane protrusions which formed larger lamellipodia as compared to the control cells [107]. Although studies have demonstrated importance of WIP in cell motility, which is a requisite for metastasis as well as interaction of

WIP with proteins important for invadopodia and filopodia activity, its direct role in promoting metastasis is poorly understood.

1.11 Role of hypoxia in cancer progression

1.11.1 Hypoxia

Oxygen supply is diminished in highly proliferative, solid tumors especially at the center of the solid tumor [109]. Proliferation rate of tumor cells is higher than endothelial cells; hence they outgrow their blood supply. This leads to hypoxia or low oxygen tension, within the tumor [110]. Hypoxia is a hallmark of various pathophysiological conditions such as cancer, tissue ischemia, inflammation and tumor growth [111]. Solid tumors have a median $[O_2]$ value of 10 mm Hg, while normal tissues with adequate blood supply have a median $[O_2]$ in the range of 40-60 mm Hg. Hypoxia is described as $\leq$ 2% O_2, and severe hypoxia (also known as anoxia) is characterized as $\leq 0.02\%$ O_2 [112]. Although low oxygen tension kills most of the normal as well as cancerous cells, it also provides a robust selective pressure for the survival of more aggressive and metastatic cells [113]. In order to survive hypoxia conditions, the expression of many genes is downregulated for conserving cellular energy and only those genes vital for cell survival under low oxygen conditions are expressed [114]. It has been suggested that hypoxia provides resistance against radiation and anti-cancer drugs through various mechanisms: 1) Lack of oxygen reduces the cytotoxic activity of some drugs and radiation 2) Hypoxia leads to genetic instability in cells which can make them drug resistant and 3) Hypoxia can alter the cellular metabolism by which cells can detoxify the drugs [115].

1.11.2 Hypoxia inducible factors

Hypoxia inducible factors (HiFs) are heterodimeric transcriptional factors consisting of an alpha subunit (HiFα) and a common constitutive beta subunit (HiFß) [116]. The alpha subunit is regulatory and unique to hypoxic response, whereas the beta subunit is expressed constitutively and plays a role in xenobiotic responses [116]. Both HiFα and HiFß belong to the basic helix-loop-helix–Per-ARNT-Sim (bHLH-PAS) protein family [116]. In mammals, there are 3 genes encoding the HiFα subunits: HiF1α, HiF2α and HiF3α. Each of the three HiFαs can form a heterodimer with HiFß and bind to hypoxia response element (HRE) 5'-RCGTG-3' of the target gene [117, 118]. HiFß is present in excess in the cell and can form heterodimer with other bHLH-PAS proteins. Hence, transcriptional activity during hypoxia response is regulated by HiFα [119]. Out of the three HiFα subunits, HiF1α and HiF2α are well characterized. HiF1α is the master regulator of hypoxia response and is expressed ubiquitously. HiF2α, referred to as endothelial PAS (EPAS) protein and HiF-like factor (HLF) share structural and functional similarities to HiF1α. Like HiF1α, it can dimerise with HiFß and bind to HRE in target genes (Figure 1.6) [120]. Expression of HiF2α is restricted to lung type II pneumocytes, vascular endothelium and kidney epithelial cells [121]. HiF3α can also dimerise with HiFß and bind to HREs [122]. A splice variant of HiF3α, known as inhibitory PAS (IPAS) can interact with the amino terminal of HiF1α and prevent it from binding to the DNA acting as a dominant negative regulator of HiF1α [123]. Expression of HiF3α is restricted to thymus, corneal epithelium of the eye and cerebellar Purkinje cells [124].

1.11.3 Regulation of HiF1α

HiF1α is the primary transcription factor responsible for inducing genes that promote survival and adaptation of cells under low oxygen conditions (~1% O_2) [116]. Under normoxia conditions, HiF1α is present at low levels in the cytoplasm and it translocates to nucleus under low oxygen conditions [125]. HiF1ß is a constitutively expressed nuclear protein and its cellular expression is independent of oxygen tension [126, 127]. HiF1ß was identified as a aryl hydrocarbon receptor binding partner and is also known as the aryl hydrocarbon nuclear translocator (ARNT) [128]. The interaction between HiF1α and HiF1ß is mediated by the bHLH and PAS motifs and further enhanced by binding to the HRE in target genes [129]. The C terminal of HiF1α consists of two transactivation domains, N terminal (N-TAD) and C terminal (C-TAD) [130]. The C-TAD plays an important role in activating gene transcription by interacting with co-activators such as CBP/p300 [131]. HiF1α also consists of an oxygen dependent degradation domain (ODDD) which regulates oxygen-mediated instability [132]. Studies have shown the role of HiF1α in transcription regulation of genes responsible for angiogenesis, iron metabolism, glucose metabolism (to counteract oxygen deficiency) and cell proliferation/survival [114].
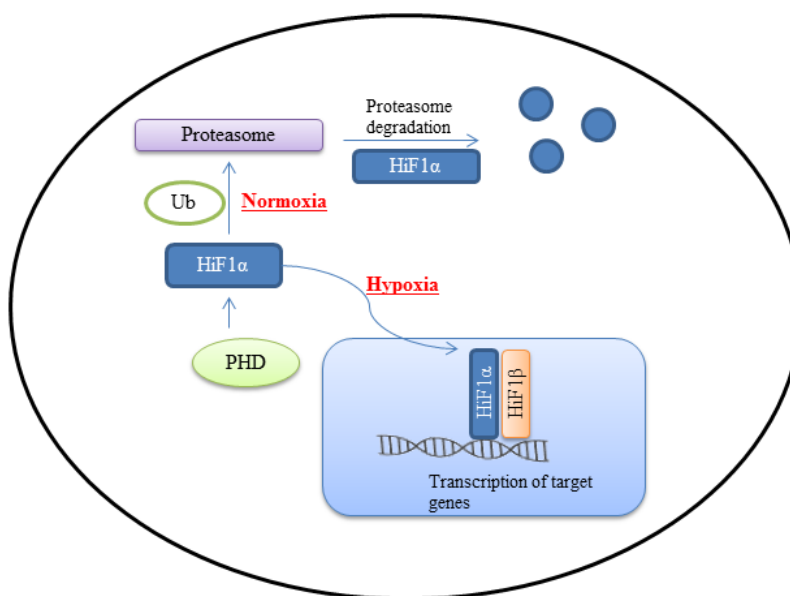
Figure.1.6: Degradation of Hypoxia inducible factor 1-alpha under normoxia condition.
In the presence of oxygen, HiF1α undergoes ubiquitination and is rapidly degraded. Under hypoxia conditions, HiF1α is stabilized in nucleus and regulates transcription of hypoxia related genes.

HiF1α protein although constitutively expressed has a short half-life and its expression is governed by oxygen levels in the tissue. Under normoxic conditions, the level of HiF1α is low in the tissues due to its proteosomal degradation. HiF1α can be targeted for degradation by hydroxylation at its conserved proline residues by a family of 2-oxoglutarate (2-OG)-dependent dioxygenases termed as Prolyl hydroxylase domain (PHD) [133]. Hydroxylation of the proline residues promotes the binding of pVHL (von Hippel-Lindau protein) ensuing ubiquitination, followed by HiF1α degradation. In the absence of oxygen, the activity of PHD is low, which prevents proline modification of HiF1α and pVHL/HIF binding. This increases the stability of HiF1α and hence its accumulation (Figure 1.7). Transacetylation of lysine residue can also promote binding of HiF1α to pVHL irrespective of the presence or absence of oxygen [126, 133].

The activity of HiF1α is also regulated by its transactivation domains: N-TAD and C-TAD. Under normal oxygen conditions, the asparagine residue (Asn803) in the C-TAD undergoes hydroxylation by FIH-1 (Factor inhibiting HiF-1), which prevents the binding of C-TAD of HiF1α to the transcriptional co-activator CBP/p300. This prevents the activation of HiF1α target genes. The transcriptional activity of HiF1α is also increased because of its phosphorylation by the MAPK pathway [114].
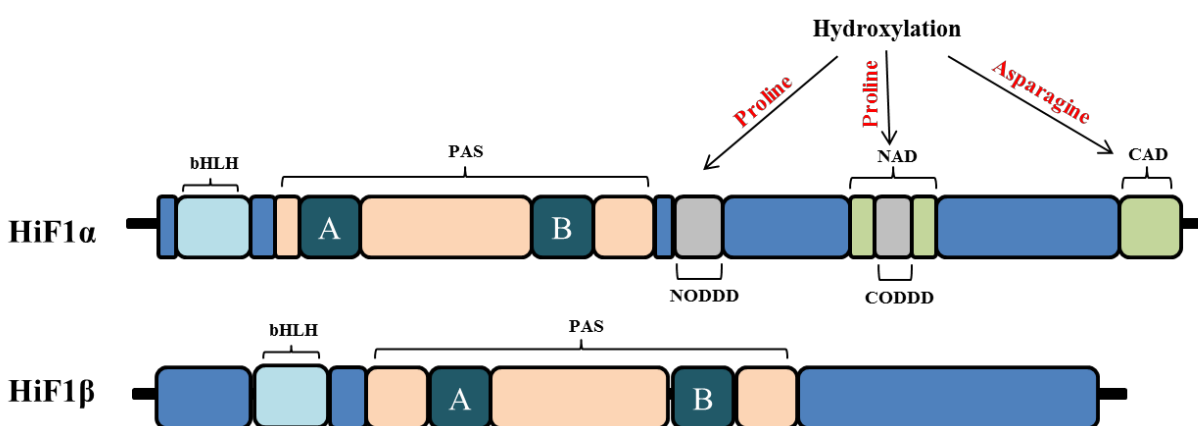
Figure 1.7: Domain structure of human HiF1α and HiF1β/ARNT
HiF1α contains basic helix–loop–helix (bHLH) domains; PAS (PCR (period circadian protein), AHR (aryl-hydrocarbon receptor), ARNT (aryl-hydrocarbon-receptor nuclear translocator), SIM (single-minded protein)) domains, which consist of directly repeating A and B sequences that are contained within a region of sequence similarity; the amino-terminal oxygen-dependent degradation domain (NODDD); the carboxy-terminal oxygen-dependent degradation domain (CODDD); the amino-terminal activation domain (NAD); and the carboxy-terminal activation domain (CAD). The NODDD, CODDD and CAD regions of HiF1α involve the oxygen-dependent enzymatic hydroxylation of specific residues in these regions.

HiFs play a important role in tumor progression and studies have demonstrated that expression levels of HiF1α and HiF2α are elevated in various human cancers [134, 135]. This may be due to genetic alterations or hypoxic conditions generated during tumor progression. The expression level of HiF1α is negligible in normal cells, low but detectable in benign tumors, high in cancerous cells and significantly higher in malignant and metastatic cells [136]. All these studies

suggest a role of HiFs in metastatic progression of tumor cells. Studies have also demonstrated that overexpression of HiF1α increases metastasis in tumor cells [114].

1.12 Epithelial Mesenchymal Transition (EMT)

EMT is a form of cell plasticity in which epithelial cells acquire mesenchymal characteristics [137]. Epithelial cells grow as layers of cells which are adjoined by cellular contacts formed by the adherens junctions, tight junctions, gap junctions and desmosomes. Epithelial cells manifest apical-basolateral polarity due to the distribution of E-cadherins and integrin molecules and are attached to basal lamina of the substratum [138]. These properties are important for maintaining the epithelial cells as highly organized sheet of cells [139]. Epithelial cells are tightly associated to their neighbouring cells which inhibit their dissociation and movement from the epithelial layer [140]. On the other hand, mesenchymal cells have a fibroblast like spindle shaped morphology. Mesenchymal cells possess front-rear polarity and do not grow as organized cell layers [141]. They are not connected to the basal lamina and exhibit FAs [137, 142]. The transition of epithelial cells to mesenchymal cells is termed as EMT and it was first observed in 1980s by Elizabeth Hay using a chick primitive streak formation model [143, 144]. EMT is thus characterized by acquisition of mesenchymal properties, loss of epithelial polarity and reorganization of cytoskeleton [145]. EMT plays an important role in normal development and organogenesis [141]. However, it is also linked to pathological conditions such as tissue fibrosis and cancer cell metastasis [146]. EMT is categorized in three subtypes each of which manifest different functional consequences depending on context.

Type 1 EMT plays a role in embryonic development and organogenesis. It involves formation of diverse cell types from the primordial epithelial cells. EMT during embryonic development is important for gastrulation and development of the migratory neural crest [147]. The mesenchymal cells formed can undergo Mesenchymal to Epithelial transition (MET) to generate secondary epithelia. This type of EMT does not induce invasion nor does it cause fibrosis**.**

Type 2 EMT is associated with organ fibrosis and regeneration of tissue. It plays a role in the inflammatory response during organ fibrosis resulting in tissue destruction. Fibrosis of tissue is a wound healing response due to continual inflammation.

Type 3 EMT occurs in carcinoma cells which undergo transition to form metastatic tumors. Metastatic tumors have the ability to invade and metastasize through the bloodstream and establish secondary tumors through MET.

Although the three subtypes of EMT represent different biological processes, they are regulated by a common set of biochemical and genetic elements [143].

1.13 Hallmarks of EMT

Epithelial cells are characterized by their adherens junctions [138]. E-cadherin, an important component of the adherens junction binds via its cytoplasmic domain to β-catenin which is a cytosolic protein. β-catenin interacts with α-catenin, which is linked to the actin cytoskeleton directly or indirectly through actin-binding proteins such as α-actinin and vinculin [139, 140]. During EMT, EMT regulators bind to the E-cadherin promoter and cause downregulation of E-cadherin expression. This leads to destabilization of adherens junction along with repression of

genes encoding desmoplakin, plakophillin, claudins and occludin [148]. E-cadherin repression abolishes E-cadherin mediated cytoplasmic sequestering of β-catenin which translocates to the nucleus. Loss of E-cadherin is accompanied by acquisition of mesenchymal markers such as N-cadherin (Neural cadherin), vimentin, α-smooth muscle actin (α-SMA), fibronectin etc (Figure 1.8) [149]. The switch from expression of E-cadherin to expression of N-cadherin is known as cadherin-switch and leads to cytoskeletal arrangement mediated by Rho GTPases to induce stress fibres, lamellipodia and filopodia eventually leading to enhanced cell motility [150, 151].
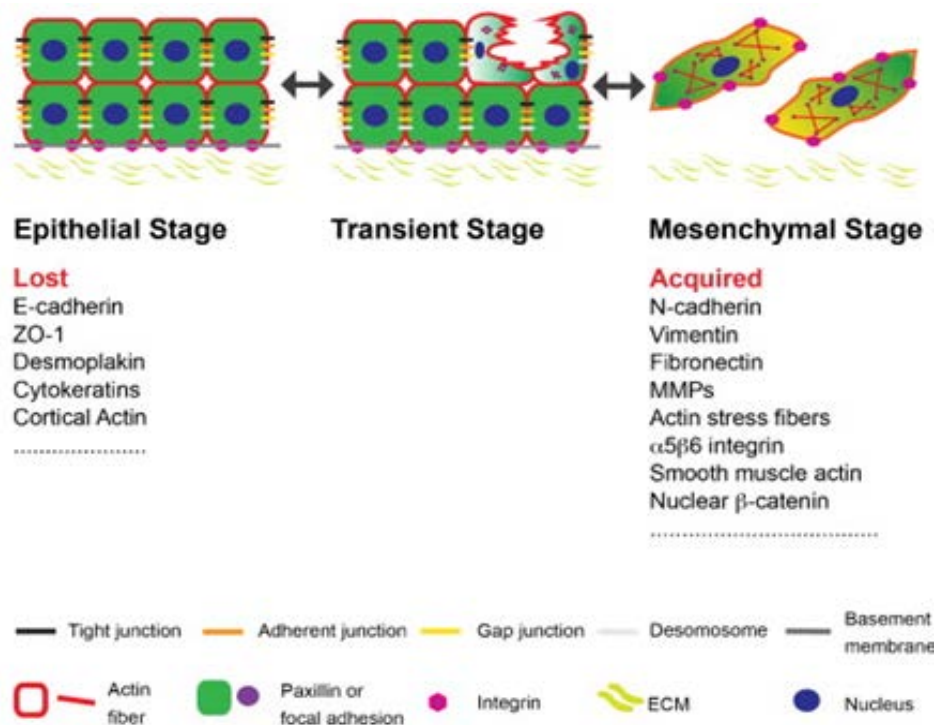
Figure.1.8: Schematic representation of epithelial to mesenchymal transition.
During epithelial to mesenchymal transition (EMT), cells lose their cell–cell contacts and re-arrange the cytoskeleton so that they can migrate, invade the neighboring tissue and metastasize to distant organs. This metastatic potential is acquired by the loss of epithelial and the acquisition of mesenchymal markers.
Reprinted from [152], with permission from Elsevier.

1.14 TGF beta signalling in EMT

Induction of EMT *in vitro* and development takes place due to a variety of signals and environmental factors [153]. EMT can be induced in cells in a stable or transient manner. Stable EMT is induced by ectopically expressing EMT related transcription factors such as Snail1, Snail2 (Slug), High-mobility group AT-hook 2 (HMGA2), ZEB1/2 and Twist [154]. These transcriptional factors cause transcriptional repression of E-cadherin and induce complete EMT. Transient EMT induction is brought about by different culture conditions or extracellular factors [155]. Several extracellular factors such as Transforming growth factor-beta (TGF-beta), Bone morphogenetic proteins (BMPs), Wnt, fibroblast growth factor, Notch ligands, epidermal growth factor (EGF), hepatocyte growth factor, can induce EMT [156].

Of these, TGF-beta is a well characterized EMT inducer during development, cancer and other pathologies [157, 158]. TGF-beta, a secreted cytokine signals via the receptor serine/threonine kinases [159]. TGF-beta is secreted in inactive form as an disulfide linked homodimeric polypeptide bound to other extracellular proteins like latent TGF-beta binding proteins (LTBPs) The latent complex is proteolytically cleaved to form the mature and bioactive TGF-beta ligand [160]. In the early stages of tumorigenesis, TGF-beta can act as tumor inhibitor by suppressing proliferation and in later stages of tumorigenesis it promotes metastasis [161].

1.14.1 Smad-dependent pathways

Transduction of signals from TGF-beta ligand to the nucleus is mediated by intracellular group of proteins known as Smads [162]. Catalytically activated TGF-beta receptor 1 (TGF-betaR1)

phosphorylates the serine residues of Smad2 and Smad3 which are known as regulatory smads (R-Smads). Upon phosphorylation, R-Smads bind to Smad4 (also known as Co-Smad) to form a trimeric complex [163]. The formation of Co-Smad/ R-Smad complex, favours its accumulation in the nucleus as well as nuclear activity. In nucleus, the trimeric complex can directly bind to Smad binding elements (SBEs) and associate with a variety of transcriptional factors [160, 164]. Thus, R-Smads play a vital role in eliciting the effects of TGF-beta. Smad7 is an inhibitory Smad (I-Smad) which competes with R-Smad for TGF-betaR1 binding and thus inhibits TGF-beta signaling [165, 166]. Studies in several cancers have shown mutations present in the TGF-beta receptors: TGFBR1, TGF-beta receptor 2 (TGFBR2) and the Smads proteins [166, 167]. TGF-beta exists in three isoforms: TGF-beta 1, 2, 3. Although TGF-beta1 isoform is the prime ligand involved in human cancers, increased levels of TGF-beta2 and TGF-beta1 have been detected in plasma of patients with metastatic melanoma. TGF-beta3 and TGF-beta1 levels also serve as a marker to monitor progression of breast cancer metastasis [168, 169].

1.14.2 Smad independent pathways

TGF-beta can activate various types of Smad independent pathways such as Extracellular signal-regulated kinases/ Mitogen activated protein kinase (Erk/MAPK), Rho GTPase, c-Jun N-terminal kinase (JNK) and phosphatidylinositol-3 (PI3) kinase/ Akt pathway [170]. TGF-beta induced direct activation of Smad independent pathways occurs via binding of TGF-beta to TGFBR1 and/or TGFBR2 or via adaptor proteins [165]. Blocking one or several of these pathways by using specific inhibitors greatly affects induction of the EMT phenotype and subsequent

responses by TGF-beta implying that activation of the Smad independent signaling augments

Smad dependent pathways in amplifying the EMT response [171].
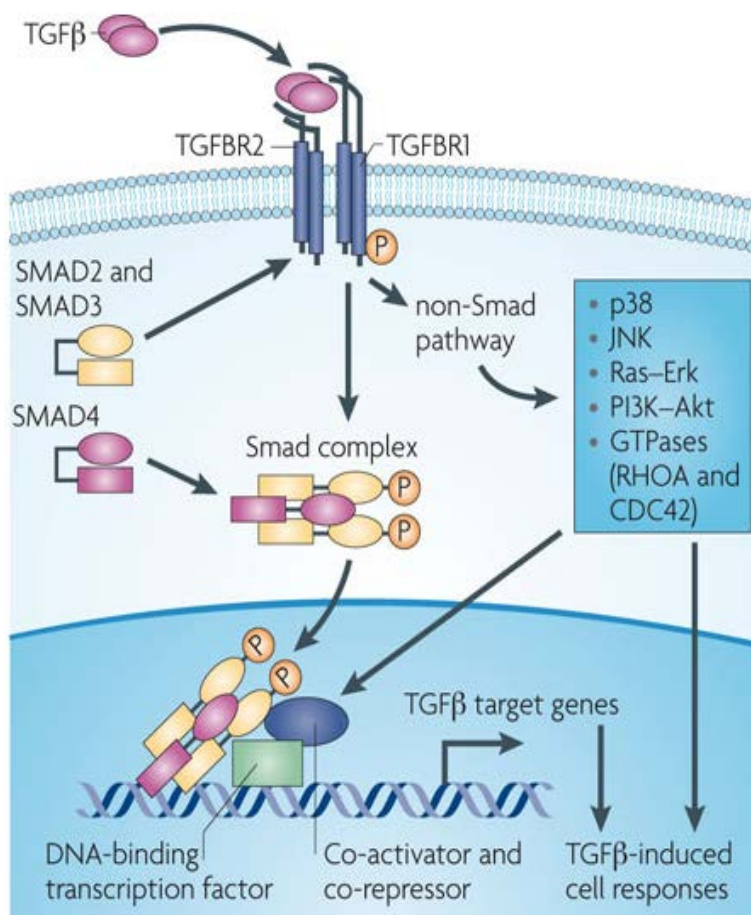
Figure.1.9: TGF-beta signaling pathway
TGF-beta signalling is transduced through Smad and non-Smad pathways. TGFβ ligand binds to TGFBR2 and TGFBR1. TGFBR2 phosphorylates (P) TGFBR1, which subsequently phosphorylates and activates Smad2 and Smad3. Activated Smad2 and Smad3 form a Smad complex with Smad4 and translocate into the nucleus. In the nucleus, the Smad complex interacts with other DNA-binding transcription factors, and co-activators and co-repressors, binds to the promoter regions of TGFβ target genes and regulates the transcription of target genes. TGFβ stimulation also activates other signalling cascades in addition to the Smad pathway. TGFβ receptors activate p38, JNK, Ras–Erk, PI3K–Akt, and small GTPases such as RhoA and Cdc42.
Reprinted by permission from Macmillan Publishers Ltd: [Nature reviews Cancer] [172] , copyright (2010).

1.15 Transcriptional regulation of EMT

Transcriptional regulators of EMT include the Snail family of zinc finger proteins such as Snail and Slug, the two-handed zinc-finger factors of δEF1 family proteins (Example: δEF1/ZEB1) and Smad-interacting proteins 1 (SIP1/ZEB2), high mobility group box-containing proteins (Example: LEF-1), basic helix-loop-helix (bHLH) factors, which are alternate splice variants of the *E2*A gene (Example: Twist and E12/E47) [156]. These transcriptional repressors bind to the E-box element present in the E-cadherin promoter and downregulate its expression. E-cadherin repression is a crucial step for EMT to progress as loss of E-cadherin leads to disruption of the adherens junction and helps the cells to attain a mesenchymal phenotype [173-175].

Id (Inhibitor of differentiation) proteins possess a helix-loop-helix domain but lack the DNA binding domain. Id proteins exist in 4 isoforms (Id 1-4) and can bind to the bHLH factors and repress their transcriptional activity [176, 177]. TGF-beta specific Smads cause repression of *Id*2 mRNA (inhibitor of differentiation 2), which is involved in downregulation of E-cadherin and zonula occludens 1 (ZO-1). Repression of Id2 causes release of the E12/E47 bHLH factors, which can downregulate E-cadherin expression by binding to the E-cadherin promoter [178]. Thus, Id proteins help in maintaining the epithelial phenotype by repressing function of *E2A* gene [165]. TGF-beta pathway leads to induction of the HMGA2 which in turn induces expression of EMT transcription factors and progression of EMT takes place [179]. Induction of EMT can be brought about by transcription factors independently or co-operatively such as Snail1-Smad3/4 co-repressor complex and the SIP1-δEF1 binding to E-cadherin promoter [175, 180].
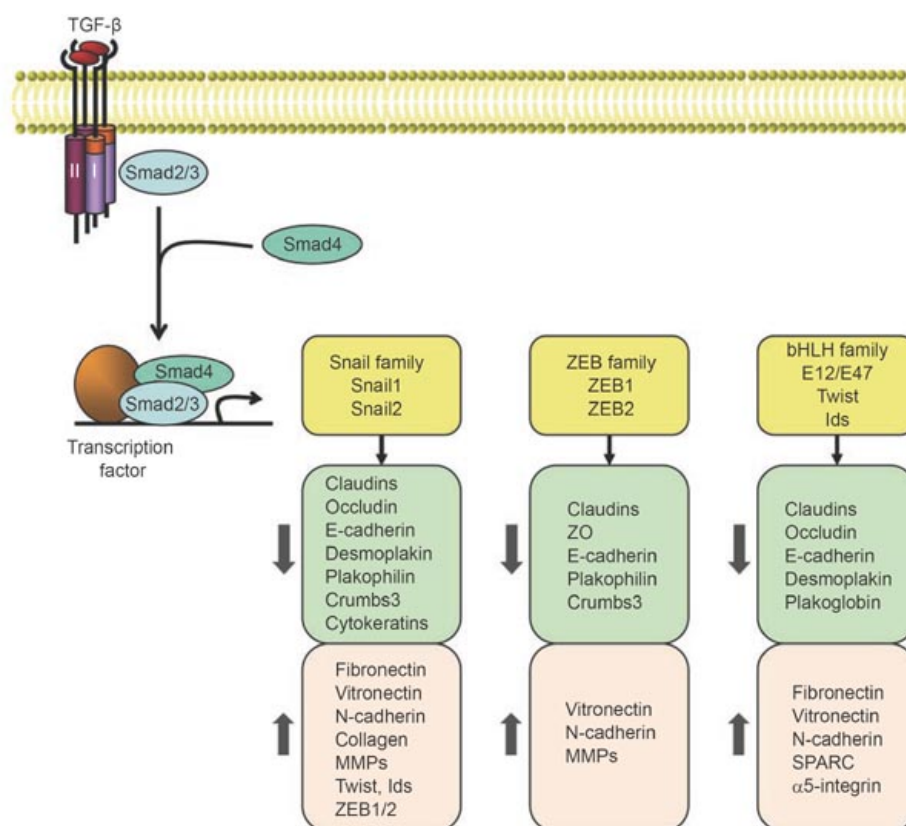
Figure.1.10: Transcriptional regulation of EMT
Transcriptional regulation of EMT induced by TGF-beta. In response to TGF-beta, Smad2 and 3 are activated, and form complexes with Smad4, which then regulate transcription of target genes through interactions with other DNA binding transcription factors. In the induction of EMT, the activated Smads mediate transcriptional regulation through three families of transcription factors, resulting in repression of epithelial marker gene expression and activation of mesenchymal gene expression.
Reprinted by permission from Macmillan Publishers Ltd: [Cell Research] [181], copyright (2009).

1.16 Actin cytoskeleton, cancer and EMT

Actin cytoskeleton is vital for maintaining epithelial cell-cell adhesion, providing shape to the cell, organizing cellular contents and serving as a platform for membrane trafficking and signaling [18]. Studies in tissue culture have demonstrated importance of actin regulators such as N-WASP, cortactin and Arp2/3 in regulating actin dynamics and maintaining epithelial polarity

at cell junctions [182]. Cortactin, a scaffolding protein is found to localize to the ZA by interacting with N-WASP and E-cadherin. At the ZA, cortactin can recruit WAVE2 and Arp2/3 and promote actin nucleation [183]. Leading edge of migrating cells is enriched with actin regulators such as N-WASP, Scar/WAVE proteins, cortactin and Arp2/3. These proteins cause a rapid polymerization of actin at the cell's leading edge and contribute to membrane dynamics and protrusions. Thus, actin regulating proteins are differentially localized and regulated during cell migration and invasion [182]. EMT leads to increased cell motility which is associated with actin cytoskeleton remodeling and formation of FAs [184]. During EMT, cortical actin is reorganized to form contractile stress fibers [185]. Stress fibers are organized structures consisting of parallel actin fibers cross-linked periodically by proteins such as myosin II and alpha-actinin [186].

Motile mesenchymal cells consist of stress fibers which are linked via FAs to the ECM. FAs are dynamic in nature and consist of proteins such as integrins, vinculin, paxillin, talin, FAK etc [187, 188]. FA are important for linking the actin cytoskeleton to ECM and allowing the cell to respond to external stimuli. Thus, FA are major sites of signal transduction events responsible for cell adhesion, migration and proliferation [189].

The members from Rho family of GTPases are responsible for transmitting signals from cell surface receptors to actin remodeling effector proteins [186]. Rho GTPases regulate cell motility and thus are crucial for EMT and invasion [190]. Like all GTPases, Rho family of GTPases can switch from an inactive GDP-bound state to an active GTP bound state [186]. Rho GTPase activation is regulated by three groups of regulatory proteins, GTPase activating proteins (GAPs),

guanine nucleotide dissociation inhibitors (GDIs) and guanine nucleotide exchange factors (GEFs) [191]. The proteins which are best studied from the Rho family of GTPases are Cdc42, RhoA and Rac1 which are important for formation of actin rich structures such as filopodia, stress fibers and lamellipodia respectively [186]. RhoA mediated actin stress fiber formation is crucial for cell-cell and cell-matrix adhesion which regulate cytoskeletal changes during EMT. The stability of the actin stress fibers is maintained by inhibiting actin depolymerization regulated by RhoA [185]. RhoA is suggested to play a role in TGF-beta induced EMT. Upon induction with TGF-beta, TGF-beta receptor is recruited to tight junctions where it interacts with Par6, a polarity protein. Par6 is phosphorylated in presence of TGF-beta causing recruitment of Smurf1, a ubiquitin ligase. RhoA is degraded by Smurf1 mediated ubiquitination which leads to the disintegration of tight junction and disassembly of the actin cytoskeleton [192].

1.17 Transcriptome analysis by RNA sequencing

Transcriptome can be defined as the entire set of transcripts in the cell and their quantities [193]. RNA sequencing (RNA-Seq) is a high throughput Next Generation Sequencing (NGS) technology for mapping and quantifying transcripts [194]. It has several advantages over microarrays and other sequencing based approaches including high resolution, reduced cost, lower technical variation, digital nature of the signal rather than analog and prior probe design knowledge is not required [195]. RNA-Seq enables us to identify novel transcripts, differentially expressed genes (DEGs), microRNAs (miRNAs) and alternative splicing events. Additionally, it provides information about untranslated transcripts, which may be essential in regulating gene expression such as UTR (untranslated region) [196].

The Illumina Hi-Seq 2000 NGS platform relies on the paired-end sequencing strategy that involves sequencing from both ends of the short cDNA fragment [197]. Workflow of a RNA-Seq experiment is depicted in the Figure 1.11. Briefly, total RNA is isolated and its purity is determined by analyzing the RNA integrity number. mRNA is enriched using Oligo (dT) beads and is fragmented into short fragments (~200 bp). Using the short strands as templates, double stranded cDNA is synthesized by random hexamer priming. Purified cDNA is ligated to sequencing adaptors and amplified using PCR. Finally, the libraries are sequenced using the Illumina Hi-Seq 2000 platform and DEGs are identified by aligning RNA-seq data with reference genome (Source: http://www.genomics.org.cn/).
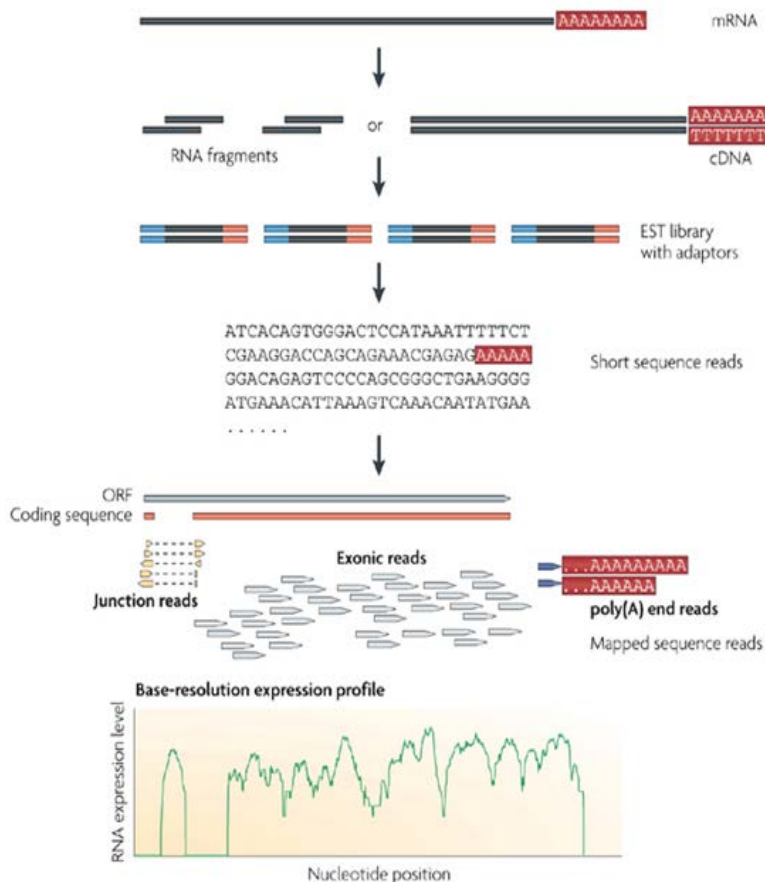
Figure.1.11: Workflow of a RNA-Seq experiment
mRNA is isolated from the samples and converted to cDNA. cDNA is fragmented, PCR amplified and ligated to sequencing adapters. cDNA library is sequenced and reads are aligned with reference genome.
Reprinted by permission from Macmillan Publishers Ltd: [Nature Review Genetics] [198], copyright (2009).

1.18 Derivation of A5-RT3 cells by malignant conversion of HaCaT cells

The cell lines used for RNA-Seq are HaCaT and A5-RT3. HaCaT is a spontaneously immortalized human keratinocyte cell line, which can maintain stable chromosome content and non-tumorigenic phenotype in-vitro for long period of time [199]. The morphogenesis and functional differentiation properties of HaCaT cultures closely resemble that of normal keratinocytes. Hence, HaCaT culture is an attractive model to study early stages of tumorigenesis

[200]. HaCaT cells were transformed using the mutated *val-12 Harvey-ras* oncogene to generate tumorigenic cells [201]. The HaCaT-ras clones when injected subcutaneously in nude mice formed epidermoid cysts (benign tumors). Two classes of tumorigenic *ras* clones where obtained: benign A5 and malignant II-4. The II-4 clones displayed well-differentiated carcinoma phenotype whereas A5 clone formed slowly enlarging, non-invasive cysts. Reinjection of the A5 clone into animals showed an increased malignancy due to the selective pressure provided by the in-vivo environment (Figure 1.12). Thus, A5-RT3 is a metastatic cell line derived by re-cultivation of the A5 clone in-vitro and re-transplanting three times in mice [202].
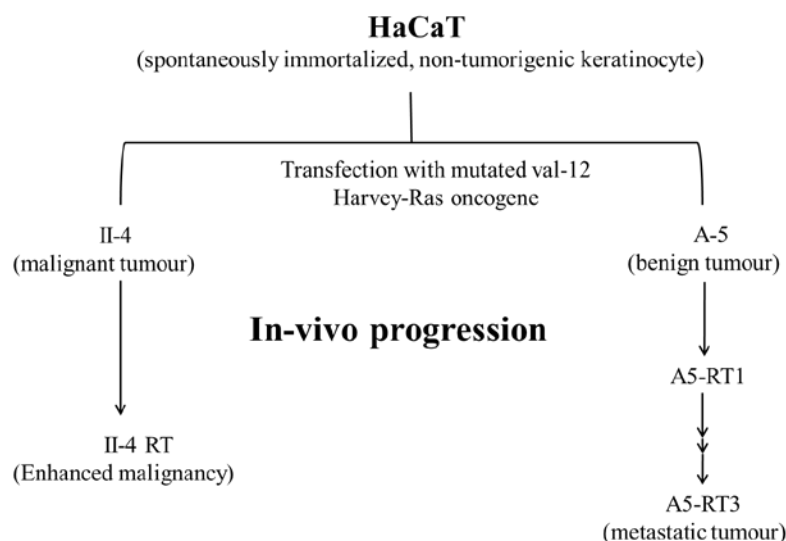
Figure.1.12: Schematic representation of the steps involved in the malignant conversion of human keratinocytes HaCaT

This skin carcinogenesis model system describes how the malignant and cancerous cell lines were derived. HaCaT A5-RT3 clone was obtained by recultivating *in vitro* the subcutaneous tumors derived from HaCaT-ras cells and re-transplanted three times in vivo.

RNA-Seq analysis of HaCaT and A5-RT3 cells will help us to explore the genetic underpinnings of the difference between the two cell lines and identify the set of DEGs during the conversion of cells from non-tumorigenic to metastatic phenotype.

1.19 Transcriptional regulation of N-WASP

Gene transcription is one of the primary biological responses that governs an organism's response to external stimuli [203]. Expression level of a protein is determined by the strength of its promoter and the regulatory elements such as enhancers or repressors interacting with the promoter region. The strength of a promoter determines the frequency of transcription initiation, which determines the rate of transcript formation. Reporter gene constructs are commonly used to study the expression pattern of a particular gene [204]. Green fluorescent protein (*GFP*) is a commonly used reporter gene to study the promoter activity. GFP protein is small in size, non-toxic, auto fluorescent and can be detected in-situ [205]. Thus, promoter activity can be monitored by fusing a *GFP* gene downstream of the gene promoter [204]. The relative fluorescence emitted by GFP can be quantified and used to monitor gene expression.

N-WASP expression pattern in different keratinocytes varies, with the highest expression observed in A5-RT3 (metastatic tumor) followed by equal expression in HaCaT (non-tumorigenic) and II-4 (malignant tumor) and the least expression in HSC-5 (tumorigenic, non-metastatic) cells. Studies suggest that N-WASP can act either as a tumor inhibitor or as a promoter of metastasis depending on the stage and type of cancer [60, 61]. Microarray studies have revealed that N-WASP is upregulated in liver metastases of human colorectal cancer

compared with primary tumor [55]. Differential N-WASP expression indicates a possible role in determining the cell phenotype and functions.

N-WASP expression is found to be elevated under hypoxia condition in squamous cell carcinoma (SCC) [56]. This differential gene expression could be due to regulation at transcription level or translation level or both. At transcriptional level of gene regulation, regulatory transcriptional factors can cause transcriptional activation or transcriptional repression of their target genes by binding to the cis-regulatory regions of the target gene [206]. Thus, characterization of the N-WASP promoter will lead to a better understanding of signaling pathways which regulate tumorigenesis by regulating N-WASP expression.

1.20 Yeast one hybrid system

Yeast one hybrid system can be used to identify and characterize DNA-protein interactions using DNA fragments of interest fused to reporter genes [206]. It is a powerful method used in the identification of proteins binding to a regulatory DNA sequence of interest. Detection is based on the interaction of a DNA binding protein with a DNA sequence (bait sequence) fused upstream of a reporter gene such as *HIS3*. The reporter gene acts as a positive growth selection marker.

(A)
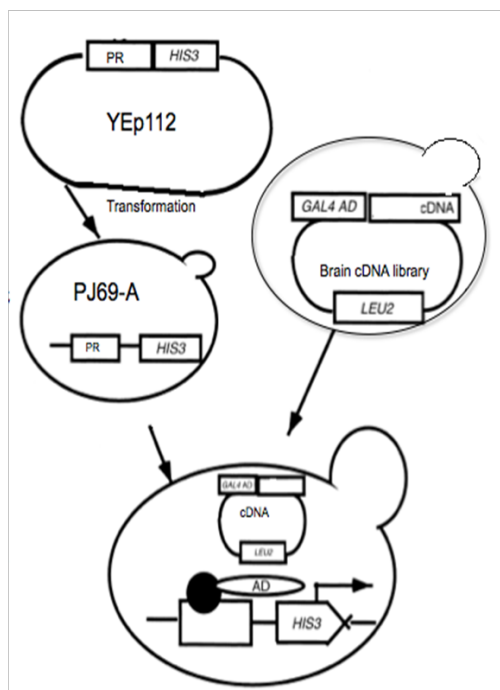
(B)
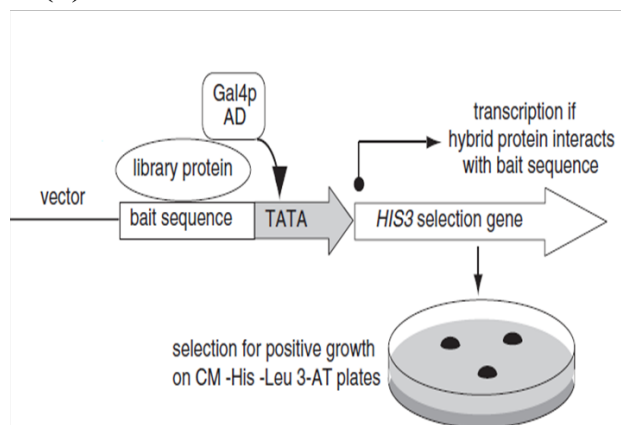
Figure.1.13: Diagrammatic representation of the HIS3 selection strategy in yeast one hybrid system

(A) Transformation of bait plasmid in yeast and subsequent mating with prey library. (B) Binding of the library protein to the bait sequence and activation of HIS3 gene.

The prey plasmid is usually a cDNA expression library consisting of a cDNA fused to a strong trans-activating domain (Figure 1.13). The cDNA expression library is usually made in a shuttle vector, which can grow in bacteria as well as in yeast. The prey plasmid and bait plasmid can be selected via auxotrophic markers for amino acids present on the plasmid (leucine and tryptophan respectively). Binding of a DNA binding protein with the regulatory sequence turns on the expression of *HIS3* reporter gene. This complements the auxotrophic HIS3 mutation and allows the growth of colonies on selective media lacking leucine, tryptophan and histidine [207]. 3-AT (3-Amino-1, 2, 4-triazole) is used to block HIS3 protein expression at low levels [206].

1.21 Objectives

N-WASP and WIP are crucial for Arp2/3-mediated actin polymerization. Transcriptome analysis of non-tumorigenic HaCaT and its metastatic clone A5-RT3 cells identified WIP as a highly upregulated gene in A5-RT3 cells as compared to HaCaT cells. Although the role of WIP in immune cell function is well established, not much is known about its role in metastatic progression. The differential expression of N-WASP in tumorigenic and non-tumorigenic cells indicates its possible role in determining the cell phenotype and function. N-WASP is suggested to be either a tumor suppressor or metastasis promoter depending on the type and stage of cancer. N-WASP expression is elevated under hypoxia conditions, and studies have shown hypoxia to be a prerequisite for metastasis. The entire focus of this dissertation would be to gain a better understanding on actin cytoskeleton regulatory proteins: WIP and N-WASP and their role in cancer progression and metastasis.

The main objectives of this project are:

1. To elucidate the role of WIP in metastasis by studying its role in TGF-beta induced EMT.

2. To study the transcriptional regulation of N-WASP by characterizing the N-WASP promoter and identifying transcription factors binding to N-WASP promoter.

3. To investigate interaction between N-WASP promoter and HiF1α and study the mechanism of upregulation of N-WASP under hypoxic condition.

CHAPTER 2: Materials and Methods

2.1 Materials

2.1.1 Plasmids and Commercial Vectors

For DNA subcloning experiments, vectors pUC19 and pUC18 were used. For yeast one hybrid assays, vectors pACT2 and YEplac112 which contain different selective markers, were used in *Saccharomyces cerevisiae* cells. For expression of proteins in mammalian cells, the vectors pcDNA3.1 HisC, pTRIPZ and pLJM1-EGFP were used. For knockdown studies, pLKO.1 and pLJM1-EGFP were used. Table 2.1 summarizes the commercial vectors used and their applications.

Vector	Resistant gene	Selective marker	Expression host	Used in	Source
pUC18	Amp	-	Bacteria	DNA subcloning	Clontech
pUC19	Amp	-	Bacteria	DNA subcloning	Clontech
pACT2	Amp	Leu	Bacteria/Yeast	Yeast two hybrid	Clontech
YEplac112	Amp	Trp	Bacteria/Yeast	Expression in yeast cells	[208]
pcDNA3.1 HisC	Amp	-	Bacteria/Mammalian	Expression in mammalian cells	Life Technologies
pGEX-4T1-RBD2	Amp	-	Bacteria	Protein expression	Gift
pLJM1-*EGFP*	Amp	-	Bacteria/Mammalian	Expression in mammalian cells	Addgene
pLKO.1 puro	Amp	-	Bacteria/Mammalian	Expression in mammalian cells	Addgene
pTRIPZ	Amp	-	Bacteria/Mammalian	Expression in mammalian cells	GE Lifesciences

Table 2.1: List of commercial vectors used.

All the constructs were checked by restriction enzyme digestion and direct sequencing according to standard protocols.

2.1.2 Bacterial strains

The bacterial strain, *Escherichia coli* (*E. coli*) DH5α was used for plasmid amplification and DNA subcloning.

2.1.3 Yeast strains

Yeast strain PJ69-4A (*MATa his3 leu2 ura3 trp1 gal 4 Δgal80Δmet2::GAL7-lacZ GAL2-ADE2 LYS2::GAL1-HIS3*) was used as described in [209].

2.1.4 Mammalian cell lines

HEK293T, HeLa, HaCaT, HSC-5, A5-RT3, A431, hSAEC, A549 and MDA-MB-231 cell lines were purchased from American Type Culture Collection (ATCC, USA).

2.1.5 Cell culture reagent and plasticware

Dulbecco's Minimal Eagles medium (DMEM)-Hyclone (Thermo Scientific) was used for culture of mammalian cells. Cell culture media additives were purchased from Hyclone or Gibco. Drugs such as DMOG and YC-1 were purchased from Enzo lifesciences. C3 transferase was purchased from Cytoskeleton Inc. Human recombinant TGF-beta1 was purchased from Peprotech. Plasticwares were bought from local representative of Costar, Corning, Nunc and Eppendorf. Transwell chamber for invasion assay was purchased from BD Biosciences.

2.1.6 Antibodies

The primary antibodies used in this study are listed in Table 2.2 and their respective dilutions used for the Western blot experiments are specified. Table 2.3 lists secondary antibodies used.

2.1.6.1 Primary antibodies

Antibody	Source	Dilution for WB	Blocking conditions	Dilution for Immuno-staining
Mouse Anti-E-cadherin monoclonal antibody	BD Transduction Laboratories (610182)	1:1000	5% skim milk	-
Mouse Anti-GAPDH monoclonal antibody	Ambion, Austin, TX, USA (AM4300)	1:10000	5% skim milk	-
Mouse Anti-HiF1α monoclonal antibody	BD Transduction Laboratories (610958)	1:500	3% skim milk	1:100
Rabbit Anti-His polyclonal antibody	Delta biolabs, Gilroy, CA, USA (DB063)	1:1000	5% skim milk	-
Mouse Anti-cortactin (p80/85) monoclonal antibody	Merck Millipore, clone 4F11, 05-180	-	-	1:50
Rabbit Anti-N-WASP polyclonal antibody	Homemade	1:1000	5% skim milk	1:50
Rabbit Anti-WIP polyclonal antibody	Santa Cruz (sc-25533)	1:500	5% skim milk	-
Mouse Anti-N-cadherin monoclonal antibody	BD Transduction Laboratories (610920)	1:1000	5% skim milk	-
Mouse Anti-RhoA monoclonal antibody	Santa Cruz (sc-418)	1:200	3% skim milk	-
Mouse Anti-ROCK-II monoclonal antibody	BD Transduction Laboratories (610623)	1:1000	5% skim milk	-
Mouse Anti-mDia1 monoclonal antibody	BD Transduction Laboratories (610848)	1:500	3% skim milk	-
Rabbit Anti-Smurf1 polyclonal antibody	Cell Signalling Technology (#2174)	1:1000	3% skim milk	-
Mouse Anti-Cdc42 monoclonal antibody	Santa Cruz (sc-8401)	1:500	3% skim milk	-
Mouse Anti-HA monoclonal antibody	Santa Cruz (sc-7392)	1:1000	3% skim milk	1:50
Mouse Anti-Rac1 monoclonal antibody	Merck Millipore, clone 23A8, 05-389	1:500	3% skim milk	-
Goat Anti-Snail monoclonal antibody	Santa Cruz (sc-10433)	1:500	3% skim milk	-

Mouse Anti-Alpha Smooth muscle actin monoclonal antibody	Santa Cruz (sc-32251)	1:1000	3% skim milk	-
Mouse Anti-vimentin monoclonal antibody	BD Transduction Laboratories (550513)	1:1000	5% skim milk	-
Mouse Anti-vinculin monoclonal antibody	Sigma (sc-73614)	1:1000	3% skim milk	1:100
Mouse Anti-paxillin monoclonal antibody	BD Transduction Laboratories (610569)	1:1000	5% skim milk	1:100
Alexa Fluor 488 Phalloidin	Molecular Probe (A12379)	-	-	1:100
Alexa Fluor 594 Phalloidin	Molecular Probe (A12381)	-	-	1:100

Table 2.2: Primary antibodies and their dilutions used for western blot analysis and immunofluorescence.

2.1.6.2 Secondary antibodies:

Antibody	Source	Dilution for WB	Dilution for IF
Anti-mouse IgG-HRP	Sigma, St. Louis, Mo, USA (A9044)	1:10000	-
Anti-rabbit IgG-HRP	Sigma, St. Louis, Mo, USA (A0545)	1:10000	-
Donkey anti goat IgG-HRP	Santa Cruz (sc-2020)	1:5000	-
Anti-mouse Alexa Fluor 488	Molecular Probe (A-11001)	-	1:500
Anti-mouse Alexa Fluor 594	Molecular Probe (A-11005)	-	1:500
Anti-rabbit Alexa Fluor 488	Molecular Probe (A-11034)	-	1:500
Anti-rabbit Alexa Fluor 594	Molecular Probe (A-11037)	-	1:500
Anti-mouse Alexa Fluor 647	Molecular Probe (A21235)	-	1:500
Anti-mouse IgG	Santa Cruz (sc-2025)	-	-

Table 2.3: List of secondary antibodies used in this study.

2.1.7 Bacterial and yeast culture media

2.1.7.1 Luria-Bertani broth

1% bacto-tryptone, 0.5% bacto-yeast extract and 0.5% NaCl was dissolved in distilled water and autoclaved.

2.1.7.2 LB agar plates

2% of bacto-agar was added to LB broth and autoclaved. Medium was left at room temperature (RT) to cool to below 60°C and 25 ml of medium was poured into each plate and left to solidify.

2.1.7.3 YPUAD medium

2% of bacto-peptone, 1% of bacto-yeast extract, 2% glucose, 0.008% of adenine hemisulphate and 0.004% of uracil were dissolved in distilled water and autoclaved.

2.1.7.4 YPUAD agar plates

2% of bacto agar was added to YPUAD medium and autoclaved. Medium was left at room temperature to cool to below 60°C and 25 ml of medium was poured into each plate and left to solidify.

2.1.7.5 Synthetic defined (SD) medium

0.67% of Yeast Nitrogen base, 2% of Glucose and the different concentrations of the dropout supplements as described in Table 2.4 were dissolved in distilled water and autoclaved.

Supplements	Amount in dropout powder (g)	Final working concentration (mg/L)
Adenine	2.5	40
L-arginine (HCl)	1.2	20
L-aspartic acid	6.0	100
L-glutamic acid (monosodium salt)	6.0	100
L-histidine	1.2	20
L-isoleucine	1.8	30

L-leucine	3.6	60
L-lysine (mono-HCl)	1.8	30
L-methionine	1.2	20
L-phenylalanine	3.0	50
L-serine	22.5	375
L-threonine	12.0	200
L-tryptophan	2.4	40
L-tyrosine	1.8	30
L-valine	9.0	150
Uracil	1.2	20

Table 2.4: List of supplements used in SD medium.

2.1.7.6 SD agar plates

2% of bacto agar was added to SD medium and autoclaved. Medium was left at room temperature to cool to ~55°C and 25 ml of medium was poured into each plate and left to solidify. For yeast one hybrid assay, SD agar plates with 2 mM 3-AT but without histidine were used. 3-AT was filter sterilized and added to SD medium containing 2% bacto-agar without histidine to a final concentration of 2 mM.

2.1.8 Enzymes and kits

The restriction endonucleases obtained from Fermentas (Hanover, MD, USA) or New England Biolabs (Ipswich, MA, USA) and T4 DNA ligase and buffer from Fermentas (Hanover, MD, USA) were used for DNA subcloning. For isolation of plasmid DNA from *E. coli* cells, Tiangen Miniprep Kit and Tiangen Midiprep Kit (Tiangen Biotech (Beijing) Co, Ltd) was used. RNA isolation was performed using PureLink RNA kit (Life Technologies). TiangenMidi Purification Kit (Tiangen) was used to extract DNA from agarose gels. Bradford solution used for measuring protein concentration was purchased from Bio-Rad (Hercules, CA, USA). The kit used for developing western blot was Millipore Immobilon (Millipore Corp, Billerica, MA, USA).

2.1.9 Chemicals and reagents

2.1.9.1 DNA work

DNA loading ladder and 6X DNA loading buffer were obtained from NEB (Ipswich, MA, USA). Ampicillin used in selective plates and medium were purchased from Sigma-Aldrich (St. Louis, Mo, USA).

2.1.9.2 Protein work

Phenylmethylsulfonyl fluoride (PMSF), 1, 4-Dithiothreitol (DTT) and protease inhibitors tablets used in cell lysis were bought from Roche (Indianapolis, IN, USA). Protein molecular weight marker was purchased from Bio-Rad Laboratories (Hercules, CA, USA) and nitrocellulose membrane was purchased from Bio-Rad (Hercules, CA, USA). The rest of the chemical reagents for protein work were purchased from Sigma Aldrich (St. Louis, Mo, USA).

2.1.10 General buffers and solutions

2.1.10.1 DNA subcloning experiments

2.1.10.1.1 50X Tris-acetate-EDTA

40 mM Tris-acetate (pH 8.3) was made in 1.0 mM EDTA.

2.1.10.1.2 Agarose gel

1% agarose was made by resuspending 1 g of agarose in 100 ml of 1X TAE buffer and microwaved for 10 mins.

2.1.10.2 Western blotting

2.1.10.2.1 10% SDS

10 g of SDS was dissolved in 100 ml of deionised water.

2.1.10.2.2 10% Ammonium persulphate

1 g of ammonium persulphate was dissolved in 10 ml of deionised water.

2.1.10.2.3 5X Tris-glycine electrophoresis buffer

125 mM Tris, 0.96 M glycine, 0.5% SDS, the pH of the solution was adjusted to 8.3.

2.1.10.2.4 Membrane transfer buffer

25 mM Tris (pH 8.3), 192 mM glycine, 0.1% SDS and 20% methanol.

2.1.10.2.5 2X SDS-PAGE gel-loading buffer

2X buffer had 100 mM Tris-HCl (pH 6.8), 200 mM DTT, 4% SDS, 0.2% bromophenol blue and 20% glycerol. The solution was stored at 4°C.

2.1.10.2.6 1M Tris buffer

121.12 g of Tris was dissolved in 1 litre of deionised water and the pH of the solution was adjusted to 8 using HCl.

2.1.10.2.7 5M NaCl

292 g of NaCl was dissolved in 1 litre of deionised water.

2.1.10.2.8 1X Tris buffered saline (TBS)

TBS had 20 mM Tris and 500 mM NaCl, the pH of the solution was adjusted to pH 7.5

2.1.10.2.9 Wash solution

5ml of 10% Triton X-100 was added to 995 ml of 1X Phosphate buffered saline (PBS). For western blot detecting phospho-proteins, 1X TBS was used.

2.1.10.2.10 Blocking solution

5%, 3% or 1% of non-fat milk powder was dissolved in 1X PBS to make the blocking solution. For western blot detecting phospho-proteins, 5% of Bovine serum albumin (BSA) was dissolved in 1X TBS.

2.1.10.2.11 Lysis buffer for His-Pull down

50 mM Tris (pH 8), 100 Mm NaCl, 1% TritonX-100, 200 mM PMSF

2.1.10.2.12 Equilibration Buffer for Ni-NTA beads

50 mM Tris (pH 8), 100 mM NaCl

2.1.10.2.13 Elution buffer for Ni beads

50 mM Tris (pH 8), 100 mM NaCl, 500 mM imidazole

2.1.11 Yeast reagents

2.1.11.1 10X LiAc

1 M lithium acetate solution was prepared in deionised water.

2.1.11.2 50% PEG 3350

50 g of PEG 3350 was dissolved in 100 ml of sterile deionised water. The solution was warmed in a microwave to enable the PEG 3350 to dissolve faster.

2.1.12 Mammalian tissue culture

2.1.12.1 Freezing media

The freezing media was prepared by adding 10% of dimethyl sulfoxide (DMSO) in FBS and filter sterilized through a 0.2 µm filter.

2.1.12.2 Lysis buffer for mammalian cells (RIPA buffer)

- 50 mM Tris–HCl (pH 7.5),
- 200 mM NaCl,
- 1% Triton X-100,
- 0.1% SDS,
- 0.5% sodium deoxycholate,
- 10% glycerol, 1 mM EDTA,
- 1mM PMSF,
- Protease inhibitor cocktail containing 10 μg/ml of leupeptin, pepstatin, and aprotinin each.

2.1.12.3 Transfection reagent

A 2 mg/ml solution of Linear Polyethyleneimine (PEI) (Sigma, St. Louis, Mo, USA) was prepared in deionised water. PEI solution was then filter sterilized through a 0.2 μm filter. 5 μg of PEI was used per microgram of DNA for transfection in mammalian cells.

2.1.13 Chromatin Immunoprecipitation assay

IP dilution buffer: 20 mM Tris-HCl (pH 8.0), 167 mM NaCl, 1.2 mM EDTA, 1.1% Triton X-100, 0.01 % SDS

Low Salt Wash buffer: 0.1% SDS, 1% Triton X-100, 2mM EDTA, 20 mM Tris-HCl pH 8.0, 150 mM NaCl

High Salt Wash Buffer: 0.1% SDS, 1% Triton X-100, 2mM EDTA, 20 mM Tris-HCl pH 8.0, 500 mM NaCl

LiCl wash buffer: 250 mM LiCl, 1% NP-40, 1% Sodium Deoxycholate, 1 mM EDTA, 10 mM Tris-HCl pH 8.0

TE buffer: 10 mM Tris HCl pH 8.0, 1 mM EDTA

Elution buffer: 1% SDS, 100 mM $NaHCO_3$

2.2 Methods

2.2.1 *Escherichia coli* cells

2.2.1.1 Growth conditions and maintenance of *E. coli* cells

E.coli was either cultured in LB broth or maintained on LB agar plates at 37°C. *E.coli* transformed with plasmids containing ampicillin selection marker were cultured in LB-broth or grown on LB agar plates supplemented with 50 µg/ml of ampicillin.

2.2.1.2 Glycerol stock of *E.coli*

For long term preservation, *E.coli* were maintained in glycerol stock as described. Single colony of the *E.coli* strain was inoculated in 5 ml LB medium containing antibiotic and cultured until mid-log phase. 200 µl of 80% glycerol solution was mixed with 800 µl of the bacterial culture and then transferred to a cryovial and stored at -80°C.

2.2.1.3 Preparation of *E. coli* competent cells ($CaCl_2$ method)

A single bacterial colony was picked from LB plate and inoculated in 2 ml of LB medium and grown overnight at 37°C shaking incubator. The culture was diluted to an OD_{600} of 0.05 in 50 ml of LB and incubated at 37°C until to an OD_{600} of 0.5. The culture was then transferred to sterile centrifuge falcon tube and kept on ice until further use. The cells were centrifuged at 4470 g at 4°C for 5 min. The supernatant was discarded and the pellet was resuspended in 25 ml of ice-cold sterile 100 mM $MgCl_2$. The cells were then centrifuged at 4470 g for 10 min at 4°C. The supernatant was discarded and the cell pellet was resuspended in 5 ml of sterile ice-cold 100 mM $CaCl_2$ and incubated on ice for 2 hr to become transformation competent. 2 ml of sterile ice-cold

50% glycerol was added to the cell suspension. The cells were later stored at -80°C as 200 μl

aliquots in eppendorf tubes.

2.2.1.4 Transformation of competent *E. coli* cells

Frozen competent cells in eppendorf tubes were first thawed on ice. For DNA amplification, 1 μl

of DNA was added to 50 μl of competent cells. For subcloning of plasmids, 20 μl of ligation

reaction was added to 100 μl of competent cells. The tubes were incubated on ice for 20 min and

heated at 42°C in a water bath for 90 sec. Tubes were then placed on ice immediately for 20 min.

Cells were plated on LB agar plates containing the selective antibiotic and incubated at 37°C

overnight.

2.2.1.5 Isolation of plasmid DNA from *E.coli*

A single bacterial colony was inoculated in 4 ml of LB containing antibiotic and grown

overnight at 37°C. The cells were centrifuged at 1200 g at 4°C for 5 min. The plasmid DNA was

isolated from the bacterial cells pellet according to the manual provided in the plasmid

purification kit.

2.2.2 *Saccharomyces cerevisiae* **culture and manipulations**

2.2.2.1 Growth and maintenance of *S.cerevisiae*

S.cerevisiae strains were cultured in YPUAD liquid culture as well as streaked on YPUAD agar

plates and maintained at 24°C. Strains harboring plasmids encoding for a nutrient selection

marker were grown in SD liquid media or SD agar plates for proper selection.

2.2.2.2 *S. cerevisiae* glycerol stocks preparation

A single colony of *S.cerevisiae* was streaked on YPUAD agar plate and grown at 30°C for 3 to 4 days. A loopful of cells was inoculated in a cryo-vial containing 500 µl of YPUAD and 20% glycerol. The cells were then stored at -80°C.

2.2.2.3 Transformation of yeast cells

Several colonies of yeast cells were inoculated in 25 ml of YPUAD and allowed to grow overnight at 24°C. The overnight culture was diluted to an OD_{600} of 0.2 and the cells were allowed to grow until they reached an OD_{600} of 0.8. Culture after reaching the OD of 0.8 was then transferred to 50 ml centrifuge tube and centrifuged at 1000 g for 5 min. Supernatant was discarded; pellet was washed with 30 ml of ddH_2O and centrifuged again at 1000 g for 5 min. The supernatant was discarded; pellet was resuspended in 1 ml of 100 mM LiAc and transferred to a 1.5 ml eppendorf tube. This time the cell suspension was centrifuged at 14,100 g in a micro-centrifuge for 15 sec. The supernatant was discarded and the pellet was resuspended in 250 µl of 100 mM LiAc. The 250 µl the pellet was redistributed in 50 µl aliquots in eppendorf tubes and employed for transformation. The cells were centrifuged at 14,100 g in a micro-centrifuge for 15 sec and the supernatant was discarded. To the pellet 240 µl of 50% PEG, 36 µl of 1 M LiAc, 72 µl of ddH_2O, 10 µl of sonicated salmon sperm DNA and 1 µl of plasmid DNA were added. The transformation tubes were vortexed for 1 min, incubated at 24°C for 30 min and given a heat shock at 42°C for 20 min. After heat shock, the cells were centrifuged again at 3,300 g for 15 sec, the supernatant was discarded and the pellet was resuspended in 400 µl of ddH_2O. 100 µl of this cells suspension was plated on selective media plates and incubated at 24°C until the colonies reached sufficient growth for further analysis.

2.2.2.4 Yeast one hybrid assay

Yeast one hybrid screening was used to identify proteins binding to regulatory DNA sequence of interest (bait sequence). *S.cerevisiae* strain pJ69-4A was grown in liquid SD (Trp⁻) culture and transformed with the bait plasmid yEP112-HIS3-400bp (Trp⁻). The *HIS3* gene was used as a reporter gene fused upstream of the DNA sequence of interest. Human foetal brain cDNA library was used for the library screening. This cDNA expression library consists of the prey plasmid pACT2 (Leu⁻), which consists of a fusion protein with GAL4 activation domain. Binding of the protein with the DNA sequence causes the activation of the reporter *HIS3* gene via the activation domain. The optimal 3AT concentration was titrated using SD Trp⁻/His⁻ plates and was found to be 2 mM. The positive interactors were analyzed on SD (Trp⁻/Leu⁻/His⁻) plates.

2.2.3 Mammalian cell culture

2.2.3.1 Growth and maintenance of mammalian cells

HEK293T, HeLa, A431, HaCaT, HSC-5, A5-RT3, hSAEC, MDA-MB-231 and A549 cell lines were maintained in complete media i.e DMEM (Dulbecco modified Eagle medium) supplemented with 10% FBS and 1% penicillin-streptomycin at 37ºC in a 5% CO_2 environment. For growth under hypoxia conditions, cells were kept under 95% N_2/5% CO_2 in Modular Incubator Chamber (Billups-Rothenberg) and maintained at 37ºC for 24 hr. For hypoxia studies, DMOG and YC-1 were dissolved in DMSO and used at a concentration of 1 mM and 60 μM as mentioned in Section 4.1. TGF-beta1 was reconstituted using sterile ddH_2O as per manufacturer's instructions.

2.2.3.2 Passaging and trypsinizing of mammalian cells

Mammalian cells were washed once with 1X PBS and detached from the culture flask by incubating them in 1 ml of 1X Trypsin EDTA solution (Gibco 10X) for 2 min at 37°C. Trypsinization of cells was stopped by adding 4 ml of pre-warmed complete DMEM media and subsequently cells were transferred at the desired density to a new tissue culture flask. The cells were then cultured at 37°C in a 5% CO_2 incubator.

2.2.3.3 Preparation of mammalian cell stocks

Cells were first trypsinised and then resuspended in the appropriate growth media followed by centrifuging at 400 g for 4 min. The supernatant was discarded and cell pellet was resuspended in freezing medium. The cell suspension was then aliquoted into cryogenic storage vials and stored at -80°C in an isopropanol cryobox, that has a controlled freezing rate, overnight. The frozen cells were then transferred to liquid nitrogen tank for long term storage.

2.2.3.4 Thawing of cells

Cryo-vials were taken from liquid nitrogen and re-suspended in 4 ml of DMEM medium supplemented with 10% FBS until the freezing medium had thawed. The thawed cells were then transferred to 5 ml of fresh DMEM medium with 10% FBS and transferred in to 25 cm^{2} culture flask. Growth medium was replaced after 24 hr with fresh complete media.

2.2.3.5 Transfection of adherent mammalian cells

One day before transfection, cells were seeded in 6-well plates to reach 60-80% confluency at the time of transfection. 4 µg of DNA was diluted in 90 µl of serum-free DMEM (SFM). In a separate Eppendorf tube, 10 µl of PEI (20 µg) was diluted in 90 µl SFM. The diluted DNA was added to the PEI solution. The DNA/PEI mixture was then allowed to stand for 15 min at RT.

After incubation, this reaction mixture was added drop-wise onto the cells. The cells were incubated for 12 hr at 37°C in a 5% CO_2-humidified incubator before changing the media to new growth media. After 36 hr of incubation at 37°C in a 5% CO_2-humidified incubator, cells were ready for further analysis.

2.2.3.6 Lentiviral transduction of cells

Day 1: HEK293T cells were seeded at a density of 3.5×10^6 cells per 100 mm dish in 10 ml complete medium. Cells should be seeded approximately 24 hr before transfection and should be 80-90% confluent at the time of transfection.

Day 2: Transfection

Dilute the DNA in a 1.5 ml Eppendorf tube as follows:

A) 3rd Generation lentivirus

3.75 µg VSVG (Envelope plasmid)

6.25 µg pDNL (Packaging plasmid)

3.125 µg REV (Envelope plasmid)

18.75 µg pLJM/ pLKO.1 (Transfer plasmid)

B) 4th Generation lentivirus

2.51 µg pVSVG

2.51 µg pTre-GAG-pro

1.37 µg pLR2P-vpr-RT-in

1.833 µg pTet-off

0.9165 µg pTre-Tat-IRES-Rev

6.11 µg pTripz (Inducible transfer plasmid)

Top up the DNA mix to 5 ml with SFM. Filter the DNA-SFM mix through a 0.2 μm filter

Dilute PEI with SFM in a separate tube at 1:3.125 DNA:PEI ratio. Top it up to 5 ml with SFM. Filter the PEI-SFM mix using a 0.2 μm filter.

Add the DNA-SFM mix to the PEI mix to make a final volume of 10 ml. Incubate the DNA-PEI-SFM mix at room temperature for 20 min. At 15 min of incubation, rinse the HEK293T cells with 5 ml of warm SFM. Add the DNA-PEI mix to the cells and incubate at 37ºC for 4 hr. After 4 hr of incubation, the DNA-PEI-SFM mix is removed and 8 ml of fresh media is added to the cells.

Day 3: 24 hr post-transfection, the cell supernatant containing virus is harvested and filtered using a 0.45 μm filter. The virus can be used immediately or stored at -80º C till further use. For transduction of cells, media is removed from the cells and equal volume of virus containing media and polybrene at final concentration of 8 μg/ml is added and incubated for 24 hr. Second infection was done 24 hr after first infection (Day 4) with fresh virus to increase the infection efficiency.

2.2.3.7 Mammalian cell lysis

Adherent cells were trypsinised and resuspended in the appropriate growth media. For both the adherent and suspension cells, the number of cells and cell viability were determined using the hemocytometer, cell counter and Trypan Blue exclusion. 2×10^6 cells were centrifuged at 400 g for 4 min. The supernatant was discarded and the cells pellet was washed with PBS and then resuspended in 50 μl of lysis buffer (Materials 2.1.12.2). Cells were left on ice for 1 hr and cellular membranes were removed by centrifugation at 14,100 g for 10 min. 50 μl (equal amounts) of 2X loading dye and 2 μl of 1M DTT was added to the lysate. Protein concentration

was quantified with Bio-Rad DC protein assays. The lysate was boiled at 100°C for 5 min and stored at -80°C until further use.

2.2.4 Cell based assays

2.2.4.1 Immunofluorescence

Cells grown on coverslips were fixed, permeabilized and blocked with 1% BSA in PBS. The cells were then incubated with appropriate primary antibodies (diluted in blocking solution) for 1 hr at room temperature. The cells were rinsed twice with PBS and then incubated with the appropriate fluorescent antibody (diluted in blocking solution) for 1 hr at room temperature. Fluorescence images were acquired using Olympus IX51 fitted with Cool SNAP^{HQ} camera and analyzed using Metamorph software (Molecular Devices).

2.2.4.2 Time-lapse microscopy

Cells were seeded at a density of 3 x 10^5 cells/ml in 6 well plates and grown in complete media at 37°C in a 5% CO_2 humidified atmosphere. Monolayer of the transfected cells was scratched using a sterile 10 μl white pipette tip. Time lapse was set up to observe the cell migration using the Olympus microscope IX51 fitted with Photometrics Cool Snap HQ2 camera over a period of 24 hr. In each experiment at least 12 randomly selected regions were monitored. Size of the scratch was measured using Metamorph software. The minimal separation between the opposing cell fronts was measured. Wound distance was measured by calculating the width of wound at the selected time point.

2.2.4.3 Matrigel Invasion assay

Invasion assay was performed using matrigel. Matrigel was thawed overnight on ice and diluted

to 2 mg/ml concentration (using cold SFM). 100 µl of matrigel was added to the upper chamber of a 8 µm 24-well transwell. The matrigel was allowed to solidify for 2 hr at 37°C in a tissue culture incubator. Cells were trypsinized, counted and resuspended in SFM. The cells were seeded at a seeding density of 1,00,000 cells/ml and the final volume of the cell suspension was adjusted to 200 µl using SFM. The cell suspension was added over the solidified matrigel. The lower chamber of the transwell was filled with 500 µl of complete media. The cells were incubated for 48 hr at 37°C in a tissue culture incubator. After 48 hr, the matrigel was removed by pipetting and the transwell was washed 3 times with PBS. The non-invaded cells were gently scraped off from the top of the transwell using a cotton swab. The invaded cells were then stained with 1% crystal violet in 25% methanol for 30 min. The transwell was washed three times with PBS and the inner chamber of transwell was cleaned thoroughly using a cotton swab. Transwell was inverted on a glass slide and the invaded cells were observed and counted under a light microscope.

2.2.4.4 Gelatin degradation assay

Coverslips were acid-washed using 20% nitric acid and coated with poly-L-lysine (Sigma) for 20 min. Coverslips were washed three times with PBS and crosslinked with 0.5% glutaraldehyde (Sigma) for 15 min on ice. The coverslips were washed with ice-cold PBS and 100 µl of 0.2 mg/ml Oregon Green 488-conjugated fluorescent gelatin (Molecular Probes) was added on the coverslips. Coverslips were incubated for 15 min in the dark at room temperature. All the subsequent steps were performed in dark. After washing thrice with PBS, the coverslips were incubated with 5 mg/ml sodium borohydride for 15 min followed by another washing with PBS

and sterilization with 70% ethanol for 30 min. Finally, fluorescent gelatin-coated coverslips were incubated with complete media for 1 hr at 37°C before plating cells.

Cells (4×10^4/ml) were cultured on fluorescent gelatin-coated coverslips for 6 hr. 1mM DMOG was added to the wells and incubated for 6 hr at 37°C. Immunostaining was performed as described previously. Alexa Fluor 594 phalloidin and cortactin antibody were used to stain F-actin and cortactin respectively. Coverslips were mounted using Dako mounting medium.

2.2.4.5 Cell spreading assay

Bovine fibronectin was diluted with 0.1 M sodium bicarbonate buffer (pH 9.1) to a final concentration of 1.4 µg/ml. 100 µl of fibronectin was added to the wells of 96-well plate and incubated at 37°C for 1.5 hr. After coating, each well was blocked with 100 µl of 0.1% (w/v) BSA at 37°C and washed once with SFM. Cells were trypsinized and allowed to recover in SFM for 30 min. Cells were then seeded at a density of 2×10^5 cells/ml, and incubated at 37°C in a CO_2 humidified incubator. Images were captured at different time intervals to monitor cell spreading (Magnification 10X). MetaMorph software was used to calculate the mean surface area of each population.

2.2.4.6 Soft agar assay

Anchorage-independent growth was assayed by the soft agar assay. Briefly, 0.8% noble agar (Sigma) was prepared using complete media and used to coat the bottom of a 6-well tissue culture plate. 1.5 ml of the agar was added to the plate and allowed to solidify at room temperature for 30 min. Meanwhile, cells were harvested by trypsinization and 2,500 cells were mixed with 1 ml of 0.3% agarose maintained at 40°C to prevent premature solidification. Cell-

agar mix was added on top of existing 0.8% bottom agar in triplicates. Plates were incubated at room temperature for 30 min and kept in 37°C incubator for 4 weeks. Agar was covered with 500 µl of complete media to prevent dessication. The covering medium was replaced every week. At the end of 4 weeks, cell colonies >0.1 mm in diameter were counted under a microscopic field. Average colony number was based on numbers from triplicate wells for each sample.

2.2.4.7 MTT assay

In brief, cells (7500 cells/well) were seeded in a 96-well plate. 10 µl of MTT (10 mg/ml) was added in each well after 24, 48 and 72 hr of seeding. The plate was incubated at 37°C in dark for 3.5 hr. After completing the incubation, the media was discarded and 150 µl of MTT solvent (0.1% NP-40 with 4mM HCl) was added to each well and incubated in dark at room temperature for 15 min. Color developed after the reaction was measured at 590 nm using Tecan microplate reader.

2.2.4.8 RNA isolation

RNA was isolated from a confluent monolayer using PureLink® Minikit by Invitrogen. Cells were trypsinized from a cell culture dish and pelleted to obtain approximately 5×10^6 cells. The cells were lysed using lysis buffer (containing 1% 2-mercaptoethanol) followed by a brief vortex to disperse the cells. The cell lysate was homogenized by passing the lysate 5-10 times through a 20-gauge needle attached to a RNase-free syringe. The homogenized lysate was added on a spin cartridge and washed with wash buffers to purify the RNA. The purified RNA was eluted using RNase free water and stored at -80°C till further use.

2.2.4.9 RNA sequencing

Enrichment of mRNA and RNA sequencing was performed by staff at Beijing Genome Institute (BGI) (Shenzen, China). Total RNA was isolated from HaCaT and A5-RT3 cells using PureLink RNA kit. The RNA yield was analyzed and 30 µg of the RNA was shipped in RNAstable tubes to BGI. The RNA integrity number was analyzed using Agilent RNA6000 Pico kit. Enrichment of the mRNA was done with Oligo (dT) magnetic beads. The mRNA was fragmented into short fragments (~200 bp) using a fragmentation buffer. Taking these short fragments as templates, first strand cDNA was synthesized by random hexamer-priming. Second-strand cDNA was synthesized using buffer, dNTPs, RNaseH and DNA polymerase I. Magnetic beads were used to purify the double strand cDNA which was then washed with EB buffer for end-polishing. Sequencing adapters were ligated to short fragments. The fragments were purified by magnetic beads and enriched by PCR amplification. Finally, the libraries were sequenced using Illumina HiSeq™2000. DEGs were identified using by aligning the RNA-Seq data obtained by mapping the short reads with a reference genome (Homo sapiens).

2.2.5 DNA manipulation

2.2.5.1 Agarose gel electrophoresis

0.5 µg/ml of Ethidium Bromide was added to 1% agarose in 1X TAE and the gel was allowed to solidify. 6X DNA Loading buffer was added to the samples and they were loaded in the wells of the gel, submerged in 1X TAE. DNA was resolved by running the gel at 110V for 50 min. DNA was visualized under the long wavelength UV light.

2.2.5.2 DNA extraction from agarose gel

The bands of desired molecular weight were excised out with a scalpel and placed in an eppendorf tube. The DNA was extracted according to the manual provided in the plasmid purification kit (Tiangen Midi-purification kit).

2.2.5.3 DNA subcloning

Restriction enzymes were used to digest the purified DNA fragments and the reaction tube was prepared according to the instructions supplied by the manufacturer. DNA sample together with restrictions enzymes were incubated at 37°C for 2 hr. In case of restriction enzymes having star activity such as BamHI and *Eco*RI, the restriction enzyme digestion was performed only up to 90 min. Agarose gel electrophoresis was used to resolve the restriction enzyme digested products; DNA fragments of interest were excised and purified from the agarose gel. 2 µl of each of the purified DNA fragment was mixed with loading dye and ddH$_2$O and subjected to agarose gel electrophoresis in order to verify the presence of sufficient quantities of DNA fragment enough for the ligation reaction. Purified insert DNA was then ligated with linearized vector DNA by using T4 DNA ligase and the ligation reaction mixture was made according to the instructions supplied by the manufacturer. The ligation reaction mixture was incubated at 24°C for 4 hr and then transformed into competent *E. coli* cells by following the transformation protocol for *E. coli*.

2.2.5.4 Verification of recombinant plasmid DNA constructs

The recombinant plasmid DNA was verified by checking with restriction enzymes that cut at restriction enzyme sites that are unique to it. The digested DNA was then resolved by agarose gel electrophoresis. The bands obtained in the gel were checked to verify for the correct sizes.

2.2.5.5 DNA quantification

Concentration of the DNA sample was calculated by using NanoDrop. Software will generate the stander curve using the DNA concentrations along with the negative control and gives the DNA concentration in ng/µl. OD_{260}/OD_{280} ratio was checked to confirm the purity of DNA sample. OD_{260}/OD_{280} less than 1.8 indicate impurity caused by proteins and/or other matter capable of absorbing UV light. OD_{260}/OD_{280} higher than 2.0 indicates possibility of RNA contamination in the DNA sample. OD_{260}/OD_{280} between 1.8 and 2.0 indicate the absorption due to DNA thus all DNA samples which had OD_{260}/OD_{280} between 1.8 to 2.0 were selected for further experiments.

2.2.5.6 Polymerase chain reaction (PCR)

PCR was performed to specifically amplify DNA from very small amount of DNA. DNA polymerase KAPA2G Robust from KAPA Biosystems (Woburn, MA, USA) was used. dNTP mix (dTTP, dATP, dGTP and dCTP) was obtained from Invitrogen (Carlsbad, CA, USA). All PCR reactions were performed using the Peltier Thermal Cycle PTC-100. A 25 µl reaction using Kapa system was set up as follows:

- 5 µl of 5x Kappa2G Robust Reaction Buffer
- 5 µl of Enhancer
- 0.5 µl of dNTP mix
- 0.75 µl of 5' primer (10 µM)
- 0.75 µl of 3' primer (10 µM)
- 0.5 µl of Template DNA
- 0.1 µl of Kappa2G Robust DNA Polymerase (1 U/µL)
- Deionised water (topped up to 25 µl)

The thermal cycle conditions used were:

- Initial Denaturation: 95ºC for 10 min

- Denaturation: 95ºC for 1 min
- Annealing: 55ºC for 1 min
- Extension: 72ºC for 30 sec per kb (30 cycles)
- Final Extension: 72ºC for 5 min

The PCR reaction was cycled 35 times for optimal amplification of the target fragment. The primers used in this study are listed in Appendix 2. The PCR products were analyzed by Agarose gel electrophoresis (Section *2.2.5.1*).

2.2.5.7 Reverse transcription of RNA to cDNA

1-5 μg of RNA was added with 1 μl of DEPC-treated water and 1 μl of Random primers. The mixture was incubated at 70°C for 5 min and incubated on ice immediately for 5 min. A reaction mixture prepared as follows was added to the RNA and incubated at 37°C for 5 min.

Reaction mixture:

- 6 μl of 5X reaction buffer
- 3 μl of 0.1M DTT
- 0.5 μl of 25 mM dNTPs
- 9 μl of DEPC-treated water

The tube was transferred to ice and incubated for 5 min. 0.5 μl of Reverse Transcriptase was added to the tube and it was incubated for 60 min at 42°C. The Reverse Transcriptase was then heat inactivated at 70°C for 5 min. The tube containing the cDNA was stored at 4°C till further use.

2.2.5.8 Real-time PCR (RT-PCR)

Total RNA was isolated from cells using the RNAeasy kit and reversed-transcribed to cDNA. 25 μl Real-time PCR reaction was set up as follows:

- 12.5 μl of SYBR Green Master Mix (Fermentas, Thermo Fisher Scientific)

- 2.5 μl of cDNA (Diluted 5 times)

- 2.5 μl of diluted primers (Forward + Reverse, 50 nM in 25 μl)

- 7.5 μl of DNAase/RNAase free water.

Each reaction was performed in triplicates and the primers used are listed in Appendix 2. The RT-PCR was performed on 7500 Real-Time PCR system (Applied Biosystems) using the comparative C_t method. Tabulation by comparing C_t values was performed to measure gene expression in target cells to that of control cells.

The formula used was $C_{tTarget} = 2^{(Ct_{Endogenous} - Ct_{GeneA})}$, and the same was applied for $Ct_{Reference}$.

2.2.5.9 Overlap extension PCR

In the overlap extension PCR, as illustrated in Figure 2.1, two halves of the gene of interest are first amplified separately with an outer flanking primer and a mutagenesis primer each (primers a and b, primers c and d).
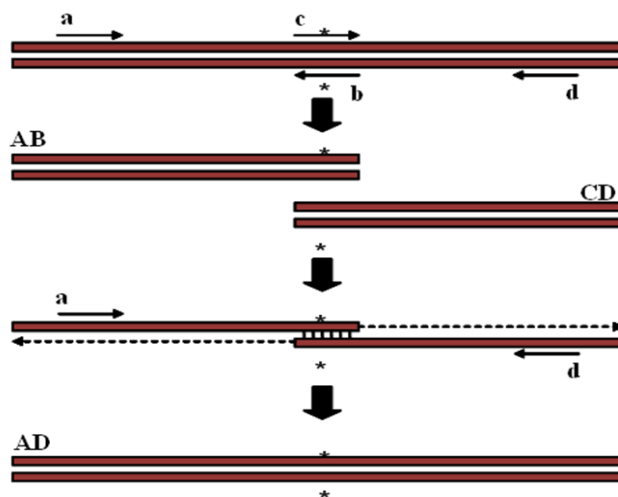
Figure.2.1: Schematic diagram of the overlap extension PCR.
b and c are the mutagenesis primers while a and d are flanking primers. AD is the final PCR product which contains the desired mutation.

The two mutagenesis primers are complementary to each other. The PCR products from the two PCR reactions (AB and CD) are purified and mixed together to be used as template for the third PCR reaction. In the third PCR reaction, the two outer flanking primers (primers a and d) are used to amplify the final full length PCR product (AD). Finally, the end product obtained is the gene of interest bearing the desired mutation.

2.2.5.10 DNA precipitation

For 20 µl of DNA mix, 2.22 µl of 3M NaOAc (1/10 of DNA mix) and 44.44 µl of 100% ethanol (2X of DNA and NaOAc mix) was added. The mixture was incubated at -20°C for 2 hr or more and centrifuged at 14,100 g for 10 min. The resulting pellet was washed with 70% ethanol. The pellet was air-dried and dissolved in appropriate amount of deionised water or 1X TE buffer according to the pellet size.

2.2.6 SDS-PAGE electrophoresis

2.2.6.1 Sample preparation for SDS-PAGE electrophoresis

Bradford assay was performed to measure the total amount of protein in samples. The protein sample was mixed with 2X loading buffer (Section 2.1.10.2.5) followed by heating at 100°C for 5 min. 30 µg of the protein sample was used to run the SDS-PAGE.

2.2.6.2 SDS-PAGE gel preparation

Proteins in samples were resolved by loading the appropriate amounts in the SDS-PAGE gel and the gel was run at 90V for 120 min, until the dye front has migrated past the end of the gel. The gel was then further processed either for the staining of proteins or western blot analysis.

A 10% SDS-PAGE gel was prepared as follows:

Resolving Gels (15 ml)

	10%	15%
1.5M Tris pH 8.8	5 ml	5 ml
30% acrylamide	4 ml	7.5 ml
water	5.9 ml	2.4 ml
20% SDS	75 µl	75 µl
10% APS	75 µl	75 µl
TEMED	25 µl	25 µl

5% Stacking Gels (5 ml)

0.5M Tris pH 6.8	0.62 ml
30% acrylamide	0.833 ml
water	3.817 ml
20% SDS	25 µl
10% APS	50 µl
TEMED	5 µl

Table 2.5: Preparation of SDS page gel

2.2.6.3 Western blot analysis

Concentration of protein in cell lysate was determined by Bradford assay and equal amount of proteins were resolved on a SDS-PAGE gel. The nitrocellulose membrane and filter papers were soaked in the transfer buffer for 5 min. The nitrocellulose membrane and the protein gel were overlaid on each other and sandwiched between 3 filter papers on each side and placed in the transfer cassette. The transfer cassette was then placed inside the transfer cell in the correct orientation such that the transfer of the proteins would take place in the direction from the protein gel and on to the nitrocellulose membrane. The transfer was carried out at a constant voltage of 90V for 2 hr at 4°C.

2.2.6.4 Immunoblotting and chemiluminescence

After blotting, the membrane was removed from the transfer cassette and blocked in the 3-5% skimmed milk solution in PBS (5% BSA in Tris buffer (pH 8.0) for phospho-proteins) for 30 min at room temperature. Primary antibody was incubated with the membrane overnight with appropriate dilution (for dilutions see Table 2.4) at 4°C. After the incubation with primary antibody, membrane was washed 3 times (5 min per wash). Subsequently, membrane was incubated in appropriate secondary antibody (for dilutions see Table 2.5) conjugated with Horseradish peroxidase (HRP) for 1 hr at room temperature. The membrane was then washed and protein bands were detected with Millipore Immobilon™ Western Chemiluminescent HRP Substrate (ECL) detection regent as per the instructions of manufacturer.

2.2.7 Hexa histidine-tag pull down assay

His tag pull down assay was performed to purify protein containing His tag. The His tag fusion protein was expressed in the HEK293T cells. HEK293T cells were grown in 10 cm^2 culture dish and transfected with the plasmid containing His tag. 36 hr post-transfection, the cells were lysed by adding 500 µl of lysis buffer (Section 2.1.14.2) and incubated on ice for 1 hr. 80 µl of bead slurry was aliquoted into eppendorf tube for each lysis sample. The Ni-NTA beads (Invitrogen, Carlsbad, CA, USA) were washed 3 times with 1 ml of equilibration buffer at 100 g for 5 min. 500 µl of equilibration buffer (Section 2.1.14.1) was added to the beads and the tubes were rocked for 1 hr at 4°C. The beads were resuspended in 400 µl of equilibration buffer. Tubes containing the lysed cells were centrifuged at 14,100 g for 5 min to remove cell debris and the supernatant was transferred to a new tube. 30 µl of the supernatant was aliquoted out as whole cell lysate (input). 40 µl of dry beads were added to the supernatant. The cell lysate was

incubated with the beads by gently rocking the tubes for 2 hr at 4°C. The beads were centrifuged for 5 min at 1000 g and the flow-through was stored in new tubes. Beads were washed 3 times with lysis buffer with 10 mM imidazole and the bound proteins were eluted with elution buffer (Section 2.1.10.2.13) containing 250 mM Imidazole. Eluted proteins in the supernatant, were boiled with 2X SDS-PAGE loading dye and 40 mM DTT at 100°C for 5 min. The samples were subjected to western blot analysis.

2.2.8 Chromatin Immunoprecipitation assay

HeLa cells were cultured in either normoxic or hypoxic (DMOG treatment) conditions for 6 hr and then fixed with 1% formaldehyde at room temperature for 10 min. Crosslinking reaction was stopped using glycine at a final concentration of 125 mM for 5 min at room temperature. The media was removed and cells were washed twice with ice cold 1X PBS. Cells were scraped in cold 1X PBS with protease inhibitors and pelleted at 1000 g at 4°C for 5 min. Supernatant was discarded and cell pellet was resuspended in RIPA lysis buffer (containing protease inhibitors) and incubated on ice for 30 min. The cross-linked chromatin suspension was sonicated for 45 min (30 sec ON/ 30 sec OFF) to generate 0.5-0.8 kb fragments. The homogenates were centrifuged at 14,100 g, 4°C for 10 min. Crosslinking efficiency was determined by running the sonicated chromatin on 2% agarose gel. 50 μl of sheared chromatin was diluted with 350 μl of IP dilution buffer, along with protease inhibitors to reach a final volume of 400 μl. One 50 μl aliquot was saved as input control for the reverse cross linking phase. The IP procedure was performed at 4°C using a rotating mixer. Diluted chromatin was pre-cleared using pre-washed protein A agarose, 50% slurry at 4°C for 60 min. Supernatants were then incubated with 1 μg anti-HiF1α antibody or mouse IgG (Santa Cruz) at 4°C for 4 hr. Protein A/G beads were blocked

using 1% BSA in IP dilution buffer at room temperature for 30 min. DNA-protein-antibody complexes were trapped by incubating each sample with blocked protein A/G beads for 2 hr. The beads were pelleted at 100 g, 4°C, 5 min and washed with low salt buffer followed by a high salt buffer. Subsequently, the beads were washed with LiCl wash buffer for 5 min. Beads were washed twice with TE buffer, pH 8 for 5 min. The bound chromatin was eluted by incubating the beads with 150 µl of elution buffer for 15 min at room temperature. The eluent by collected by centrifugation at 14,100 g for 5 min at room temperature. The elution step was repeated with 150 µl of fresh elution buffer and the two elutes were combined. DNA-protein cross-linking was reversed by adding 200 mM NaCl to each sample, followed by overnight incubation at 65°C. The eluates were then treated with RNase (50 µg/ml) at 37°C for 60 min followed by digestion with proteinase K at 45°C for 2 hr. DNA was recovered by using phenol/chloroform/isoamyl alcohol (25:24:1) extraction, followed by ethanol precipitation. The DNA was resuspended in TE buffer and subjected to PCR analysis by primers mentioned in Appendix C.

2.2.9 Quantification of GFP fluorescence by fluorimetry

Cells were seeded in a 6-well plate 24 hr prior to transfection. PEI transfection was performed using 4 µg of DNA at 60-80% confluency. After 36 hr of transfection, cells were lysed using 350 µl of lysis buffer (20 mM Tris-HCl, 2 mM EGTA, 2 mM EDTA, 30 mM NaF, 30mM $Na_4O_7P_2$, 2 mM Na_2VO_4, 1% Triton X-100, 0.03% SDS, pH 7.4) and incubated on a shaker for 10 min in dark at room temperature. The lysate was centrifuged at 14,100 g for 5 min to remove the cell debris. The supernatant was divided in three wells of a 96-well plate. The fluorescence intensity was measured using Tecan plate reader using following excitation and emission wavelengths (GFP: Excitation-480 nm, Emission-530 nm and RFP: Excitation-550 nm, Emission 630 nm). In

case of a co-transfection using two plasmids, 2 μg of each plasmid was transfected for a 6-well plate. GFP/RFP normalization was performed to ensure equal uptake of each of the plasmids.

2.2.10 Bioinformatic analysis

Bioinformatic analysis of the genomic region at the 5' end of the *WASL* gene was performed using web-based software programs. Analysis of the GC nucleotide content used the CpG-plot tool at the EMBL-EBI European Bioinformatics Institute, [http://www.ebi.ac.uk/Tools/emboss/cpgplot]. The conservation profile was obtained with the tools for comparative genomics of the VISTA Genome Browser [http://genome.lbl.gov/vista/index.shtml]. The search for transcription factor binding sites in selected DNA region was performed with MatInspector software [http://www.genomatix.de/solutions/genomatix-software-suite.html] [210]. Gene and biological process analysis for RNA sequencing data was done using PANTHER software [http://pantherdb.org/tools/index.jsp] [211].

2.2.11 Statistics

All the statistical data was generated from at least three independent experiments. Statistical analysis was performed using two-tailed unpaired student's t-test to compare the difference between groups. Significance is indicated by stars * $p \leq 0.05$, ** $p \leq 0.01$, *** $p \leq 0.001$.

RESULTS

CHAPTER 3:
Role of WIP in Epithelial Mesenchymal transition

Introduction:

RNA-Seq involves sequencing of cDNA and mapping the sequencing reads to reference genome. It allows identification of introns and exons, mapping their boundaries and identifying the TSS as well as the 5' and 3' ends of genes [212, 213]. The A5-RT3 clone was derived from normal human keratinocytes HaCaT by transforming with *Ras* oncogene and subcutaneous transplantation in mice [202]. This gave rise to a highly metastatic and malignant A5-RT3 clone which grows to form poorly differentiated SCCs with local lymph node metastases. Mapping and quantifying the transcriptome of normal HaCaT keratinocyte and metastatic A5-RT3 cell using RNA sequencing was performed to identify the set of DEGs during metastasis.

3.1 RNA sequencing analysis

HaCaT and A5-RT3 cells were grown to 90% confluence and total RNA was extracted using PureLink® Minikit (Invitrogen). RNA concentration and purity was determined using a Nanodrop spectrophotometer and RNA sequencing was performed at BGI. Transcriptome sequencing using Illumina Hi-SeQ ™2000 yielded a total of 11322436 and 11929023 reads with

554799364 and 584522127 bp of HaCaT and A5-RT3 cells respectively. The sequencing reads were mapped to reference human genome sequence hg19 using the aligner SOAP2. SOAP2 is a fast method for aligning cDNA to reference genome with a better accuracy at gene level [214].

3.2 Mapping results

Mapping of the sequencing reads generated files containing alignment information. Summary of the mapping is generated in Table 3.1 for HaCaT and A5-RT3. As a result of the mapping of reads against the human genome hg19 build, a total of 85.98% and 85.03% reads mapped out of which 73.52% and 73.02% reads showed a perfect match in HaCaT and A5-RT3 cells respectively (Table 3.1).

Map to Gene	HaCaT	A5-RT3
Total mapped reads	9734896 (85.98%)	9785441 (82.03%)
Perfect match	8324541(73.52%)	8471592 (71.02%)
<=2 mismatch	1410355 (12.46%)	1313849(11.01%)
Unique match	9143255(80.75%)	9278397(77.78%)
Multi position match	591641(5.23%)	507044 (4.25%)
Total unmapped reads	1587540(14.02%)	2143582 (17.97%)

Table 3.1: Mapping statistics for transcriptome of HaCaT and A5-RT3 cells.

#	HaCaT	A5-RT3
Total Gene Number	22748	22748
Unique matched genes	15072	15607
Percentage	66.26%	68.61%

Table 3.2: Coverage analysis for HaCaT and A5-RT3 cells

Table 3.2 represents the integral gene coverage analysis of the two samples. The coverage analysis aims to know number of detectable genes and is calculated by the ratio of unique matched genes number to total gene number. Gene expression level was determined using the RPKM method (Reads per kilobase transcriptome per million mapped reads). After determining the gene expression level, the level of differential expression was examined for the two samples.

3.3 Differentially expressed genes

As shown in Figure 3.1 (A), 4488 genes were found to be upregulated and 1403 genes were found to be downregulated in A5-RT3 cells relative to HaCaT cells. Both gene groups (upregulated and downregulated) were analyzed with Panther software (http://pantherdb.org/tools/index.jsp) [211] to identify the biological processes and associated genes in HaCaT and A5-RT3 cells (Figure 3.2). Panther software is an online annotation software for identifying a gene's molecular function, protein class, involvement in biological processes and associated signaling pathways [211]. Analysis of the DEGs, showed a 5.6 fold-increase for N-WASP, 9.5 fold-increase for HiF1α and 1000 fold-increase for WIP in A5-RT3

cells in comparison to HaCaT cells (Figure 3.1 B). Table 3.3 and Table 3.4 enlists the top 10 upregulated and downregulated genes in A5-RT3 cells in comparison to HaCaT cells.
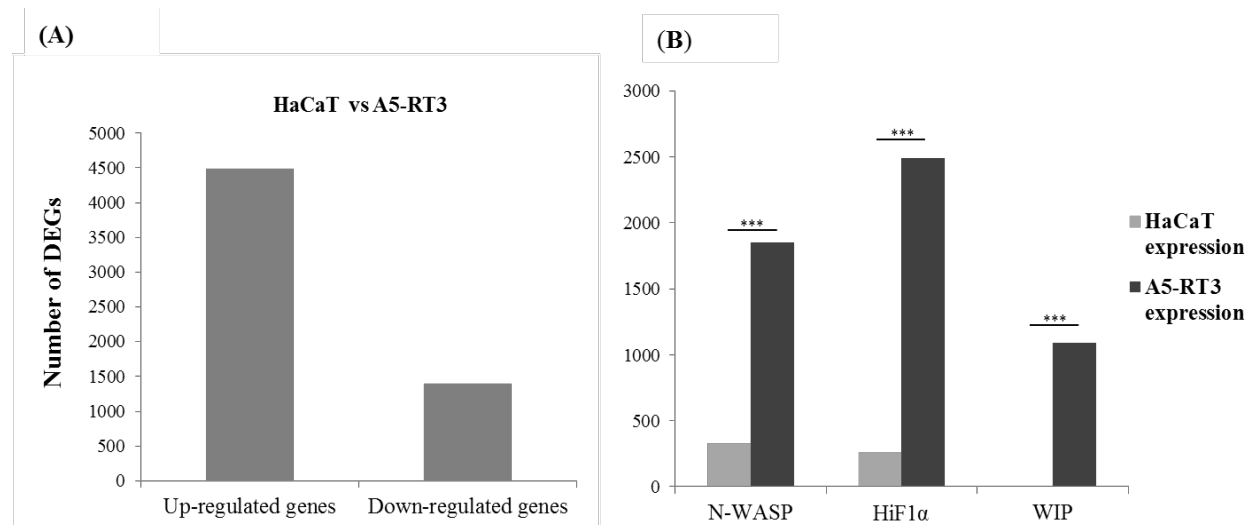
Figure.3.1: Differential gene expression in HaCaT and A5-RT3 cells.

(A) RNA sequencing showed 4488 genes are upregulated and 1403 genes are downregulated in A5-RT3 cells as compared to HaCaT cells (B) Relative expression of N-WASP, HiF1α and WIP in HaCaT and A5-RT3 cells showed significantly high expression of all three proteins in A5-RT3 cells as compared to HaCaT cells. (Significance is indicated by stars * $p \leq 0.05$, ** $p \leq 0.01$, *** $p \leq 0.001$).

(A) Top 100 upregulated genes in A5-RT3 as compared to HaCaT cells

Legend:
- 1 cellular component organization or biogenesis
- 2 cellular process
- 3 localization
- 4 apoptotic process
- 5 reproduction
- 6 biological regulation
- 7 response to stimulus
- 8 developmental process
- 9 multicellular organismal process
- 10 biological adhesion
- 11 metabolic process
- 12 growth
- 13 immune system process

(B) Top 100 downregulated genes in A5-RT3 as compared to HaCaT cells

Legend:
- 1 cellular component organization or biogenesis
- 2 cellular process
- 3 localization
- 4 apoptotic process
- 5 reproduction
- 6 biological regulation
- 7 response to stimulus
- 8 developmental process
- 9 multicellular organismal process
- 10 locomotion
- 11 biological adhesion
- 12 metabolic process
- 13 immune system process

Figure.3.2: Panther analysis of genes upregulated and downregulated in A5-RT3 cells as compared to HaCaT cells.

Pie chart denoting the biological processes associated with top 100 upregulated genes (A) and top 100 down regulated genes (B) in A5-RT3 as compared to HaCaT cells (Percentages in the pie chart represent number of genes against total identifications).

Gene Symbol	Description	log2 Ratio(A5-RT3/HaCaT)	HaCaT-Expression	A5-RT3 Expression	P-value
WIPF1	*WAS/WASL* interacting protein family, member 1	14.62	0	1091	0
FMOD	fibromodulin	12.86	1	7580	0
CDH2	cadherin 2, type 1, N-cadherin (neuronal)	9.01	4	2107	0
CFB	complement factor B	8.69	11	4642	0
PDZK1IP1	PDZK1 interacting protein 1	7.95	8	2009	0
C1S	complement component 1, s subcomponent	7.37	8	1351	0
PLLP	plasmolipin	7.31	8	1295	0
C3	complement component 3	7.24	66	10183	0
DPYSL3	dihydropyrimidinase-like 3	6.29	24	1909	0
LCN2	lipocalin 2	6.01	243	15982	0

Table 3.3: List of top 10 genes upregulated genes in A5-RT3 cells as compared to HaCaT cells

Gene Symbol	Description	log2 Ratio(A5-RT3/HaCaT)	HaCaT-Expression	A5-RT3 Expression	P-value
KRT1	keratin 1	-10.07	2131	2	0
SPON2	spondin 2, extracellular matrix protein	-9.24	1794	3	0
KLK5	kallikrein-related peptidase 5	-8.63	2358	6	0
KRT4	keratin 4	-8.13	11090	40	0
SPRR1B	small proline-rich protein 1B	-6.42	1520	18	0
H19	H19, imprinted maternally expressed transcript	-6.12	2205	32	0
MDK	midkine (neurite growth-promoting factor 2)	-5.44	5183	121	0
KRT13	keratin 13	-5.26	120308	3165	0
PI3	peptidase inhibitor 3, skin-derived	-5.04	1270	39	0
AQP3	aquaporin 3 (Gill blood group)	-4.42	3124	148	0

Table 3.4: List of top 10 genes down regulated genes in A5-RT3 cells as compared to HaCaT cells

3.4 Expression of WIP is enhanced in A5-RT3 cells as compared to HaCaT cells

Analysis of the DEGs obtained by RNA-seq revealed *WIPF1* gene to be highly upregulated in A5-RT3 cells relative to HaCaT cells. *WIPF1* gene encodes for the WIP protein, which is a WASP and N-WASP binding protein. WIP is a known actin regulator and its role in hematopoietic cells is well established [89]. However, the role of WIP in cancer progression and metastasis has not been characterized. In order to investigate the correlation of WIP expression with tumorigenicity, western blot was performed with the cell lysates of HaCaT and its tumorigenic clone, A5-RT3. Western blot analysis showed that expression of WIP was upregulated in the A5-RT3 cells relative to parental HaCaT cells (Figure 3.3 A). mRNA expression of WIP was determined in HaCaT and A5-RT3 cells by RT-PCR analysis. As seen in Figure 3.3 C, the number of transcripts of WIP was significantly downregulated in HaCaT cells as compared to A5-RT3 cells which is in concordance with the RNA sequencing results. WIP transcripts were undetectable in RNA-seq for HaCaT cells. Hence, it may be possible that the transcripts were too low to be detected since RNA-Seq is a comparative study.

(A) **(B)** **(C)**
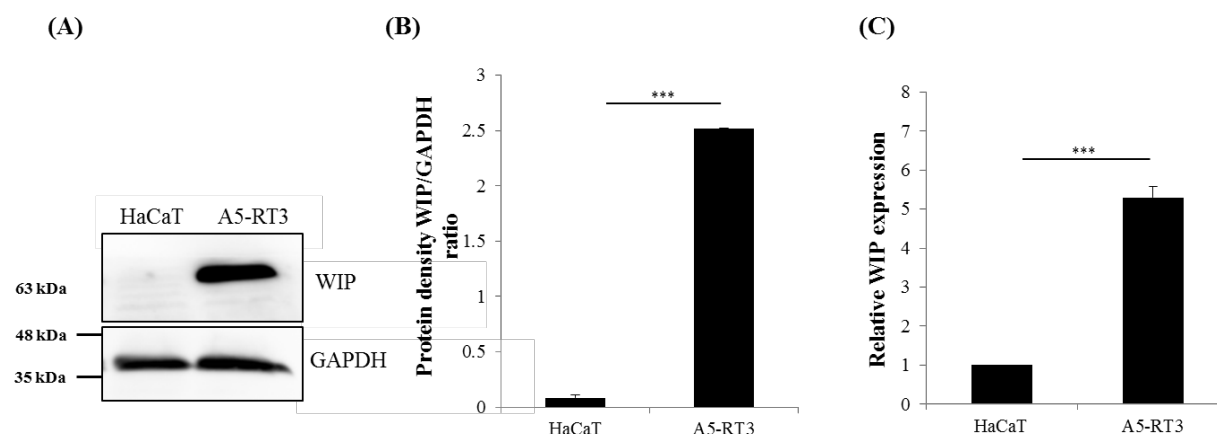
Figure.3.3: Expression of WIP is enhanced in metastatic A5-RT3 cells as compared to non-tumorigenic HaCaT cells

(A) HaCaT and A5-RT3 cells were lysed and the lysate was used for western blot analysis. Equal concentration of the protein resolved on 10% SDS PAGE. Proteins were probed for anti-WIP and anti-GAPDH. (B) Densitometric analysis of WIP expression in HaCaT and A5-RT3 (C) Real time PCR analysis shows upregulation of WIP mRNA expression in A5-RT3 relative to HaCaT cells. (Significance is indicated by stars * $p \leq 0.05$, ** $p \leq 0.01$, *** $p \leq 0.001$).

3.5 Generation of stable cell lines

In order to determine the role of WIP in metastasis, stable WIP overexpressing and WIP knockdown cell lines were generated using A549 lung carcinoma cells. A western blot analysis was performed to determine WIP expression using A549 cells and non-cancerous Human Small Airway Epithelial Cells (SAEC). As shown in Figure 3.4 A, expression of WIP was found to be increased in A549 cells as compared to SAEC consistent with the expression analysis in skin cancer cells.

A) WIP overexpressing cells

Lentivirus was generated using pLJM-linker and pLJM-WIP plasmids, which were transfected into HEK293T packaging cells along with lentiviral packaging plasmids as described in Section

2.2.3.6. pLJM-EGFP plasmid was transfected separately to monitor transfection and infection efficiency by observing cells expressing GFP. Transfection efficiency was determined by comparing number of GFP transduced cells to the total number of cells in a microscopic field. Viral supernatants were collected at 24 hr and 48 hr after transfection. A549 cells were plated in a 6-well plate and infected twice with the harvested virus using 8 µg/ml polybrene followed by puromycin selection (1.5 µg/ml) to get rid of the uninfected cells. As shown in Figure 3.4 B, the efficiency of infection was estimated to be 90% by the number of GFP expressing cells. Two stable sublines were generated in A549 cells: 1) WIP overexpressing cells: A549^{WIP} (A549 cells infected with pLJM1-WIP lentivirus). 2) Control cells with empty plasmid: A549^{CTR} (A549 cells infected with pLJM1 lentivirus). Following puromycin selection, the overexpression was analyzed by western blot analysis. Expression of WIP was found to increase by 85% for A549 cells respectively (Figure 3.4 C-D).
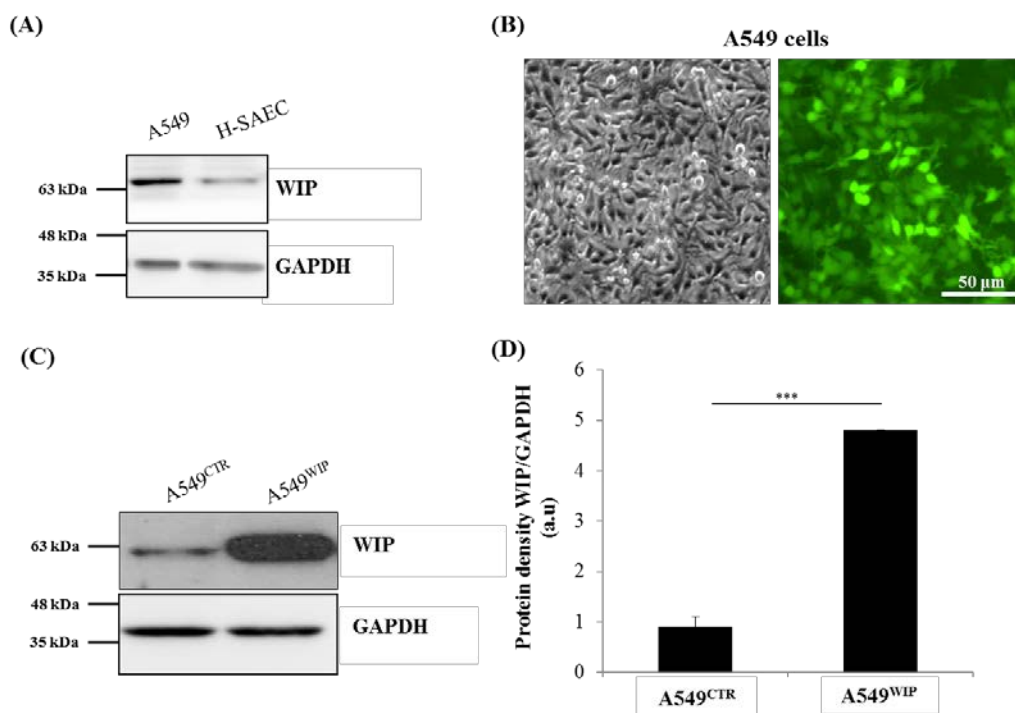
Figure.3.4: Overexpression of WIP in A549 cells by lentiviral transduction
(A) Expression of WIP was compared by western blot analysis in non-cancerous SAEC and cancerous A549 lung cells (B) HEK293T cells were transiently transfected with GFP lentiviral plasmid. Lentivirus was harvested after 24 and 48 hr and uses to transduce A549 cells. Images of GFP virus infected cells were taken using a fluorescence microscope. Scale bar: 50 μm. (C) Infected cells were lysed and expression of WIP was confirmed by western blotting. GAPDH was used as an endogenous control to ensure equal loading of the protein. (D) Densitometric quantification was performed for WIP/GAPDH protein density using ImageJ. (Significance is indicated by stars * p ≤ 0.05, ** p ≤ 0.01, *** p ≤ 0.001).

B) WIP knockdown cells

WIP knockdown cells were generated for A549 cells using lentiviral vectors encoding shRNA targeting the WIP coding region. The efficacy and specificity of the shRNA was tested and stable knockdown cell lines were generated.

Lentivirus was generated using HEK293T cells as described in Section 2.2.3.6. pLKO.1 and pLKO.1-WIP shRNA were transfected into HEK293T packaging cells along with lentiviral packaging plasmids. Viral supernatants were collected at 24 hr and 48 hr after transfection. A549

cells were seeded in a 6-well plate and infected twice with the harvested virus using 8 μg/ml

polybrene followed by puromycin selection (1.5 μg/ml) to get rid of the uninfected cells.

Two stable sublines were generated in A549 cells: 1) WIP knockdown cells: A549$^{WIP\ KD}$ (A549

cells infected with pLKO.1 WIP shRNA lentivirus). 2) Control cells with empty plasmid:

A549^{VECTOR} (A549 cells infected with pLKO.1 lentivirus)

Following puromycin selection, the knockdown was confirmed by western blot analysis.

Expression of WIP was found to decrease by 99% for A549 cells (Figure 3.5).

(A)   **(B)**
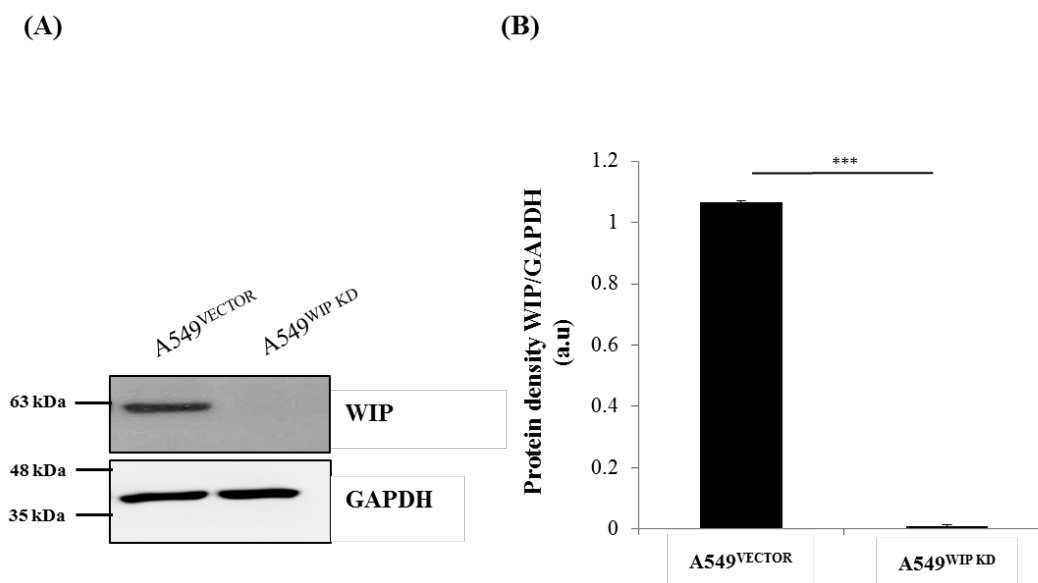
Figure.3.5: Knockdown of WIP expression using human WIP specific shRNA

(A)   Lentiviral   plasmid   encoding   human   WIP   specific   shRNA   (knockdown)   [Sequence:
CCGGCCAATACTGGACAAACCTAAACTCGAGTTTAGGTTTGTCCAGTATTGGTTTTT] and empty plasmid
(control) was used to general lentiviral particles. The virus was used to transduce A549 cells. Infection was
performed twice followed by 1.5 μg/ml puromycin selection for one week. Cells lysate was resolved on 10% SDS-
PAGE. Knockdown of WIP was analyzed by western blot analysis using anti-WIP antibody. GAPDH was used as
an endogenous control (B) Densitometric quantification was performed for WIP/GAPDH protein using ImageJ.
(Significance is indicated by stars * $p \leq 0.05$, ** $p \leq 0.01$, *** $p \leq 0.001$).

3.6 Overexpression of WIP enhanced the migration of cells in a wound healing assay

Cell migration is an important step during metastasis through which cancer cells lose cell-ECM contact by loss of FAs and migrate to neighboring tissues to establish secondary tumors [215]. WIP has been shown to be important for migration of T-cell and macrophages [93]. Since WIP expression is associated with poor prognosis as observed in clinical colorectal specimens [100], we hypothesized that WIP may be essential for cell migration, which is critical for invasion and metastasis. In order to study the role of WIP in migration of epithelial cells, a wound healing assay was performed in WIP overexpressing stable cells. Briefly, cells were allowed to grown to 100% confluency after which a scratch was generated using a sterile pipette tip. Gap closure was observed for 48 hr using a time lapse microscope. Scratch width was measured at timepoints of 0 hr and 24 hr and it was observed that WIP overexpressing cells were able to close the gap faster relative to control cells (Figure 3.6).
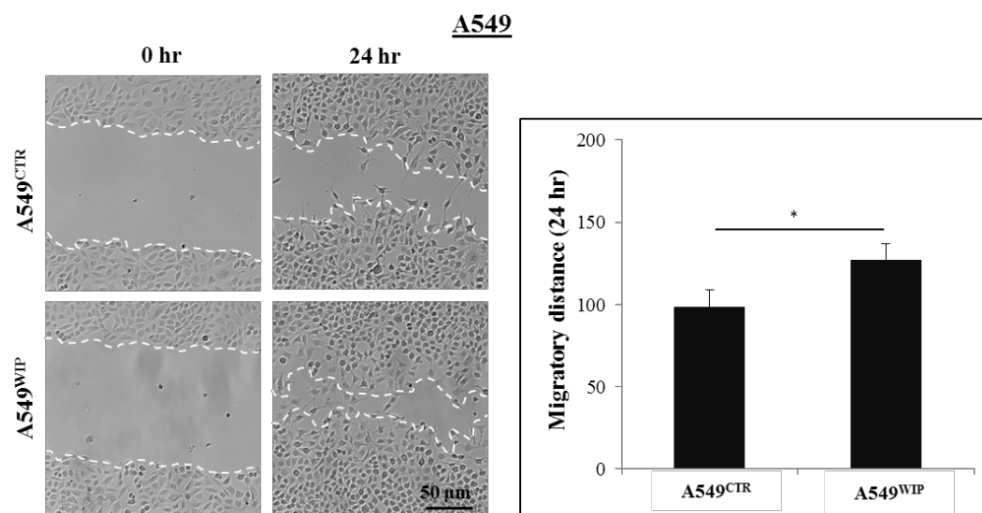
Figure.3.6: WIP overexpressing cells display increased migration in wound healing assay

(A) A549[CTR] and A549[WIP] cells were seeded in a 6 well plate and grown to confluence. A scratch was made in the middle of the culture using a sterile white pipette tip. Cell migration was studied using time lapse microscopy by acquiring images at timepoints of 0 and 24 hr. (B) Distance between edges of wound was measured using Metamorph software and plotted. Data shown are representative of three independent experiments. (Significance is indicated by stars * $p \leq 0.05$, ** $p \leq 0.01$, *** $p \leq 0.001$).

3.7 Knockdown of WIP reduces the migration of cells in a wound healing assay

Overexpression of WIP enhances migration in A549 cells as shown in the wound healing assay (Figure 3.6). Hence, to further investigate whether knockdown of WIP has an effect on cell migration, a wound healing assay was performed. Cells were allowed to migrate for 48 hr and the scratch width was quantified at time points of 0 and 36 hr. It was observed that A549[WIP KD] cells closed the gap slower than the control cells indicating that knockdown of WIP reduced cell migration (Figure 3.7 B).
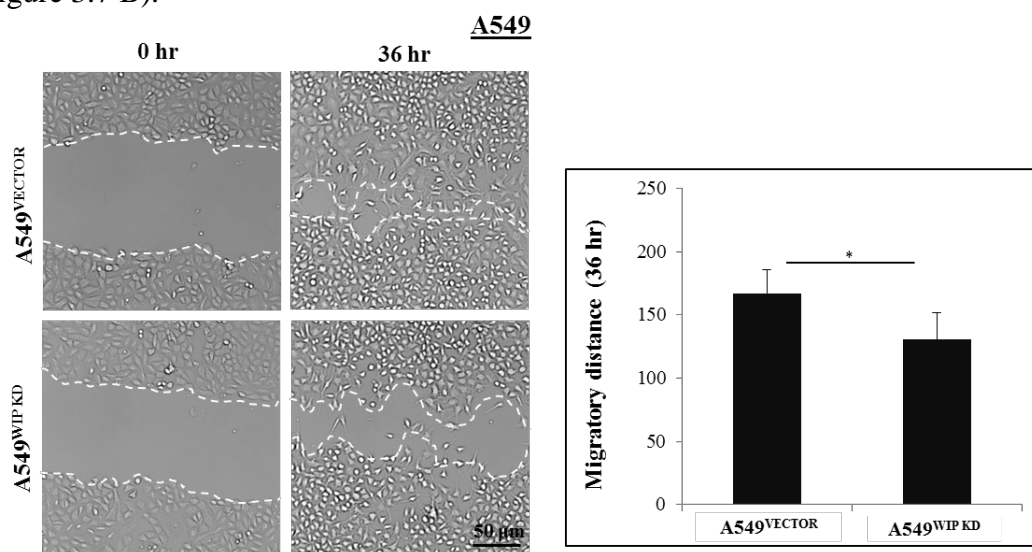
Figure.3.7: WIP deficient cells display decreased migration in wound healing assay
(A) A549[VECTOR] and A549[WIP KD] cells were seeded in equal number onto wells of a 6 well plate and grown to 100% confluence. A scratch was made in the middle of the culture using a sterile white pipette tip. Cell migration was studied using time lapse microscopy by acquiring images at timepoints of 0 and 36 hr. (B) Distance between edges of wound was measured using Metamorph software and plotted. Data shown are representative of three independent experiments. (Significance is indicated by stars * $p \leq 0.05$, ** $p \leq 0.01$, *** $p \leq 0.001$).

3.8 WIP overexpression leads to reduction of vinculin and paxillin patches

Cell-ECM adhesion is facilitated by adhesive structures consisting of integrins and intracellular associated protein clusters known as FAs [216]. FA formation is a key event in cell migration.

Therefore, it was of interest to analyze the effect of knockdown and overexpression of WIP on the localization of FA proteins. Vinculin and paxillin are important proteins present in FAs and are responsible for the assembly and turnover of FAs [217, 218]. Studies have demonstrated that cells with increased motility had reduced number of vinculin patches and knockout of vinculin in MEFs leads to enhanced cell motility [5, 43, 219]. Similarly, paxillin is an adaptor protein which is responsible for integrin mediated signaling at the FAs [220].

Overexpression of WIP enhanced cell migration and knockdown of WIP reduced cell migration in A549 cells (Figure 3.6 and Figure 3.7). Hence, vinculin and paxillin staining was performed to determine if enhanced motility by WIP overexpression is due to the change in the number of vinculin and paxillin patches. Briefly, cells were fixed and stained with anti-vinculin/ anti-paxillin antibody. Phalloidin staining was performed to stain actin filaments. A vinculin/paxillin patch count was performed by manually counting the number of observable patches in 30 randomly selected cells.

As shown in Figure 3.8 and Figure 3.9, A549^{WIP} cells had decreased number of vinculin as well as paxillin patches relative to the control cells. Similarly, knockdown of WIP led to increase in the number of vinculin and paxillin patches in comparison to the control cells. Western blot analysis using WIP overexpression and knockdown cell lines showed that expression of vinculin was unchanged by WIP overexpression (Figure 3.8 C). It is possible that the reduced number of vinculin patches in A549^{WIP} cells may be due to reduced recruitment of vinculin to the FAs and not due to reduced expression of vinculin.

However, expression of paxillin was found to be reduced in WIP overexpressing cells (Figure 3.9 C). Similarly, A549$^{WIP\ KD}$ cells showed increased expression of paxillin which was consistent with the observation in immunostaining (Figure 3.9).
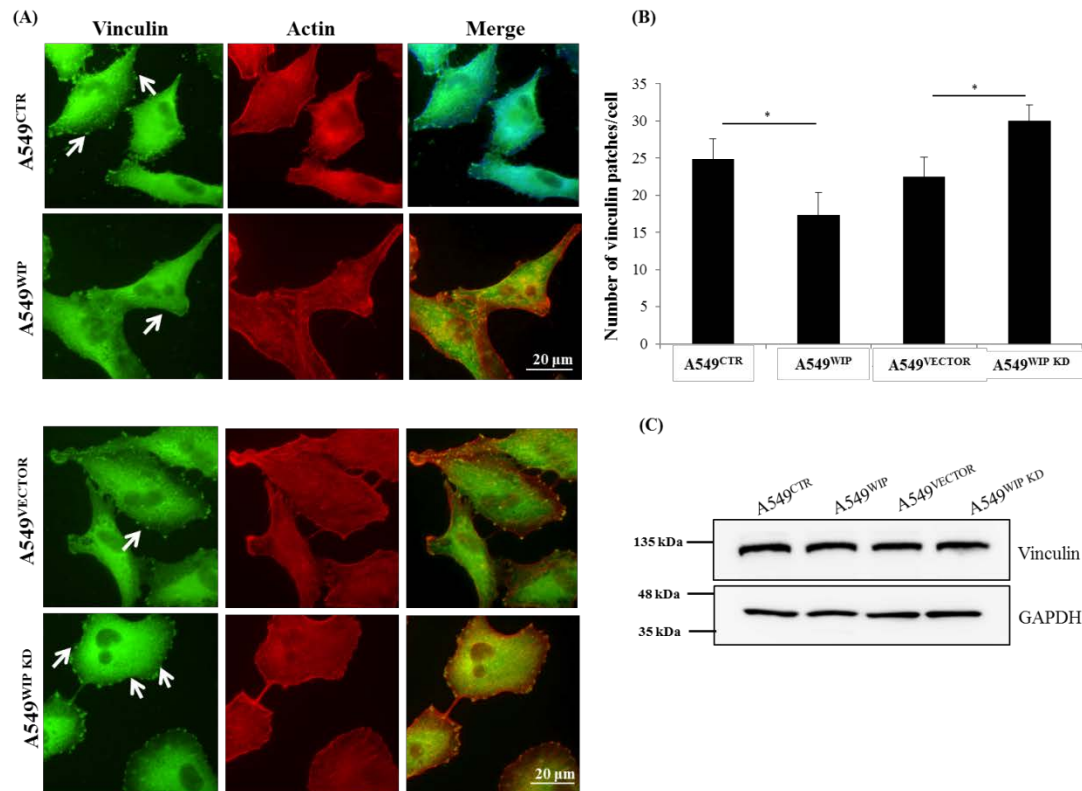
Figure.3.8: WIP overexpression leads to reduced localization of vinculin patches and WIP knockdown leads to increased localization of vinculin patches

(A) Cells were grown on glass coverslips, fixed using formaldehyde and immunostained with anti-vinculin primary antibody and anti-mouse Alexa Fluor (488 nm) secondary antibody. Actin filaments were visualized by phalloidin (594 nm) staining. Arrows denote vinculin patches. Cells were observed under 40X oil lens. Scale bar: 20μm (B) The number of patches per cells were quantified in a total of 30 cells per experiment, which was repeated thrice (C) Cells were lysed and 30 μg of protein was resolved on 10% SDS-PAGE gel and blotted with anti-vinculin antibody. GAPDH was used as a loading control. (Significance is indicated by stars * $p \leq 0.05$, ** $p \leq 0.01$, *** $p \leq 0.001$).
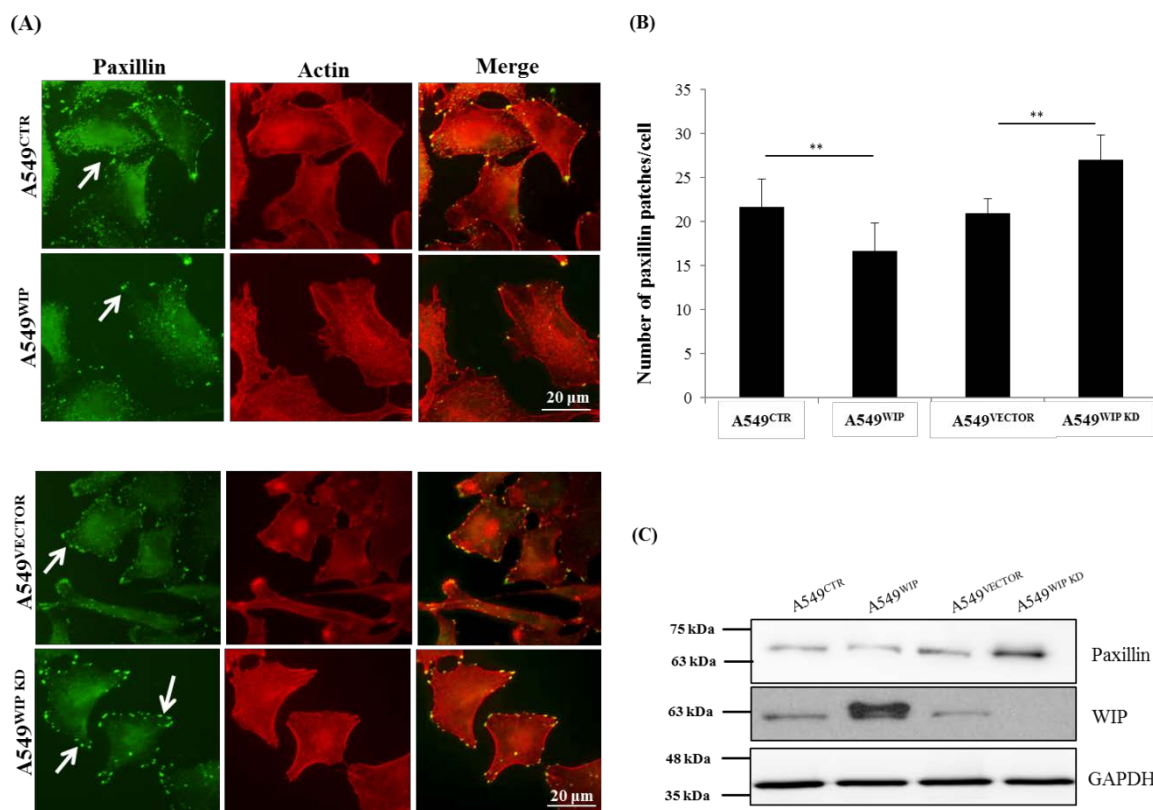
Figure.3.9: WIP overexpression leads to reduced number of paxillin patches and WIP knockdown leads to increased number of paxillin patches

A) Cells were seeded on glass coverslips, fixed using formaldehyde and immunostained with anti-paxillin primary antibody and anti-mouse Alexa Fluor (488 nm) secondary antibody. Actin filaments were visualized by phalloidin staining. Cells were observed under 40X oil lens. Arrows denote paxillin patches. Scale bar: 20µm (B) The number of patches per cells were quantified in a total of 30 cells per experiment, which was repeated thrice (C) Cells were lysed and 30 µg of protein was resolved on 10% SDS-PAGE gel and blotted with anti-paxillin, anti-WIP and anti-GAPDH antibody (loading control). (Significance is indicated by stars * $p \leq 0.05$, ** $p \leq 0.01$, *** $p \leq 0.001$).

3.9 Overexpression of WIP in A549 cells enhanced invasion in a matrigel invasion assay

Cell invasion is an integral step involved in processes such as embryonic development as well as adult immune surveillance [221]. Invasive ability is restricted to specific cell types in adult tissues such as immune cells. This restriction of invasion is lost in cancerous cells which can invade through ECM degradation and metastasize to distant organs [8]. A549 cells are highly invasive and are known to exhibit invasion on basement membrane matrix such as matrigel. WIP

is known to localize at invadopodia and studies in breast cancer cells have shown that WIP is essential for matrix degradation [107]. To determine whether overexpression of WIP affects the invasive ability of epithelial cancer cells, an invasion assay was performed using a transwell coated with matrigel. As shown in Figure.3.10, overexpression of WIP increased the invasiveness of A549 cells. Cells with empty vector showed lesser invasive ability as compared to WIP overexpressing cells, as indicated by a marked reduction in the number of cells that invaded the bottom chamber of the transwell (Figure 3.10 A).

(A)   **(B)**
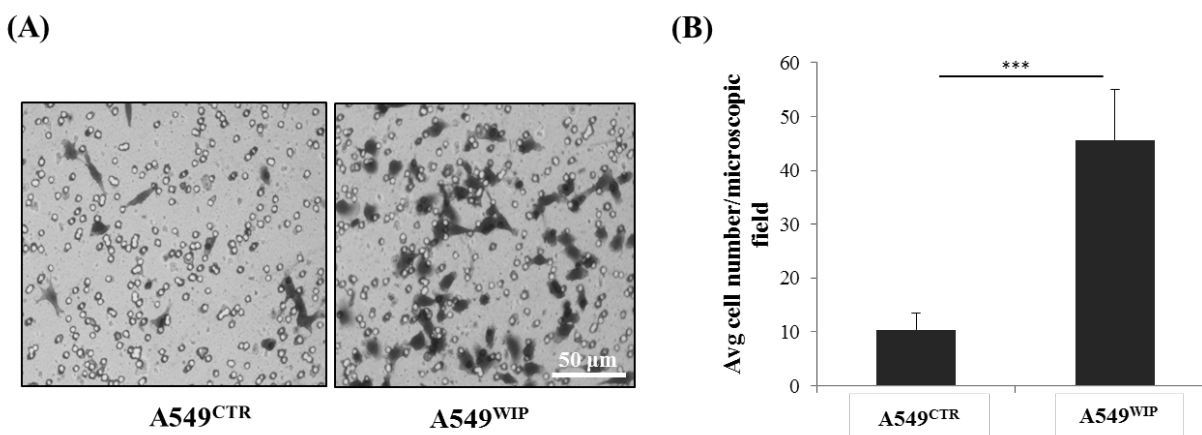
Figure.3.10: Overexpression of WIP increases invasive ability in A549 cells.

(A) Matrigel (2mg/ml) was used to coat the upper chamber of an 8 μm transwell. Cells were allowed to invade through the matrigel for 36 hr. Invasive cells at the bottom of the chamber were fixed with formaldehyde and stained with 1% crystal violet in methanol. (B) The number of cells/microscopic field was calculated for five microscopic fields using a 10X objective lens. Data shown are representative of three independent experiments. (Significance is indicated by stars * $p \leq 0.05$, ** $p \leq 0.01$, *** $p \leq 0.001$).

3.10 WIP regulates cell proliferation in A549 cells

Dysregulation of the cell cycle is a fundamental feature of cancer pathogenesis. Genes important for cell cycle and proliferation are found to be upregulated in most tumor microarray datasets and indicate poor prognosis [222]. After establishing a role of WIP in cell migration and cell spreading, we wanted to check if WIP influences the proliferation of cancer cells. MTT assay was performed on WIP overexpressing and WIP knockdown cells to analyze the effect of WIP on cell proliferation. As shown in Figure.3.11, WIP overexpression significantly increased the cell proliferation till 48 hr relative to the control A549^{CTR} cells. On the contrary, WIP knockdown cells showed reduced proliferation as compared to the control cells which was also evident by the slow growth during routine subculture of cells.
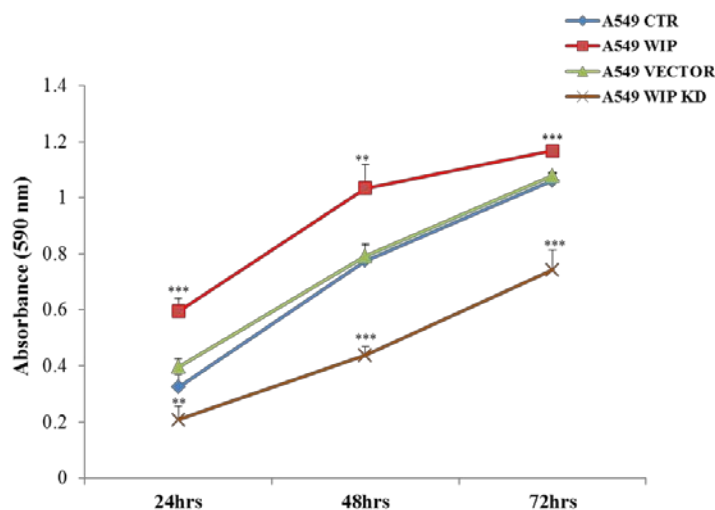
Figure.3.11: Overexpression of WIP enhanced cell proliferation and knockdown of WIP lowered cell proliferation rate

Proliferation of the cells was analyzed by performing MTT assay. 5000 cells were seeded in triplicates in a 96-well plate. Cell proliferation was measured at 24-, 48- and 72- hr intervals as described in Section (2.2.4.7). The absorbance was measured at 590 nm using Tecan plate reader. Wells containing media were used to subtract the background. (Significance is indicated by stars * $p \leq 0.05$, ** $p \leq 0.01$, *** $p \leq 0.001$).

3.11 Knockdown of WIP alters the cell morphology and cytoskeleton organization in A549 cells

Actin cytoskeleton plays a critical role in cell physiology and disease because of its importance in cell migration and cell adhesion [223]. Previous studies with WIP have shown that WIP directly binds to actin and regulates actin polymerization [79]. To determine the effect of WIP knockdown on cell spreading and cytoskeleton, phalloidin staining was carried out for F-actin visualization in WIP overexpressing and WIP knockdown cells. Knockdown of WIP led to progressive shrinkage of cells with reduction in cell size and overexpression of WIP led to a more elongated cell phenotype (Figure 3.12). Cell area and cell perimeter was quantified using ImageJ software to analyze the differences in cell morphology. As shown in Figure 3.12 (B-I and B-II), cell area and cell perimeter was significantly reduced by knockdown of WIP in A549 cells. There was no significant change observed for cell area and cell perimeter for WIP overexpressing cells.

(A)

(B-I)

(B-II)
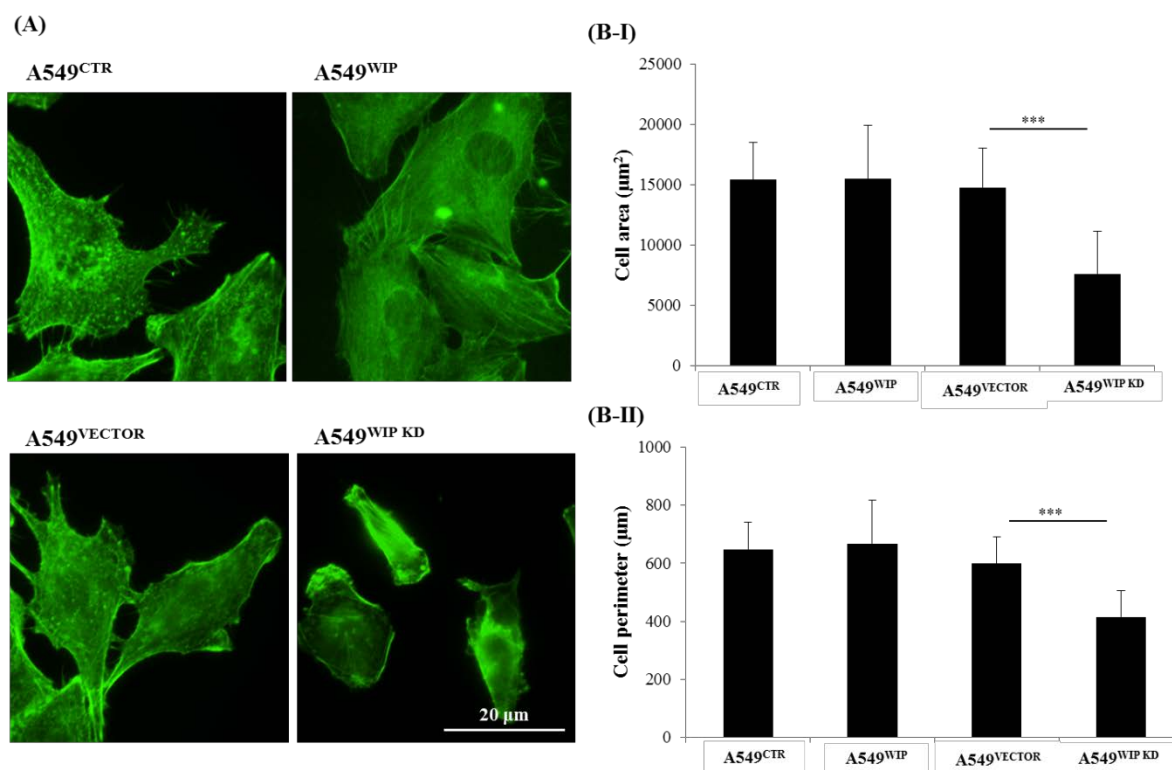
Figure.3.12: Knockdown of WIP causes reduction in cell size of A549 cells

(A) Cells were grown to a 40-50% confluence on coverslips, fixed and stained with phalloidin to visualize actin filaments. Images were captured using a 40X objective lens. Scale bar: 20μm (B) Quantification of cell area (I) and cell perimeter (II) was performed for 30 cells/experiment using ImageJ. (Significance is indicated by stars * $p \leq 0.05$, ** $p \leq 0.01$, *** $p \leq 0.001$).

3.12 Knockdown of WIP leads to enhanced cell spreading on fibronectin coated surface

Cell spreading is tightly linked with cell adhesion and well-defined cell spreading depends on integrity and assembly of actin cytoskeleton in terms of FA assembly and cell contractility [224]. As shown in Figure 3.12, A549$^{WIP\ KD}$ show reduced cell size as well as reduced cell perimeter. Hence, it was of interest to determine the adhesion characteristics of WIP deficient cells by analyzing their ability to spread on fibronectin coated surface. Spreading assay was performed as described in section 2.2.4.5. Briefly, cells were trypsinised, washed with PBS and seeded in 96-well plate coated with fibronectin followed by blocking with BSA. Cells were monitored for

different time intervals for their ability to spread on fibronectin surface. As shown in Figure 3.13

A, A549$^{WIP\ KD}$ cells spread faster on fibronectin coated surface as compared to A549^{VECTOR} cells.

No significant difference was observed for spreading of A549^{WIP} cells in comparison to A549^{CTR}

cells (Figure 3.13 B). Surface area of cells was quantified at different time points of spreading

and plotted. As shown in Figure 3.13 B, knockdown of WIP enhanced spreading of A549 cells

on fibronectin coated surface.
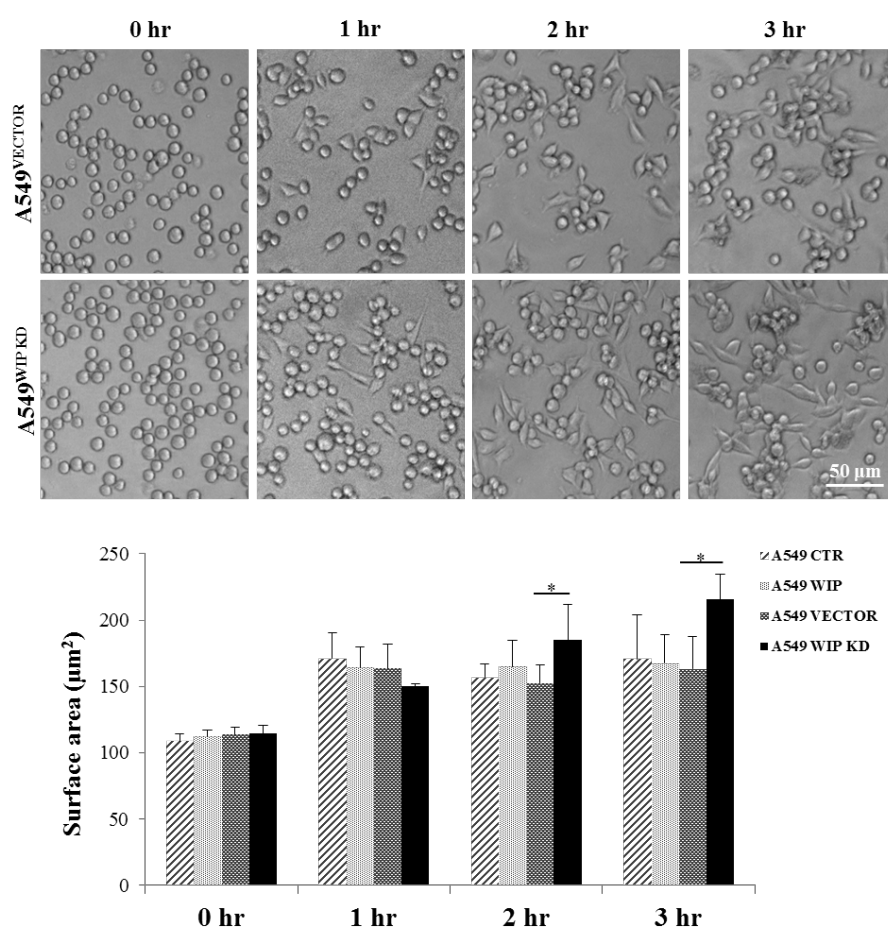
Figure.3.13: WIP knockdown cells show enhanced spreading on fibronectin coated surface
(A) A549^{VECTOR} and A549$^{WIP\ KD}$ cells were trypsinised and serum starved for 30 min. After starvation, cells were seeded onto the wells of a 96 well plate coated with fibronectin (1.41 µg/ml). Cells were allowed to spread for 3 hr and images were captured after every 60 min using Metaview software. Scale bar: 50µm. (B) Surface area of the cells was measured at each of the time points using ImageJ. (Significance is indicated by stars * $p \leq 0.05$, ** $p \leq 0.01$, *** $p \leq 0.001$).

3.13 Overexpression of WIP enhances anchorage independent growth of A549 cells in soft agar

Anchorage independent cell growth also referred to as anoikis resistance is a feature of malignant transformation [225]. The effect of WIP on anchorage independent growth was analyzed by performing soft agar colony formation assay. This assay helps to characterize the anchorage independent growth ability of adherent cells. Cells are grown in soft agar to prevent attachment to tissue culture plate and allowed to form colonies. Briefly, a 6-well plate was coated with 0.8% noble agar in complete media (DMEM + 10% FBS) to form a bottom layer of agar. After the bottom agar layer is solidified, cells were suspended in 0.3% agar maintained at 40°C and added on the bottom layer. The top layer was allowed to solidify and topped up with 500 ul complete media periodically to prevent dessication. Plates were incubated at 37°C for 4 weeks. The colonies were stained using nitroblue tetrazolium chloride and the number of colonies was quantified. As shown in Figure 3.14, overexpression of WIP led to significant increase in the number of colonies in soft agar as compared to the control cells. A549^{WIP} cells formed larger colonies relative to A549^{CTR} cells (Figure 3.14 B).

Since, overexpression of WIP was found to enhance the proliferation rate of A549 cells (Figure 3.11), it may be one of the reasons for larger sized colonies in soft agar assay. Another possible reason can be that overexpression of WIP makes the cells highly transformed and allows them to grow independent of substrate attachment.

Knockdown of WIP did not significantly affect the number of colonies growing in soft agar. However, the colonies formed by A549$^{WIP\ KD}$ cells were smaller in size in comparison to control

cells. This may be due to the reduced proliferation rate of WIP knockdown cells. Thus, soft agar

assay suggests that WIP positively promotes anchorage independent cell growth in A549 cells.
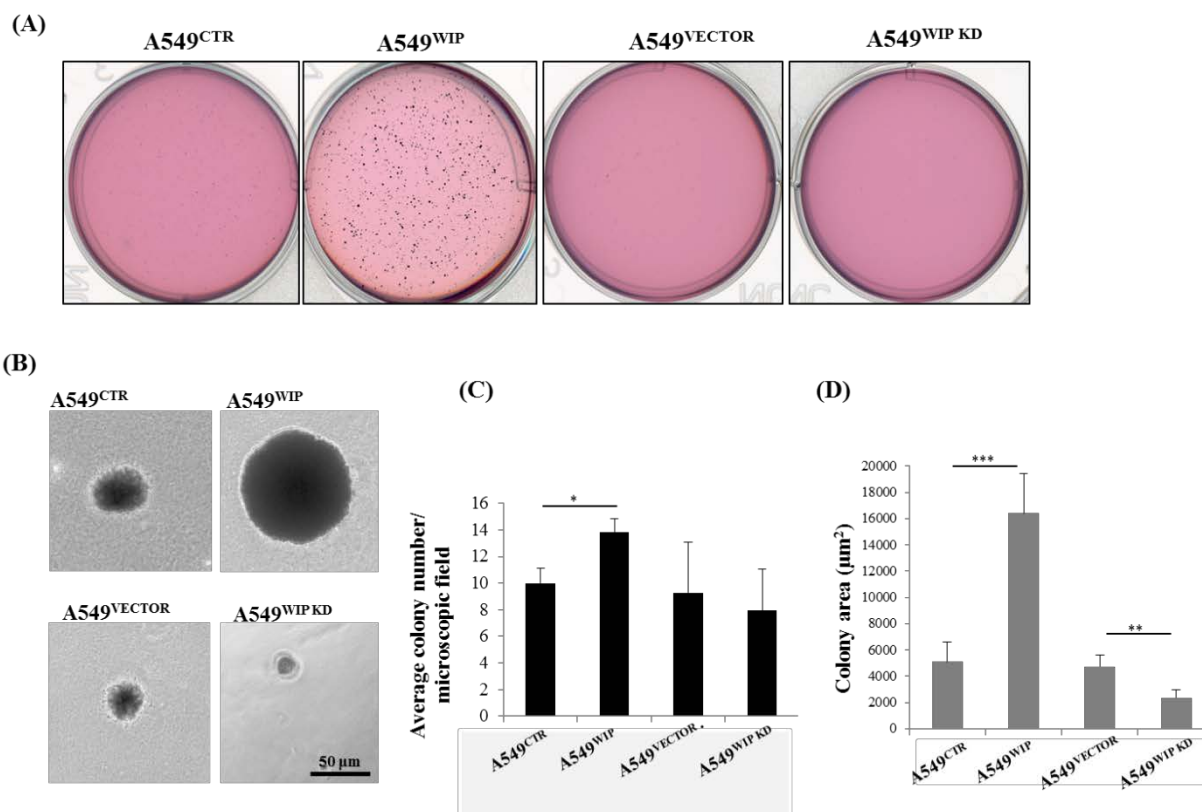
Figure 3.14 : Overexpression of WIP enhances anchorage independent growth of A549 cells in soft agar

(A) A549^{CTR}, A549^{WIP}, A549^{VECTOR} and A549$^{WIP\ KD}$ cells were subjected to soft agar assay. 6-well plate was coated with 0.8% noble agar. 2 x 10^5 cells were mixed with 0.3% noble agar and added on the solidified bottom agar. Plates were incubated for 4 weeks at 37°C and the resulting colonies were stained with 1 mg/ml nitroblue tetrazolium chloride. Plates were scanned and scanned digital images are shown (B) Images from the soft agar assay were captured with a 10X objective using a phase contrast microscope. Scale bar: 50 μm (C) Graph represents number of colonies per microscopic field. Images were caputured using a 4X objective and average number of colonies per microscopic field was quantified. 10 fields were counted for each sample in triplicates (D) Graph represents average colony size which is quantified by quantifying the area of colonies (μm^2) using ImageJ software (Significance is indicated by stars * p $\leq$ 0.05, ** p $\leq$ 0.01, *** p $\leq$ 0.001).

3.14 Induction of EMT in A549 cells using TGF-beta

Overexpression of WIP has shown to enhance cell proliferation, migration and invasion in A549 cells. It is possible that WIP may be regulating metastasis or it may be an effector of metastasis. Hence, the next step was to investigate if WIP is important for malignant transformation of cells during metastasis by investigating its role in EMT. Induction of EMT was carried out using TGF-beta. TGF-beta mediated EMT is widely studied in A549 cells, as these cells show distinct morphological changes in presence of TGF-beta. Hence, A549 cells were used to study role of WIP in TGF-beta induced EMT. For EMT induction, A549 cells were allowed to grow to 40-50% confluence. The cells were serum starved for 12 hr and varying concentrations (2 ng, 5 ng, 10 ng) of TGF-beta were added to the cells (Figure 3.15 A). After 48 hr of TGF-beta induction, analysis of EMT markers expression was performed by western blotting. 5 ng TGF-beta was found to be optimum in inducing EMT with the loss of epithelial marker E-cadherin and gain of mesenchymal markers N-cadherin, vimentin and α-SMA (Figure 3.15 B). Immunostaining was performed to analyze the morphological changes in the actin cytoskeleton. As shown in Figure 3.15 C, TGF-beta treated cells looked elongated and dispersed which was evident in F-actin staining.

A549 cells

(A)

Control   2ng   5ng   10ng   TGF-beta

50 μm

(B)

Control 2ng 5ng 10ng TGF-beta

135 kDa —
100 kDa —
E-cadherin

63 kDa —
Vimentin

63 kDa —
α-Smooth muscle actin
48 kDa —

135 kDa —
N-cadherin
100 kDa —

35 kDa —
GAPDH

(C)

F-Actin staining

TGF-beta
(5 ng)   -   +

20 μm
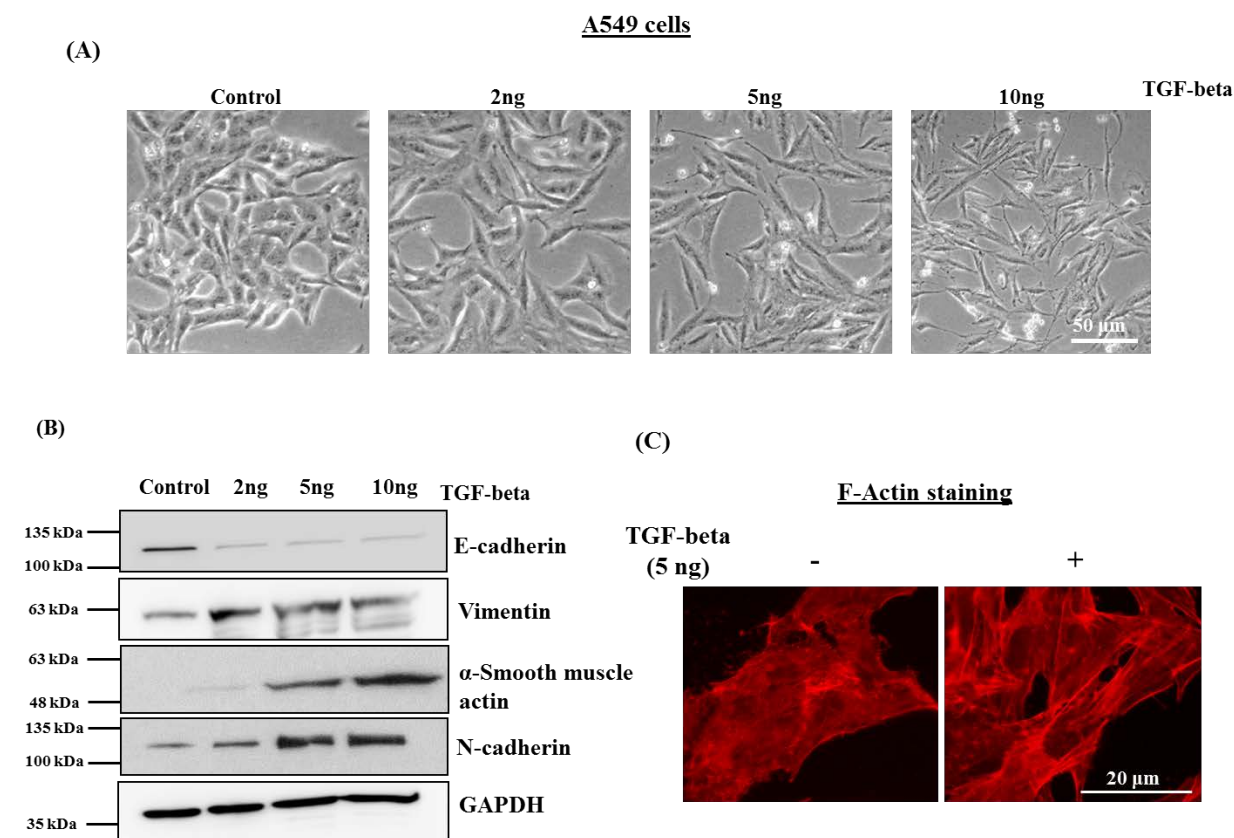
Figure.3.15: Induction of EMT in A549 cells using TGF-beta

(A) Morphological changes induced by different concentration of TGF-beta in A549 cells. A549 cells were grown to 40% confluence and serum starved for 12 hr. Cells were cultured in serum free medium without (control) and with TGF-beta at varying concentrations (2 ng, 5 ng and 10 ng) for 48 hr. Cell morphology was photographed with a 10X objective using a phase contrast microscope. Scale bar: 50μm (B) Effect of TGF-beta on A549 cells was analyzed by checking expression E-cadherin, N-cadherin, vimentin and α-SMA. Cells were lysed with/without TGF-beta and resolved on a 10% SDS-PAGE gel. GAPDH was used as loading control to ensure equal loading of the samples. (C) Phalloidin staining was performed to visualise actin cytoskeleton changes in control and TGF-beta treated A549 cells. Images were captured using a fluorescence microscope and 40X objective lens. Scale bar: 20 μm.

3.15 Expression of WIP increases in TGF-beta induced EMT in A549 cells

EMT was induced in A549 cells using 5 ng TGF-beta. Briefly, cells were allowed to grow till 40-50% confluency and serum starved for 12 hr. Cells were treated with 5 ng TGF-beta and incubated at 37°C for 48 hr. The cells were lysed in lysis buffer and western blotting was

performed to analyze expression of WIP. As shown in Figure 3.16 A-B, expression of WIP was

found to increase in a time-dependent manner in presence of TGF-beta as compared to the

untreated (control) cells. This suggests that expression of WIP is regulated by TGF-beta and WIP

may play a role in TGF-beta induced EMT.
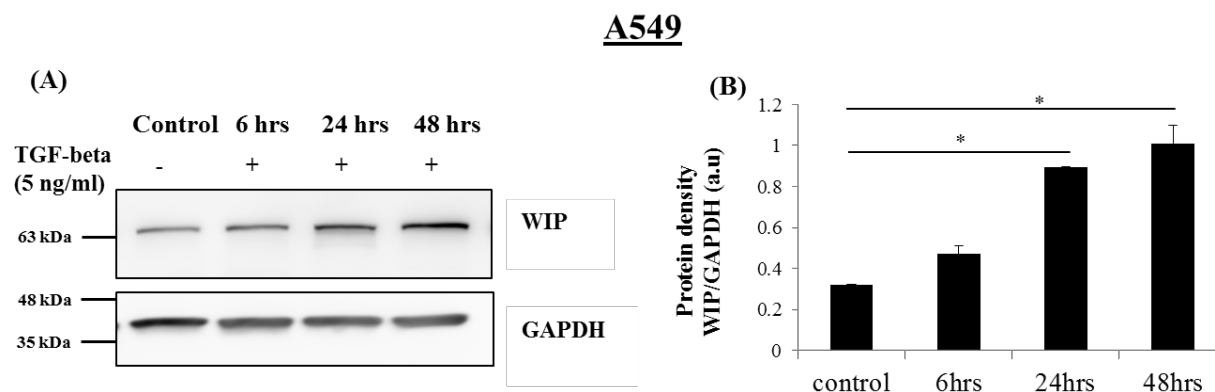
A549

Figure.3.16: Expression of WIP increases in presence of TGF-beta
(A) A549 cells were serum starved for 12 hrs followed by treatment with 5 ng/ml TGF-beta for various time points (6 hr, 12 hr, 24 hr and 48 hr). Cells were lysed and cell lysate was resolved on a 10% SDS-PAGE gel. Expression of WIP was analyzed by western blot analysis and GAPDH was used to ensure equal loading (B) Densitometric analysis of WIP/GAPDH ratio using ImageJ software. (Significance is indicated by stars * $p \leq 0.05$, ** $p \leq 0.01$, *** $p \leq 0.001$).

In order to determine if the localization of WIP is affected in presence of TGF-beta, A549 cells

were seeded in coverslips and transfected with a plasmid expressing WIP-GFP. Expression of

WIP was determined by western blot analysis and is shown in Figure 3.17 B. Transfected cells

were serum starved and EMT was induced with TGF-beta for 48 hr. As shown in Figure 3.17 A,

in presence of TGF-beta, A549 cells underwent morphological changes to become more

elongated. Interestingly, WIP-GFP was found to localize to membrane protrusions (denoted by

arrows) after 48 hr in presence of TGF-beta. These membrane protrusion were found to co-

localize with F-actin as seen by phalloidin staining. Staining for FA proteins such as vinculin and

paxillin did not reveal co-localization with WIP-GFP. Since overexpression of WIP led to enhanced cell migration and invasion in A549 cells, it may be possible that WIP positively regulates cell migration and invasion during EMT.
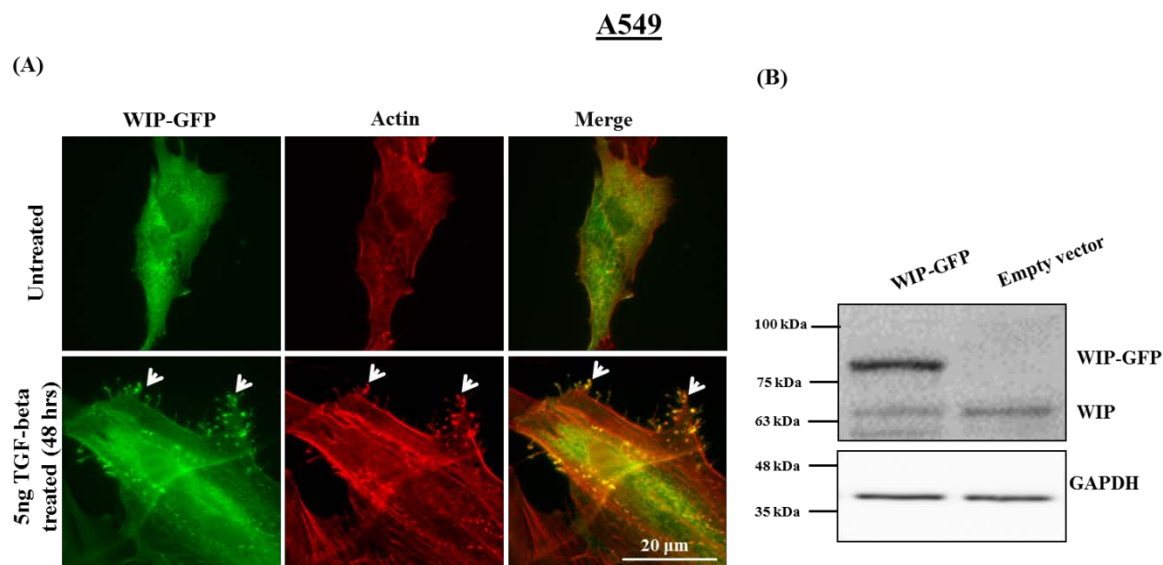
Figure 3.17: TGF-beta causes WIP to localize to membrane protrusions in A549 cells
(A) WIP-GFP was transfected in A549 cells and the cells were treated with 5 ng TGF-beta. After 48 hrs, the cells were fixed and stained for F-actin. Localization of WIP was observed using a fluorescence microscope and 40X objective lens. Arrows indicate membrane protrusive structures showing co-localization of WIP-GFP with F-actin. Scale bar: 20 μm (B) Western blot showing expression of WIP-GFP and control empty plasmid in A549 cells. Cells were transfected with empty plasmid and WIP-GFP expressing plasmid and EMT was induced using 5 ng/ml TGF-beta.

3.16 Overexpression of WIP enhances E-cadherin loss/ EMT progression in A549 cells

Expression of WIP was found to be elevated during TGF-beta induced EMT. Therefore, it was of interest to investigate whether overexpression of WIP would accelerate EMT progression. For this purpose, A549^{WIP} and A549^{CTR} cells were treated with TGF-beta to undergo EMT. After 48 hr of TGF-beta treatment, the cells were lysed and western blotting was performed to analyze expression of EMT markers. As shown in Figure 3.18 B, A549^{WIP} cells showed greater

repression of E-cadherin as compared to A549^{CTR} cells in presence of TGF-beta. Increase in expression of mesenchymal markers α-SMA, N-cadherin and vimentin was enhanced in TGF-beta treated A549^{WIP} cells as compared to the A549^{CTR} cells. TGF-beta treated A549^{WIP} cells showed a more slender and elongated phenotype (Figure 3.18 A) in comparison to A549^{CTR} cells.
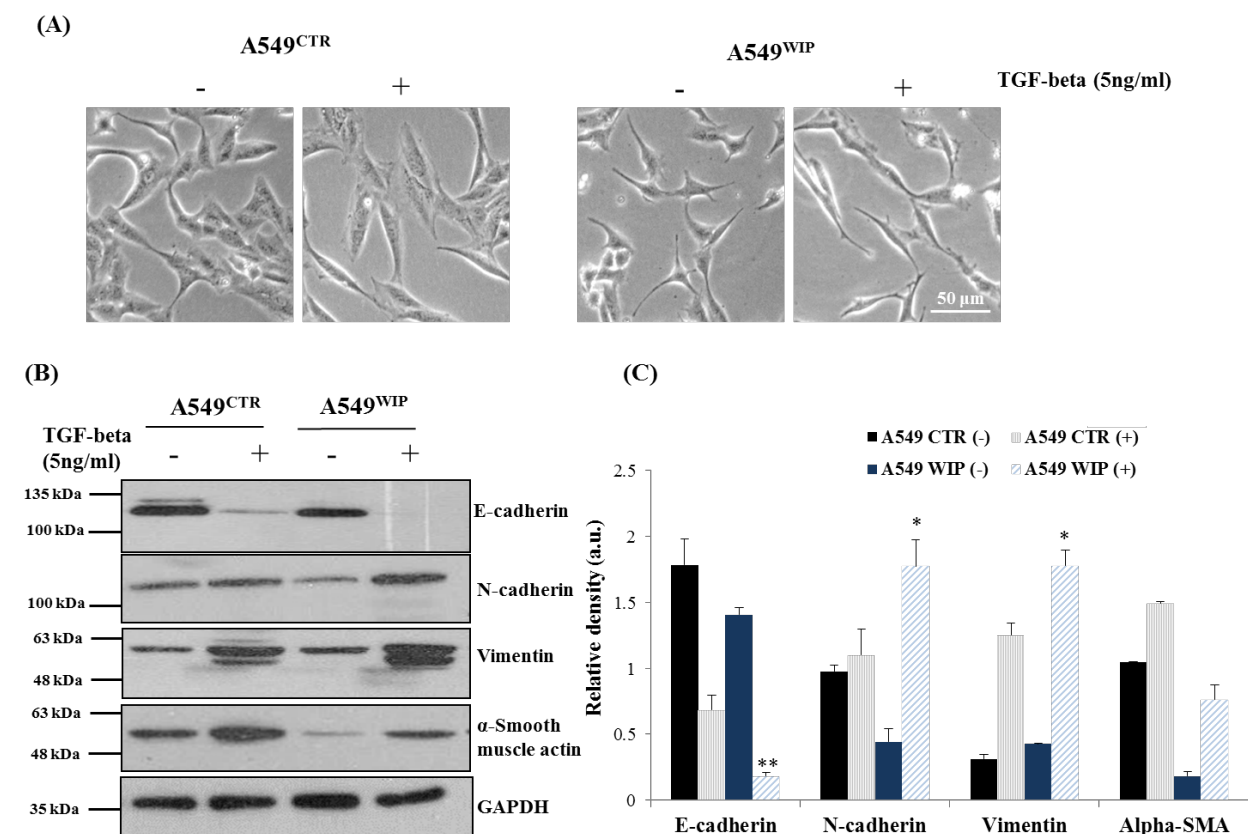
Figure.3.18: Overexpression of WIP enhances E-cadherin loss/ EMT progression in A549 cells

(A) A549^{CTR} and A549^{WIP} cells were induced with 5ng/ml TGF-beta to study the effect of WIP overexpression in TGF-beta induced EMT. Morphological changes during EMT were observed by capturing images of the cells using a 10X objective lens. Scale bar: 50μm. (B) TGF-beta treated A549^{CTR} and A549^{WIP} cells were lysed and blotted for expression of EMT markers E-cadherin, N-cadherin, vimentin and α-SMA. GAPDH was used to ensure equal loading of lysates (C) Densitometric quantification of EMT markers was performed using ImageJ software. (Significance is indicated by stars * $p \leq 0.05$, ** $p \leq 0.01$, *** $p \leq 0.001$).

(D)
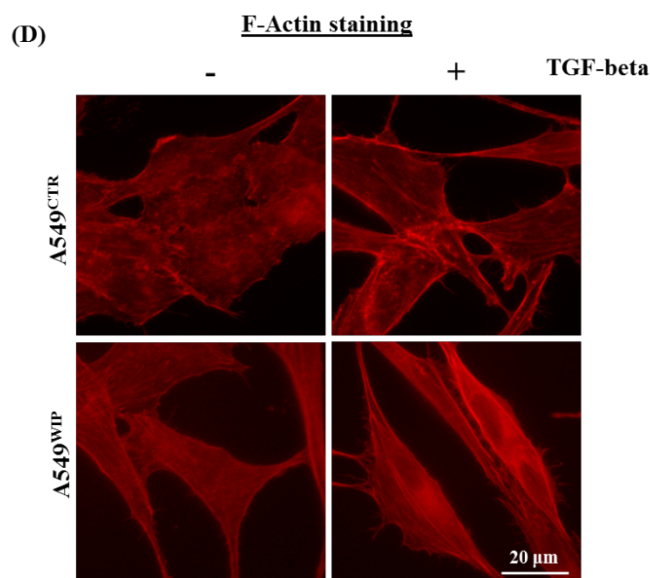
F-Actin staining

Figure.3.18: Overexpression of WIP enhances E-cadherin loss/ EMT progression in A549 cells

(D) A549^{CTR} and A549^{WIP} cells were seeded on coverslips and treated with 5 ng TGF-beta for 48 hr. Phalloidin staining was performed to observe changes in actin cytoskeleton during EMT progression and images were captured using 40X objective lens using a fluorescence microscope. Scale bar: 20 μm.

Phalloidin staining was performed to visualize actin cytoskeleton. A549^{WIP} cells showed a more elongated and spindle shaped morphology as observed by phalloidin staining (Figure 3.18 D). This suggests that overexpression of WIP helps the cells to acquire a migratory and mesenchymal phenotype.

3.17 Knockdown of WIP in A549 cells inhibited morphological changes associated with EMT

Increased expression of WIP during TGF-beta induced EMT suggests that WIP might be playing a role in EMT progression. Therefore, it was of interest to investigate whether knockdown of WIP influences TGF-beta induced EMT. For this purpose, A549$^{WIP\ KD}$ and A549^{VECTOR} cells were treated with TGF-beta for 48 hr. Western blot was performed at the end of 48 hr to analyze

the expression of EMT markers (Figure 3.19 A). After TGF-beta treatment, it was observed that A549$^{WIP\ KD}$ cells failed to acquire the characteristic morphological changes observed for cells undergoing EMT. A549^{VECTOR} cells treated with TGF-beta were elongated, dispersed and assumed a fibroblast like morphology (Figure 3.19 C). However, TGF-beta treated A549$^{WIP\ KD}$ cells did not show any dramatic morphological changes as compared to the TGF-beta treated A549^{VECTOR} cells. This result was evident by immunostaining with F-actin staining as shown in Figure 3.19 D. Although the loss in E-cadherin expression for TGF-beta treated A549$^{WIP\ KD}$ cells was slightly lower than A549^{VECTOR} cells, the gain in vimentin and α-SMA was not significant as A549^{VECTOR} cells (Figure 3.19 B-C). A549$^{WIP\ KD}$ cells treated with TGF-beta showed reduced levels of mesenchymal markers α-SMA and N-cadherin as compared to the untreated A549$^{WIP\ KD}$ cells (Figure 3.19 A-B). This suggests that knockdown of WIP in A549 cells inhibited the expression of mesenchymal markers associated with TGF-beta induced EMT.
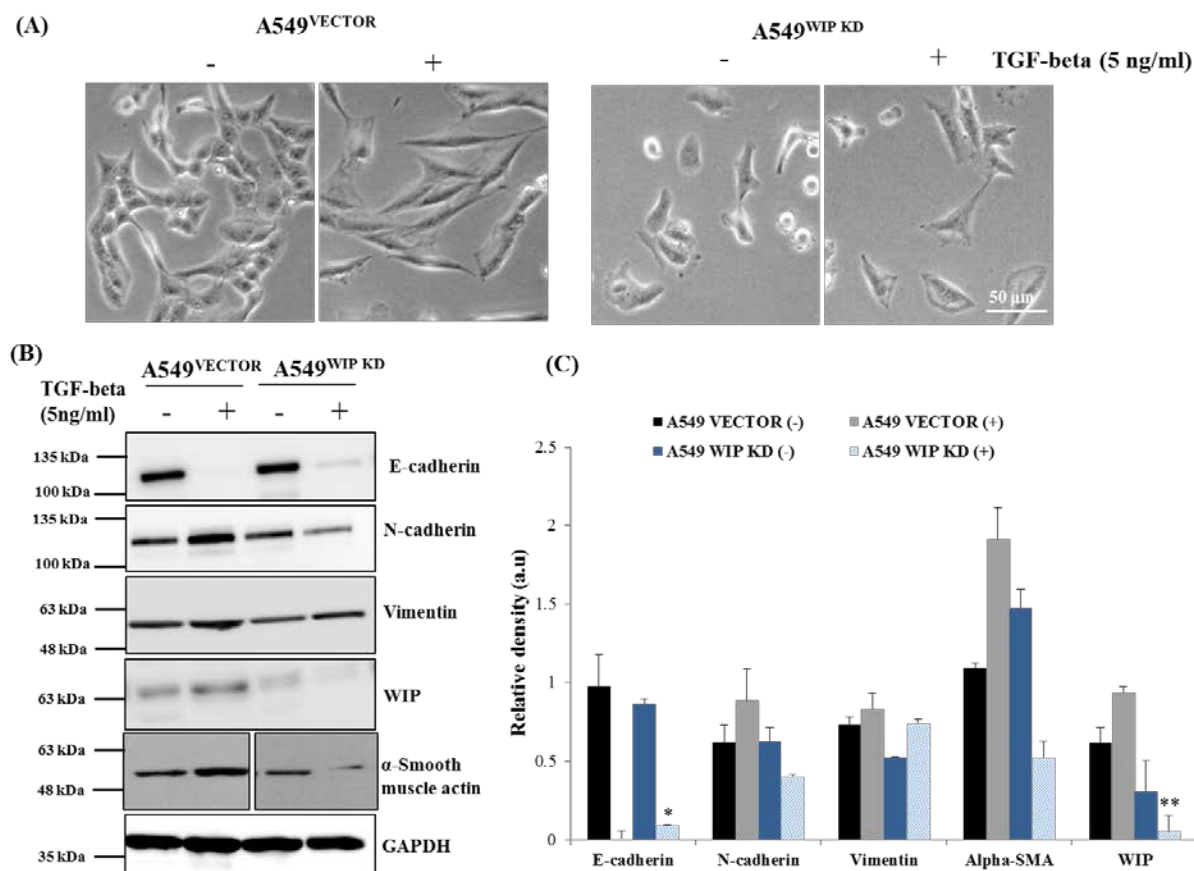
Figure.3.19: Knockdown of WIP in A549 cells antagonized morphological changes induced by TGF-beta

(A) A549^{VECTOR} and A549$^{WIP\,KD}$ cells were induced with 5 ng/ml TGF-beta to study the effect of WIP knockdown in TGF-beta induced EMT. Morphological changes during EMT were observed by capturing images of the cells using a 10X objective lens. Scale bar: 50 μm (B) TGF-beta treated A549^{VECTOR} and A549$^{WIP\,KD}$ cells were lysed and the lysates were resolved on a 10% SDS-PAGE gel. Expression of WIP and EMT markers such as E-cadherin, N-cadherin, vimentin and α-SMA was analyzed by western blotting. GAPDH was used to ensure equal loading of lysates (C) Densitometric quantification of EMT markers was performed using ImageJ software. (Significance is indicated by stars * p ≤ 0.05, ** p ≤ 0.01, *** p ≤ 0.001).

F-Actin staining

(D)
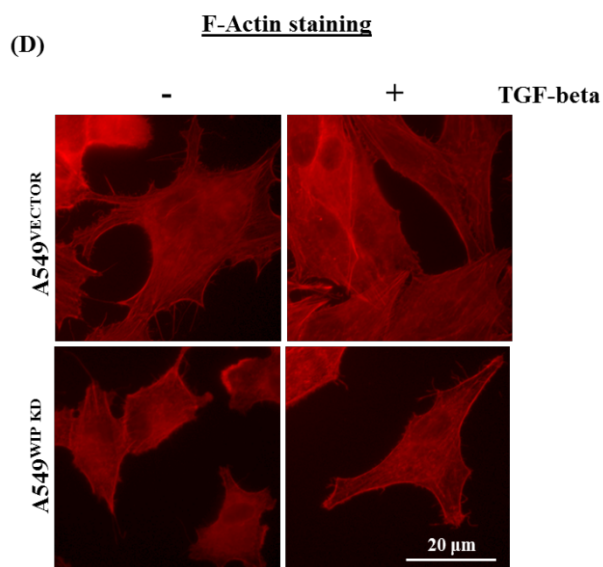
Figure.3.19: Knockdown of WIP in A549 cells antagonized morphological changes induced by TGF-beta

(D) A549^{VECTOR} and A549$^{WIP\ KD}$ cells were seeded on coverslips and treated with 5 ng TGF-beta for 48 hr. Phalloidin staining was performed to observe changes in actin cytoskeleton during EMT progression and images were captured using 40X objective lens using a fluorescence microscope. Scale bar: 20 μm.

As shown in Figure 3.19, A549$^{WIP\ KD}$ cells failed to undergo the morphological changes induced by TGF-beta as compared to A549^{VECTOR} cells. To confirm this result, stable induction of EMT was performed by ectopic expression of Snail transcription factor. Snail is direct repressor of E-cadherin expression and it has been reported that exogenous expression of Snail causes loss of cell-cell adhesion and induction of EMT phenotype [226, 227]. Snail was overexpressed in A549^{VECTOR} and A549$^{WIP\ KD}$ cells using a inducible lentivirus system. The vector used for inducible snail expression (pTripz-Snail) is engineered to be Tetracycline-on (Tet-on) and causes tightly controlled expression of Snail in the presence of doxycycline. The control plasmid (pTripz) contains a RFP reporter driven by the Tetracycline response element (TRE) which helps to monitor delivery efficiency and activity of promoter. In presence of doxycycline, the control

plasmid (pTripz) expressed RFP and the Snail inducible plasmid (pTripz-Snail) induces expression of Snail protein. 2 μg/ml of Doxycycline was found to be optimal for inducing maximum expression without causing cell toxicity. As shown in Figure 3.20 A, addition of control plasmid to A549^{VECTOR} and A549$^{WIP\,KD}$ cells led to expression of RFP in ~90-100% cells. Expression of Snail in control and WIP knockdown cells was assessed by western blot (Figure 3.20 C). Expression of WIP was not affected by Snail induction which indicates that Snail may not be regulating WIP expression. As shown in Figure 3.20 B, A549^{VECTOR} cells infected with Snail inducing plasmid underwent morphological changes to become more elongated and dispersed in presence of doxycycline. However, no morphological changes were observed for WIP knockdown cells by the overexpression of Snail. This confirmed that knockdown of WIP did not allow the cells to attain morphological changes associated with transient as well as stable EMT.
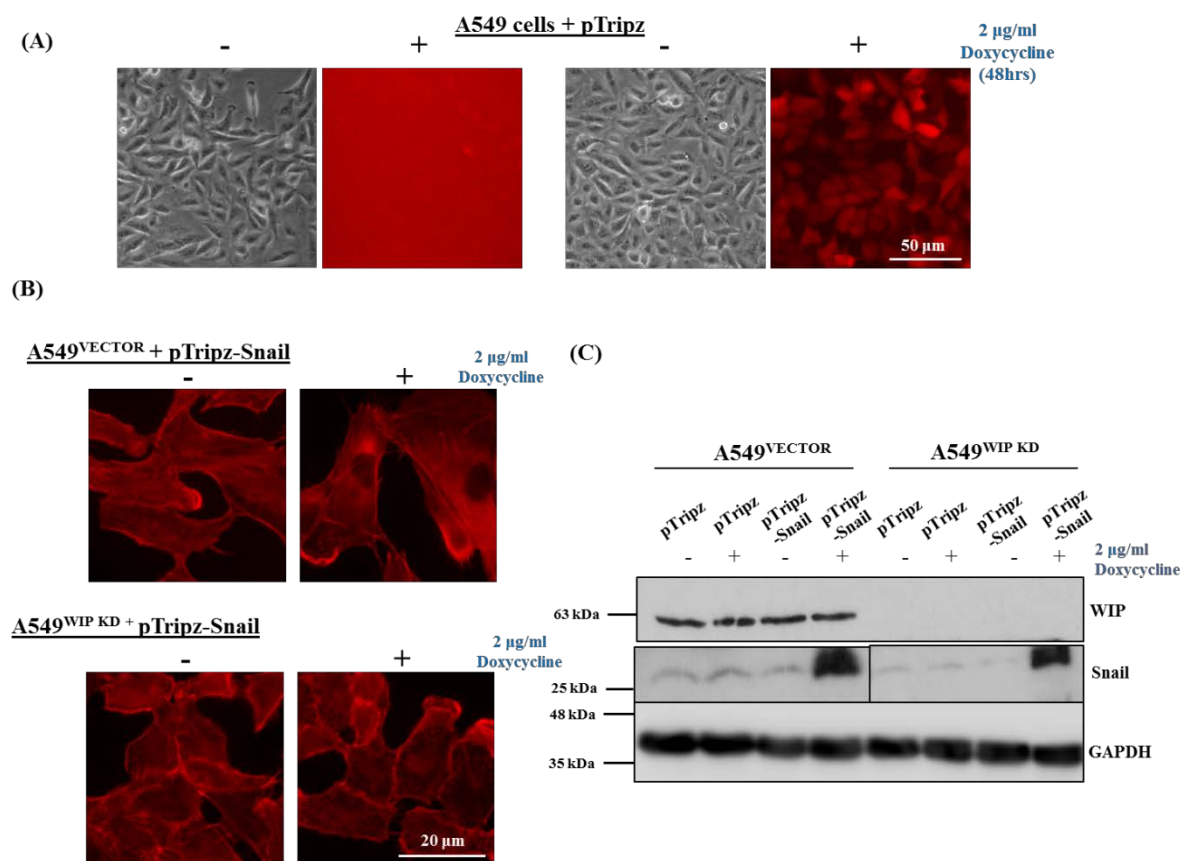
Figure.3.20: WIP knockdown cells do not attain EMT morphological changes in Snail induced stable EMT

(A) HEK293T were transiently transfected with pTripz-RFP plasmid using the inducible lentiviral system. Virus was harvested at 24 hr and 48 hr. A549^{VECTOR} and A549$^{WIP\ KD}$ cells were infected twice with the lentivirus and selected with puromycin. Doxycycline (2 μg/ml) was added for 48 hr to determine the transfection efficiency. Induction of RFP was observed in 80-90% of cells in presence of 2 μg/ml of doxycycline. Images were taken using 10X objective of a fluorescent microscope. Scale bar: 50 μm (B) pTripz-Snail virus was added to A549^{VECTOR} and A549$^{WIP\ KD}$ cells. Cells were selected with puromycin and seeded on coverslips for immunostaining. 2 μg/ml doxycycline was added for 48 hr after which cells were fixed and stained for phalloidin. Images were taken using a 40X oil objective lens of a fluorescent microscope. Scale bar: 20 μm (C) Expression of Snail was analyzed by western blotting for A549^{VECTOR} and A549$^{WIP\ KD}$ cells infected with pTripz-Snail and induced with doxycycline for 48 hr.

3.18 Knockdown of WIP led to reduction in number of stress fibers in A549 cells

Knockdown of WIP in A549 cells caused reduction in cell perimeter and area as shown by phalloidin staining (Figure 3.12). Also, A549$^{WIP\ KD}$ cells did not show the morphological changes associated with TGF-beta induced EMT. TGF-beta mediated cell scattering, elongation was

inhibited by knockdown of WIP in A549 cells (Figure 3.19). Actin reorganization is a crucial step during EMT progression by which cells attain characteristic mesenchymal morphology [185]. Hence, in order to examine the status of actin during EMT, phalloidin staining was performed in TGF-beta treated A549$^{\text{VECTOR}}$ and A549$^{\text{WIP KD}}$ cells. Cells were seeded on glass coverslips and treated with TGF-beta to induce EMT. After 48 hr of TGF-beta induction, the cells were fixed and stained with phalloidin to visualize actin filaments. In contrast to the untreated control cells, TGF-beta dramatically induced actin stress fibers formation typical of EMT in A549$^{\text{VECTOR}}$ cells (Figure 3.21 A). However, A549$^{\text{WIP KD}}$ cells treated with TGF-beta did not display stress fiber formation despite the presence of TGF-beta (Figure 3.21 B).

(A) A549^{VECTOR}
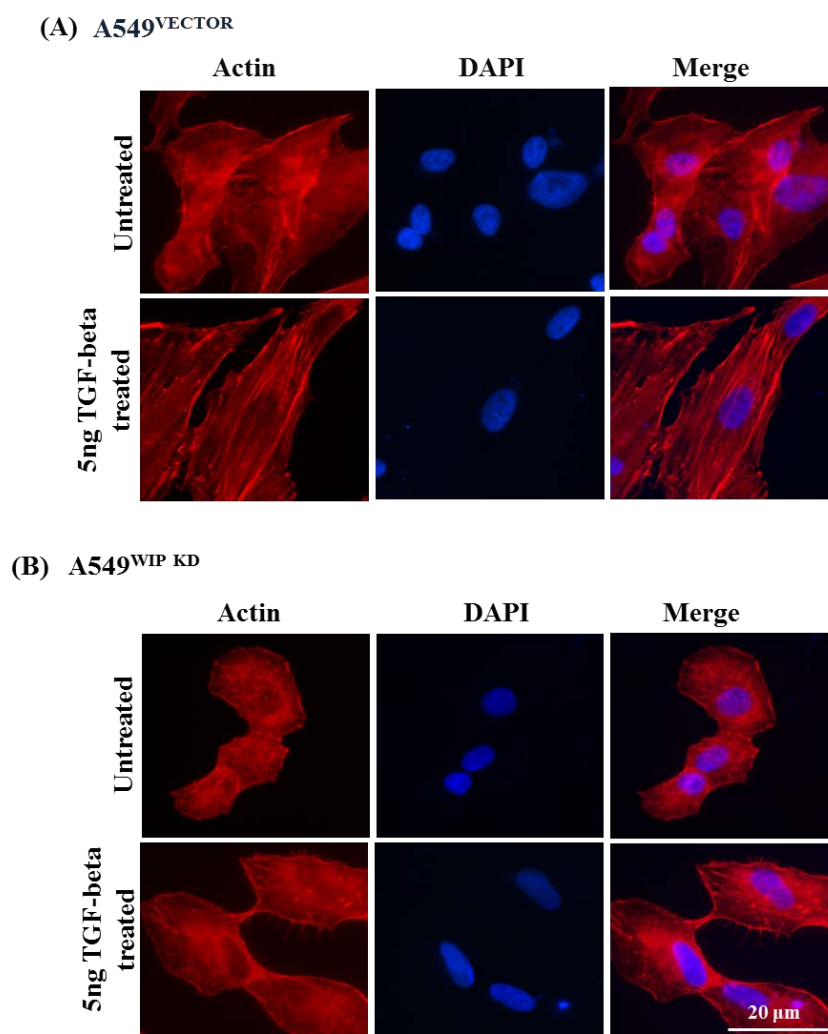
(B) A549^{WIP KD}

Figure.3.21: Knockdown of WIP reduced stress fiber formation during EMT
A549^{VECTOR} and A549^{WIP KD} cells were seeded on coverslips and EMT was induced using TGF-beta. After 48 hr of TGF-beta treatment, the cells were fixed and stained with phalloidin to visualize actin cytoskeleton. Nucleus was visualized by DAPI staining. Images were captured with a 40X objective lens using a fluorescence microscope. (A) Phalloidin staining for A549^{VECTOR} cells (B) Phalloidin staining for A549^{WIP KD} cells. Scale bar: 20μm

3.19 A549^{WIP KD} cells showed significant reduction in RhoA content

Epithelial cells are characterized by cortical actin filaments whereas mesenchymal cells consist

of actin stress fibers. EMT is characterized by disassembly of adherens junction complex and

reorganization of actin cytoskeleton from cortical arrangement to form actin stress fibers [228].

RhoA, a *Ras* superfamily small GTPase is crucial for the formation of actin stress fibers [186, 229]. With respect to EMT, RhoA activation leads to disruption of E-cadherin based adhesion junctions. This leads to actin cytoskeleton remodeling and formation of stress fibers [230]. Knockdown of WIP in A549 cells led to reduced cell area and diminished number of stress fibers (Figure 3.12). A549$^{WIP\ KD}$ cells displayed reduced number of stress fibers as compared to the control cells during TGF-beta induced EMT (Figure 3.21). During EMT, RhoA is activated from its inactive (GDP-bound form) to the active (GTP-bound) form [228]. Activation of RhoA leads to remodeling of the actin cytoskeleton which helps in attaining the classic EMT phenotype [190].

Knockdown of WIP in A549 cells significantly reduced the total RhoA content (Figure 3.22). This could explain the reduced number of stress fibers as well as the reduced cell area in A549$^{WIP\ KD}$ cells. Expression of RhoA was determined in A549 cells with WIP overexpression and WIP knockdown. As shown in Figure 3.22 A, A549$^{WIP\ KD}$ cells had reduced RhoA content and A549^{WIP} cells showed elevated expression of RhoA as compared to control cells. This indicates a possible regulation of RhoA expression by WIP.

The next step was to determine if WIP lies upstream of RhoA or whether WIP is an effector of RhoA. For this purpose, A549 cells were treated with exoenzyme C3 transferase which is a commonly used cell permeable Rho inhibitor [231]. As shown in Figure (3.22 B), addition of C3 transferase to the cells, led to disruption of actin stress fibers. This was also confirmed by performing actin staining for C3 transferase treated/untreated A549 cells. Figure 3.22 D shows loss of stress fibers and collapse of the cell body in presence of C3 transferase for A549 cells.

The expression of RhoA and WIP with/without C3 transferase was determined by western blot analysis (3.22 B). As expected, C3 transferase treated cells had reduced RhoA content. Interestingly, the amount of WIP protein was unchanged after C3 treatment. This implies that the expression of WIP is not affected by inhibition of RhoA and indicates that WIP may regulate RhoA expression.
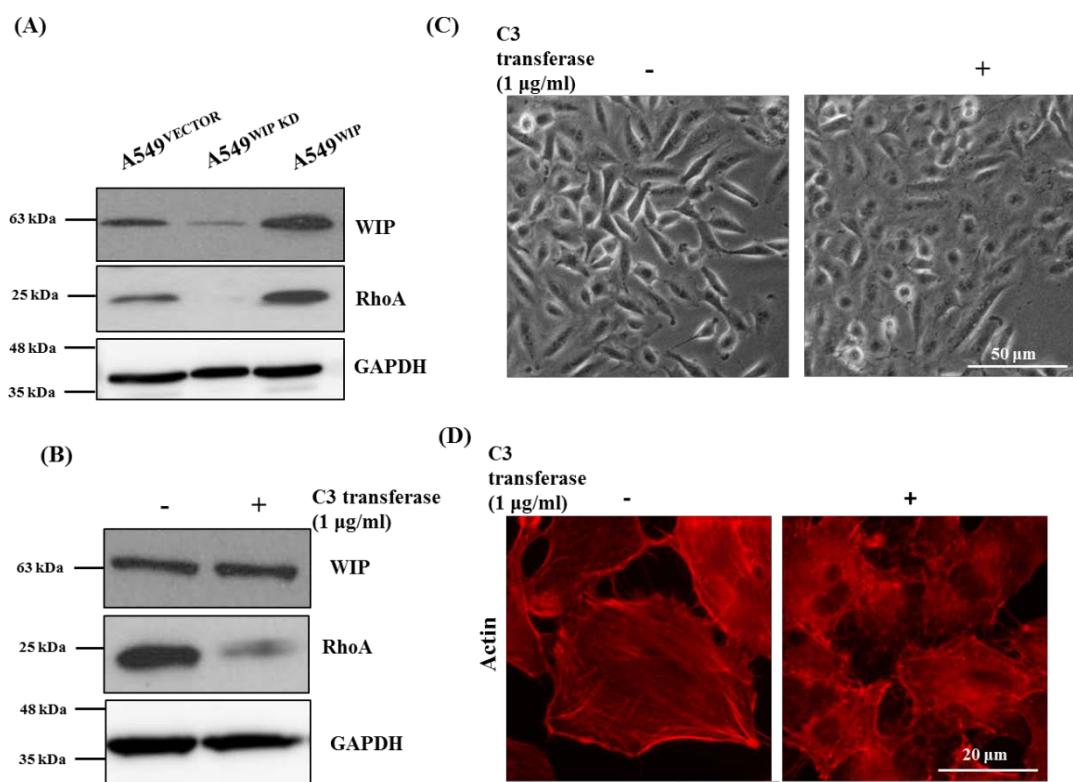
Figure 3.22: Knockdown of WIP leads to reduced total RhoA content in A549 cells.

(A) A549^{VECTOR}, A549$^{WIP\ KD}$ and A549^{WIP} cell lysates were resolved on a 15% SDS-PAGE gel and blotted with Anti-RhoA and Anti-WIP antibody. (B) Western blot analysis of WIP and RhoA in the presence/absence of C3 transferase. Cells were treated with C3 transferase (1 µg/ml) and lysed after 5 hrs using RIPA lysis buffer. Lysates were resolved on a 15% SDS-PAGE gel and probed for RhoA and WIP protein. GAPDH was used as endogenous control to ensure equal loading (C) A549 cells were treated with 1 µg/ml of C3 transferase (Cytoskeleton Inc.) for 5 hr at 37°C. Images were captured using 10X objective lens using a phase contrast microscope. Scale bar: 50µm (D) Immunostaining was performed for C3 transferase treated/untreated cells. Cells were seeded on coverslips and grown till 60-70% confluence. C3 transferase was added to the cells followed by incubation for 5 hr at 37°C. For visualizing actin filaments, the cells were fixed and phalloidin staining was performed. Scale bar: 20 µm.

To determine if WIP regulates RhoA at mRNA level, a real-time PCR analysis was performed using A549^{VECTOR} and A549$^{WIP\ KD}$ cells. As shown in Figure 3.23A, A549$^{WIP\ KD}$ had reduced mRNA levels of WIP. However, knockdown of WIP did not affect the mRNA levels of RhoA. This suggests that WIP causes reduction in RhoA protein level.

Rho-associated kinase (ROCK) and Formin homology protein mDia1 (mDia1) are RhoA downstream effectors and mediate effects of RhoA on the actin cytoskeleton. ROCK and mDia1 jointly act to stabilize normal cell shape by controlling actin cytoskeletal rearrangements [232]. ROCK causes phosphorylation of myosin light chain (MLC) leading to actomyosin-based cell contractility [233]. ROCK is also essential for formation of stress fibers and FAs [234]. mDia1 promotes actin polymerization and plays a role in actin-dependent FA formation as well as regulates the alignment of stress fibers with the microtubules [235-237]. Overexpression or knockdown of WIP did not show changes in expression of RhoA downstream effectors such as ROCK-II (ROKα) and mDia1 (Figure 3.23 B). Expression of other Rho GTPase family members such as Cdc42 and Rac1 was analyzed in A549^{WIP} and A549$^{WIP\ KD}$ cells and was found to be unchanged. Similarly, expression of Smurf1, an E3 ubiquitin ligase responsible for degradation of RhoA was also found to be unaffected by knockdown of WIP (Figure 3.23 B).

(A)

(B)
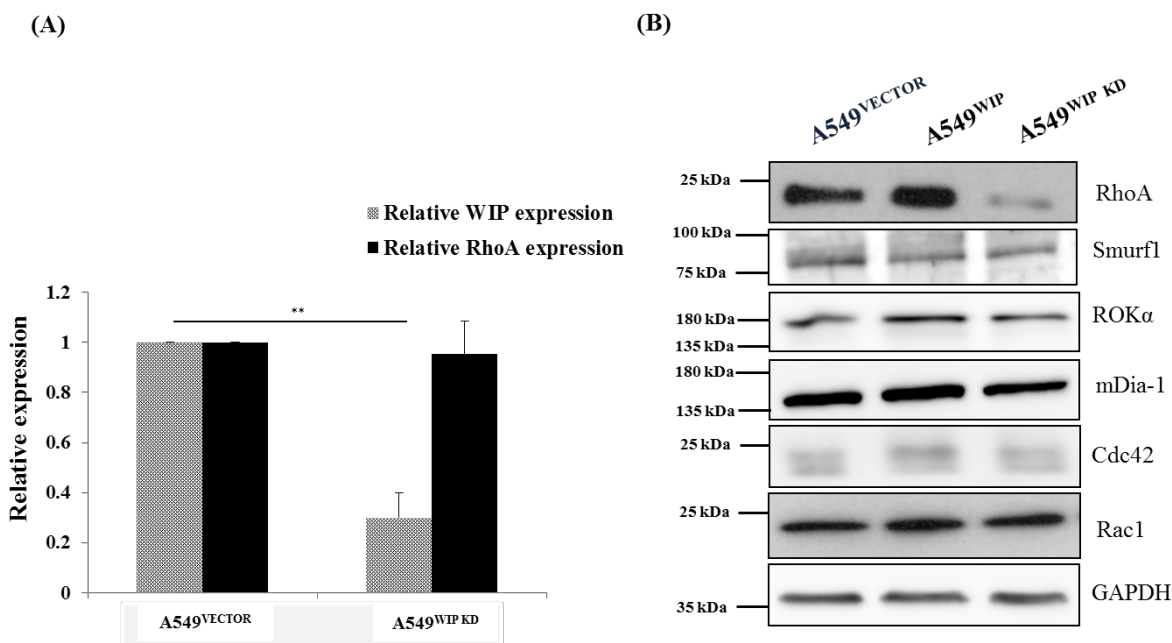
Figure.3.23: Knockdown of WIP in A549 cells does not affect mRNA level of RhoA

(A) Real time PCR analysis showing relative expression of WIP and RhoA mRNA in A549^{VECTOR} and A549$^{WIP\ KD}$ cells (B) A549^{VECTOR}, A549^{WIP} and A549$^{WIP\ KD}$ cells were lysed and subjected to western blot analysis. Lysates were resolved using SDS-PAGE gel and blotted with Anti-RhoA, Anti-Smurf1, Anti-ROKα, Anti-mDia1, Anti-Cdc42, Anti-Rac1 antibodies. GAPDH was used as the loading control. (Significance is indicated by stars * $p \leq 0.05$, ** $p \leq 0.01$, *** $p \leq 0.001$).

3.20 WIP specifically interacts with RhoA

In order to determine if reduction in RhoA is specifically due to loss of WIP, WIP was re-expressed in WIP knockdown stable cells. These cells are referred to as A549$^{WIP\ RESCUE}$ cells. Interestingly, expression of RhoA was also increased in A549$^{WIP\ RESCUE}$ cells as compared to A549$^{WIP\ KD}$ cells (Figure 3.24 A). Next, A549$^{WIP\ KD}$ cells were transfected with plasmid expressing WIP-GFP and control plasmid expressing GFP. Phalloidin staining was performed to visualize F-actin filaments in the GFP and WIP-GFP transfected cells. As shown in Figure 3.24 B, reconstitution of WIP causes appearance of stress fibers and recovers cell size similar to

control A549^{VECTOR} cells. This implies that phenotypic defect and reduction in RhoA levels in A549$^{WIP KD}$ cells is specifically caused by knockdown of WIP.

In order to determine if WIP interacts with RhoA and regulates its expression, a His tag pulldown was performed. Since the endogenous level of RhoA was low in A549 cells, HEK293T cells were used to perform the pulldown experiment. Briefly, cells were co-transfected with full length RhoA expressing plasmid with a HA tag (RhoA-HA) alongwith a plasmid expressing WIP with a His tag (WIP-His). A plasmid expressing GFP with a His tag was used as a control (GFP-His). 36 hr after transfection, cells were lysed followed by incubation with Ni-NTA beads. However, it was observed that cells co-transfected with WIP-His showed enhanced expression of RhoA-HA as compared to cells co-transfected with GFP-His and RhoA-HA which may be due to stabilization of RhoA by WIP. Hence, to maintain equal RhoA expression in the lysated, cells were transfected with individual plasmids. 36 hr post-transfection, cell lysates were mixed in equal volume as follows: 1) RhoA-HA + WIP-His and 2) RhoA-HA + GFP-His. Lysates were subjected to His tag pulldown followed by western blot analysis. As shown in Figure 3.24 C, RhoA-HA was specifically pulled down by WIP-His and not GFP-His in HEK293T cells.
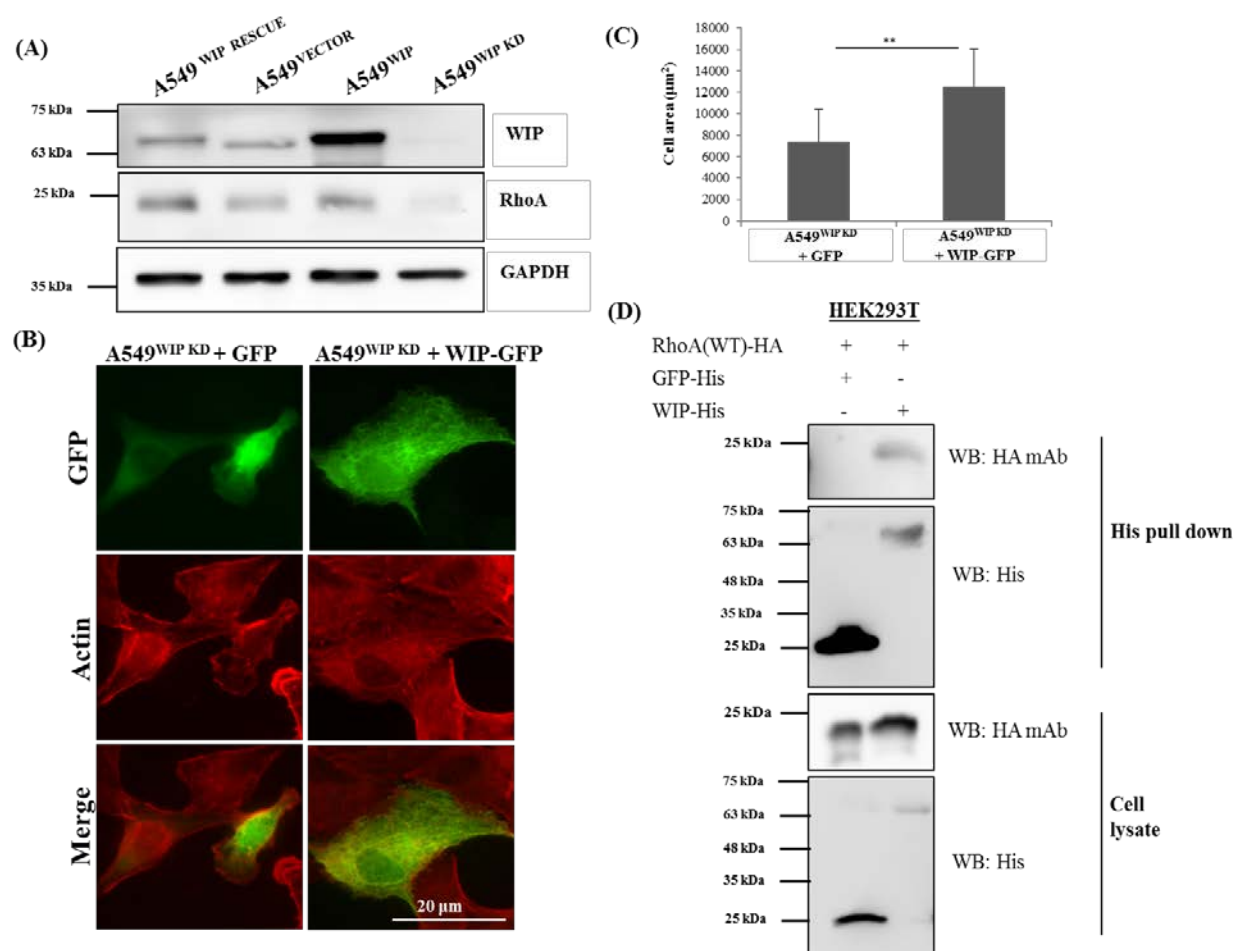
Figure.3.24: WIP specifically interacts with RhoA and reconstitutes the phenotype of WIP knockdown cells

(A) A549$^{WIP KD}$ cells were transduced with control plasmid and WIP-His expressing plasmid. Cells were lysed and western blot analysis was performed to determine expression of WIP and RhoA. GAPDH was used as the loading control (B) A549^{VECTOR} and A549$^{WIP KD}$ cells were transiently transfected with plasmids expressing GFP and WIP-GFP. 36 hr post-transfection, cells were immunostained for phalloidin 568 to stain F-actin filaments. Scale bar: 20 µm (C) HEK293T cells were transfected with plasmids expressing RhoA-HA, WIP-His and GFP-His. 36 hr post-transfection, cells were lysed and cell lysates were mixed in equal volumes as 1) RhoA-HA + WIP-His and 2) RhoA-HA + GFP-His. His tag pulldown was performed and samples were resolved on a 12% SDS-PAGE gel and blotted with Anti-His and Anti-HA antibodies.

CHAPTER 4: Transcriptional Regulation of N-WASP

A) Characterization of N-WASP promoter

Introduction:

N-WASP regulates actin polymerization and plays a vital role in cell adhesion, motility and cell spreading [43, 238]. Differential expression of N-WASP in tumorigenic and non-tumorigenic cells indicates its possible role in determining the cell phenotype and function. N-WASP expression is enhanced in hypoxia induced EMT as well as in the presence of EGF [56]. Expression of N-WASP is found to be decreased in breast cancer and colorectal cancers and is inversely-correlated with cancer progression suggesting that N-WASP is a potential tumor suppressor [61]. On the contrary, cDNA microarray analysis of liver metastases showed N-WASP to be significantly upregulated in liver metastases as compared to primary colon tumors [55]. Several *in-vitro* studies have demonstrated the role of N-WASP in cancer progression [57, 239, 240]. N-WASP is present at leading edge of lamellipodia and invadopodia in melanoma and breast cancer cells [30, 241] and N-WASP activation is critical for cell motility and invasion in breast cancer cells [58]. These studies suggest that N-WASP can be a tumor suppressor as well as a metastasis promoter depending on the type and stage of cancer progression.

4.1 Differential expression of N-WASP

Role of N-WASP in actin polymerization and cancer progression has been well-studied. However, the mechanism of regulation of N-WASP at transcriptional level is poorly understood. To correlate the expression of N-WASP with tumorigenicity, a western blot was performed to determine N-WASP expression in various cancer cell lines. As shown in Figure 4.1, N-WASP expression was found to be upregulated in metastatic clones II-4 and A5-RT3 cells, compared to the parental non-tumorigenic HaCaT cells. However, N-WASP expression was found to be low in HSC-5 (squamous cell carcinoma) as compared to HaCaT cells (Figure 4.1 C). N-WASP expression is upregulated under conditions of hypoxia as well as in the presence of EGF (Figure 4.10 A and B). Hence, in order to gain a better understanding of regulation of N-WASP expression, a characterization of genomic region containing the N-WASP promoter was carried out to identify the regulatory elements.
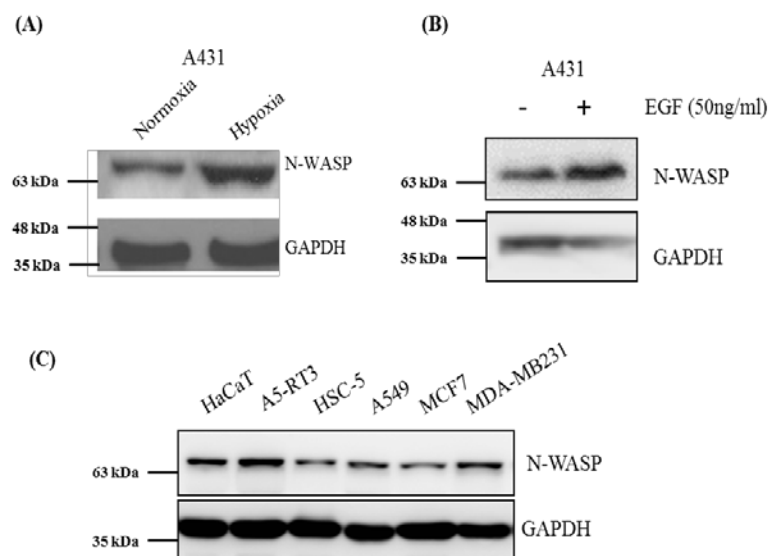
Figure.4.1: Expression of N-WASP is altered under different culture conditions
(A) A431 epidermoid carcinoma cells were cultured for 24 hrs in a hypoxia chamber. Cells were lysed and lysates were resolved on a 10% SDS PAGE gel to analyze expression of N-WASP and GAPDH. (B) A431 cells were grown till 30-40% confluence and serum starved for 12 hrs. After 12 hrs, cells were treated with EGF (50ng/ml) for 48 hrs. Cells were lysed and expression of N-WASP was determined with/without EGF. (C) HaCaT, A5-RT3, HSC-5, A549, MCF7, MDA-MB-231 cells were lysed and the expression of N-WASP was analyzed by western blotting. GAPDH was used as the endogenous control.

4.2 Characterization of the N-WASP promoter by bioinformatics analysis

The human N-WASP protein is coded by *WASL* gene, which is located on chromosome 7 and consists of 11 exons (Source: www.ensembl.org). Identification and characterization of *WASL* gene promoter sequence was carried out by performing bioinformatic analysis of genomic region located at the 5' upstream region of *WASL* gene. N-WASP candidate promoter region was identified as the region spanning from -1295 bp upstream of the first exon / transcription start site (TSS). This region was selected based on analysis of *WASL* gene using Ensembl software, which identified -1295 bp upstream region as the region containing binding sites for DNA binding proteins. The TATA box was identified present at ~1200 bp upstream relative to TSS.

N-WASP promoter contains a long stretch of GC nucleotides as observed in the GC plot (Figure 4.2 A). This region contains 60% of GC nucleotides and is referred to as CpG island. Comparative analysis of the 1.3 kb upstream of the TSS of human and mouse *WASL* gene was performed using the rVista tool at Vista Genome Browser [http://genome.lbl.gov/vista/index.shtml]. A 100 bp region was found to be conserved (70%) between the two species (highlighted in red) (Figure 4.2 B).
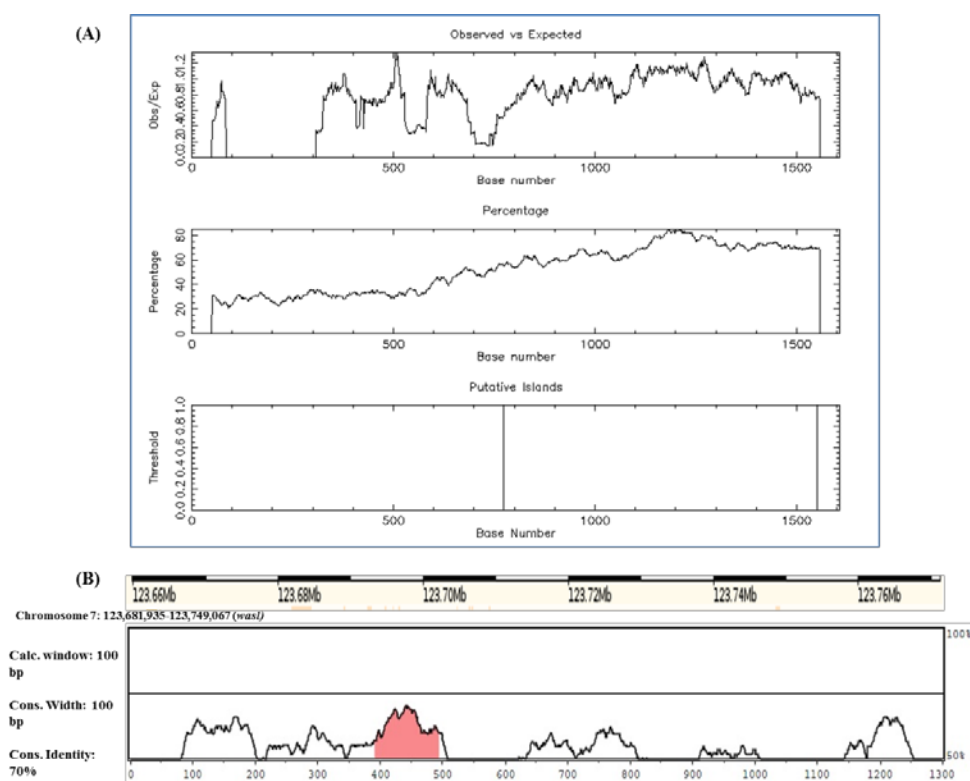
Figure.4.2: Base composition of the human *WASL* promoter
(A) CpG islands plot reporting the analysis of GC-nucleotide content and structure of the *WASL* 1.6 kb genomic region upstream of the TSS using CpG-plot tool at the EMBL-EBI European Bioinformatics Institute (http://www.ebi.ac.uk/Tools/emboss/cpgplot). Plot of ratio of the observed over the expected GC content. Middle panel: GC content expressed as percentage (minimum percentage required to identify the presence of a CpG islands is 50%). Lower panel: identification of a 777 bp CpG island upstream and proximal to the first 5'UTR exon of the *WASL* gene. (B) Output of the comparative genomic analysis obtained with dedicated software available at the Vista Genome Browser (http://genome.lbl.gov/vista/index.shtml, tools for comparative analysis). Conserved sequences with a percentage of identity (vertical axis) that is higher than 70% are represented as red peaks and are shown relative to their position in the human genome (horizontal axis) compared to mouse.

4.3 Assessment of N-WASP promoter constructs in GFP reporter assay

To identify the functional region of N-WASP promoter, a mammalian expression vector with a series of deletion fragments of the N-WASP promoter ranging from -1295, -902, -726, -575 and -288 bp relative to the TSS were constructed (Figure 4.3 A). Deletion constructs were synthesized using Human BAC clone 746L19-BAC RP11 as the template and selected based on the proximity to start codon, presence of GC-clusters and putative recognition sites for transcription factors. These deletion constructs were generated to specifically identify the regulatory elements present in the N-WASP promoter. Each of these promoter constructs was verified by sequencing and fused upstream of a *GFP* gene (Figure 4.3 A).
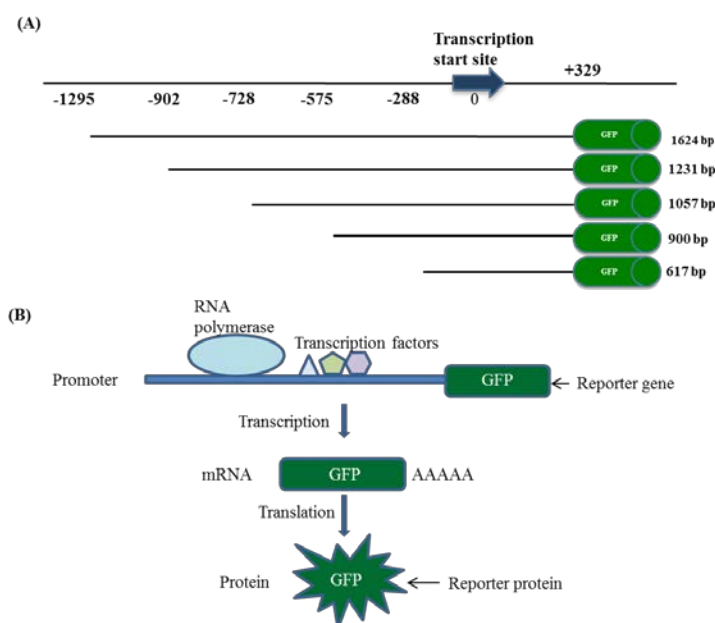
Figure.4.3: Generation of N-WASP promoter constructs.
(A) Series of deletion fragments of N-WASP promoter were generated. The size of fragments ranged from 1624 bp, 1231 bp, 1057 bp, 900 bp and 617 bp. All the 5 promoter constructs were sequenced and cloned in an expression vector upstream of a *GFP* gene. Sequencing accuracy was determined by comparing with the sequences at UCSC Genome Bioinformatics [https://genome.ucsc.edu/index.html]. (B) Schematic representation of the principle of GFP reporter assay. GFP fluorescence emitted is proportional to number of transcripts generated which is determined by the promoter activity.

N-WASP promoter constructs fused with *GFP* gene were transfected in HEK293T cells to analyze the expression of GFP and determine promoter activity. CMV-GFP, which consists of *GFP* gene regulated by CMV promoter, was used as a positive control. The GFP fluorescence was quantified using ImageJ software by individually measuring the fluorescent intensity of the cells. The relative fluorescence pattern is shown in Figure 4.4. Significant drop in fluorescent intensity was observed by deletion of 393 bp region between 1624 bp and 1231 bp N-WASP promoter region. This suggests that regulatory elements important for activity of the promoter may be present in -1624 to -1231 bp region and deletion of this region causes a drop in the promoter activity.

(A)
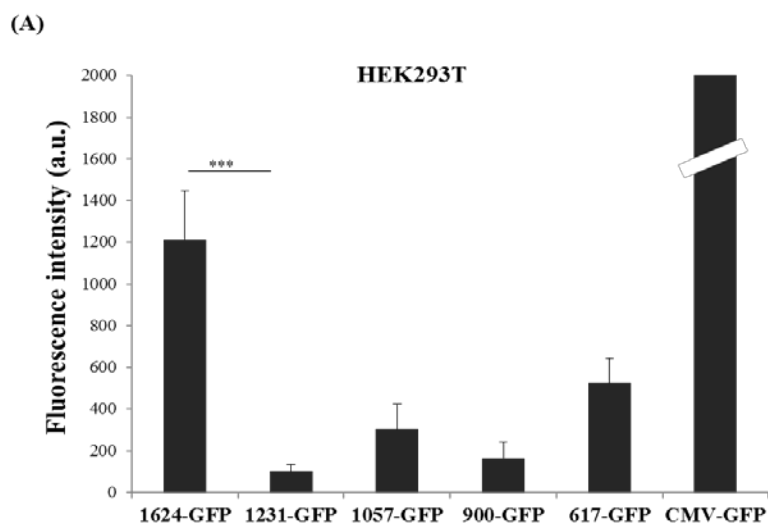
Figure.4.4: Functional characterization of 1624 bp promoter region of N-WASP

(A) HEK293T cells were seeded in a 6-well plate and grown till 50-60% confluence. 4 μg of DNA was used to transfect the cells in triplicates. Fluorescence was quantified from 90 cells for each transfection using ImageJ software. Graph represents data from 3 independent experiments. (Significance is indicated by stars * $p \leq 0.05$, ** $p \leq 0.01$, *** $p \leq 0.001$).

In order to avoid transfection variability from well to well, vector normalization was performed by using a control plasmid expressing RFP. Fluorescence intensity was measured 36 hr post-transfection and normalization was performed by dividing GFP intensity by RFP intensity (Figure 4.4 B). Significant drop in fluorescent intensity was observed from 1624 bp to 1231 bp of N-WASP promoter.
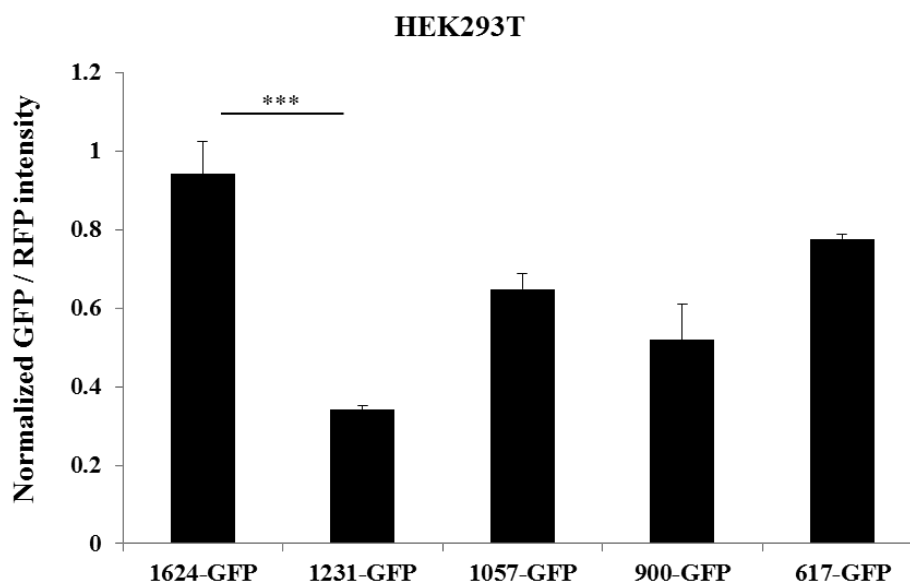
HEK293T

Figure.4.4: Functional characterization of 1624 bp promoter region of N-WASP
(B) HEK293T cells were seeded in a 6-well plate and grown till 50-60% confluence. 2 μg of promoter constructs expressing GFP were co-transfected with 2 μg of control plasmid expressing RFP. 36 hr post transfection, cells were lysed and fluorescence was measured using fluorimetry. The fluorescence was quantified from 3 independent experiments. (Significance is indicated by stars * $p \le 0.05$, ** $p \le 0.01$, *** $p \le 0.001$).

Similar transfections were performed in epithelial cells (HaCaT and HSC-5) to analyze the expression pattern of N-WASP promoter constructs (Figure 4.5). Quantification of the relative fluorescence revealed a significant drop in fluorescent intensity from 1624 bp to 1231 bp fragments which was consistent with the results obtained with HEK293T cells.
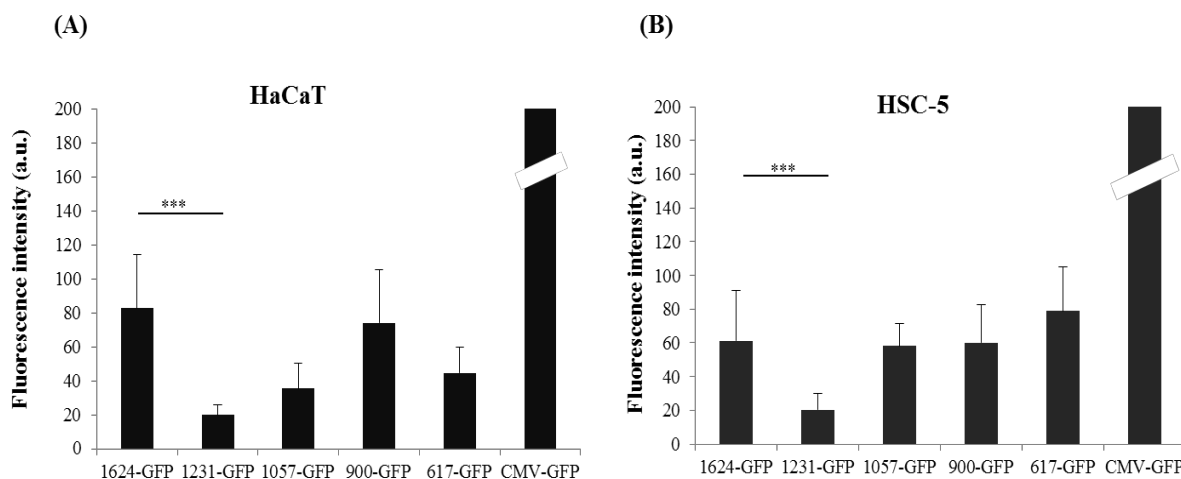
Figure.4.5: Transfection of N-WASP promoter constructs in HaCaT and HSC-5 cells.
HaCaT (A) and HSC-5 (B) cells were seeded in a 6-well plate and grown till 50-60% confluence. 4 μg of DNA was used to transfect the cells in triplicates. Fluorescence was quantified from 90 cells for each transfection using ImageJ software. Graph represents data from 3 independent experiments. (Significance is indicated by stars * p ≤ 0.05, ** p ≤ 0.01, *** p ≤ 0.001).

As shown in Figure 4.4 and Figure 4.5, deletion of 393 bp region between 1624 bp and 1231 bp of N-WASP promoter showed a significant drop in the relative GFP fluorescence intensity for HEK293T, HaCaT and HSC-5 cell lines. This suggests that the 393 bp region may contain potential binding sites for several cis-regulatory elements, enhancers and repressors.

To confirm the importance of the 393 bp region in N-WASP promoter, this region was cloned with a SV40 minimal promoter fused to a reporter *GFP* gene (393-SV40 GFP)(Figure 4.6 A). Empty plasmid containing SV40 minimal promoter fused to a reporter *GFP* gene was used as a control (SV40 GFP). HEK293T cells were transfected with 4 μg of the plasmid. 36 hr post transfection, cells were lysed and GFP fluorescence was measured and quantified as described in Section (2.2.9). As seen in Figure 4.6 B, transfection of plasmid containing 393 bp significantly

enhanced the fluorescent intensity by three fold. This confirmed that the 393 bp region between -1295 and -902 of N-WASP promoter could be a regulatory region.
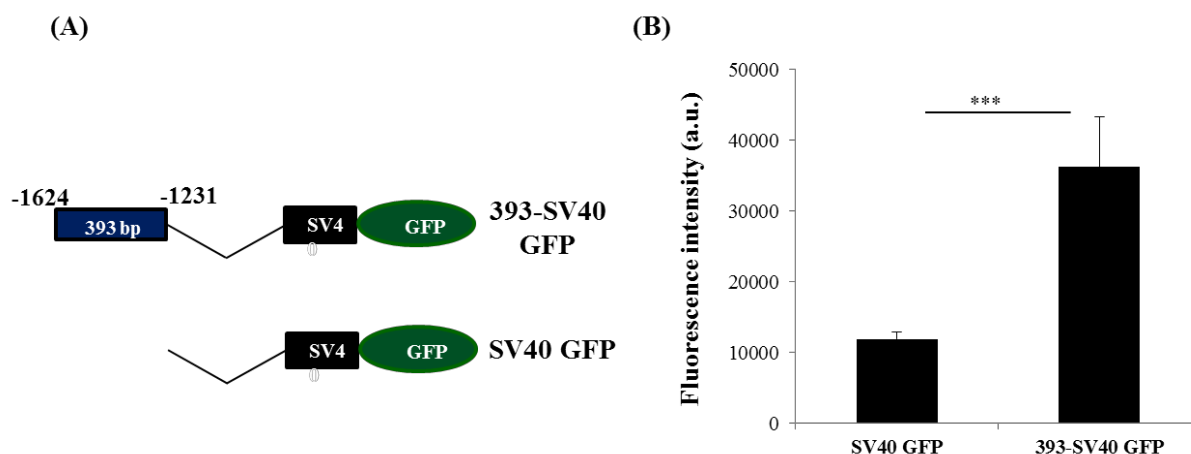
Figure.4.6: 393 bp regulatory region in N-WASP promoter enhances activity of minimal promoter

(A) Cloning of 393 bp regulatory region with SV40 minimal promoter fused to *GFP* gene to generate 393-SV40 GFP. SV40 GFP was used as the control plasmid (B) HEK293T cells were seeded in a 6-well plate and grown till 50-60% confluence. 4 µg of DNA was used to transfect the cells in triplicates. 36 hr post transfection, the cells were lysed and fluorescence was measured using fluorimetry. The fluorescence was quantified from 3 independent experiments. (Significance is indicated by stars * $p \leq 0.05$, ** $p \leq 0.01$, *** $p \leq 0.001$).

4.4 Identification of DNA binding proteins using yeast one hybrid system

The deletion between -1295 and -902 genomic region of N-WASP promoter reduced the activity of N-WASP promoter. Hence it was vital to perform a functional analysis of this region for identifying regulatory elements in the promoter.

Yeast one hybrid screening was performed to identify DNA binding proteins to the 393 bp region in N-WASP promoter. The 393 bp region was used as the bait sequence and it was cloned in bait plasmid (YEp112) with a *HIS3* selection gene. The prey plasmid was a brain cDNA expression library, which consisted of transcription factors fused to Gal4 activation domain

(Gal4-AD). Brain cDNA library was used for the yeast one hybrid screen as N-WASP expression is found to be elevated in the brain [20]. 2mM 3-AT was determined to be optimal concentration to inhibit leaky HIS3 expression. The bait plasmid was transformed into yeast PJ694A strain and was allowed to mate with *Saccharomyces cerevisiae* cells transformed with brain cDNA expression library. Using yeast one hybrid screen, 32 colonies were identified which were able to grow on media lacking histidine (positive interaction). The positive clones from the screening plate were used for plasmid isolation. Isolated plasmids were confirmed to be the prey plasmids by restriction digestion. Prey plasmids was sequenced and BLAST search was performed to identify genes present in prey plasmids. Sequence analysis revealed that the colonies had cDNA encoding 6 DNA binding proteins (Table 4.1), while the remainder colonies had an out-of-frame fusion with Gal4-AD. The prey plasmid was re-transformed in yeast to confirm binding specificity with the 393 bp basal promoter region in the bait plasmid.

The following is the list of interactors obtained from the yeast one hybrid screening:

Serial no.	Interactor	Number of clones
1	Homo sapiens msh homeobox 1 (MSX1), mRNA	4
2	Homo sapiens ISL LIM homeobox 1 (ISL1), mRNA	4
3	Homo sapiens POU class 3 homeobox 2 (POU3F2), mRNA	1
4	Homo sapiens H3 histone, family 3A (H3F3A), mRNA	4
5	Homo sapiens tubulin, alpha 1a (TUBA1A), mRNA	1
6	Homo sapiens kinesin family member 22 (KIF22), mRNA	1

Table 4.1: List of positive interactors obtained in brain cDNA library screening

The presence of histones from the one-hybrid screening was expected as they are known sequence-independent DNA binding proteins. A single colony was obtained for Alpha tubulin and Kinesin family member 22. Hence, it was of interest to analyze the role of Msx1, ISL1 and POU3F2 in regulation of N-WASP expression.

A) **Msx1 msh homeobox 1 (Homo sapiens)**: *MSX1* gene encodes a member of muscle segment homeobox (*MSX*) gene family. Studies have indicated a role of Msx1 protein in craniofacial development particularly odontogenesis, limb-pattern formation, and inhibiting tumor progression [242, 243]. Mutations harbored in *MSX1* gene have been associated with Witkop syndrome, Wolf-Hirschom syndrome and autosomal dominant hypodontia [244, 245]. The protein encoded by *MSX1* gene interacts with TATA binding protein via its homeodomain and acts as a transcriptional repressor during embryogenesis [246]. *MSX1*-deficient mice die prenatally due to defects in cranio-facial features caused by incomplete development of maxillae and mandibles and missing teeth [247]. Mutations in the *MSX1* gene causes tooth agenesis and orofacial cleft in humans [248, 249]. Msx1 was thought to be expressed exclusively during embryogenesis; however studies have demonstrated its presence in highly differentiated pituitary cells [250].

B) **ISL1 LIM homeobox 1 (Homo sapiens)**: Insulin gene enhancer protein ISL-1 is a protein encoded by the *ISL1* gene. ISL-1 protein is a transcription factor, which comprises of two LIM domains (N-terminal) and one homeodomain (C-terminal). ISL1 is a marker for progenitor cardiac cells and helps in the formation of multipotent cardiac cell lineages [251]. Also ISL1 binds to the enhancer of the insulin gene and positively regulates insulin gene expression [252]. N-WASP is involved in mobilizing F-actin which promotes recruitment of GLUT4 receptors to

the plasma membrane and uptake of glucose from blood. [253]. It may be possible that ISL1 enhances insulin gene expression which causes membrane localization of N-WASP. Thus, N-WASP and ISL1 might be working in co-ordination to maintain blood glucose levels.

C) **POU class 3 homeobox 2 (POU3F2) (Homo sapiens):** POU domain, class 2, transcription factor 3 (POU3F2) is a transcription factor involved in neuronal differentiation. It plays a role in the production and positioning of neocortical neurons [254]. N-WASP expression is found to be elevated in brain tissue [20]. POU3F2 is highly active in the brain tissue which is indicated by its role in neuronal differentiation and production of cortical neurons. It may be possible that POU3F2 interacts with the N-WASP promoter and enhances the promoter activity leading to high levels of N-WASP in brain. Overexpression of POU3F2 protein in melanoma cells has been shown to increase proliferation and invasive ability of cells [255].

4.5 Mapping yeast one hybrid interactors in the N-WASP promoter

The list of interactors obtained from yeast one hybrid screening were analyzed and Msx1, ISL1 and POU3F2 were selected for determining their role in regulating N-WASP promoter. The first step was to confirm if the three interactors have their consensus binding sequence in the 393 bp region of N-WASP promoter. Sequence analysis was performed using Matinspector software and it was observed that all the three interactors have their consensus binding sequences in the promoter region (Figure 4.7).
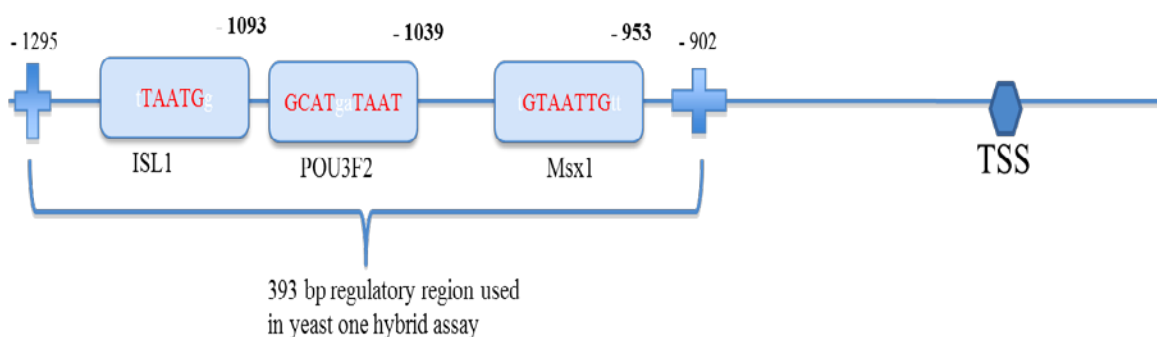
Figure.4.7: Binding of the yeast one hybrid interactors in the N-WASP promoter

Sequence analysis of the 393 bp regulatory region of the N-WASP promoter shows presence of consensus binding sequence of Msx1, ISL1 and POU3F2. Sequence analysis was performed using MatInspector software [http://www.genomatix.de/solutions/genomatix-software-suite.html] [210]. The consensus binding sequence is highlighted in bold red font.

4.6 Msx1 causes significant increase in activity of N-WASP promoter

MSX1, ISL1 and *POU3F2* genes were cloned in an expression plasmid with His tag. The sequence of the three genes was confirmed and their expression was analyzed by performing western blotting (Figure 4.8 A). In order to check if the interactors enhance the activity of N-WASP promoter, expression plasmids for Msx1, ISL1 and POU3F2 were co-transfected with the full-length N-WASP promoter (1624-GFP) in HEK293T cells. Quantification of relative fluorescence showed that transfection of plasmid expressing Msx1 had a strong activating effect on 1624 bp of N-WASP promoter. There was a consistent and significant enhancement of transcriptional activity in presence of Msx1 (Figure 4.8 B). However, no significant change in N-WASP promoter activity was observed in presence of ISL1 and POU3F2. To confirm if the binding of interactors in 393 bp regulatory region is specific, the expression vectors for the interactors were co-transfected with 1231 bp of N-WASP promoter which lacks the 393 bp

regulatory region. As seen in Figure 4.8 B, expression of the interactors did not affect transcriptional activity of N-WASP in absence of the 393 bp regulatory region which suggests that 393 bp region of N-WASP promoter is crucial for its activation.

(A)

Blot : Anti-His

Control Msx1 ISL1 POU3F2

75 kDa
63 kDa
48 kDa ← POU3F2
← ISL1
35 kDa ← Msx1
25 kDa

48 kDa GAPDH
35 kDa

(B)
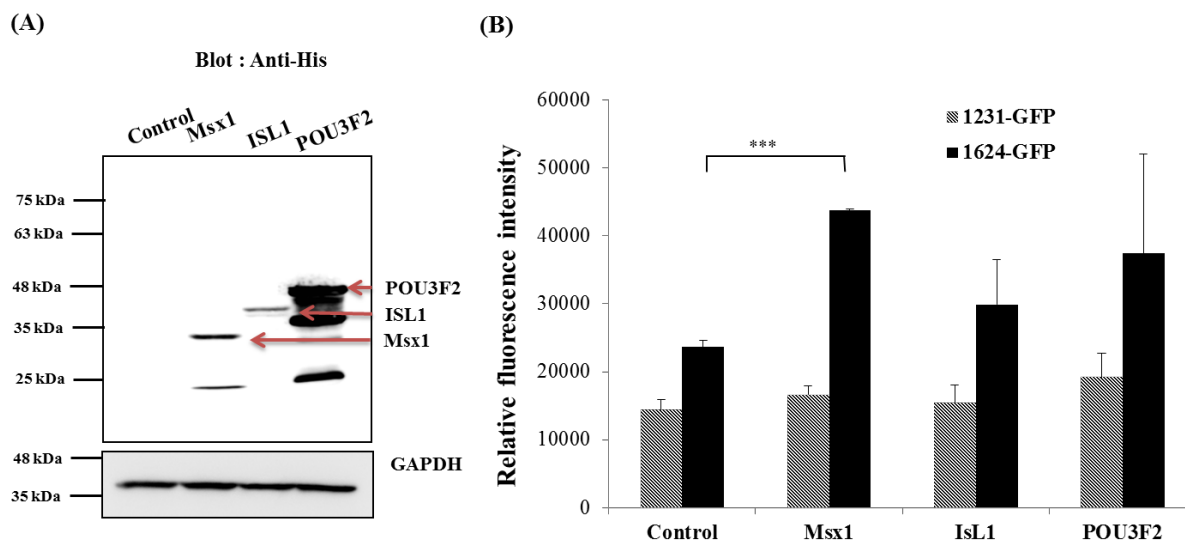
Figure.4.8: Cloning and transfection of yeast one hybrid interactors
(A) *Msx1, ISL1* and *POU3F2* were cloned in an expression plasmid with His tag and 4 μg of each plasmid was transfected in HEK293T cells to check the expression of the interactors. Lysates were resolved on a 12% SDS-PAGE gel and probed with Anti-His antibody. (B) Msx1, ISL1 and POU3F2 were co-transfected with full length N-WASP promoter as well as the N-WASP promoter lacking the 393 bp regulatory region tagged with a *GFP* gene and the relative fluorescence was quantified using fluorimetry. (Significance is indicated by stars * $p \leq 0.05$, ** $p \leq 0.01$, *** $p \leq 0.001$).

As shown in Figure 4.8 B, Msx1 caused a significant enhancement in N-WASP promoter activity. To confirm this result, Msx1 was co-transfected with 393-SV40 GFP (Figure 4.6 A). HEK293T cells were co-transfected with 2 μg of individual plasmid to a total of 4 μg DNA/well of a 6-well plate (Figure 4.9 A). 36 hrs post-transfection, cells were lysed and GFP fluorescence was measured and quantified. As shown in Figure 4.9 B, co-transfection of Msx1 further enhanced the activity of 393 bp of N-WASP promoter. This strongly implied that Msx1 could positively enhance N-WASP promoter activity by binding to the regulatory region of N-WASP

promoter. Interestingly, co-transfection of 1624-GFP with Msx1 showed a 6-fold higher fluorescent intensity as compared to co-transfection of 393-SV40 GFP with Msx1 (Figure 4.8 and Figure 4.9). This suggests that apart from the 393 bp regulatory region, the remaining 1231 bp of N-WASP promoter may contain binding sites for other regulatory elements which enhance N-WASP promoter activity.
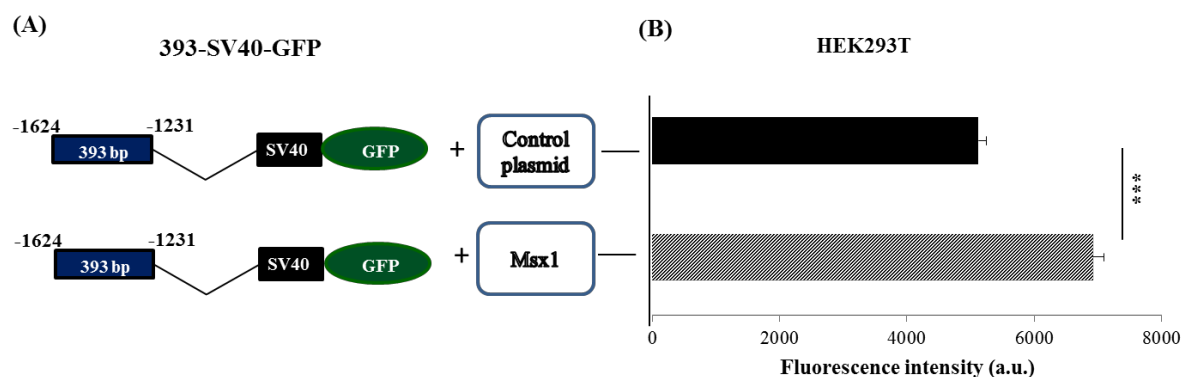
Figure.4.9: Msx1 enhances the activity of 393 bp regulatory region of the N-WASP promoter
(A) SV40 minimal promoter-GFP was fused to 393 bp and co-transfected with empty/ Msx1 plasmid (B) HEK293T cells were seeded in a 6-well plate and co-transfected with 2 μg of individual plasmids as shown in (A). Cells were lysed after 36 hr of transfection to quantify fluorescence intensity using fluorimetry. (Significance is indicated by stars * $p \leq 0.05$, ** $p \leq 0.01$, *** $p \leq 0.001$).

4.7 Msx1 binds to its consensus binding site in 393 bp regulatory region of N-WASP promoter

To determine the functionality of the Msx1 binding site in the N-WASP promoter, ChIP assay was performed. Since the endogenous levels of Msx1 were too low to be detected, HEK293T cells were transfected with an expression vector coding for the Msx1 protein with His tag (Msx1-his). Cells transfected with an empty vector containing a His tag were used as a control. 36 hr post-transfection, cells were cross-linked using formaldehyde followed by pulldown of Msx1-his

protein with Ni-NTA beads. Protein-bound DNA was eluted and amplified by PCR using

primers flanking the Msx1 binding site in the N-WASP promoter region. Primers flanking a

region of exon 1 of the *WASL* gene were used as the negative control. Figure 4.10 shows a

distinct PCR amplification band by using Msx1 primers. The band was absent in the negative

control primers as well as the empty vector transfected cells. This suggests that Msx1 is capable

of direct binding to its predicted binding site in the 393 bp region of N-WASP promoter.
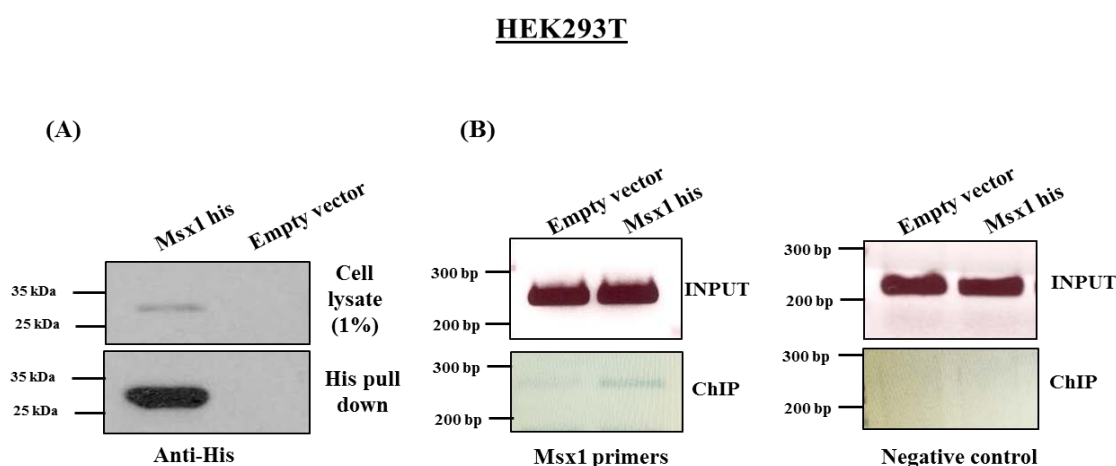
<u>**HEK293T**</u>

Figure.4.10: Interaction of Msx1 with its consensus sequence in N-WASP promoter
(A) Plasmid expressing Msx1 with His tag was transfected in HEK293T cells and His-tag pulldown was performed
to confirm Msx1 protein pulldown (B) ChIP assay was performed to analyze in-vivo binding of Msx1 to the N-
WASP promoter. Msx1 tagged with His tag was transfected in HEK293T cells and chromatin was crosslinked.
Msx1-his protein was purified using Ni-NTA beads and the bound DNA was extracted. Primers specific for Msx1
consensus sequence in N-WASP promoter were used for PCR analysis. Primers flanking a region in exon1 of *WASL*
gene were used as negative control. Input refers to the cell lysate before performing Ni-NTA pulldown.

4.8 Delineation of 393 bp promoter region

The 393 bp region between -1295 and -902 of N-WASP promoter was found to regulate

promoter activity (Figure 4.4 - 4.7). Hence, further 100 bp deletions were generated in the 1624

bp promoter construct by PCR amplification to identify the regulatory regions within the 393 bp

region (Figure 4.11 A). HEK293T cells were transfected using series of deletion constructs (Figure 4.11 A) and the promoter activity was measured. As shown in Figure 4.11 B, a significant loss of promoter activity between -1324 bp and -1231 bp indicating that the 100 bp region may be vital for promoter activity. Sequence analysis of the 100 bp region was performed using Matinspector software [http://www.genomatix.de/solutions/genomatix-software-suite.html] which predicted binding sites of DNA binding elements. Interestingly, Msx1 binding site was predicted in the 100 bp region, which further strengthened our hypothesis that Msx1 may be a integral regulator of N-WASP promoter.
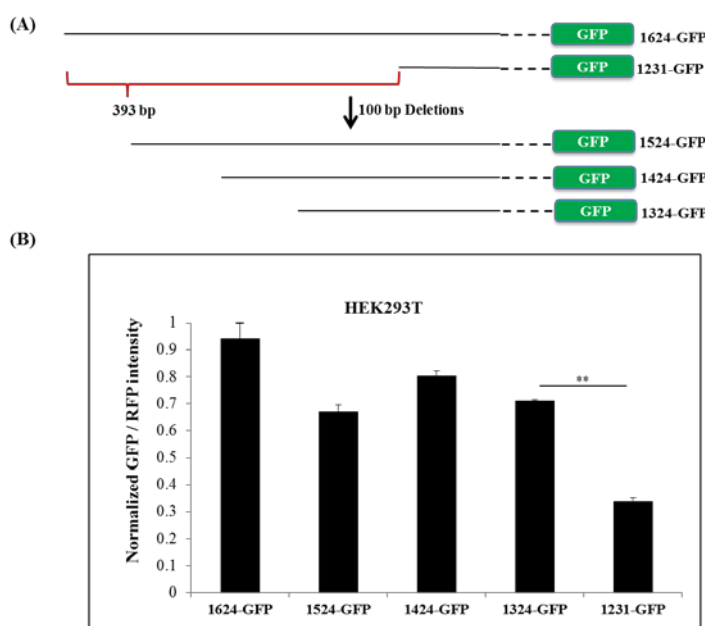
Figure.4.11: Delineation of 393 bp promoter region
(A) Series of deletion fragments of N-WASP promoter were generated. The size of fragments ranged from 1524 bp, 1424 bp and 1324 bp. All the 3 promoter constructs were sequenced and cloned in an expression vector upstream of a *GFP* gene. Sequencing accuracy was determined by comparing with the sequences at UCSC Genome Bioinformatics [https://genome.ucsc.edu/index.html]. (B) HEK293T cells were transfected with 1624-GFP, 1524-GFP, 1424-GFP, 1324-GFP, 1231-GFP promoter constructs. Plasmid expressing RFP was used as the internal control. 36 hr post transfection, the cells were lysed and fluorescence was measured using fluorimetry. The fluorescence intensity was normalized by GFP/RFP ratio and plotted. Graph represents three independent experiments. (Significance is indicated by stars * $p \leq 0.05$, ** $p \leq 0.01$, *** $p \leq 0.001$).

B) Regulation of N-WASP promoter under hypoxia conditions

Introduction:

Significant fraction of cells in solid tumors are subjected to either acute or chronic hypoxia [115]. Emerging evidences have suggested that cells exposed to hypoxia conditions acquire metastatic potential [256]. Cancer cells have a high proliferation rate and hypoxia provides a selective pressure for the survival of most aggressive tumor cells. Hence, tumor cells are resistant to anti-cancer drugs and can metastasize leading to cancer-related deaths [257].

Metastasis is a multi-step process in which cancer cells undergo changes to promote cell invasion and establish secondary tumors. Reorganization of actin cytoskeleton takes place which helps the cancer cells to acquire migratory and invasive properties. Actin and actin related proteins play a crucial role in formation of migratory organelles such as filopodia, lamellipodia, podosomes and invadopodia [185]. Actin regulatory protein, N-WASP is an important component of actin-rich motile structures and expression of N-WASP is increased under hypoxia conditions [56]. However, the exact mechanism of N-WASP upregulation and its downstream effect under hypoxia remains to be explored.

4.9 Expression of N-WASP is upregulated in response to hypoxia

Expression of N-WASP has been shown to be increased under hypoxia conditions in A431 cells [56]. To further investigate whether hypoxia affects expression of N-WASP, HeLa cells were incubated under hypoxia (24 hr) conditions using a hypoxia chamber. Since HiF1α is easily

degraded in presence of oxygen, cells were immediately lysed using 2X SDS sample buffer to

prevent degradation of HiF1α. Protein expression was analyzed by western blotting and as

shown in Figure 4.12 A, expression of HiF1α was markedly increased in HeLa cells under

hypoxia condition. Interestingly, expression of N-WASP was found to be significantly

upregulated in hypoxia treated cells as compared to control cells maintained in normoxia. Similar

trend was observed in regards to N-WASP expression in hypoxia treated A431 cells (Figure 4.12

B).
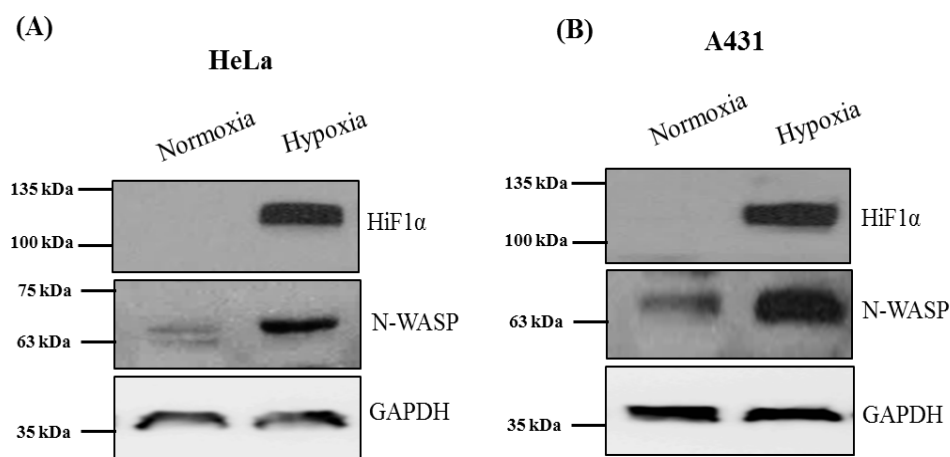
Figure.4.12: Hypoxia stimulation enhanced N-WASP expression in HeLa and A431 cells.

HeLa (A) and A431 (B) cells were grown under hypoxia conditions for 24 hr at 37°C. Cells were lysed and lysates were resolved on a 10% SDS-PAGE gel. Western blot was performed to check the expression of HiF1α and N-WASP. GAPDH was used as a loading control.

4.10 1 mM DMOG stabilizes HiF1α expression under normoxia conditions and leads to enhanced expression of N-WASP

HiF1α is rapidly degraded in presence of oxygen. This occurs within 5 min of exposure to a

normoxic environment even after hypoxia treatment [258]. In order to mimic hypoxia conditions,

Di-methyl-oxaloyl-glycine (DMOG) was used. DMOG is a cell-permeable pan hydroxylase

inhibitor which is commonly used to mimic hypoxia-mediated stabilization of HiF1α in cells [259]. In presence of DMOG, HeLa cells showed increase in HiF1α expression within 6 hrs of DMOG treatment which remained stable for 24 hr without causing cell toxicity.

HeLa cells were treated with 1mM DMOG for 6 hr in a normal tissue culture incubator. As shown in Figure 4.15 A-B, DMOG treatment caused nuclear localization of HiF1α and stabilized its expression. Cells were lysed immediately in 2X SDS sample buffer and expression of N-WASP and HiF1α was analyzed. As shown in Figure 4.13 B, HeLa cells treated with DMOG showed significant increase in expression of HiF1α as compared to the control DMSO treated cells. Real Time PCR of DMOG treated cells showed increase in N-WASP mRNA (Figure 4.13 C). N-WASP protein expression was upregulated after treatment with 1 mM DMOG which was consistent with observations using the hypoxia chamber (Figure 4.13 D).
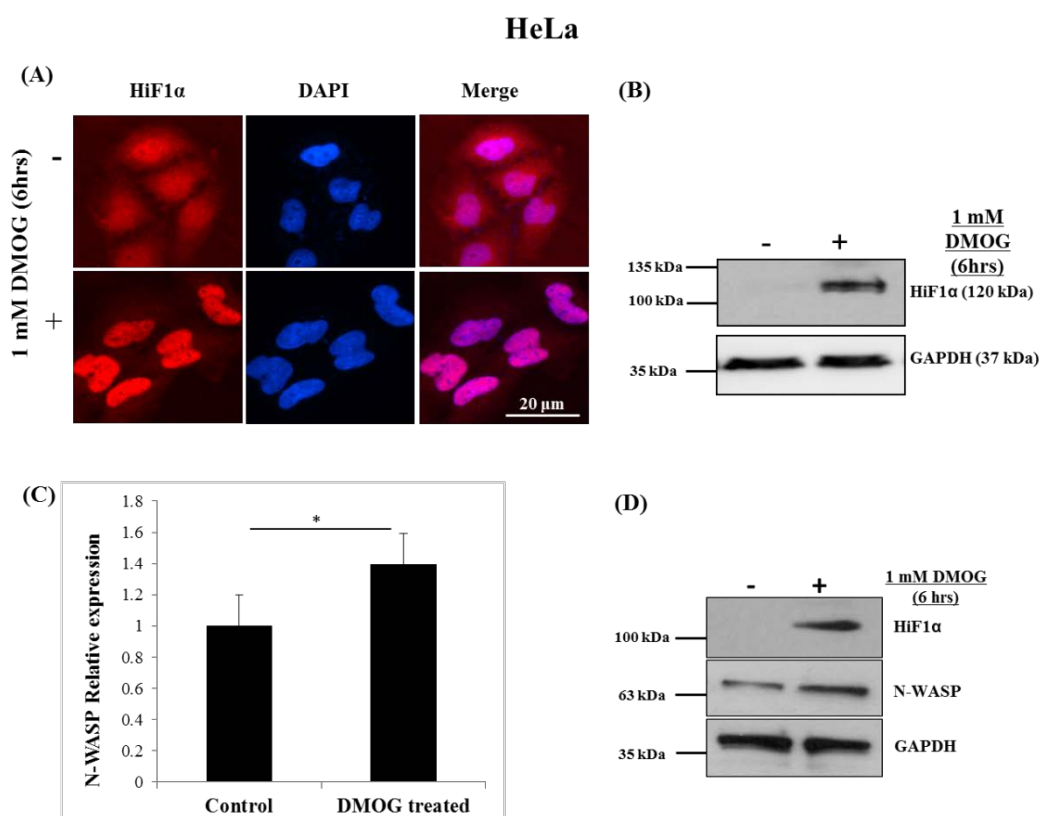
HeLa

Figure.4.13: Expression of N-WASP is enhanced in the presence of hypoxia mimic: DMOG in HeLa cells

(A) HiF1α is stabilized in presence of 1mM DMOG and translocates to the nucleus (B) Stabilization of HiF1α protein under normoxia conditions was determined by western blot analysis (C) N-WASP mRNA levels were found to be elevated in presence of DMOG by RT-PCR analysis (D) N-WASP protein expression is enhanced under DMOG treatment. (Significance is indicated by stars * $p \leq 0.05$, ** $p \leq 0.01$, *** $p \leq 0.001$).

4.11 N-WASP promoter activity is enhanced in the presence of HiF1α

Hypoxia condition leads to changes in expression of several transcription factors necessary for cell survival [256]. HiFs are transcription factors which are upregulated under low oxygen conditions [119]. HiFs bind to the HREs in the promoter of the target genes which leads to enhanced expression of genes important for adaptation under hypoxia conditions [117]. HiF1α is the chief regulator of hypoxia response [207]. To investigate whether HiF1α is responsible for

the upregulation of N-WASP in hypoxia, N-WASP promoter constructs were co-transfected with plasmid expressing HiF1α in HEK293T cells. HiF1α was cloned in an expression vector upstream of a *RFP* gene (Figure 4.14 B). The N-WASP promoter constructs (GFP) were co-transfected with HiF1α and the relative fluorescence intensity was measured. GFP/RFP normalization was performed to ensure equal uptake of both plasmids. As seen in Figure 4.15 A, the N-WASP promoter activity was found to be enhanced in the presence of HiF1α suggesting that enhanced expression of N-WASP under hypoxia condition may be due to activation of the promoter by HiF1α.

Expression of HiF1α and DNA-binding activity of HiF1 has been shown to increase exponentially to decreasing oxygen tension in HeLa cells [119]. Hence, HeLa cells were used for further experiments in this study. DMOG is an inhibitor of prolyl 4-hydroxylases and may have HiF1α-independent role. To ensure that increased expression of N-WASP in presence of DMOG is specifically due to HiF1α, YC-1 which is an down-regulator of HiF1α was used. YC-1 downregulates HiF1α post-translationally by causing functional inactivation of HiF1α [260]. As shown in Figure 4.15 C, YC-1 blocked upregulation of N-WASP expression despite the presence of DMOG suggesting that hypoxia-induced N-WASP expression is due to HiF1α.

HEK293T
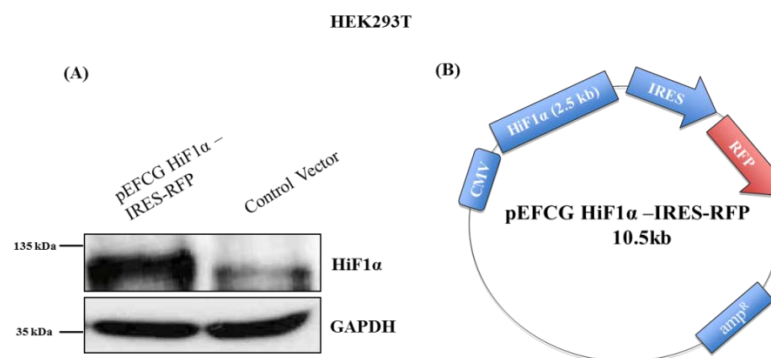
Figure.4.14: Cloning of HiF1α expression plasmid

(A) Western blot analysis of HiF1α expression plasmid. The expression of HiF1α was found to be high in presence of the plasmid gene encoding HiF1α as compared to the control vector. (B) Plasmid map of pEFCG HiF1α-IRES-RFP. The HiF1α gene was fused upstream of the IRES element and *RFP* gene.
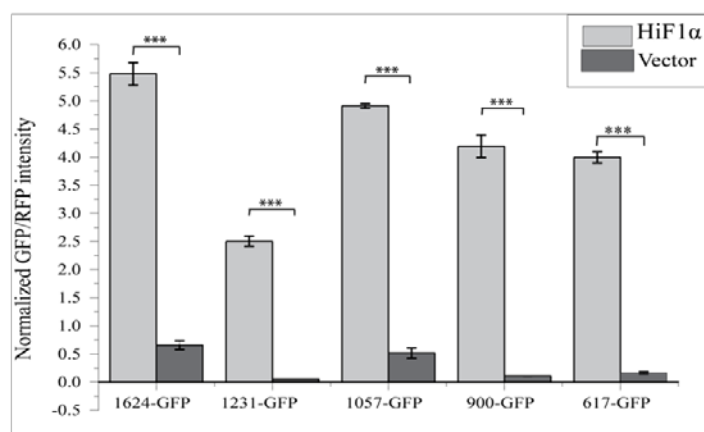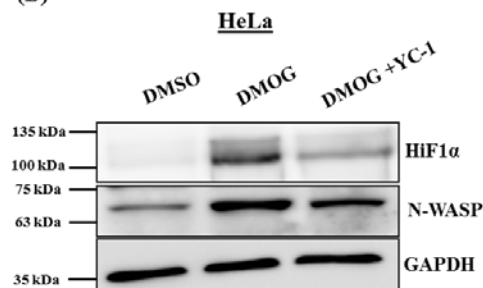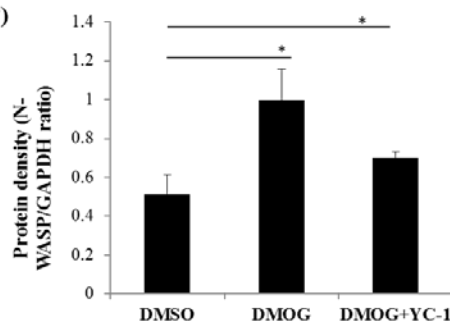
Figure.4.15: Increased N-WASP expression in hypoxia is dependent on HiF1α

(A) Fluorescent signal quantification from HEK293T cells after co-transfection with N-WASP promoter constructs and HiF1α. Cells were lysed and GFP and RFP fluorescence was measured as described in section 2.2.9. GFP/RFP normalization was done to ensure equal plasmid uptake. (B) Western blot analysis of N-WASP expression in presence of DMSO, DMOG and DMOG+YC-1 (C) Densitometric analysis of N-WASP/GAPDH protein density. (Significance is indicated by stars * $p \leq 0.05$, ** $p \leq 0.01$, *** $p \leq 0.001$).

4.12 N-WASP promoter contains two HREs

HiF1α binds to the consensus HRE sequence present in the promoter of target genes and enhances the target gene expression. In order to elucidate the mechanism of upregulation of N-WASP in hypoxia condition, sequence analysis of upstream region of human *WASL* gene (Genbank® accession number NP_003932) was performed. This was done to identify potential HiF1α binding sites in the N-WASP promoter. Analysis of the sequence upstream of the *WASL* gene revealed two putative HREs that resembled the canonical A/G/CGTG sequence (Figure 4.16 A) [261]. The first potential HiF1α binding site, HRE1 was at position -132 and the second site, HRE2 was at position -662 relative to the TSS. Both the HREs in N-WASP promoter consisted of consensus HRE sequence 5' GCGTG 3'. Figure 4.16 A-B indicate the position of HREs in N-WASP promoter.

(A)

(B)
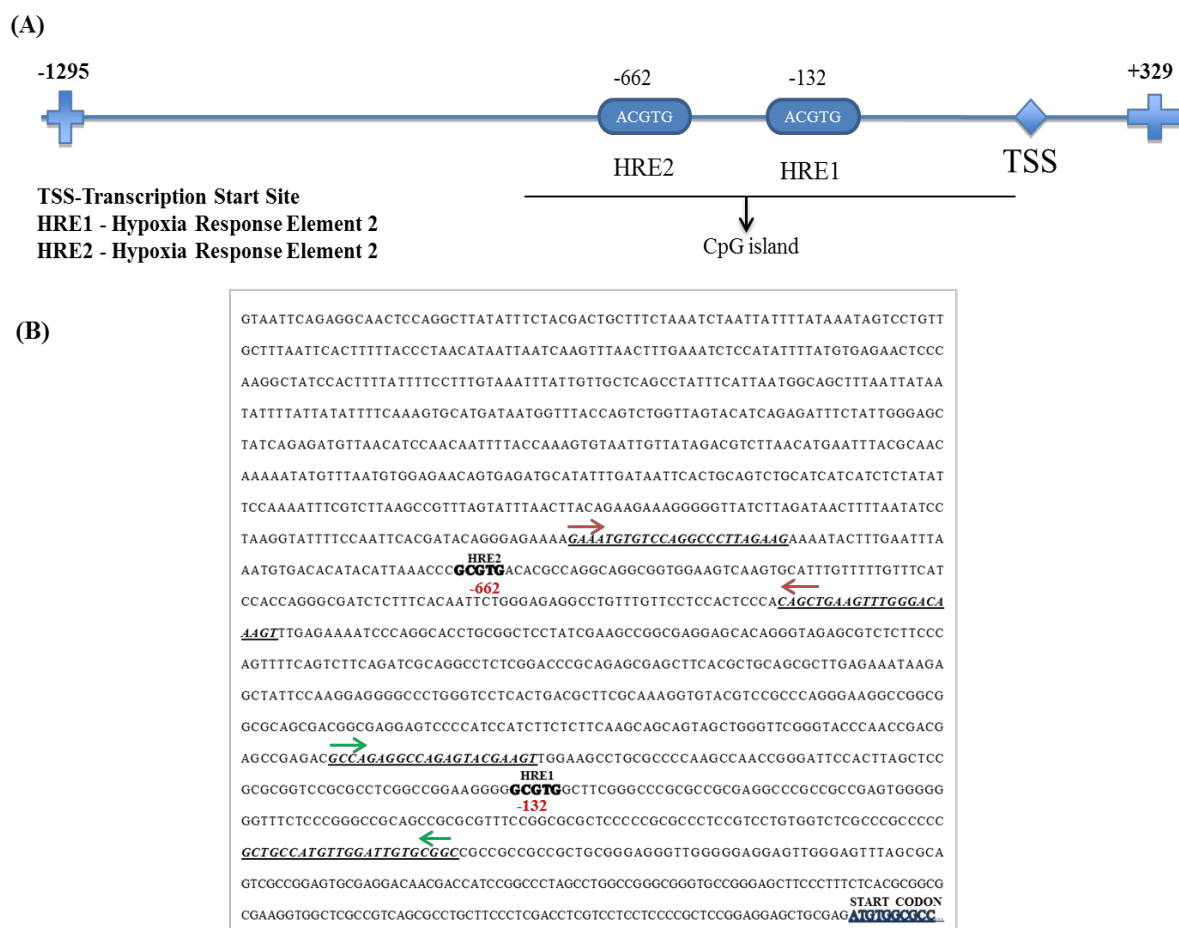
Figure.4.16: Presence of hypoxia response elements in N-WASP promoter

(A) Sequence analysis of *WASL* gene promoter consists of two HRE elements (B) Sequence of the human N-WASP promoter region encompassing ~1295 bp upstream of the start codon. Primer sequences used for the ChIP assay are highlighted and underlined. The putative HRE sequences are highlighted in bold and labelled as HRE1(-132) and HRE2(-662).

4.13 Site directed mutagenesis of the HREs in N-WASP promoter

To check whether the two HREs found in the N-WASP promoter are functional, the consensus HRE sequence was mutated and the promoter activity was analyzed. Site directed mutagenesis was performed to mutate the consensus HRE sequence from 5' GCGTG 3' to 5'GAAAG 3' in the N-WASP promoter. N-WASP promoter constructs with mutation in HRE1(-132), HRE2(-

662) and a double mutant with mutations in both HREs were generated by PCR and their sequence was confirmed. HeLa cells were transiently co-transfected with the N-WASP promoter constructs and HiF1α expression plasmid (Figure 4.14 B) and relative fluorescence intensity was measured (Figure 4.17 A). It was observed that N-WASP promoter activity was enhanced in the presence of HiF1α. HRE1(-132) mutant activity was significantly decreased in the presence of HiF1α whereas, HRE2(-662) mutant activity remained unchanged. The double mutant HRE which had mutations in both HRE1(-132) and HRE2(-662) showed a decreased activity in presence of HiF1α. This indicates that HRE1(-132) may be a potential HiF1α binding site and mutating the consensus sequence may have abolished the binding site for HiF1α resulting in decreased promoter activity.

Similar results were observed in the presence of DMOG. HeLa cells were transiently co-transfected with the N-WASP promoter constructs (wild type and HRE mutants) and were treated with 1 mM DMOG for 6 hr. Treatment with DMOG enhanced the activity of wild type promoter and decreased the activity of HRE1 mutant (Figure 4.17 B). The activities of HRE2(-662) mutant remained unchanged with/without DMOG. This suggests that HRE1(-132) may be a functional binding site of HiF1α, whereas HRE2(-662) may not be involved in hypoxia-mediated upregulation of N-WASP promoter activity.

(A)

(B)
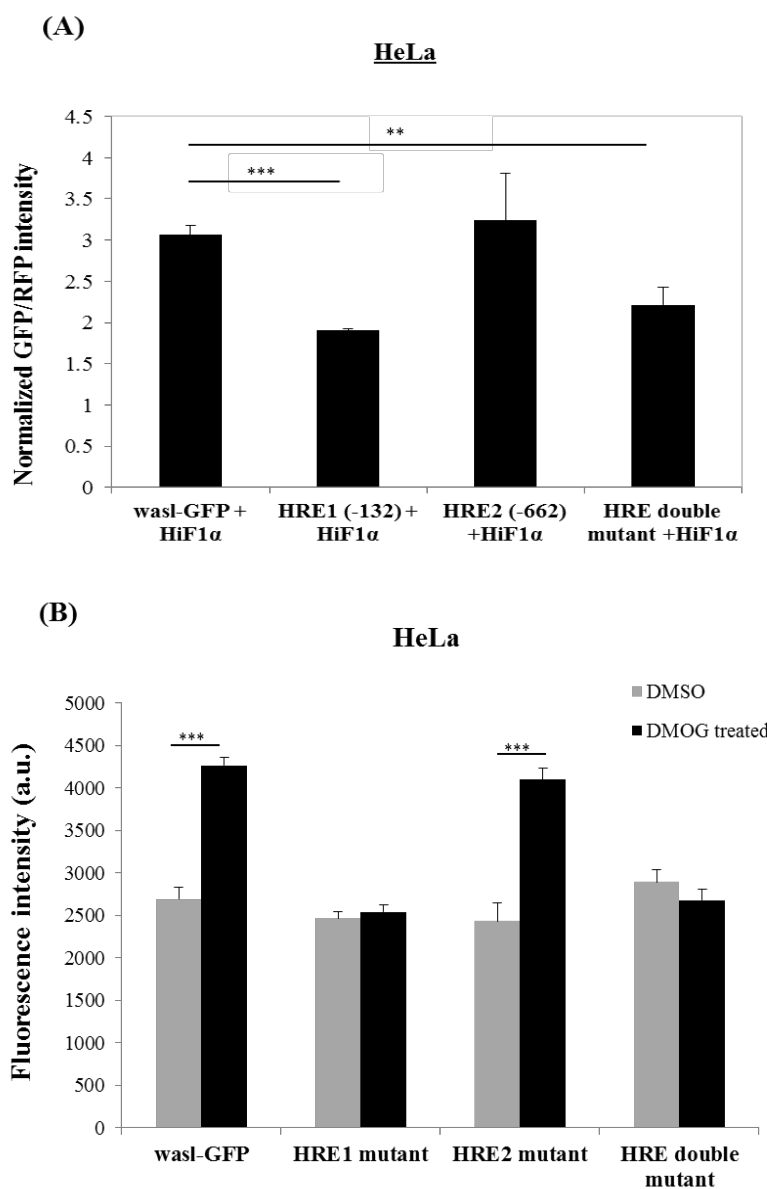
Figure.4.17: HRE1(-132) of N-WASP promoter is important for promoter activity in presence of HiF1α and DMOG

(A) Site directed mutagenesis was performed in HREs of N-WASP promoter. HeLa cells were co-transfected with HiF1α expression plasmid (RFP) and N-WASP promoter with mutation in HREs (GFP). GFP and RFP fluorescence intensity was measured after 36 hrs of transfection and normalized (B) HeLa cells were transfected with wild type N-WASP promoter and N-WASP promoter with mutations in HREs. Cells were incubated with/without 1 mM DMOG for 6 hr and the fluorescence intensity was quantified. (Significance is indicated by stars * $p \leq 0.05$, ** $p \leq 0.01$, *** $p \leq 0.001$).

4.14 HiF1α binds to HRE1(-132) in N-WASP promoter

Sequence analysis of the N-WASP promoter showed the presence of two HRE elements. Site-directed mutagenesis of the two HREs showed that HRE1(-132) may be the binding site of HiF1α during hypoxia response. Hence, ChIP assay was performed to check for an *in vivo* binding of HiF1α to the HREs in N-WASP promoter.

HeLa cells were grown till 80% confluence and cultured for 6 hr with/without DMOG. Chromatin was crosslinked using formaldehyde and the crosslinking reaction was stopped using glycine. Cells were scraped in ice-cold PBS containing protease inhibitors. Cells were lysed in lysis buffer and sheared chromatin was prepared as described in section 2.2.8. Lysates were pre-cleared and immunoprecipitation was performed using HiF1α antibody from cells with/without DMOG treatment. Mouse IgG antibody as well as no-antibody control was used as a negative control to check for specificity of the interaction. After the immunoprecipitation, the DNA was isolated and purified by phenol-chloroform method. PCR primers were used to amplify the region flanking HRE1(-132) and HRE2(-662) in N-WASP promoter. Negative control reaction was set up using a primer flanking a region in exon 1 of N-WASP. As seen in Figure 4.18, a visible PCR band was observed in DMOG-treated cells immunoprecipitated with HiF1α and input. In contrast, there was no PCR amplified product for the primers flanking HRE2(-662) in the N-WASP promoter. PCR amplification was not observed for mouse IgG as well as no-antibody control indicating the specificity of the interaction between HiF1α and HRE1(-132). These findings confirm that HiF1α specifically binds to the HRE1(-132) present in the N-WASP promoter under hypoxia condition.
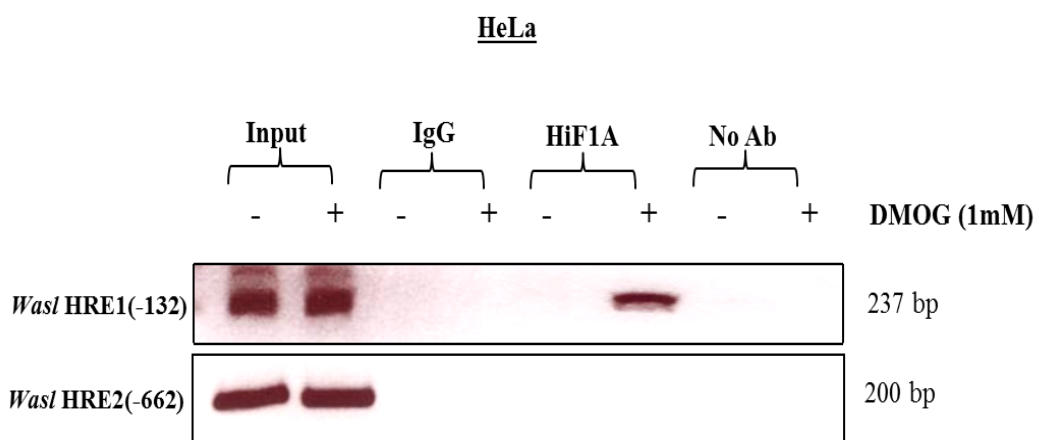
Figure.4.18: HiF1α interacts with HRE1(-132) of the N-WASP promoter

ChIP assay was performed using HeLa cells with/without DMOG treatment. PCR primers flanking HRE1(-132) and HRE2(-662) in N-WASP promoter were used for PCR amplification. Monoclonal HiF1α antibody was used for immunoprecipitation. For negative control, IgG and No antibody control was used. Crosslinked chromatin was used as the input.

4.15 Gelatin degradation assay

(A) HeLa cells are unable to degrade gelatin in invadopodia formation assay

Hypoxia leads to upregulation of HiF1α and HiF1α has been linked to increased metastatic potential in several types of cancer [134, 262]. Emerging evidences have linked HiF1α to invasive ability of cancer cells [221, 257]. Invasive cancer cells employ invadopodia to degrade underlying matrix and metastasize to distant organs [263]. HiF1α is shown to be necessary for hypoxia induced invadpodia formation [221, 264]. N-WASP plays a role in trafficking of MMPs to the invadopodia and N-WASP is also shown to localize to the leading edge of invadopodia [30, 104]. Hence, the next step was to assess whether increase in N-WASP expression during hypoxia had functional relevance in invadopodia formation.

Gelatin degradation assay was performed to observe invadopodia activity in HeLa cells. Briefly, coverslips were acid-washed, coated with poly-L-lysine and cross-linked with 0.5% glutaraldehyde (ice-cold). Coverslips were washed with PBS and coated with Oregon Green 488-conjugated fluorescent gelatin for 10 min in dark. Excess gelatin was removed and residual glutaraldehyde was quenched using sodium borohydride. Coverslips were washed, sterilized and quenched with complete media for 1 hr at 37°C before seeding of the cells. Hela cells were used for gelatin degradation assay and immunostained with phallodin 594 to visualize actin filaments. As shown in Figure 4.19, no gelatin degradation was observed for HeLa cells which may be due to low ECM degradative capacity of HeLa cells.

MDA-MB-231 cell line is an invasive breast carcinoma cell line which was used to study invadopodia activity in the gelatin degradation assay. MDA-MB-231 cells are commonly used to study invadopodia as they express high levels of MMPs and hence can degrade ECM [8]. As shown in Figure 4.19, gelatin degradation (black spots) were observed which co-localized with actin puncta (red dots) indicating areas of matrix degradation (indicated by arrows). Hence, MDA-MB-231 cells were used to study the role of N-WASP in hypoxia-induced invadopodia formation.
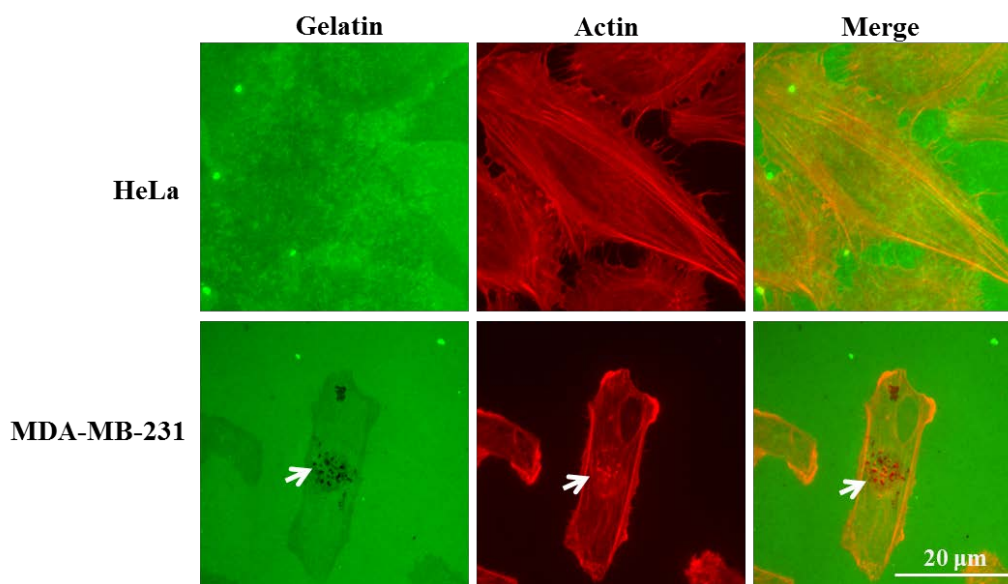
Figure.4.19: HeLa cells are unable to degrade gelatin matrix whereas MDA-MB-231 showed distinct gelatin degradation spots

HeLa cells were seeded on Oregon green gelatin coated coverslips for 6 hr. Cells were fixed and stained with Phalloidin 594 (red) to stain F-actin. MDA-MD-231 cells were seeded on Oregon green fluorescent gelatin coated coverslips for 6 hr and fixed. Cells were stained with Phalloidin 594 (red) to stain actin (Bottom). Images were captured using 40X objective of a fluorescence microscope. Arrows indicate areas of gelatin degradation. Merge images show co-localization of gelatin degraded areas with F-actin. Scale bar: 20 µm.

(B) Generation of N-WASP knockdown MDA-MB-231cells

In order to determine if N-WASP affects the cell phenotype in hypoxia, MDA-MB-231 cells with stable knockdown of N-WASP were generated. Lentivirus was generated using HEK293T cells as described in Section 2.2.3.6. pLJM1 and pLJM-N-WASP shRNA plasmids were transfected in HEK293T cells along with lentiviral packaging plasmids. Lentiviral supernatants were collected at 24 hr and 48 hr after transfection. MDA-MB-231 cells were seeded in a 6-well plate and infected twice with the harvested lentivirus using 8 µg/ml polybrene. Uninfected cells were eliminated by puromycin selection (1 µg/ml). N-WASP specific shRNA (pLJM-N-WASP shRNA) was used to knockdown the expression of N-WASP in MDA-MB-231 cells. This cell

line will be referred to as N-WASP^{KD}. Cells infected with the empty plasmid (pLJM1) will be referred to as Control. After selection with puromycin, knockdown of N-WASP was analyzed by western blotting (Figure 4.20 B).

Human N-WASP specific shRNA targets the coding region of N-WASP which can also affect the expression of exogenous N-WASP. Therefore, shRNA resistant version of human N-WASP (N-WASP^{Rescue}) was generated. Site directed mutagenesis was performed by PCR for introducing four silent mutations in shRNA targeted region of N-WASP gene (Figure 4.20 A). N-WASP^{KD} cells were infected with lentivirus for shRNA resistant N-WASP gene (pLJM-N-WASP^{Rescue}) to generate N-WASP^{Rescue} cell line. Reconstitution of N-WASP in knockdown cells was confirmed by performing a western blot (Figure 4.20 B).
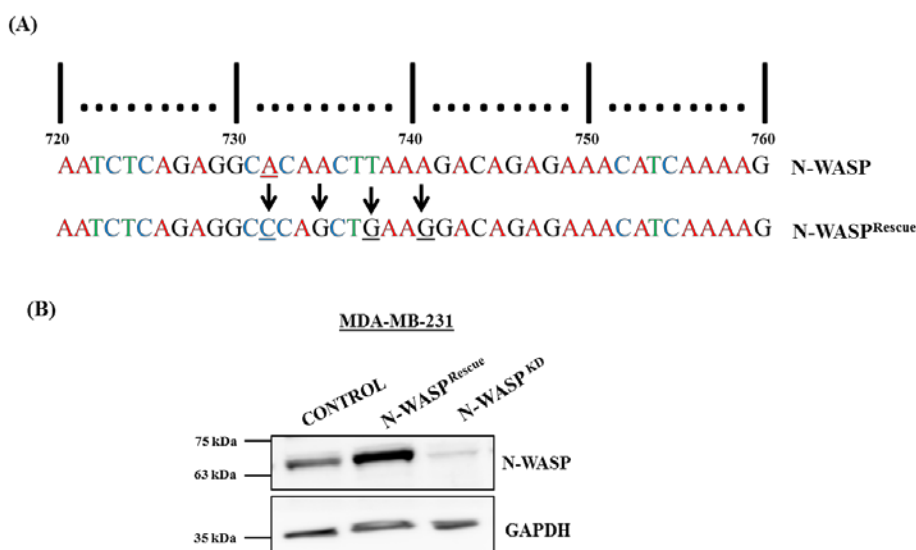
Figure.4.20: Knocking down of endogenous N-WASP expression and reconstitution of N-WASP in MDA-MB-231 cells
(A) shRNA resistant N-WASP gene was generated by introducing 4 silent point mutations in N-WASP coding sequence which abolishes shRNA binding sequence (B) MDA-MB-231 cells with N-WASP knockdown were generated by lentiviral transduction using a shRNA specific for N-WASP. Knockdown was confirmed by western blot analysis. Expression of N-WASP was reconstituted using shRNA resistant N-WASP gene (N-WASP^{Rescue}).

4.17 N-WASP is important for hypoxia-induced invadopodia formation

Gelatin degradation assay was performed to measure gelatin degradation in MDA-MB-231 stable cells . In order to mimic hypoxia conditions and stabilize HiF1α, 1 mM DMOG was used. In MDA-MB-231 cells, DMOG has been shown to increase the number of cells forming invadopodia as well as to increase the gelatin degradation capacity of invading cells [264-266]. Cells were seeded on fluorescent gelatin coated coverslips and incubated for 6 hr at 37°C in the presence of 1 mM DMOG. After 6 hr of DMOG treatment, the cells were fixed and stained with Alexa Fluor 594 phalloidin to stain F-actin. Cortactin was used as an invadopodia markers as it plays a role in regulating invadopodia formation and activity [106]. As shown in Figure 4.21 A, treatment with DMOG increased the number of invadopodia which can be seen by enhanced degradation of gelatin (indicated by arrow). N-WASP[KD] cells caused a reduction in the number of invadopodia per cell as well as the percentage of cells with invadopodia (Figure 4.21 B and D). Interestingly, DMOG treatment did not increase the number of invadopodia forming cells in N-WASP[KD] cells as the number of cells degrading the gelatin with/without DMOG were found to be same. Reconstitution of N-WASP in knockdown cells could rescue the gelatin degradation capacity of MDA-MB-231 cells which was further enhanced in presence of DMOG (Figure 4.21 C-D). This suggests that N-WASP plays a vital role in hypoxia induced invadopodia formation.

MDA-MB-231
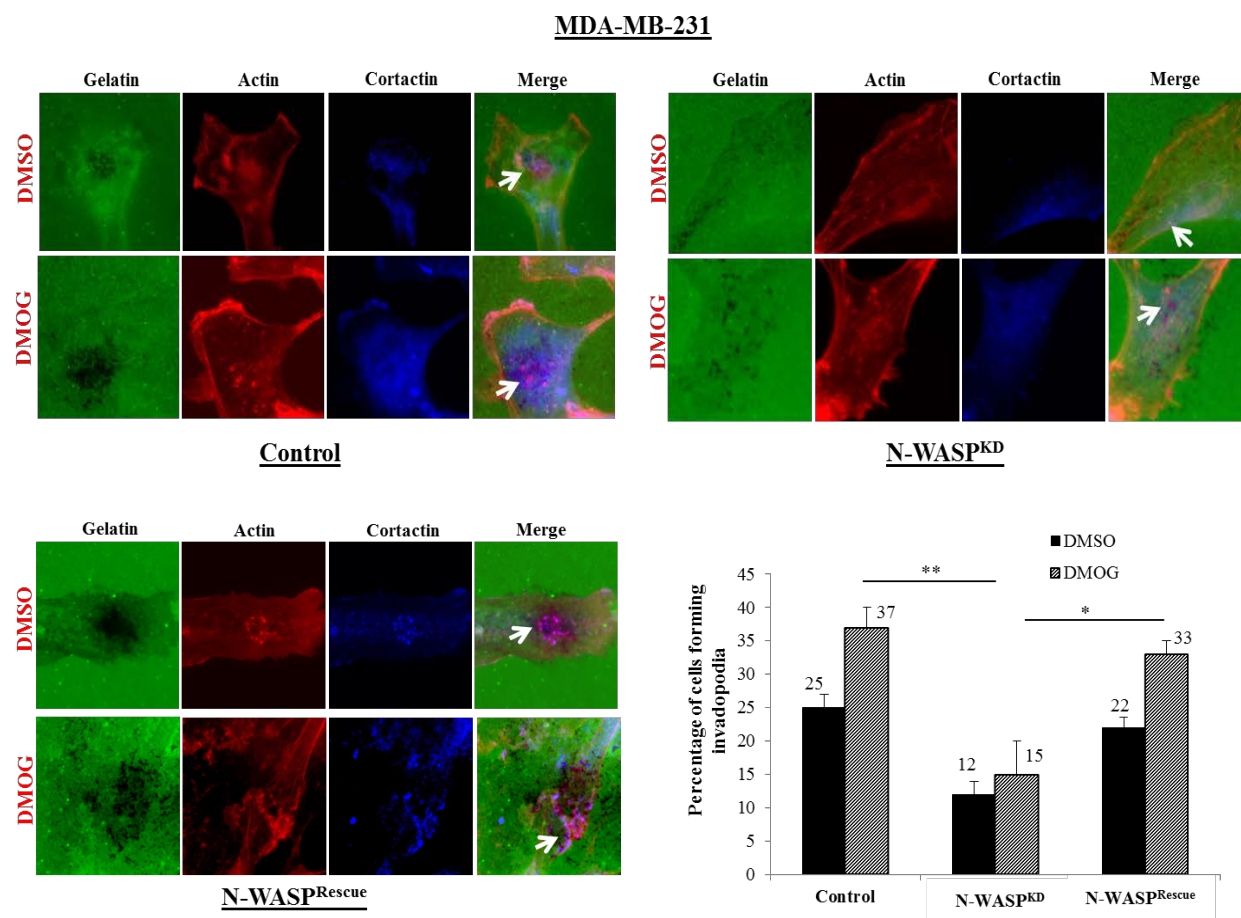
Figure.4.21: N-WASP is important for hypoxia induced invadopodia formation

(A-C) Cells were seeded on fluorescent gelatin coated coverslips for 6 hrs and treated with 1 mM DMOG. After 6 hr of DMOG treatment, cells were fixed and stained for phalloidin 594 (actin) and cortactin. Degraded areas of fluorescent gelatin alongwith co-localization of F-actin (red) and cortactin (blue) indicate presence of invadopodia. Images were taken using 40X oil objective lens. Presence of actin dots (red), cortactin (blue) with underlying degraded gelatin (black areas) was used to identify degradation areas (pink dots on gelatin degradaed areas). Arrows indicate areas of gelatin degradation. Scale bar: 10 μm (D) Percentage of cells with invadopodia was counted for DMSO and DMOG treated cells. To quantify invadopodia formation, the total number of cells forming invadopodia were counted on each captured image and normalized to the total cells in the same image. (Significance is indicated by stars * p ≤ 0.05, ** p ≤ 0.01, *** p ≤ 0.001).

CHAPTER 5: DISCUSSION

Introduction:

Metastasis is a multi-step process involving numerous cellular events. In early stages of metastasis, cancers of epithelial origin (carcinomas) abolish cell-cell adhesion and are able to degrade the underlying basement membrane [152]. Cancer cells are highly motile and can degrade the ECM by MMPs present in the invadopodia [267]. During invasion, cells undergo EMT, which enables them to invade neighbouring tissues and blood vessels and establish secondary tumors [148]. Actin cytoskeleton is the primary driver of cell motility, an essential function of normal body tissues. However, the same processes of motility and invasion are at the heart of cancer cell metastasis and invasion [185]. Understanding the regulation of cell motility and how it is affected in cancer cells will provide a better understanding of metastasis and how to prevent it.

5.1 Transcriptome analysis of HaCaT and A5-RT3 by RNA sequencing

RNA-Seq is a next generation sequencing technology which provides a genome-scale transcriptome map and gives detailed information regarding expression of the whole genome [194]. The current study provides a comprehensive analysis of transcriptome data of HaCaT and A5-RT3 cells obtained through the Illumina Hi-SeQ™2000 platform. cDNA reads were mapped to their genomic counterparts to obtain accurate information about alternate splicing and differential gene expression [268]. Analysis of the DEGS showed that 4408 genes are upregulated and 1403 genes are downregulated in metastatic A5-RT3 as compared to non-

tumorigenic HaCaT cells. Since A5-RT3 cells are derived from HaCaT cells, the differential expression of genes helps in understanding altered cellular functions in metastasis.

Downregulation of certain genes in A5-RT3 as compared to HaCaT may be an indication of the negative role played by these genes in metastatic progression. These genes may be involved in suppressing metastatic progression and their downregulation may promote metastasis. Likewise, upregulation of certain genes in A5-RT3 as compared to HaCaT may be an indication of the significant role played by these genes to promote metastasis. Analysis of DEGs showed an increase in expression of N-WASP, HiF1α and WIP in A5-RT3 as compared to HaCaT. Studies have already shown that N-WASP and HiF1α play a role in metastatic progression [60, 114]. However, the role of WIP in cancer progression and metastasis has not been well studied.

Analysis of the top 10 upregulated genes in A5-RT3 shows N-cadherin and fibromodulin to be highly upregulated as compared to HaCaT cells. N-cadherin, a mesenchymal marker is highly expressed in metastatic cells and plays a role in transendothelial migration [269, 270]. Fibromodulin is a proteoglycan which is known to regulate activity of TGF-beta by sequestering TGF-beta in ECM [271]. This suggests that a large majority of upregulated genes in A5-RT3 may be involved in promoting metastasis. Of all the transcripts found, WIP transcripts were found to be highly upregulated in metastatic A5-RT3 cells and undetectable in non-tumorigenic HaCaT cells. This provided a strong indication that WIP may play a role in promoting metastasis.

5.2 Differential expression of WIP during metastatic progression

WIP is a regulator of actin cytoskeleton and forms an important component of actin-rich motile structures such as filopodia and invadopodia [69, 86, 89]. Enhanced expression of WIP at mRNA and protein level in A5-RT3 cells relative to HaCaT cells confirmed the RNA-Seq results. (Figure 3.3). Tumor metastasis is characterized by alterations in cell-ECM adhesion followed by increase in cell motility, invasion and proliferation [65]. The hypothesis that WIP is important for metastasis was based on two observations. Firstly, RNA-Seq analysis of non-tumorigenic HaCaT and its metastatic clone A5-RT3 showed WIP to be highly upregulated in A5-RT3 cells. Secondly, WIP has been shown to promote migratory and invasive properties of cells [101, 107]. In order to analyze the role of WIP in metastasis, analysis of each of these steps was done using stable cell lines with overexpression and knockdown of WIP (Figure 3.4-3.5).

5.3 Role of WIP in cell migration and cell invasion

To study the role of WIP in metastasis, A549 cancer cell line was used as the model system. A549 is an adenocarcinoma alveolar basal epithelial cell line [272, 273]. Expression of WIP was found to be increased in A549 cells as compared to non-cancerous SAEC cells (Figure 3.4 A). Wound healing assay was performed to study the role of WIP in cell migration. As seen in Section 3.6, overexpression of WIP in A549 cells enhanced cell migration relative to the control cells. On the contrary, knockdown of WIP led to slower migration in comparison to the control cells (Section 3.7). Studies performed in NIH3T3 fibroblast cells have demonstrated WIP as a negative regulator of fibroblast migration [101]. Since A549 cells are carcinoma cells, it may be possible that WIP plays a differential role in enhancing epithelial cancer cell motility.

Directed cell migration is the result of changes in cytoskeleton and reorganization of the cell adhesion in response to extracellular stimuli [5]. Vinculin and paxillin are components of the FAs, which are adhesive structures formed during cell migration [216]. Vinculin is a structural protein linked to actin and talin and is necessary for adhesion strengthening. Paxillin is a signalling and adaptor protein which binds to vinculin and plays a role in integrin mediated signalling [217]. Vinculin null MEFs show enhanced motility, delayed cell spreading and possess reduced number of FAs [219]. Cells lacking vinculin are highly motile and metastatic and studies have shown vinculin to regulate cell motility via ERK pathway by mediating accessibility of paxillin for FAK interaction [274]. Similarly, focal complexes containing low levels of paxillin have been reported to enhance movement of lamellipodium [275]. Vinculin and paxillin staining was performed to study the FAs in A549 cells overexpressing WIP. As shown in Figure 3.8-3.9, overexpression of WIP led to reduction in number of vinculin and paxillin patches. Lesser number of vinculin patches in A549^{WIP} cells may be due to reduced number of FAs which explains enhanced migration of WIP overexpressing cells in wound healing assay. Although expression of vinculin was not affected in WIP overexpressing cells as compared to control cells, the difference in number of vinculin patches may be due to reduced localization of vinculin at the FAs. Similarly, number of paxillin patches were found to be reduced in A549^{WIP} cells and enhanced in A549$^{WIP\ KD}$ cells which indicates increased FAs in A549$^{WIP\ KD}$ cells. Thus, reduced localization of vinculin and reduced expression of paxillin could be due to reduced FAs in WIP overexpressing cells which explains the enhanced migration.

Tumor cell invasion is an important step in metastasis and is mediated by invadopodia [276]. Role of WIP in invasion was studied using matrigel invasion assay. It was found that overexpression of WIP in A549 cells lead to enhanced invasion through matrigel as compared with the control cells (Figure 3.13). This is consistent with a recent study which demonstrated the necessity of WIP for invasion in breast cancer cells using a 2D and 3D culture system [107]. WIP is present in invadopodia and plays a role in formation and activity of invadopodia [31, 88]. Moreover, WIP interacts with cortactin, Nck and N-WASP, each of which play a positive role in regulating formation and activity of invadopodia [31, 83, 106, 277]. Thus, it may be possible that WIP plays a role in ECM degradation by recruiting either of these proteins at the site of invadopodia which explains the enhanced invasion in matrigel invasion assay.

5.4 Role of WIP in cell spreading, cell proliferation and anchorage independent growth

During sub-culturing of A549$^{\text{WIP KD}}$ cells, it was observed that A549$^{\text{WIP KD}}$ cells proliferated at a slower rate and displayed reduced cell size. Proliferation of WIP overexpressing and knockdown cells was analyzed by MTT assay and it was found that proliferation rate of A549 cells was directly proportional to the expression level of WIP (Figure 3.11). Till date, studies on WIP have demonstrated its role in regulating cell motility and adhesion by actin polymerization. However, its effect on cell growth and proliferation is intriguing and remains unknown. Nonetheless, recent studies have demonstrated the importance of actin polymerization in regulating transcriptional programs and signalling pathways linked to cell proliferation which indicates a possible role of WIP in regulating cell proliferation [57, 278].

Reduction in cell size for A549$^{\text{WIP KD}}$ cells was also evident in the F-actin staining (Figure 3.12). Hence, it was of interest to study the role of WIP in cell spreading. Cell spreading assay was performed for A549$^{\text{WIP}}$ and A549$^{\text{WIP KD}}$ cells and it was observed that overexpression of WIP did not affect the spreading of cells on fibronectin coated surface. However, A549$^{\text{WIP KD}}$ cells were observed to spread faster on fibronectin coated surface (Figure 3.13). This differs from previous results which showed A549$^{\text{WIP KD}}$ cells had reduced cell size and looked less spread (Figure 3.12). A possible reason for this may be the increased number of FAs in WIP knockdown cells as compared to the control cells. As fibronectin is a known activator of integrin signaling, it may be possible that increased number of FAs lead to enhanced integrin signaling and thus better spreading of WIP knockdown cells on fibronectin coated dishes [279].

WIP plays a role in maintaining the closed conformation of N-WASP by binding to the WH1 domain of N-WASP and preventing N-WASP activation by Cdc42 [39]. N-WASP has been shown to positively regulate cell spreading in fibroblast [43]. It may be possible that reduced WIP levels lead to higher amount of N-WASP in open conformation which leads to enhanced actin polymerization and faster spreading of WIP knockdown cells.

Metastic potential of WIP was also demonstrated in the soft agar assay. Overexpression of WIP was found to enhance the size and number of colonies growing in soft agar in comparison to the control cells (Figure 3.14). Cells which possess high proliferation rates can grow faster in soft agar. Anchorage independent growth is a sign of highly transformed cells as these cells can survive and proliferate in the absence of ECM transmitted signals [280]. Thus, high proliferation rate coupled with increased metastatic potential may cause enhanced anchorage independent

growth of WIP overexpressing cells. Acquisition of invasive, migratory and proliferative properties as well as anchorage independent growth is a primary step in metastatic progression [222, 225, 276]. WIP was found to positively promote all of the above steps which strongly affirmed the hypothesis that WIP may be a pro-metastatic gene.

5.5 Role of WIP in TGF-beta induced EMT

TGF-beta is a prototypical cytokine for inducing in-vitro EMT, whereas other cytokines such as EGF, HGF are context dependent and variable [281]. TGF-beta causes distinct morphological changes as well as induces expression of mesenchymal markers in A549 cells. TGF-beta plays a crucial role in inducing lung fibrosis and is found to be upregulated in lungs of patients with idiopathic pulmonary fibrosis, which involves scarring of lung tissue [281]. Hence, it was of interest to study the role of WIP in TGF-beta induced EMT in A549 cells, which are human adenocarcinomic epithelial cells.

Different concentrations of TGF-beta (2 ng, 5 ng, 10 ng) were used to induce EMT and 5ng TGF-beta treatment for 48 hrs was found to be optimal to give rise to the distinct morphological changes characteristic of EMT. An optimal concentration of TGF-beta would be effective in allowing higher level of functional TGF-beta receptor activity to maintain the TGF-beta signalling in a more sustained condition [282]. Also, TGF-beta is a known regulator of cell proliferation and high amount of TGF-beta can exert an inhibitory effect on cell growth [161]. Reduction in expression of epithelial markers such as E-cadherin and increased expression of mesenchymal markers such as N-cadherin, vimentin, α-SMA and snail was confirmed by

western blot analysis of TGF-beta treated A549 cells (Figure 3.15 B). Reduction of E-cadherin and reorganization of actin cytoskeleton was also observed by immunofluorescence (Figure 3.15 C).

Expression of WIP was increased in the presence of TGF-beta suggesting that WIP may be regulated by TGF-beta (Figure 3.16). Enhanced localization of WIP was observed at the membrane protrusions which co-localized with actin in TGF-beta treated A549 cells indicating a possible role of WIP in EMT induced cell migration and invasion (Figure 3.17). Similar studies have been performed for WAVE3, an actin cytoskeleton regulator belonging to the WASP/WAVE family of proteins. WAVE3 was found to be necessary for promoting TGF-beta induced EMT in breast cancer cells and inactivating WAVE3 mitigated metastasis stimulated by TGF-beta [283].

A549 cells with stable WIP overexpression and WIP knockdown were generated to determine if TGF-beta induced EMT progression would be altered by varying levels of WIP. WIP overexpressing cells subjected to TGF-beta treatment demonstrated a more elongated and spindle shaped morphology in comparison to the control cells. Loss in E-cadherin expression was significantly higher and faster in WIP overexpressing cells as compared to TGF-beta treated control cells (Figure 3.18). Down-regulation of E-cadherin is a critical step in cancer progression and leads to a more invasive and de-differentiated phenotype [284]. Studies on breast cancer cells have demonstrated that loss in E-cadherin expression can confer metastatic ability to otherwise non-metastatic cells [285]. Expression of mesenchymal markers such as vimentin and

N-cadherin was significantly enhanced in WIP overexpressing cells relative to control cells in the presence of TGF-beta. This indicates that expression of WIP enhanced EMT progression.

On the contrary, knockdown of WIP inhibited the cells from attaining mesenchymal phenotype during EMT. As seen in Figure 3.19 A, WIP knockdown cells failed to give rise to an elongated and fibroblast-like morphology compared to TGF-beta treated control cells (A549^{VECTOR}). The cell size was smaller in WIP knockdown cells with reduced number of stress fibers and induction with TGF-beta did not show any dramatic morphological changes (Figure 3.20-3.21). Although, western blot analysis demonstrated TGF-beta mediated loss of epithelial marker E-cadherin, the gain of N-cadherin and α-SMA was not significant as compared to the control cells (A549^{VECTOR}). Induction of stable EMT by overexpression of Snail also failed to induce mesenchymal morphology in WIP knockdown cells (Figure 3.20). Thus, knockdown of WIP inhibited the cells from attaining the morphological changes associated with transient as well as stable EMT.

A549$^{WIP\ KD}$ cells displayed a retracted morphology and reduced cell size (Figure 3.12). WIP regulates actin polymerization by directly binding to actin as well as by interacting with actin polymerizing proteins such as N-WASP [97]. Hence, visualization of actin cytoskeleton was performed for WIP knockdown cells during TGF-beta induced EMT. As shown in Figure 3.21, knockdown of WIP severely diminished the number of stress fibers associated with EMT. Similarly, knockdown of WIP itself reduced the number of stress fibers in A549 cells. Formation of stress fibers is controlled by RhoA, a small GTPase belonging to Rho family of GTPases [186]. RhoA plays a crucial role in actin cytoskeleton remodeling during EMT and blockage of

RhoA inhibited TGF-beta induced EMT [230]. Studies have shown that RhoA activation level is associated with reduced E-cadherin expression [286]. Rearrangement of the actin cytoskeleton by RhoA is essential to accomplish EMT phenotype as well as migratory properties characteristic of EMT [287]. RhoA is a well-studied regulator of cell migration, proliferation and invasion and alteration in RhoA signaling has been found to promote cancer invasion and metastasis [288, 289]. A recent study has demonstrated anti-tumor effect of RhoA depletion in ovarian cancer cells [290]. It was observed that knockdown of RhoA in ovarian cancer cells led to reduced tumor cell migration and invasion as well as suppressed tumorigenic ability of these cells in nude mice. Silencing of RhoA has also been shown to suppress human colorectal xenografts in-vivo [291].

It was observed that A549$^{WIP\ KD}$ cells showed significantly reduced levels of RhoA and A549^{WIP} cells showed increased levels of RhoA as compared to control cells (Figure 3.22). Thus, reduced RhoA content in A549$^{WIP\ KD}$ cells may lead to decreased number of stress fibers and reduced cell size in A549 cells. Likewise, low RhoA expression can be a reason for inhibition of EMT morphological changes in A549$^{WIP\ KD}$ cells. RhoA levels were significantly reduced in WIP knockdown cells, which strongly implied that reduced proliferation, migration and invasion of A549$^{WIP\ KD}$ cells may be due to low RhoA levels. Treatment of A549 cells with C3 transferase disrupted actin stress fibers and inhibited RhoA levels. However, there was no change in WIP expression as shown in Figure 3.22. This indicates that WIP may lie upstream of RhoA and may play a role in regulating RhoA expression. Rescue experiment was performed by reconstituting WIP expression in A549$^{WIP\ KD}$ cells which showed increase in RhoA protein expression as well

as appearance of stress fibers in A549^{Rescue} cells as compared to A549$^{WIP\ KD}$ cells (Figure 3.24 A-B).

Knockdown of WIP did not affect RhoA mRNA expression suggesting that WIP regulates RhoA post-translationally (Figure 3.23 A). Expression of immediate downstream effectors of RhoA such as ROKα and mDia1 remained unchanged by knockdown of WIP (Figure 2.23 B). It may be possible that WIP reduces the expression of other RhoA effectors or affects only the functional activity of RhoA effectors. WIP was found to specifically interact with RhoA (Figure 3.24 C) which strenthened our hypothesis that RhoA expression is regulated by WIP.
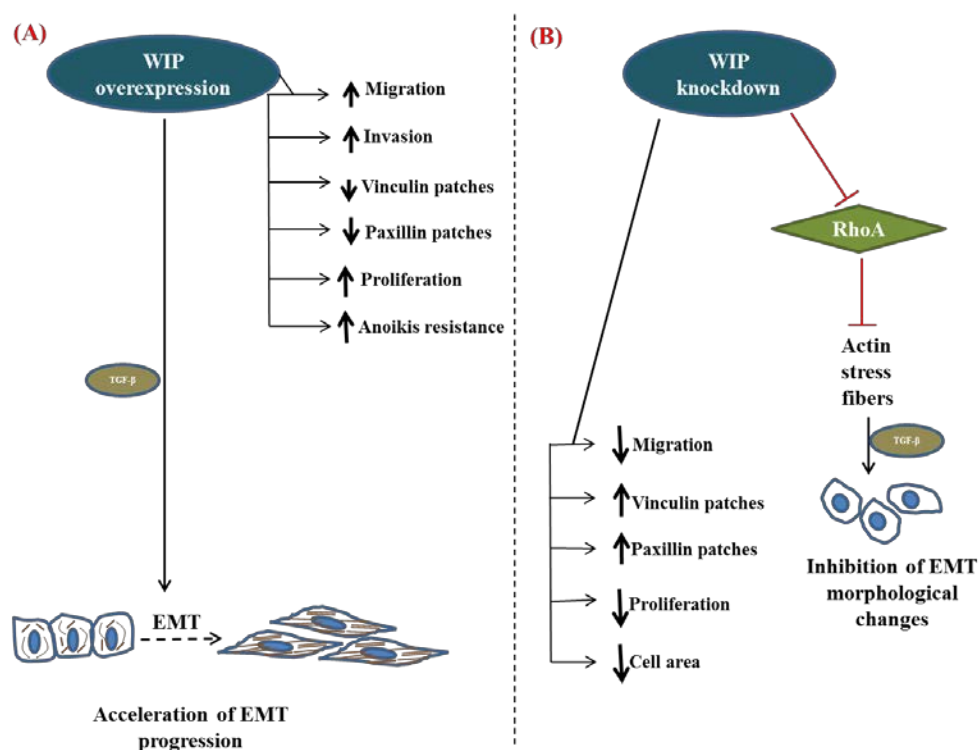
Figure.5.1: Summary of the role of WIP in metastasis
WIP positively regulates cell migration, invasion, proliferation and anchorage independent growth of A549 cells. Knockdown of WIP reduced RhoA content leading to loss of stress fibers and thus inhibits morphological changes in TGF-beta induced EMT.

5.6 Characterization of N-WASP promoter

N-WASP expression is elevated under conditions of hypoxia and EGF induced EMT [56]. N-WASP expression was found to vary in different cancer cells depending on progression of cancer (Figure 4.1). Differential expression of N-WASP may be due to transcriptional regulation of N-WASP which is determined by regulatory elements binding to N-WASP promoter.

N-WASP promoter has not been characterized and this is the first study carried out to study transcriptional regulation of N-WASP. To characterize the N-WASP promoter, a bioinformatics analysis of the genomic region located 5' upstream of the *WASL* gene was done. N-WASP promoter contains a CpG island at ~ -800 position, relative to the TSS (Figure 4.2). CpG islands are regions of DNA with a high GC content and high frequency of CpG dinucleotides relative to size of the genome [292]. CpG island is a characteristic of constitutively active genes, which explains the ubiquitous expression of N-WASP. The CpG island in N-WASP promoter has 60% of GC nucleotides clustered in long stretches predominantly mapping to the proximal 1kb segment as indicated in Figure 4.2. Thus, the CpG island allows N-WASP promoter to remain constitutively active regardless of the deletion of 393 bp regulatory region from the 1624 bp promoter fragment. No TATA boxes were present in the region near the transcription site. Although a TATA element is present at ~ -1250 bp upstream of the TSS, its functionality has to be checked. Interestingly, ~76% of human core promoters lack the TATA box, have a high GC content and are enriched with Sp1 binding sites [293]. Sequence analysis of the N-WASP promoter region also shows presence of three Sp1 binding sites as well as ~60% GC content indicating that a initiator element may be regulating N-WASP expression in absence of TATA box.

5.7 N-WASP promoter contains a 393 bp regulatory element

Differential expression of a gene is determined by regulatory proteins which bind to the cis-regulatory element located in the gene promoter [206]. In this study, N-WASP promoter was characterized using GFP reporter assay and yeast one hybrid system. Studies have shown that intensity of GFP fluorescence is directly proportional to the abundance of GFP mRNA, which in turn depends on the copy number of *GFP* gene [205].

For the GFP reporter assay, series of deletion constructs of N-WASP promoter were cloned upstream of the *GFP* gene and transfected in HEK293T cells. 1624 bp of N-WASP promoter region was cloned from -1295 bp to +329 bp relative to TSS (+1) into a GFP reporter plasmid. Analysis of N-WASP promoter constructs revealed a reduction in promoter activity when the promoter region was deleted from -1295 bp to -902 bp from the TSS. Thus, the 393 bp region between -1295 bp and -902 bp might be a cis-acting regulatory sequence for the N-WASP promoter.

5.8 DNA binding proteins obtained by yeast one hybrid screening

Gene expression is a tightly regulated process that involves interactions of various proteins with the gene promoter, enhancer and repressor elements. Yeast one hybrid system, is a powerful in vivo genetic assay used to identify the DNA binding proteins using a large DNA fragment (promoter) as well as a small cis-regulatory element [294]. Yeast one hybrid assay was used to study DNA binding proteins that interact with the 393 bp N-WASP promoter region and regulate its activity. Yeast one hybrid screening identified 6 positive interactors out of which three interactors are histone, tubulin and kinesin proteins, which were expected as they are known DNA binding proteins. The remaining three interactors are transcripts for Homo sapiens msh

homeobox 1 (Msx1), Homo sapiens ISL LIM homeobox 1 (ISL1) and Homo sapiens POU class 3 homeobox 2 (POU3F2). N-WASP promoter activity was assayed in presence of the yeast one hybrid interactors and it was observed that Msx1 significantly enhanced the activity of N-WASP promoter (Figure 4.9).

5.9 Interaction of Msx1 with N-WASP promoter region

Muscle segment homeobox 1 (Msx1) is a protein coded by the *MSX1* gene in humans. The 393 bp regulatory region in N-WASP promoter revealed presence of an Msx1 binding consensus sequence 5' GXATTG 3' and ChIP assay was performed to demonstrate direct interaction of Msx1 protein with the N-WASP promoter (Figure 4.10).

Msx1 belong to the *MSX* family of vertebrate homeobox genes which consists of three members: *MSX1*, *MSX2* and *MSX3*. These genes were originally isolated by homology with *msh* gene in Drosophila and show highly conserved structural organization. Vertebrate Msx proteins are vital in regulating development of cardiac, neuronal and craniofacial structures and are usually expressed at sites of epithelial mesenchymal interactions in the developing embryo [295]. Although Msx1, Msx2 and Msx3 share functional redundancies, they show differences in their expression pattern and specific roles [295]. Although Msx1 is a known transcriptional repressor, recent studies have demonstrated its role in transcriptional activation. [296, 297].

EMT is a distinct cellular differentiation process which occurs during metastasis as well as embryonic development [298]. Studies have shown that Msx2, another member of Msx family, is important for inducing EMT in mouse mammary epithelial cells [299]. Msx1 and Msx2 exhibit similarity in their DNA binding consensus sequence as well as DNA binding properties [300]. This gives rise to a possibility that Msx2 may be binding to its consensus sequence in N-WASP

promoter but it could not be identified during the yeast one hybrid screen which may be due to absence of Msx2 in the brain cDNA library.

Thus, although the role of Msx1 in EMT and cancer is poorly studied, it may be possible that like Msx2, Msx1 could be involved in promoting metastasis. Cancer cells acquire this embryonic trait of being able to migrate by expressing early embryonic transcription factors. These transcription factors control genes, when turned on help the cells to proliferate more, become invasive, resist programmed cell death [152]. Since, expression of N-WASP is found to be upregulated in metastatic lesions as compared to the primary tumor [55], it may be possible that Msx1 is an embryonic transcription factor expressed during metastasis, which binds to N-WASP promoter and upregulates N-WASP expression.

Furthermore, 100 bp deletion in the N-WASP promoter region between -1324 bp and -1231 bp caused a 5-fold reduction in promoter activity (Figure 4.11). Sequence analysis of this 100 bp region exhibited presence of Msx1 binding site and this binding site was shown to be functional by ChIP assay (Figure 4.10). Expression of Msx1 is shown to be reduced in adult epithelial-derived tissues [301]. Since Msx1 expression could not be detected in most of the cancer cell lines, it was not possible to deplete Msx1 and study its effects on N-WASP function. However, it will be interesting to study Msx1-mediated N-WASP function during embryonic development by using *MSX1* knockout mice.
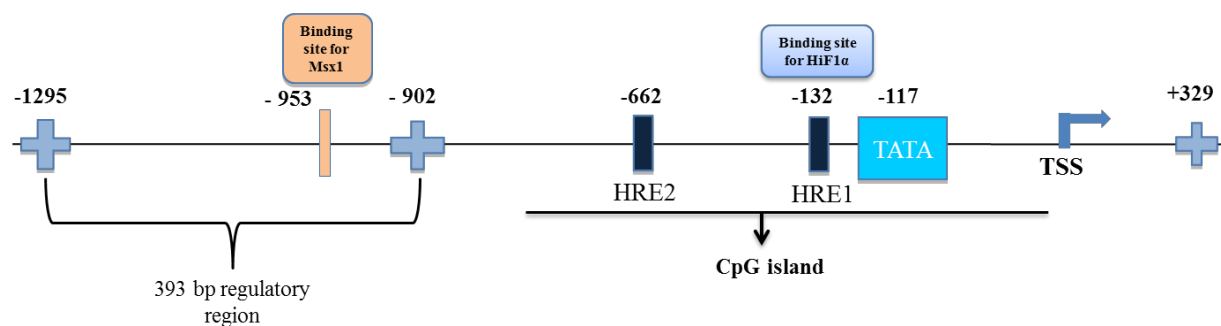
Figure.5.2: Model for N-WASP promoter
Schematic representation of N-WASP promoter indicating the position of 393 bp regulatory region and the two hypoxia response elements.

5.10 Regulation of N-WASP expression under hypoxia conditions

Hypoxia is shown to cause a repertoire of changes in gene expression [207]. Although both HiF1α and HiF2α are upregulated in hypoxia, HiF1α is the primary transcription factor responsible for differential expression of genes involved in hypoxia response [116]. Microarray studies have revealed that 89% of genes upregulated under hypoxia were dependent on HiF1α. Thus, HiF1α is important for the cells to survive in low oxygen conditions [207]. Expression of N-WASP was increased under hypoxia, it was of interest to check if this enhanced expression is due to HiF1α.

The first step was to analyze N-WASP promoter activity in presence of HiF1α. As shown in Figure 4.14, activity of N-WASP promoter was significantly enhanced in the presence of HiF1α. Hypoxia conditions were mimicked by using 1mM DMOG, which is used commonly to stabilize HiF1α expression under normoxia conditions and N-WASP promoter activity was found to be enhanced in presence of DMOG (Figure 4.14 B) [264, 265, 302, 303]. Expression of N-WASP

protein was enhanced in presence of DMOG and reduced in present of YC-1, which is an down-regulator of HiF1α (Figure 4.15). This suggested that HiF1α is involved in regulating N-WASP expression under hypoxia.

Expression of N-WASP was enhanced at protein as well as mRNA level under hypoxia conditions (Figure 4.15). Hence, N-WASP promoter analyzed to gain a better understanding of the underlying mechanism. Bioinformatics analysis identified two putative hypoxia-response elements [294] (5' NCGTG 3') at position -132 and -662 relative to the transcription start site. As shown in Fig.4.5, the two putative HREs are not present in the 393 bp region which can be another reason for the lack of positive interaction in yeast one hybrid system. Since two HREs were found in the N-WASP promoter region, it was important to determine if one or both of the HREs were functional and responsible for upregulation of N-WASP under hypoxia. Site-directed mutagenesis of the HREs provided first evidence that HRE1 may be functional as mutating HRE1 caused a decrease in N-WASP promoter activity. Mutating HRE2 did not affect the activity of N-WASP promoter suggesting that HRE2 may not be functional and may not be regulated by HiF1α. ChIP assay confirmed the functionality of HRE1 in N-WASP promoter as the binding site for HiF1α (Figure 4.18). Thus, binding of HiF1α to HRE1 was responsible for hypoxia-induced activation of N-WASP promoter.

5.11 Role of N-WASP under hypoxia conditions

Low oxygen tension is a characteristic of tumor microenvironment which is referred to as hypoxia. Under hypoxia conditions, tumor cells undergo a number of molecular and biological responses by activation of signaling pathways critical for adapting in an oxygen deprived environment [256]. A number of proteins regulated in a hypoxic response are instrumental in

enhancing the migration and invasiveness of tumor cells [304]. Although low oxygen enhances the migration and invasion of cancerous cells, the exact molecular mechanism is poorly understood.

Members of the WASP family of proteins are critical for actin polymerization mediated cell motility and invasion. N-WASP is an important regulator of actin cytoskeleton and it does so by activating the Arp2/3 complex [39]. The VCA-domain of N-WASP binds to the Arp2 and Arp3 subunits of the Arp2/3 complex bringing the two subunits together for formation of F-actin [16]. Studies have demonstrated the importance of N-WASP in cancer cell motility [59] and cell adhesion [72]. Expression of N-WASP is enhanced in metastatic lesions as compared to primary tumors indicating that N-WASP may be playing a role in actin remodeling events during metastasis [55]. N-WASP is also an important component of invadopodia and is responsible for recruiting MT1-MMP from the late endosomes into invasive pseudopods [63]. In this study, it was shown that N-WASP expression is enhanced under hypoxia conditions due to the direct binding of HiF1α to the HRE1(-132) in the N-WASP promoter. It may be possible that N-WASP is responsible for the enhanced cell motility under hypoxia.

A number of genes which are important for cancer invasion are regulated by HiF1α [305, 306] and HiF1α governs cell migration by regulating JMY expression [304]. Studies in MDA-MB231 cells have shown that overexpression of HiF1α increases invadopodia formation and enhanced matrix degradative capacity compared to control (normoxia) cells. PCR array analysis of DMOG treated cells revealed increased expression of cytoskeleton related genes for invadopodia formation [264]. N-WASP is vital for invadopodia function and hypoxia environment induces formation of invadopodia [30, 57, 221]. Also, HiF1α regulates expression of N-WASP in

hypoxia conditions which suggests a role of N-WASP in hypoxia-induced invadopodia formation. It is possible that HiF1α may induce invadopodia formation through multiple cytoskeletal pathways. Studies in human glioblastoma cell lines have identified c-Src and N-WASP as the key mediators for enhanced motility under low oxygen conditions. Downregulation of N-WASP by siRNA abrogated the low oxygen induced enhanced motility in glioma cell lines. This shows that N-WASP along with Src plays a crucial role in mediating the molecular pathogenesis of hypoxia induced-enhanced brain invasion by gliomas [307].

The increased levels of N-WASP in hypoxia, along with the requirement of N-WASP for invadopodia activity indicated that N-WASP may be regulating hypoxia-induced invadopodia formation. For this purpose, N-WASP knockdown cells were generated and a gelatin degradation assay was performed using MDA-MB-231 cells. It was found that DMOG treatment enhanced the gelatin degradative capacity of MDA-MB-231 cells which was consistent with previous reports [264]. Knockdown of N-WASP significantly reduced the number of cells forming invadopodia (Figure 4.21 B) and reconstitution of N-WASP in knockdown cells could compensate for the reduced number of invadopodia forming cells (Figure 4.21 C-D). This further strengthened our hypothesis that N-WASP may play a role in promoting invasion under hypoxia conditions by regulating the formation of invadopodia.
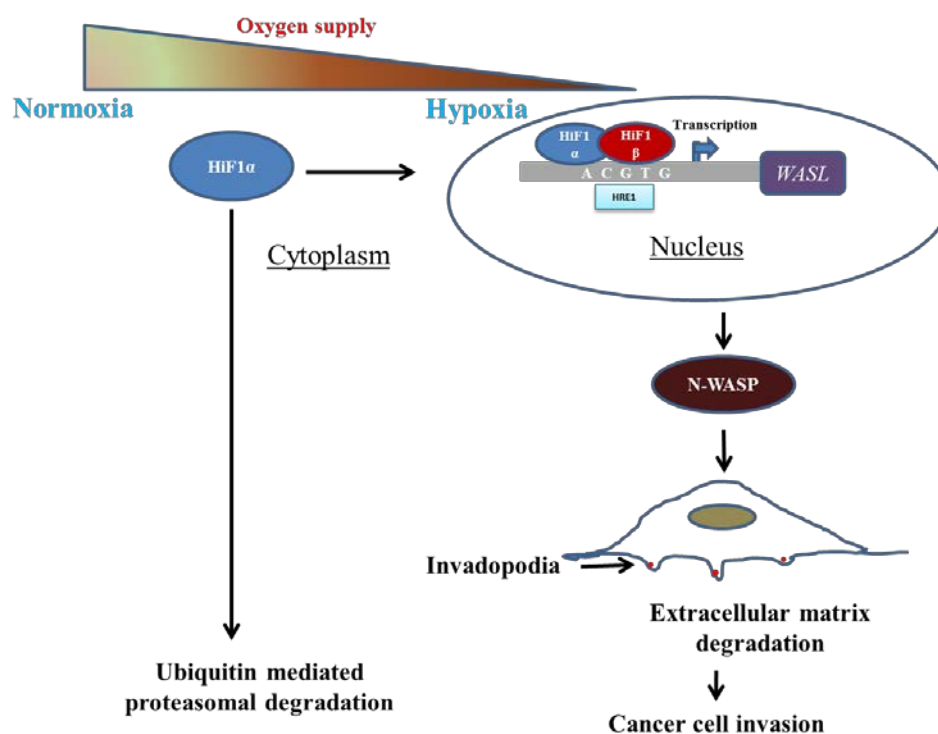
Figure.5.3: Proposed mechanism of role of N-WASP in hypoxia conditions
(A) Presence of oxygen, leads to the proteasomal degradation of HiF1α (B) In the absence of oxygen, HiF1α translocates to the nucleus and binds to HRE1 of N-WASP promoter. This leads to enhanced invadopodia formation mediated by N-WASP.

CONCLUSION AND FUTURE DIRECTIONS

(A) Conclusion

1) WIP is an actin cytoskeleton regulator and is important for immune cell function [82]. In this study, the role of WIP in metastatic progression was studied. WIP was found to positively promote migration, invasion and proliferation in A549 cells. Overexpression of WIP led to anchorage independent growth in A549 cells indicating the pro-metastatic role of WIP. Expression of WIP is regulated by TGF-beta and WIP overexpression accelerated progression of TGF-beta induced EMT. Knockdown of WIP in A549 cells inhibited EMT related morphological changes in presence of TGF-beta and it was found that knockdown of WIP led to a marked decrease in RhoA protein levels. This was consistent with the reduction of stress fibers and reduced cell area in WIP knockdown A549 cells. WIP was found to interact with RhoA, indicating the importance of WIP for RhoA regulated cellular functions.

2) Characterisation of N-WASP promoter was performed which led to the identification of a 393 bp regulatory region. Yeast one hybrid screen helped in identifying Msxl, ISL1 and POU3F2 as a potential interactors binding to the 393 bp regulatory region. Reporter assay and ChIP assay confirmed that Msx1 interacts with N-WASP promoter and enhances promoter activity.

3) Expression of N-WASP was found to increase in hypoxia condition as well as in presence of hypoxia mimicking agent, DMOG. N-WASP promoter contains 2 HREs, out of which, HRE1 was identified as the binding site of HiF1α by ChiP assay. N-WASP was also found to be

important for hypoxia induced invadopodia activity as N-WASP knockdown cells showed significant reduction in gelatin degradation in the presence of DMOG .

(B) Future directions:

1) Knockdown of WIP in A549 cells led to loss of stress fibers and inhibited the morphological changes associated with TGF-beta induced EMT. Although, WIP was found to specifically interact with RhoA, the questions arises whether WIP interacts with the active form (RhoA-GTP) or inactive form (RhoA-GDP) of RhoA. Till date, RhoA is known to be degraded by ubiquitin mediated proteasomal degradation [308, 309]. Hence, it would be interesting to know whether loss of RhoA in the absence of WIP involves degradation of RhoA via proteasomal pathway. Thus, further characterization of RhoA-WIP interaction will help to gain a better understanding about the regulation of RhoA by WIP.

2) Knockdown of WIP did not change the expression of RhoA downstream effectors such as ROKα and mDia1. It would be interesting to study if WIP affects the expression and/or functional activity of RhoA effectors.

3) Although results obtained by in-vitro studies indicate a positive role of WIP in promoting metastasis, it would be interesting to study the role of WIP using an in-vivo model. A549 cells with WIP overexpression and WIP knockdown can be injected in nude mice to check for development of tumors and metastases of lung, which would confirm the invasive potential of the cells in an in-vivo environment. These models could be studied over a period of time to study tumor progression.

4) To determine if there are any additional transcription factors binding to the 100 bp regulatory region between -1324 and -1231 bp of the N-WASP promoter.

<u>REFERENCES</u>

1. Fletcher, D.A. and R.D. Mullins, *Cell mechanics and the cytoskeleton.* Nature, 2010. **463**(7280): p. 485-92.
2. Bruce Alberts, A.J., Julian Lewis, Martin Raff, Keith Roberts, and Peter Walter, *Molecular Biology of the Cell.* 2002.
3. Janmey, P.A., *The cytoskeleton and cell signaling: component localization and mechanical coupling.* Physiol Rev, 1998. **78**(3): p. 763-81.
4. Harvey Lodish, A.B., S Lawrence Zipursky, Paul Matsudaira, David Baltimore, and James Darnell, *Molecular cell biology.* 2000.
5. Ridley, A.J., et al., *Cell migration: integrating signals from front to back.* Science, 2003. **302**(5651): p. 1704-9.
6. Mitchison, T.J. and L.P. Cramer, *Actin-based cell motility and cell locomotion.* Cell, 1996. **84**(3): p. 371-379.
7. Rotty, J.D., C. Wu, and J.E. Bear, *New insights into the regulation and cellular functions of the ARP2/3 complex.* Nat Rev Mol Cell Biol, 2013. **14**(1): p. 7-12.
8. Murphy, D.A. and S.A. Courtneidge, *The 'ins' and 'outs' of podosomes and invadopodia: characteristics, formation and function.* Nat Rev Mol Cell Biol, 2011. **12**(7): p. 413-26.
9. Visa, N. and P. Percipalle, *Nuclear functions of actin.* Cold Spring Harb Perspect Biol, 2010. **2**(4): p. a000620.
10. Pollard, T.D. and G.G. Borisy, *Cellular motility driven by assembly and disassembly of actin filaments.* Cell, 2003. **112**(4): p. 453-65.
11. Oda, T., et al., *The nature of the globular-to fibrous-actin transition.* Nature, 2009. **457**(7228): p. 441-445.
12. Lee, S.H. and R. Dominguez, *Regulation of actin cytoskeleton dynamics in cells.* Mol Cells, 2010. **29**(4): p. 311-25.
13. Raftopoulou, M. and A. Hall, *Cell migration: Rho GTPases lead the way.* Developmental Biology, 2004. **265**(1): p. 23-32.
14. Goode, B.L. and M.J. Eck, *Mechanism and function of formins in the control of actin assembly.* Annual Review of Biochemistry, 2007. **76**: p. 593-627.
15. Mullins, R.D., J.A. Heuser, and T.D. Pollard, *The interaction of Arp2/3 complex with actin: nucleation, high affinity pointed end capping, and formation of branching networks of filaments.* Proc Natl Acad Sci U S A, 1998. **95**(11): p. 6181-6.
16. Egile, C., et al., *Activation of the CDC42 effector N-WASP by the Shigella flexneri IcsA protein promotes actin nucleation by Arp2/3 complex and bacterial actin-based motility.* J Cell Biol, 1999. **146**(6): p. 1319-32.

17. Chesarone, M.A. and B.L. Goode, *Actin nucleation and elongation factors: mechanisms and interplay.* Curr Opin Cell Biol, 2009. **21**(1): p. 28-37.

18. Lee, S.H. and R. Dominguez, *Regulation of actin cytoskeleton dynamics in cells.* Molecules and Cells, 2010. **29**(4): p. 311-325.

19. Derry, J.M., H.D. Ochs, and U. Francke, *Isolation of a novel gene mutated in Wiskott-Aldrich syndrome.* Cell, 1994. **78**(4): p. 635-44.

20. Miki, H., K. Miura, and T. Takenawa, *N-WASP, a novel actin-depolymerizing protein, regulates the cortical cytoskeletal rearrangement in a PIP2-dependent manner downstream of tyrosine kinases.* Embo Journal, 1996. **15**(19): p. 5326-5335.

21. Remold-O'Donnell, E. and F.S. Rosen, *Sialophorin (CD43) and the Wiskott-Aldrich syndrome.* Immunodefic Rev, 1990. **2**(2): p. 151-74.

22. Ramesh, N., et al., *WIP, a protein associated with Wiskott–Aldrich syndrome protein, induces actin polymerization and redistribution in lymphoid cells.* Proceedings of the National Academy of Sciences, 1997. **94**(26): p. 14671-14676.

23. Imai, K., S. Nonoyama, and H.D. Ochs, *WASP (Wiskott-Aldrich syndrome protein) gene mutations and phenotype.* Curr Opin Allergy Clin Immunol, 2003. **3**(6): p. 427-36.

24. Lyubimova, A., et al., *Neural Wiskott-Aldrich syndrome protein modulates Wnt signaling and is required for hair follicle cycling in mice.* J Clin Invest, 2010. **120**(2): p. 446-56.

25. Lommel, S., et al., *Actin pedestal formation by enteropathogenic Escherichia coli and intracellular motility of Shigella flexneri are abolished in N-WASP-defective cells.* EMBO Rep, 2001. **2**(9): p. 850-7.

26. Snapper, S.B., et al., *N-WASP deficiency reveals distinct pathways for cell surface projections and microbial actin-based motility.* Nat Cell Biol, 2001. **3**(10): p. 897-904.

27. Miki, H., et al., *Induction of filopodium formation by a WASP-related actin-depolymerizing protein N-WASP.* Nature, 1998. **391**(6662): p. 93-6.

28. Banon-Rodriguez, I., et al., *WIP regulates persistence of cell migration and ruffle formation in both mesenchymal and amoeboid modes of motility.* PLoS One, 2013. **8**(8): p. e70364.

29. Krueger, E.W., et al., *A dynamin-cortactin-Arp2/3 complex mediates actin reorganization in growth factor-stimulated cells.* Mol Biol Cell, 2003. **14**(3): p. 1085-96.

30. Lorenz, M., et al., *Imaging sites of N-wasp activity in lamellipodia and invadopodia of carcinoma cells.* Curr Biol, 2004. **14**(8): p. 697-703.

31. Yamaguchi, H., et al., *Molecular mechanisms of invadopodium formation: the role of the N-WASP-Arp2/3 complex pathway and cofilin.* J Cell Biol, 2005. **168**(3): p. 441-52.

32. Desmarais, V., et al., *N-WASP and cortactin are involved in invadopodium-dependent chemotaxis to EGF in breast tumor cells.* Cell Motil Cytoskeleton, 2009. **66**(6): p. 303-16.

33. Weiler, M.C., J.L. Smith, and J.N. Masters, *CR16, a novel proline-rich protein expressed in rat brain neurons, binds to SH3 domains and is a MAP kinase substrate.* J Mol Neurosci, 1996. **7**(3): p. 203-15.

34. Aspenstrom, P., *The WASP-Binding Protein WIRE Has a Role in the Regulation of the Actin Filament System Downstream of the Platelet-Derived Growth Factor Receptor.* Experimental Cell Research, 2002. **279**(1): p. 21-33.

35. Kato, M., et al., *WICH, a novel verprolin homology domain-containing protein that functions cooperatively with N-WASP in actin-microspike formation.* Biochem Biophys Res Commun, 2002. **291**(1): p. 41-7.

36. Symons, M., et al., *Wiskott-Aldrich syndrome protein, a novel effector for the GTPase CDC42Hs, is implicated in actin polymerization.* Cell, 1996. **84**(5): p. 723-734.

37. Abdul-Manan, N., et al., *Structure of Cdc42 in complex with the GTPase-binding domain of the 'Wiskott-Aldrich syndrome' protein.* Nature, 1999. **399**(6734): p. 379-383.

38. Takenawa, T. and H. Miki, *WASP and WAVE family proteins: key molecules for rapid rearrangement of cortical actin filaments and cell movement.* Journal of Cell Science, 2001. **114**(10): p. 1801-1809.

39. Rohatgi, R., et al., *The interaction between N-WASP and the Arp2/3 complex links Cdc42-dependent signals to actin assembly.* Cell, 1999. **97**(2): p. 221-231.

40. Padrick, S.B., et al., *Hierarchical regulation of WASP/WAVE proteins.* Mol Cell, 2008. **32**(3): p. 426-38.

41. Wu, X.Y., et al., *Focal adhesion kinase regulation of N-WASP subcellular localization and function.* Journal of Biological Chemistry, 2004. **279**(10): p. 9565-9576.

42. Cory, G.O.C., et al., *Phosphorylation of tyrosine enhances the ability of WASp to stimulate actin polymerization and filopodium formation.* Journal of Biological Chemistry, 2002. **277**(47): p. 45115-45121.

43. Misra, A., et al., *N-WASP plays a critical role in fibroblast adhesion and spreading.* Biochem Biophys Res Commun, 2007. **364**(4): p. 908-12.

44. Jain, N., et al., *Conditional N-WASP knockout in mouse brain implicates actin cytoskeleton regulation in hydrocephalus pathology.* Experimental Neurology, 2014. **254**: p. 29-40.

45. Gruenbaum-Cohen, Y., et al., *The actin regulator N-WASp is required for muscle-cell fusion in mice.* Proc Natl Acad Sci U S A, 2012. **109**(28): p. 11211-6.

46. Kessels, M.M. and B. Qualmann, *Syndapins integrate N-WASP in receptor-mediated endocytosis.* EMBO J, 2002. **21**(22): p. 6083-94.

47. Benesch, S., et al., *N-WASP deficiency impairs EGF internalization and actin assembly at clathrin-coated pits.* J Cell Sci, 2005. **118**(Pt 14): p. 3103-15.

48. Basquin, C., et al., *Membrane protrusion powers clathrin-independent endocytosis of interleukin-2 receptor.* EMBO J, 2015.

49.   Wegner, A.M., et al., *N-wasp and the arp2/3 complex are critical regulators of actin in the development of dendritic spines and synapses.* J Biol Chem, 2008. **283**(23): p. 15912-20.

50.   Suetsugu, S. and T. Takenawa, *Translocation of N-WASP by nuclear localization and export signals into the nucleus modulates expression of HSP90.* Journal of Biological Chemistry, 2003. **278**(43): p. 42515-42523.

51.   Wu, X., et al., *Regulation of RNA-polymerase-II-dependent transcription by N-WASP and its nuclear-binding partners.* Nat Cell Biol, 2006. **8**(7): p. 756-763.

52.   Park, S.J. and T. Takenawa, *Neural Wiskott-Aldrich Syndrome Protein Is Required for Accurate Chromosome Congression and Segregation.* Molecules and Cells, 2011. **31**(6): p. 515-521.

53.   Mareel, M., M.J. Oliveira, and I. Madani, *Cancer invasion and metastasis: interacting ecosystems.* Virchows Arch, 2009. **454**(6): p. 599-622.

54.   Bacac, M. and I. Stamenkovic, *Metastatic cancer cell.* Annu Rev Pathol, 2008. **3**: p. 221-47.

55.   Yanagawa, R., et al., *Genome-wide screening of genes showing altered expression in liver metastases of human colorectal cancers by cDNA microarray.* Neoplasia, 2001. **3**(5): p. 395-401.

56.   Misra, A., et al., *Hypoxia activated EGFR signaling induces epithelial to mesenchymal transition (EMT).* PLoS One, 2012. **7**(11): p. e49766.

57.   Gligorijevic, B., et al., *N-WASP-mediated invadopodium formation is involved in intravasation and lung metastasis of mammary tumors.* Journal of Cell Science, 2012. **125**(3): p. 724-734.

58.   Pichot, C.S., et al., *Cdc42-interacting protein 4 promotes breast cancer cell invasion and formation of invadopodia through activation of N-WASp.* Cancer Res, 2010. **70**(21): p. 8347-56.

59.   Gadea, G., et al., *DOCK10-mediated Cdc42 activation is necessary for amoeboid invasion of melanoma cells.* Curr Biol, 2008. **18**(19): p. 1456-65.

60.   Yu, X., et al., *N-WASP coordinates the delivery and F-actin-mediated capture of MT1-MMP at invasive pseudopods.* J Cell Biol, 2012. **199**(3): p. 527-44.

61.   Martin, T.A., et al., *N-WASP is a putative tumour suppressor in breast cancer cells, in vitro and in vivo, and is associated with clinical outcome in patients with breast cancer.* Clinical & Experimental Metastasis, 2008. **25**(2): p. 97-108.

62.   Machesky, L.M. and H.R. Tang, *Actin-based protrusions: promoters or inhibitors of cancer invasion?* Cancer Cell, 2009. **16**(1): p. 5-7.

63.   Yu, X. and L.M. Machesky, *Cells assemble invadopodia-like structures and invade into matrigel in a matrix metalloprotease dependent manner in the circular invasion assay.* PLoS One, 2012. **7**(2): p. e30605.

64. Aspenstrom, P., *The verprolin family of proteins: regulators of cell morphogenesis and endocytosis.* FEBS Lett, 2005. **579**(24): p. 5253-9.

65. Donnelly, S.F., et al., *A proline-rich protein, verprolin, involved in cytoskeletal organization and cellular growth in the yeast Saccharomyces cerevisiae.* Mol Microbiol, 1993. **10**(3): p. 585-96.

66. Sujuan Ye1, A.A.a.Y.L., *CpGIF: an algorithm for the identification of CpG islands.* 2008.

67. Nichols, N.R., J.N. Masters, and C.E. Finch, *Changes in gene expression in hippocampus in response to glucocorticoids and stress.* Brain Res Bull, 1990. **24**(5): p. 659-62.

68. Suetsugu, S., et al., *Male-specific sterility caused by the loss of CR16.* Genes Cells, 2007. **12**(6): p. 721-33.

69. Martinez-Quiles, N., et al., *WIP regulates N-WASP-mediated actin polymerization and filopodium formation.* Nat Cell Biol, 2001. **3**(5): p. 484-91.

70. Misra, A., et al., *The mammalian verprolin, WIRE induces filopodia independent of N-WASP through IRSp53.* Exp Cell Res, 2010. **316**(17): p. 2810-24.

71. Kato, M. and T. Takenawa, *WICH, a member of WASP-interacting protein family, cross-links actin filaments.* Biochem Biophys Res Commun, 2005. **328**(4): p. 1058-66.

72. Kovacs, E.M., et al., *N-WASP regulates the epithelial junctional actin cytoskeleton through a non-canonical post-nucleation pathway.* Nat Cell Biol, 2011. **13**(8): p. 934-43.

73. Vaduva, G., et al., *The human WASP-interacting protein, WIP, activates the cell polarity pathway in yeast.* J Biol Chem, 1999. **274**(24): p. 17103-8.

74. Anton, I.M., et al., *WIP deficiency reveals a differential role for WIP and the actin cytoskeleton in T and B cell activation.* Immunity, 2002. **16**(2): p. 193-204.

75. de la Fuente, M.A., et al., *WIP is a chaperone for Wiskott-Aldrich syndrome protein (WASP).* Proc Natl Acad Sci U S A, 2007. **104**(3): p. 926-31.

76. Koduru, S., et al., *A novel anti-WIP monoclonal antibody detects an isoform of WIP that lacks the WASP binding domain.* Biochem Biophys Res Commun, 2007. **353**(4): p. 875-81.

77. Thanabalu, T., et al., *Verprolin function in endocytosis and actin organization. Roles of the Las17p (yeast WASP)-binding domain and a novel C-terminal actin-binding domain.* FEBS J, 2007. **274**(16): p. 4103-25.

78. Chou, H.-C., et al., *WIP Regulates the Stability and Localization of WASP to Podosomes in Migrating Dendritic Cells.* Current biology : CB, 2006. **16**(23): p. 2337-2344.

79. Ramesh, N., et al., *Binding of the WASP/N-WASP-interacting protein WIP to actin regulates focal adhesion assembly and adhesion.* Mol Cell Biol, 2014. **34**(14): p. 2600-10.

80. Antón, I.M., et al., *WASP-interacting protein (WIP): working in polymerisation and much more.* Trends in cell biology, 2007. **17**(11): p. 555-562.

81. Ramesh, N. and R. Geha, *Recent advances in the biology of WASP and WIP.* Immunol Res, 2009. **44**(1-3): p. 99-111.

82. Anton, I.M., et al., *WASP-interacting protein (WIP): working in polymerisation and much more.* Trends Cell Biol, 2007. **17**(11): p. 555-62.

83. Kinley, A.W., et al., *Cortactin interacts with WIP in regulating Arp2/3 activation and membrane protrusion.* Curr Biol, 2003. **13**(5): p. 384-93.

84. Ho, H.Y., et al., *CR16 forms a complex with N-WASP in brain and is a novel member of a conserved proline-rich actin-binding protein family.* Proc Natl Acad Sci U S A, 2001. **98**(20): p. 11306-11.

85. Volkman, B.F., et al., *Structure of the N-WASP EVH1 domain-WIP complex: insight into the molecular basis of Wiskott-Aldrich Syndrome.* Cell, 2002. **111**(4): p. 565-76.

86. Martinez-Quiles, N., Rohatgi, R., Anton, I. M, *WIP regulates nwasp mediated actin polymerization and filopodium formation.pdf.* 2001.

87. Konno, A., et al., *The expression of Wiskott-Aldrich syndrome protein (WASP) is dependent on WASP-interacting protein (WIP).* Int Immunol, 2007. **19**(2): p. 185-92.

88. García, E., et al., *WIP: WASP-interacting proteins at invadopodia and podosomes.* European Journal of Cell Biology, 2012. **91**(11–12): p. 869-877.

89. Fried, S., et al., *WIP: more than a WASp-interacting protein.* J Leukoc Biol, 2014. **96**(5): p. 713-27.

90. Krzewski, K., X. Chen, and J.L. Strominger, *WIP is essential for lytic granule polarization and NK cell cytotoxicity.* Proc Natl Acad Sci U S A, 2008. **105**(7): p. 2568-73.

91. Lanzi, G., et al., *A novel primary human immunodeficiency due to deficiency in the WASP-interacting protein WIP.* J Exp Med, 2012. **209**(1): p. 29-34.

92. Stewart, D.M., L. Tian, and D.L. Nelson, *Mutations that cause the Wiskott-Aldrich syndrome impair the interaction of Wiskott-Aldrich syndrome protein (WASP) with WASP interacting protein.* J Immunol, 1999. **162**(8): p. 5019-24.

93. Calle, Y., et al., *WASP and WIP regulate podosomes in migrating leukocytes.* J Microsc, 2008. **231**(3): p. 494-505.

94. Tsuboi, S., *Requirement for a complex of Wiskott-Aldrich syndrome protein (WASP) with WASP interacting protein in podosome formation in macrophages.* J Immunol, 2007. **178**(5): p. 2987-95.

95. Vijayakumar, V., et al., *Tyrosine phosphorylation of WIP releases bound WASP and impairs podosome assembly in macrophages.* J Cell Sci, 2015. **128**(2): p. 251-65.

96. Fried, S., et al., *Triple-color FRET analysis reveals conformational changes in the WIP-WASp actin-regulating complex.* Sci Signal, 2014. **7**(331): p. ra60.

97. Moreau, V., et al., *A complex of N-WASP and WIP integrates signalling cascades that lead to actin polymerization.* Nat Cell Biol, 2000. **2**(7): p. 441-8.

98. Franco, A., et al., *WIP is a negative regulator of neuronal maturation and synaptic activity.* Cereb Cortex, 2012. **22**(5): p. 1191-202.

99. Mattila, P.K. and P. Lappalainen, *Filopodia: molecular architecture and cellular functions.* Nat Rev Mol Cell Biol, 2008. **9**(6): p. 446-54.

100. Staub, E., et al., *An expression module of WIPF1-coexpressed genes identifies patients with favorable prognosis in three tumor types.* J Mol Med (Berl), 2009. **87**(6): p. 633-44.

101. Lanzardo, S., et al., *A role for WASP Interacting Protein, WIP, in fibroblast adhesion, spreading and migration.* Int J Biochem Cell Biol, 2007. **39**(1): p. 262-74.

102. Gryaznova, T., et al., *Intersectin adaptor proteins are associated with actin-regulating protein WIP in invadopodia.* Cellular Signalling, 2015. **27**(7): p. 1499-1508.

103. Gimona, M., et al., *Assembly and biological role of podosomes and invadopodia.* Curr Opin Cell Biol, 2008. **20**(2): p. 235-41.

104. Yamaguchi, H., et al., *Molecular mechanisms of invadopodium formation: the role of the N-WASP–Arp2/3 complex pathway and cofilin.* The Journal of Cell Biology, 2005. **168**(3): p. 441-452.

105. Li, A., et al., *The actin-bundling protein fascin stabilizes actin in invadopodia and potentiates protrusive invasion.* Curr Biol, 2010. **20**(4): p. 339-45.

106. Clark, E.S., et al., *Cortactin is an essential regulator of matrix metalloproteinase secretion and extracellular matrix degradation in invadopodia.* Cancer Res, 2007. **67**(9): p. 4227-35.

107. Garcia, E., et al., *WIP is necessary for matrix invasion by breast cancer cells.* Eur J Cell Biol, 2014. **93**(10-12): p. 413-23.

108. Gu, X., et al., *Reduced PDEF expression increases invasion and expression of mesenchymal genes in prostate cancer cells.* Cancer Res, 2007. **67**(9): p. 4219-26.

109. Vaupel, P., D.K. Kelleher, and M. Hockel, *Oxygenation status of malignant tumors: Pathogenesis of hypoxia and significance for tumor therapy.* Seminars in Oncology, 2001. **28**(2): p. 29-35.

110. Folkman, J., *What Is the Evidence That Tumors Are Angiogenesis Dependent.* Journal of the National Cancer Institute, 1990. **82**(1): p. 4-6.

111. Ryan, H.E., et al., *Hypoxia-inducible factor-1 alpha is a positive factor in solid tumor growth.* Cancer Research, 2000. **60**(15): p. 4010-4015.

112. Brown, J.M., *The hypoxic cell: A target for selective cancer therapy - Eighteenth Bruce F. Cain Memorial Award lecture.* Cancer Research, 1999. **59**(23): p. 5863-5870.

113. Yan, W., et al., *PI3 kinase/Akt signaling mediates epithelial-mesenchymal transition in hypoxic hepatocellular carcinoma cells.* Biochem Biophys Res Commun, 2009. **382**(3): p. 631-6.

114. Ke, Q. and M. Costa, *Hypoxia-inducible factor-1 (HIF-1).* Mol Pharmacol, 2006. **70**(5): p. 1469-80.

115. Teicher, B.A., *Hypoxia and drug resistance.* Cancer Metastasis Rev, 1994. **13**(2): p. 139-68.

116. Wang, G.L., et al., *Hypoxia-Inducible Factor-1 Is a Basic-Helix-Loop-Helix-Pas Heterodimer Regulated by Cellular O-2 Tension.* Proceedings of the National Academy of Sciences of the United States of America, 1995. **92**(12): p. 5510-5514.

117. Semenza, G.L., et al., *Hypoxia-Inducible Nuclear Factors Bind to an Enhancer Element Located 3' to the Human Erythropoietin Gene.* Proceedings of the National Academy of Sciences of the United States of America, 1991. **88**(13): p. 5680-5684.

118. Fukasawa, M., et al., *Identification and characterization of the hypoxia-responsive element of the human placental 6-phosphofructo-2-kinase/fructose-2,6-bisphosphatase gene.* J Biochem, 2004. **136**(3): p. 273-7.

119. Jiang, B.H., et al., *Hypoxia-inducible factor 1 levels vary exponentially over a physiologically relevant range of O-2 tension.* American Journal of Physiology-Cell Physiology, 1996. **271**(4): p. C1172-C1180.

120. Mojsilovic-Petrovic, J., et al., *Hypoxia-inducible factor-1 (HIF-1) is involved in the regulation of hypoxia-stimulated expression of monocyte chemoattractant protein-1 (MCP-1/CCL2) and MCP-5 (Ccl12) in astrocytes.* J Neuroinflammation, 2007. **4**: p. 12.

121. Tian, H., S.L. McKnight, and D.W. Russell, *Endothelial PAS domain protein 1 (EPAS1), a transcription factor selectively expressed in endothelial cells.* Genes & Development, 1997. **11**(1): p. 72-82.

122. Gu, Y.Z., et al., *Molecular characterization and chromosomal localization of a third alpha-class hypoxia inducible factor subunit, HIF3 alpha.* Gene Expression, 1998. **7**(3): p. 205-213.

123. Makino, Y., et al., *Inhibitory PAS domain protein (IPAS) is a hypoxia-inducible splicing variant of the hypoxia-inducible factor-3 alpha locus.* Journal of Biological Chemistry, 2002. **277**(36): p. 32405-32408.

124. Makino, Y., et al., *Inhibitory PAS domain protein is a negative regulator of hypoxia-inducible gene expression.* Nature, 2001. **414**(6863): p. 550-554.

125. Semenza, G.L., *HIF-1, O-2, and the 3 PHDs: How animal cells signal hypoxia to the nucleus.* Cell, 2001. **107**(1): p. 1-3.

126. Jaakkola, P., et al., *Targeting of HIF-alpha to the von Hippel-Lindau ubiquitylation complex by O2-regulated prolyl hydroxylation.* Science, 2001. **292**(5516): p. 468-72.

127. Maxwell, P.H., C.W. Pugh, and P.J. Ratcliffe, *Activation of the HIF pathway in cancer.* Current Opinion in Genetics & Development, 2001. **11**(3): p. 293-299.

128. Reyes, H., S. Reiszporszasz, and O. Hankinson, *Identification of the Ah Receptor Nuclear Translocator Protein (Arnt) as a Component of the DNA-Binding Form of the Ah Receptor.* Science, 1992. **256**(5060): p. 1193-1195.

129. Crews, S.T., *Control of cell lineage-specific development and transcription by bHLH-PAS proteins.* Genes & Development, 1998. **12**(5): p. 607-620.

130. Ruas, J.L., L. Poellinger, and T. Pereira, *Functional analysis of hypoxia-inducible factor-1 alpha-mediated transactivation - identification of amino acid residues critical for transcriptional activation and/or interaction with CREB-binding protein.* Journal of Biological Chemistry, 2002. **277**(41): p. 38723-38730.

131. Lando, D., et al., *Asparagine hydroxylation of the HIF transactivation domain: A hypoxic switch.* Science, 2002. **295**(5556): p. 858-861.

132. Pugh, C.W., et al., *Activation of hypoxia-inducible factor-1; Definition of regulatory domains within the alpha subunit.* Journal of Biological Chemistry, 1997. **272**(17): p. 11205-11214.

133. Maxwell, P.H., *Hypoxia-inducible factor as a physiological regulator.* Experimental Physiology, 2005. **90**(6): p. 791-797.

134. Harris, A.L., *Hypoxia--a key regulatory factor in tumour growth.* Nat Rev Cancer, 2002. **2**(1): p. 38-47.

135. Bos, R., et al., *Overexpression of HIF-1 alpha in breast carcinogenesis.* Journal of Pathology, 2001. **193**: p. 30a-30a.

136. Semenza, G.L., *HIF-1: upstream and downstream of cancer metabolism.* Current Opinion in Genetics & Development, 2010. **20**(1): p. 51-56.

137. Thiery, J.P. and J.P. Sleeman, *Complex networks orchestrate epithelial-mesenchymal transitions.* Nat Rev Mol Cell Biol, 2006. **7**(2): p. 131-42.

138. Schock, F. and N. Perrimon, *Molecular mechanisms of epithelial morphogenesis.* Annu Rev Cell Dev Biol, 2002. **18**: p. 463-93.

139. Niessen, C.M. and C.J. Gottardi, *Molecular components of the adherens junction.* Biochimica Et Biophysica Acta-Biomembranes, 2008. **1778**(3): p. 562-571.

140. Niessen, C.M., *Tight junctions/adherens junctions: basic structure and function.* J Invest Dermatol, 2007. **127**(11): p. 2525-32.

141. Lee, J.M., et al., *The epithelial–mesenchymal transition: new insights in signaling, development, and disease.* The Journal of Cell Biology, 2006. **172**(7): p. 973-981.

142. Friedl, P., K. Wolf, and J. Lammerding, *Nuclear mechanics during cell migration.* Curr Opin Cell Biol, 2011. **23**(1): p. 55-64.

143. Kalluri, R. and R.A. Weinberg, *The basics of epithelial-mesenchymal transition.* J Clin Invest, 2009. **119**(6): p. 1420-8.

144. Vanderburg, C. and E. Hay, *Role of the E-Cadherin Gene and Tissue Interaction in Epithelial-Mesenchymal Transformation.* Faseb Journal, 1995. **9**(4): p. A1067-A1067.

145. Yeaman, C., K.K. Grindstaff, and W.J. Nelson, *New perspectives on mechanisms involved in generating epithelial cell polarity.* Physiological Reviews, 1999. **79**(1): p. 73-98.

146. Kalluri, R. and E. Neilson, *Epithelial-mesenchymal transition and its implications for fibrosis.* J Clin Invest, 2003. **112**: p. 1776 - 1784.

147.   Thiery, J.P., et al., *Molecular Mechanism of Avian Neural Crest Cells Migration and Homing.* Biology of the Cell, 1982. **45**: p. 38-38.

148.   Huang, R.Y., P. Guilford, and J.P. Thiery, *Early events in cell adhesion and polarity during epithelial-mesenchymal transition.* J Cell Sci, 2012. **125**(Pt 19): p. 4417-22.

149.   Valcourt, U., et al., *TGF-beta and the Smad signaling pathway support transcriptomic reprogramming during epithelial-mesenchymal cell transition.* Mol Biol Cell, 2005. **16**(4): p. 1987-2002.

150.   Cavallaro, U. and G. Christofori, *Cell adhesion and signalling by cadherins and Ig-CAMs in cancer.* Nat Rev Cancer, 2004. **4**(2): p. 118-32.

151.   van Zijl, F., G. Krupitza, and W. Mikulits, *Initial steps of metastasis: cell invasion and endothelial transmigration.* Mutat Res, 2011. **728**(1-2): p. 23-34.

152.   Tiwari, N., et al., *EMT as the ultimate survival mechanism of cancer cells.* Semin Cancer Biol, 2012. **22**(3): p. 194-207.

153.   Sleeman, J.P. and J.P. Thiery, *SnapShot: The epithelial-mesenchymal transition.* Cell, 2011. **145**(1): p. 162 e1.

154.   Peinado, H., D. Olmeda, and A. Cano, *Snail, ZEB and bHLH factors in tumour progression: an alliance against the epithelial phenotype?* Nature Reviews Cancer, 2007. **7**(6): p. 415-428.

155.   Moreno-Bueno, G., et al., *The morphological and molecular features of the epithelial-to-mesenchymal transition.* Nat Protoc, 2009. **4**(11): p. 1591-613.

156.   Moustakas, A. and C.H. Heldin, *Signaling networks guiding epithelial-mesenchymal transitions during embryogenesis and cancer progression.* Cancer Sci, 2007. **98**(10): p. 1512-20.

157.   Zavadil, J. and E.P. Bottinger, *TGF-beta and epithelial-to-mesenchymal transitions.* Oncogene, 2005. **24**(37): p. 5764-74.

158.   Massague, J., *A very private TGF-beta receptor embrace.* Mol Cell, 2008. **29**(2): p. 149-50.

159.   Pardali, K. and A. Moustakas, *Actions of TGF-beta as tumor suppressor and pro-metastatic factor in human cancer.* Biochim Biophys Acta, 2007. **1775**(1): p. 21-62.

160.   Keski-Oja, J., K. Koli, and H. von Melchner, *TGF-beta activation by traction?* Trends Cell Biol, 2004. **14**(12): p. 657-9.

161.   Akhurst, R.J. and R. Derynck, *TGF-beta signaling in cancer--a double-edged sword.* Trends Cell Biol, 2001. **11**(11): p. S44-51.

162.   Kretzschmar, M. and J. Massague, *SMADs: mediators and regulators of TGF-beta signaling.* Curr Opin Genet Dev, 1998. **8**(1): p. 103-11.

163.   Schmierer, B. and C.S. Hill, *Kinetic analysis of smad nucleocytoplasmic shuttling reveals a mechanism for transforming growth factor beta-dependent nuclear accumulation of Smads.* Molecular and Cellular Biology, 2005. **25**(22): p. 9845-9858.

164.   Wotton, D. and J. Massague, *Smad transcriptional corepressors in TGF beta family signaling.* Curr Top Microbiol Immunol, 2001. **254**: p. 145-64.

165.   Miyazono, K., *Transforming growth factor-β signaling in epithelial-mesenchymal transition and progression of cancer.* Proceedings of the Japan Academy, Series B, 2009. **85**(8): p. 314-323.

166.   Moustakas, A., S. Souchelnytskyi, and C.H. Heldin, *Smad regulation in TGF-beta signal transduction.* Journal of Cell Science, 2001. **114**(24): p. 4359-4369.

167.   Hata, A., Y. Shi, and J. Massague, *TGF-beta signaling and cancer: structural and functional consequences of mutations in Smads.* Mol Med Today, 1998. **4**(6): p. 257-62.

168.   Ghellal, A., et al., *Prognostic significance of TGF beta 1 and TGF beta 3 in human breast carcinoma.* Anticancer Res, 2000. **20**(6B): p. 4413-8.

169.   Krasagakis, K., et al., *Elevated plasma levels of transforming growth factor (TGF)-beta1 and TGF-beta2 in patients with disseminated malignant melanoma.* Br J Cancer, 1998. **77**(9): p. 1492-4.

170.   Derynck, R. and Y.E. Zhang, *Smad-dependent and Smad-independent pathways in TGF-beta family signalling.* Nature, 2003. **425**(6958): p. 577-84.

171.   Moustakas, A. and C.H. Heldin, *Signaling networks guiding epithelial-mesenchymal transitions during embryogenesis and cancer progression.* Cancer Science, 2007. **98**(10): p. 1512-1520.

172.   Ikushima, H. and K. Miyazono, *TGFbeta signalling: a complex web in cancer progression.* Nat Rev Cancer, 2010. **10**(6): p. 415-24.

173.   Peinado, H., F. Portillo, and A. Cano, *Transcriptional regulation of cadherins during development and carcinogenesis.* Int J Dev Biol, 2004. **48**(5-6): p. 365-75.

174.   Comijn, J., et al., *The two-handed E box binding zinc finger protein SIP1 downregulates E-cadherin and induces invasion.* Mol Cell, 2001. **7**(6): p. 1267-78.

175.   Vandewalle, C., et al., *SIP1/ZEB2 induces EMT by repressing genes of different epithelial cell-cell junctions.* Nucleic Acids Res, 2005. **33**(20): p. 6566-78.

176.   Miyazono, K. and K. Miyazawa, *Id: a target of BMP signaling.* Sci STKE, 2002. **2002**(151): p. pe40.

177.   Kondo, M., et al., *A role for Id in the regulation of TGF-beta-induced epithelial-mesenchymal transdifferentiation.* Cell Death Differ, 2004. **11**(10): p. 1092-101.

178.   Kowanetz, M., et al., *Id2 and Id3 define the potency of cell proliferation and differentiation responses to transforming growth factor beta and bone morphogenetic protein.* Mol Cell Biol, 2004. **24**(10): p. 4241-54.

179.   Thuault, S., et al., *Transforming growth factor-beta employs HMGA2 to elicit epithelial-mesenchymal transition.* J Cell Biol, 2006. **174**(2): p. 175-83.

180. Vincent, T., et al., *A SNAIL1-SMAD3/4 transcriptional repressor complex promotes TGF-beta mediated epithelial-mesenchymal transition.* Nat Cell Biol, 2009. **11**(8): p. 943-50.

181. Xu, J., S. Lamouille, and R. Derynck, *TGF-beta-induced epithelial to mesenchymal transition.* Cell Res, 2009. **19**(2): p. 156-72.

182. Morris, H.T. and L.M. Machesky, *Actin cytoskeletal control during epithelial to mesenchymal transition: focus on the pancreas and intestinal tract.* Br J Cancer, 2015. **112**(4): p. 613-20.

183. Han, S.P., et al., *Cortactin scaffolds Arp2/3 and WAVE2 at the epithelial zonula adherens.* J Biol Chem, 2014. **289**(11): p. 7764-75.

184. Thiery, J.P., *Epithelial-mesenchymal transitions in tumour progression.* Nat Rev Cancer, 2002. **2**(6): p. 442-54.

185. Yilmaz, M. and G. Christofori, *EMT, the cytoskeleton, and cancer cell invasion.* Cancer Metastasis Rev, 2009. **28**(1-2): p. 15-33.

186. Hall, A., *Rho GTPases and the actin cytoskeleton.* Science, 1998. **279**(5350): p. 509-514.

187. Mitra, S.K., D.A. Hanson, and D.D. Schlaepfer, *Focal adhesion kinase: in command and control of cell motility.* Nat Rev Mol Cell Biol, 2005. **6**(1): p. 56-68.

188. Hu, K., et al., *Differential transmission of actin motion within focal adhesions.* Science, 2007. **315**(5808): p. 111-5.

189. Cox, B.D., et al., *New concepts regarding focal adhesion kinase promotion of cell migration and proliferation.* J Cell Biochem, 2006. **99**(1): p. 35-52.

190. Masszi, A., et al., *Central role for Rho in TGF-beta(1)-induced alpha-smooth muscle actin expression during epithelial-mesenchymal transition.* American Journal of Physiology-Renal Physiology, 2003. **284**(5): p. F911-F924.

191. Lozano, E., M. Betson, and V.M. Braga, *Tumor progression: Small GTPases and loss of cell-cell adhesion.* Bioessays, 2003. **25**(5): p. 452-63.

192. Ozdamar, B., et al., *Regulation of the polarity protein Par6 by TGF beta receptors controls epithelial cell plasticity.* Science, 2005. **307**(5715): p. 1603-1609.

193. Mortazavi, A., et al., *Mapping and quantifying mammalian transcriptomes by RNA-Seq.* Nat Methods, 2008. **5**(7): p. 621-8.

194. Nagalakshmi, U., K. Waern, and M. Snyder, *RNA-Seq: a method for comprehensive transcriptome analysis.* Curr Protoc Mol Biol, 2010. **Chapter 4**: p. Unit 4 11 1-13.

195. Shendure, J., *The beginning of the end for microarrays?* Nat Methods, 2008. **5**(7): p. 585-7.

196. Nookaew, I., et al., *A comprehensive comparison of RNA-Seq-based transcriptome analysis from reads to differential gene expression and cross-comparison with microarrays: a case study in Saccharomyces cerevisiae.* Nucleic Acids Res, 2012. **40**(20): p. 10084-97.

197.   McIntyre, L.M., et al., *RNA-seq: technical variability and sampling.* BMC Genomics, 2011. **12**: p. 293.

198.   Wang, Z., M. Gerstein, and M. Snyder, *RNA-Seq: a revolutionary tool for transcriptomics.* Nat Rev Genet, 2009. **10**(1): p. 57-63.

199.   Boukamp, P., et al., *Sustained nontumorigenic phenotype correlates with a largely stable chromosome content during long-term culture of the human keratinocyte line HaCaT.* Genes Chromosomes & Cancer, 1997. **19**(4): p. 201-214.

200.   Schoop, V.M., N. Mirancea, and N.E. Fusenig, *Epidermal organization and differentiation of HaCaT keratinocytes in organotypic coculture with human dermal fibroblasts.* Journal of Investigative Dermatology, 1999. **112**(3): p. 343-353.

201.   Boukamp, P., et al., *C-Ha-Ras Oncogene Expression in Immortalized Human Keratinocytes (Hacat) Alters Growth-Potential Invivo but Lacks Correlation with Malignancy.* Cancer Research, 1990. **50**(9): p. 2840-2847.

202.   Mueller, M.M., et al., *Tumor Progression of Skin Carcinoma Cells in Vivo Promoted by Clonal Selection, Mutagenesis, and Autocrine Growth Regulation by Granulocyte Colony-Stimulating Factor and Granulocyte-Macrophage Colony-Stimulating Factor.* The American Journal of Pathology, 2001. **159**(4): p. 1567-1579.

203.   Schwede, A., S. Kramer, and M. Carrington, *How do trypanosomes change gene expression in response to the environment?* Protoplasma, 2012. **249**(2): p. 223-238.

204.   Lu, C., W.E. Bentley, and G. Rao, *A high-throughput approach to promoter study using green fluorescent protein.* Biotechnol Prog, 2004. **20**(6): p. 1634-40.

205.   Soboleski, M.R., J. Oaks, and W.P. Halford, *Green fluorescent protein is a quantitative reporter of gene expression in individual eukaryotic cells.* FASEB J, 2005. **19**(3): p. 440-2.

206.   Deplancke, B., et al., *A gateway-compatible yeast one-hybrid system.* Genome Res, 2004. **14**(10B): p. 2093-101.

207.   Greijer, A.E., et al., *Up-regulation of gene expression by hypoxia is mediated predominantly by hypoxia-inducible factor 1 (HIF-1).* J Pathol, 2005. **206**(3): p. 291-304.

208.   Gietz, R.D. and A. Sugino, *New Yeast-Escherichia-Coli Shuttle Vectors Constructed with Invitro Mutagenized Yeast Genes Lacking 6-Base Pair Restriction Sites.* Gene, 1988. **74**(2): p. 527-534.

209.   James, P., J. Halladay, and E.A. Craig, *Genomic libraries and a host strain designed for highly efficient two-hybrid selection in yeast.* Genetics, 1996. **144**(4): p. 1425-36.

210.   Cartharius, K., et al., *MatInspector and beyond: promoter analysis based on transcription factor binding sites.* Bioinformatics, 2005. **21**(13): p. 2933-42.

211.   Mi, H.Y., A. Muruganujan, and P.D. Thomas, *PANTHER in 2013: modeling the evolution of gene function, and other gene attributes, in the context of phylogenetic trees.* Nucleic Acids Research, 2013. **41**(D1): p. D377-D386.

212. Nagalakshmi, U., et al., *The transcriptional landscape of the yeast genome defined by RNA sequencing.* Science, 2008. **320**(5881): p. 1344-1349.

213. Tsuchihara, K., et al., *Massive transcriptional start site analysis of human genes in hypoxia cells.* Nucleic Acids Res, 2009. **37**(7): p. 2249-63.

214. Li, R.Q., et al., *SOAP2: an improved ultrafast tool for short read alignment.* Bioinformatics, 2009. **25**(15): p. 1966-1967.

215. Li, M. and D.S. Sakaguchi, *Expression patterns of focal adhesion associated proteins in the developing retina.* Developmental Dynamics, 2002. **225**(4): p. 544-553.

216. Webb, D.J., C.M. Brown, and A.F. Horwitz, *Illuminating adhesion complexes in migrating cells: moving toward a bright future.* Curr Opin Cell Biol, 2003. **15**(5): p. 614-20.

217. Huttenlocher, A. and A.R. Horwitz, *Integrins in cell migration.* Cold Spring Harb Perspect Biol, 2011. **3**(9): p. a005074.

218. Parsons, J.T., A.R. Horwitz, and M.A. Schwartz, *Cell adhesion: integrating cytoskeletal dynamics and cellular tension.* Nat Rev Mol Cell Biol, 2010. **11**(9): p. 633-43.

219. Rodriguez Fernandez, J.L., et al., *Suppression of vinculin expression by antisense transfection confers changes in cell morphology, motility, and anchorage-dependent growth of 3T3 cells.* J Cell Biol, 1993. **122**(6): p. 1285-94.

220. Deakin, N.O. and C.E. Turner, *Paxillin comes of age.* J Cell Sci, 2008. **121**(Pt 15): p. 2435-44.

221. Diaz, B., et al., *Notch increases the shedding of HB-EGF by ADAM12 to potentiate invadopodia formation in hypoxia.* Journal of Cell Biology, 2013. **201**(2): p. 279-292.

222. Whitfield, M.L., et al., *Common markers of proliferation.* Nature Reviews Cancer, 2006. **6**(2): p. 99-106.

223. Schmidt, A. and M.N. Hall, *Signaling to the actin cytoskeleton.* Annual Review of Cell and Developmental Biology, 1998. **14**: p. 305-338.

224. Wiesner, S., K.R. Legate, and R. Fassler, *Integrin-actin interactions.* Cell Mol Life Sci, 2005. **62**(10): p. 1081-99.

225. Taddei, M.L., et al., *Anoikis: an emerging hallmark in health and diseases.* Journal of Pathology, 2012. **226**(2): p. 380-393.

226. Cano, A., et al., *The transcription factor Snail controls epithelial-mesenchymal transitions by repressing E-cadherin expression.* Nature Cell Biology, 2000. **2**(2): p. 76-83.

227. Peinado, H., M. Quintanilla, and A. Cano, *Transforming growth factor beta-1 induces snail transcription factor in epithelial cell lines - Mechanisms for epithelial mesenchymal transitions.* Journal of Biological Chemistry, 2003. **278**(23): p. 21113-21123.

228. Bhowmick, N.A., et al., *Transforming growth factor-beta1 mediates epithelial to mesenchymal transdifferentiation through a RhoA-dependent mechanism.* Mol Biol Cell, 2001. **12**(1): p. 27-36.

229. Ridley, A.J. and A. Hall, *The Small Gtp-Binding Protein Rho Regulates the Assembly of Focal Adhesions and Actin Stress Fibers in Response to Growth-Factors.* Cell, 1992. **70**(3): p. 389-399.

230. Bhowmick, N., et al., *Transforming growth factor-beta1 mediates epithelial to mesenchymal transdifferentiation through a RhoA-dependent mechanism.* Mol Biol Cell, 2001. **12**: p. 27 - 36.

231. Sekine, A., M. Fujiwara, and S. Narumiya, *Asparagine Residue in the Rho Gene-Product Is the Modification Site for Botulinum Adp-Ribosyltransferase.* Journal of Biological Chemistry, 1989. **264**(15): p. 8602-8605.

232. Watanabe, N., et al., *Cooperation between mDia1 and ROCK in Rho-induced actin reorganization.* Nature Cell Biology, 1999. **1**(3): p. 136-143.

233. Kimura, K., et al., *Regulation of myosin phosphatase by Rho and Rho-associated kinase (Rho-kinase).* Science, 1996. **273**(5272): p. 245-8.

234. Kawano, Y., et al., *Phosphorylation of myosin-binding subunit (MBS) of myosin phosphatase by Rho-kinase in vivo.* J Cell Biol, 1999. **147**(5): p. 1023-38.

235. Palazzo, A.F., et al., *mDia mediates Rho-regulated formation and orientation of stable microtubules.* Nature Cell Biology, 2001. **3**(8): p. 723-729.

236. Riveline, D., et al., *Focal contacts as mechanosensors: Externally applied local mechanical force induces growth of focal contacts by an mDia1-dependent and ROCK-independent mechanism.* Journal of Cell Biology, 2001. **153**(6): p. 1175-1185.

237. Ishizaki, T., et al., *Coordination of microtubules and the actin cytoskeleton by the Rho effector mDia1.* Nature Cell Biology, 2001. **3**(1): p. 8-14.

238. Machesky, L.M., et al., *Scar, a WASp-related protein, activates nucleation of actin filaments by the Arp2/3 complex.* Proc Natl Acad Sci U S A, 1999. **96**(7): p. 3739-44.

239. Kurisu, S. and T. Takenawa, *WASP and WAVE family proteins: friends or foes in cancer invasion?* Cancer Sci, 2010. **101**(10): p. 2093-104.

240. Yamaguchi, H., H. Miki, and T. Takenawa, *Neural Wiskott-Aldrich syndrome protein is involved in hepatocyte growth factor-induced migration, invasion, and tubulogenesis of epithelial cells.* Cancer Research, 2002. **62**(9): p. 2503-2509.

241. Takenawa, T. and S. Suetsugu, *The WASP-WAVE protein network: connecting the membrane to the cytoskeleton.* Nat Rev Mol Cell Biol, 2007. **8**(1): p. 37-48.

242. Jezewski, P.A., et al., *Complete sequencing shows a role for MSX1 in non-syndromic cleft lip and palate.* J Med Genet, 2003. **40**(6): p. 399-407.

243. van den Boogaard, M.J.H., et al., *MSX1 mutation is associated with orofacial clefting and tooth agenesis in humans.* Nature Genetics, 2000. **24**(4): p. 342-343.

244.	Mostowska, A., A. Kobielak, and W.H. Trzeciak, *Molecular basis of non-syndromic tooth agenesis: mutations of MSX1 and PAX9 reflect their role in patterning human dentition.* Eur J Oral Sci, 2003. **111**(5): p. 365-70.

245.	Jumlongras, D., et al., *A nonsense mutation in MSX1 causes Witkop syndrome.* Am J Hum Genet, 2001. **69**(1): p. 67-74.

246.	Catron, K.M., et al., *Transcriptional repression by Msx-1 does not require homeodomain DNA-binding sites.* Mol Cell Biol, 1995. **15**(2): p. 861-71.

247.	Satokata, I. and R. Maas, *Msx1 deficient mice exhibit cleft palate and abnormalities of craniofacial and tooth development.* Nat Genet, 1994. **6**(4): p. 348-56.

248.	Vastardis, H., et al., *A human MSX1 homeodomain missense mutation causes selective tooth agenesis.* Nat Genet, 1996. **13**(4): p. 417-21.

249.	Blanco, R., et al., *Evidence of a sex-dependent association between the MSX1 locus and nonsyndromic cleft lip with or without cleft palate in the Chilean population.* Hum Biol, 2001. **73**(1): p. 81-9.

250.	Sarapura, V.D., et al., *Msx1 is present in thyrotropic cells and binds to a consensus site on the glycoprotein hormone alpha-subunit promoter.* Mol Endocrinol, 1997. **11**(12): p. 1782-94.

251.	Stevens, K.N., et al., *Common variation in ISL1 confers genetic susceptibility for human congenital heart disease.* PLoS One, 2010. **5**(5): p. e10855.

252.	Zhang, H., et al., *The LIM-homeodomain protein ISL1 activates insulin gene promoter directly through synergy with BETA2.* J Mol Biol, 2009. **392**(3): p. 566-77.

253.	Jiang, Z.Y., et al., *A phosphatidylinositol 3-kinase-independent insulin signaling pathway to N-WASP/Arp2/3/F-actin required for GLUT4 glucose transporter recycling.* J Biol Chem, 2002. **277**(1): p. 509-15.

254.	Pang, Z.P., et al., *Induction of human neuronal cells by defined transcription factors.* Nature, 2011. **476**(7359): p. 220-3.

255.	Kobi, D., et al., *Genome-wide analysis of POU3F2/BRN2 promoter occupancy in human melanoma cells reveals Kitl as a novel regulated target gene.* Pigment Cell Melanoma Res, 2010. **23**(3): p. 404-18.

256.	Hockel, M. and P. Vaupel, *Biological consequences of tumor hypoxia.* Seminars in Oncology, 2001. **28**(2): p. 36-41.

257.	Sullivan, R. and C.H. Graham, *Hypoxia-driven selection of the metastatic phenotype.* Cancer Metastasis Rev, 2007. **26**(2): p. 319-31.

258.	Huang, L.E., et al., *Activation of hypoxia-inducible transcription factor depends primarily upon redox-sensitive stabilization of its alpha subunit.* J Biol Chem, 1996. **271**(50): p. 32253-9.

259. Milkiewicz, M., C.W. Pugh, and S. Egginton, *Inhibition of endogenous HIF inactivation induces angiogenesis in ischaemic skeletal muscles of mice.* Journal of Physiology-London, 2004. **560**(1): p. 21-26.

260. Li, S.H., et al., *A novel mode of action of YC-1 in HIF inhibition: stimulation of FIH-dependent p300 dissociation from HIF-1{alpha}.* Mol Cancer Ther, 2008. **7**(12): p. 3729-38.

261. Semenza, G.L., et al., *Hypoxia response elements in the aldolase A, enolase 1, and lactate dehydrogenase A gene promoters contain essential binding sites for hypoxia-inducible factor 1.* Journal of Biological Chemistry, 1996. **271**(51): p. 32529-32537.

262. Hockel, M., et al., *Association between tumor hypoxia and malignant progression in advanced cancer of the uterine cervix.* Cancer Research, 1996. **56**(19): p. 4509-4515.

263. Hanahan, D. and R.A. Weinberg, *Hallmarks of Cancer: The Next Generation.* Cell, 2011. **144**(5): p. 646-674.

264. Md Hashim, N.F., et al., *Hypoxia-induced invadopodia formation: a role for beta-PIX.* Open Biol, 2013. **3**(6): p. 120159.

265. Cheung, E.C., R.L. Ludwig, and K.H. Vousden, *Mitochondrial localization of TIGAR under hypoxia stimulates HK2 and lowers ROS and cell death.* Proc Natl Acad Sci U S A, 2012. **109**(50): p. 20491-6.

266. Zhdanov, A.V., et al., *A novel effect of DMOG on cell metabolism: direct inhibition of mitochondrial function precedes HIF target gene expression.* Biochimica Et Biophysica Acta-Bioenergetics, 2015. **1847**(10): p. 1254-1266.

267. Buccione, R., G. Caldieri, and I. Ayala, *Invadopodia: specialized tumor cell structures for the focal degradation of the extracellular matrix.* Cancer Metastasis Rev, 2009. **28**(1-2): p. 137-49.

268. Jakhesara, S.J., et al., *RNA-Seq reveals differentially expressed isoforms and novel splice variants in buccal mucosal cancer.* Gene, 2013. **516**(1): p. 24-32.

269. Vleminckx, K. and R. Kemler, *Cadherins and tissue formation: integrating adhesion and signaling.* Bioessays, 1999. **21**: p. 211 - 220.

270. Ramis-Conde, I., et al., *Multi-scale modelling of cancer cell intravasation: the role of cadherins in metastasis.* Physical Biology, 2009. **6**(1).

271. Hildebrand, A., et al., *Interaction of the Small Interstitial Proteoglycans Biglycan, Decorin and Fibromodulin with Transforming Growth-Factor-Beta.* Biochemical Journal, 1994. **302**: p. 527-534.

272. Giard, D.J., et al., *In vitro cultivation of human tumors: establishment of cell lines derived from a series of solid tumors.* J Natl Cancer Inst, 1973. **51**(5): p. 1417-23.

273. Foster, K.A., et al., *Characterization of the A549 cell line as a type II pulmonary epithelial cell model for drug metabolism.* Exp Cell Res, 1998. **243**(2): p. 359-66.

274. Subauste, M.C., et al., *Vinculin modulation of paxillin-FAK interactions regulates ERK to control survival and motility.* J Cell Biol, 2004. **165**(3): p. 371-81.

275. Zaidel-Bar, R., et al., *Early molecular events in the assembly of matrix adhesions at the leading edge of migrating cells.* J Cell Sci, 2003. **116**(Pt 22): p. 4605-13.

276. Bravo-Cordero, J.J., L. Hodgson, and J. Condeelis, *Directed cell invasion and migration during metastasis.* Current Opinion in Cell Biology, 2012. **24**(2): p. 277-283.

277. Donnelly, S.K., et al., *WIP provides an essential link between Nck and N-WASP during Arp2/3-dependent actin polymerization.* Curr Biol, 2013. **23**(11): p. 999-1006.

278. Zipfel, P.A., et al., *Role for the Abi/wave protein complex in T cell receptor-mediated proliferation and cytoskeletal remodeling.* Curr Biol, 2006. **16**(1): p. 35-46.

279. Wozniak, M.A., et al., *Focal adhesion regulation of cell behavior.* Biochim Biophys Acta, 2004. **1692**(2-3): p. 103-19.

280. Guadamillas, M.C., A. Cerezo, and M.A. Del Pozo, *Overcoming anoikis--pathways to anchorage-independent growth in cancer.* J Cell Sci, 2011. **124**(Pt 19): p. 3189-97.

281. Willis, B.C. and Z. Borok, *TGF-beta-induced EMT: mechanisms and implications for fibrotic lung disease.* American Journal of Physiology-Lung Cellular and Molecular Physiology, 2007. **293**(3): p. L525-L534.

282. Vilar, J.M.G., R. Jansen, and C. Sander, *Signal Processing in the TGF-β Superfamily Ligand-Receptor Network.* PLoS Comput Biol, 2006. **2**(1): p. e3.

283. Taylor, M.A., et al., *Upregulated WAVE3 expression is essential for TGF-beta-mediated EMT and metastasis of triple-negative breast cancer cells.* Breast Cancer Res Treat, 2013. **142**(2): p. 341-53.

284. Birchmeier, W. and J. Behrens, *Cadherin expression in carcinomas: role in the formation of cell junctions and the prevention of invasiveness.* Biochim Biophys Acta, 1994. **1198**(1): p. 11-26.

285. Mani, S.A., et al., *The Epithelial-Mesenchymal Transition Generates Cells with Properties of Stem Cells.* Cell, 2008. **133**(4): p. 704-715.

286. Shankar, J. and I.R. Nabi, *Actin Cytoskeleton Regulation of Epithelial Mesenchymal Transition in Metastatic Cancer Cells.* Plos One, 2015. **10**(3).

287. Guarino, M., *Epithelial–mesenchymal transition and tumour invasion.* The International Journal of Biochemistry & Cell Biology, 2007. **39**(12): p. 2153-2160.

288. Karlsson, R., et al., *Rho GTPase function in tumorigenesis.* Biochim Biophys Acta, 2009. **1796**(2): p. 91-8.

289. Narumiya, S., M. Tanji, and T. Ishizaki, *Rho signaling, ROCK and mDia1, in transformation, metastasis and invasion.* Cancer Metastasis Rev, 2009. **28**(1-2): p. 65-76.

290. Wang, X., et al., *Knockdown of RhoA expression alters ovarian cancer biological behavior in vitro and in nude mice.* Oncol Rep, 2015. **34**(2): p. 891-9.

291. Wang, H., et al., *Silencing of RhoA and RhoC expression by RNA interference suppresses human colorectal carcinoma growth in vivo.* J Exp Clin Cancer Res, 2010. **29**: p. 123.

292. Gardinergarden, M. and M. Frommer, *Cpg Islands in Vertebrate Genomes.* Journal of Molecular Biology, 1987. **196**(2): p. 261-282.

293. Chuhu Yang, E.B., Tao Jiang, Frances M. Sladek, and Ernest Martinez, *Prevalence of the Initiator over the TATA box in human and yeast genes and identification of DNA motifs enriched in human TATAless core promoters.* 2007.

294. Reece-Hoyes, J.S., et al., *Enhanced yeast one-hybrid assays for high-throughput gene-centered regulatory network mapping.* Nature Methods, 2011. **8**(12): p. 1059-+.

295. Davidson, D., *The function and evolution of Msx genes: pointers and paradoxes.* Trends Genet, 1995. **11**(10): p. 405-11.

296. Bendall, A.J., et al., *Msx1 antagonizes the myogenic activity of Pax3 in migrating limb muscle precursors.* Development, 1999. **126**(22): p. 4965-76.

297. Duval, N., et al., *Msx1 and Msx2 act as essential activators of Atoh1 expression in the murine spinal cord.* Development, 2014. **141**(8): p. 1726-1736.

298. Thiery, J.P., et al., *Epithelial-mesenchymal transitions in development and disease.* Cell, 2009. **139**(5): p. 871-90.

299. Di Bari, M.G., et al., *Msx2 Induces Epithelial-Mesenchymal Transition in Mouse Mammary Epithelial Cells Through Upregulation of Cripto-1.* Journal of Cellular Physiology, 2009. **219**(3): p. 659-666.

300. Catron, K.M., et al., *Comparison of MSX-1 and MSX-2 suggests a molecular basis for functional redundancy.* Mech Dev, 1996. **55**(2): p. 185-99.

301. Stelnicki, E.J., et al., *The human homeobox genes MSX-1, MSX-2, and MOX-1 are differentially expressed in the dermis and epidermis in fetal and adult skin.* Differentiation, 1997. **62**(1): p. 33-41.

302. Zhdanov, A.V., et al., *A novel effect of DMOG on cell metabolism: Direct inhibition of mitochondrial function precedes HIF target gene expression.* Biochim Biophys Acta, 2015.

303. Zhdanov, A.V., et al., *A novel effect of DMOG on cell metabolism: direct inhibition of mitochondrial function precedes HIF target gene expression.* Biochim Biophys Acta, 2015. **1847**(10): p. 1254-66.

304. Coutts, A.S., et al., *Hypoxia-driven cell motility reflects the interplay between JMY and HIF-1 alpha.* Oncogene, 2011. **30**(48): p. 4835-4842.

305. Krishnamachary, B., et al., *Regulation of colon carcinoma cell invasion by hypoxia-inducible factor 1.* Cancer Research, 2003. **63**(5): p. 1138-1143.

306. Victor, N., et al., *Involvement of HIF-1 in invasion of Mum2B uveal melanoma cells.* Clinical & Experimental Metastasis, 2006. **23**(1): p. 87-96.

307.   Tang, Z., L.M. Araysi, and H.M. Fathallah-Shaykh, *c-Src and neural Wiskott-Aldrich syndrome protein (N-WASP) promote low oxygen-induced accelerated brain invasion by gliomas.* PLoS One, 2013. **8**(9): p. e75436.

308.   Wang, H.R., et al., *Regulation of cell polarity and protrusion formation by targeting RhoA for degradation.* Science, 2003. **302**(5651): p. 1775-9.

309.   Chen, Y.Z., et al., *Cullin Mediates Degradation of RhoA through Evolutionarily Conserved BTB Adaptors to Control Actin Cytoskeleton Structure and Cell Movement.* Molecular Cell, 2009. **35**(6): p. 841-855.

Appendix

Appendix A : List of primers used for this study

Sr. No	Primer name	Sequence (5'-3')
1	cmvMin-5	CGGAATTCACTAGTGCACCAAAATCAACGGGACTTTCC
2	cmvBgES-5	GGAAGATCTGAATTCATACTAGTATTATGCCCAGTACATGAC
3	dtom5N	GCGAATTCGGGTCTAGAAGATCT
4	dtom3N	CGGGATCCGTCGACCAATTGTTA
5	Ghis-5	CGGGATCCGCTAGCATGCATCACCATCACCATCACCATCAC
6	HiF1a-5	CATGCCATGGAGGGCGCCGGCGGCGC
7	HiF1a-3	CGCGGATCCGTTAACTTGATCCAAAGCTCTGAG
8	His31Hy-5	CGGAATTCGTCGACTCTAGATGGCATTATCACATAATGAATTATAC
9	His31Hy-3	CGGGATCCCTGCAGCTACATAAGAACACCTTTGGTGGAG
10	HSna1-f	GCTCTAGAATGCCGCGCTCTTTCCTCG
11	HSna1-r	CGGAATTCTCAGCGGGGACATCCTGA
12	Isl5	AACTGCAGGTCTAGGTCTAGAATGGGAGACAT
13	Isl3	CGGGAATTCTAGGATCCTGCCTCAA
14	Msx5	AACTGCAGGTCTAGAATGACTTCTT

Sr.No	Primer name	Sequence (5'-3')
15	Msx3	CGGGAATTCTAGGATCCTGTCAGGTG
16	NWAS-5	CATGCCATGGGACATATGAGCTCCGTCCAG CAGCAGC
17	NWAS-3	CCGGAATTCTCAACTCGAGTCTTCCCACTCATCATCATCCTC
18	NWAST1R-F	GAGGCCCAGCTGAAGGACAGAGAAACATCA
19	NWAST1R-R	GTCCTTCAGCTGGGCCTCTGAGATTCCACA
20	POU5	AACTGCAGGTCTAGAATGGCGACCG
21	POU3	CGGGAATTCTAGGATCCCTGGACGGG
22	waslPF1295	CGGAATTCACTAGTGTAATTCAGAGGCAACTCCAGG
23	waslPF1195	CGGAATTCATAATTAATCAAGTTTAACTTTGAAATCTC
24	waslPF1095	CGGAATTCTATTTCATTAATGGCAGCTTTAATTATA
25	waslPF995	CGGAATTCGGGAGCTATCAGAGATGTTAACATC
26	waslPF902	CGGAATTCACTAGTAATGTGGAGAACAGTGAGATGC
27	waslPF728	CGGAATTCACTAGTAAGAAATGTGTCCAGGCCCTTAG
28	waslPF575	CGGAATTCACTAGTGGCCTGTTTGTTCCTCCACTC
29	waslPF288	CGGAATTCACTAGTCCCATCCATCTTCTTCAAGCAG
30	waslPR902	GCTCTAGAGCATCTCACTGTTCTCCACATT
31	waslPR329	GCTCTAGAGCTCATGGTTTCGCCGGCGGG
32	WIP5	CATGCCATGGCAATGCCTGTCCCTCCCCCTCCAGC
32	WIP3	GGAAGATCTCCTCGGGATGGGAGGGAGTGGTG

Appendix B : List of shRNAs used in this study

Sr.No	Primer	Sequence
1	hWIPshRNA-F	5' CCAATACTGGACAAACCTAAA 3'
2	hNWAS-shRNA-F	5' GCACAACTTAAAGACAGAGAA 3'

Appendix C: List of ChiP primers

Sr.No	Primer name	Sequence
1	Chipmsx1-F	5' CATGATAATGGTTTACCAGTCTGGT 3'
2	Chipmsx1-R	5' TTCTTCTGTAAGTTAAATACTAAACGGC 3'
3	ChipNeg-F	5' GTCCTAATCTACCCATGGCTACAGT 3'
4	ChipNeg-R	5' TCTGTCTTTAAGTTGTGCCTCTGAGA 3'
5	ChipHRE1-F	5' GCCAGAGGCCAGAGTACGAAGT 3'
6	ChipHRE1-R	5' GCCGCACAATCCAACATGGCAGC 3'
7	ChipHRE2-F	5' GAAATGTGTCCAGGCCCTTAGAAG 3'
8	ChipHRE2-R	5' AACTTTGTCCCAAACTTCAGCTG 3'

Appendix D: List of real time PCR primers

Sr.No	Primer name	Sequence
1	h-MRPL27-F	5'CTGGTGGCTGGAATTGACCGCTA 3'
2	h-MRPL27-R	5'CAAGGGGATATCCACAGAGTACCTTG3'
3	h-NWASPrt-F	5'AAGGATGGGAAACTATTGTGGGA 3'
4	h-NWASPrt-R	5'GACGGCCCAAAAGGTCTGTAA 3'
5	h-WIPrt-F	5' GTTACCTTCGCCAGGACGTTCA 3'
6	h-WIPrt-R	5' TGCGTTTCTGCTTACTGGAGG 3'